SMART MAGNETIC AFFINITY ADSORBENTS

By

Kalliopi Zourna

A thesis submitted to the University of Birmingham
for the degree of
DOCTOR OF PHILOSOPHY

School of Chemical Engineering
College of Engineering and Physical Sciences
2009

Thesis Abstract

As the focus of research on ‘adaptive/responsive’ surfaces has in recent years contributed strongly towards the design of surface materials with ‘intelligent’ or ‘smart’ behaviour, current superparamagnetic adsorbents being employed both in small and large scale operations can be surface modified and improved by gaining dual functionalities. In this work, modification of M-PVA supports with polymer brushes of dual properties has been explored for their intended use in bioseparation technology, i.e. for both selectively protein binding and enhanced temperature elution of especially difficult to elute species such as haemoglobin. Tethering of polymer brushes was achieved by employing two different ‘grafting from’ routes, i.e. cerium (IV) initiated polymerisation and Atom Transfer Polymerisation Reaction (ATRP). By identifying the optimum cerium (IV) reaction conditions, the said chemistry was further utilised to attach different polymers (thermoresponsive and affinity ligands) and their combination (thermo-affinity) at fixed positions onto M-PVA supports, either as di-block or mixed functionality polymer brushes. The configuration of introduced polymer chains as well as the haemoglobin binding characteristics of the above materials was evaluated, and their efficiency for haemoglobin and GFP desorption via sequential temperature transitions was demonstrated. Mixed polymer brushes manufactured using sequential ATRP after partial bromination of AGE activated magnetic supports were characterised and tested likewise. Protein binding and release efficiency was dependent on brush configuration (length and spacing between the graft sites of polymers), pNIPAAm content, type of affinity ligand and type of protein employed. From the above materials those with polymer chains of sufficient pNIPAAm length and at such spacing allowing their ‘free’ expansion/collapse upon temperature change (especially those grafted via cerium (IV) route) were found efficient, as brush behaviour favour enhanced desorption of difficult to elute species.

Acknowledgments

I would like to express my sincere gratitude to Professor Owen Thomas, for entrusting me with this research and for his excellent scientific guidance. I am also indebted to my mentor and friend, Dr. Eirini Theodosiou: without her continuous support and input I would not have managed to complete this task.

I would like also to thank all the students and staff from the 'bio' group for their valuable assistance: Tom Willet as a genuine collaborator and advisor in chemistry. Yao Yu for providing me with his VBIDA. Chia Chang Hsu (Evan) for helping me to finish off my last experimental work. Geoff Brown, Haiyang Liu and Alison Liddy for their collaboration. Ms Hazel Jennings and Ms Elaine Mittchel, for their willing assistance in the lab.

I am grateful to supervise the MSc student Dhiraj Kumar Ramnath. His work contributed to Chapter 3.

Many thanks to Dr Jörg Becker from the Institute of Technical Chemistry at the Forschungszentrum Karlsruhe, Germany, for supplying the GFP extract and the purification protocol for it.

Finally, I would like to thank my family and Nick for standing by me through the difficult times.

Contents and Appendices

List of Figures

List of Tables

1. Introduction

1.1 Background of the Project

This work has been part of a European Commission funded Specific Targeted Research Project (STREP) entitled 'Magnetic Field Assisted Biomaterials Processing–NanoBioMag', with the overall objective to "enhance the competitiveness of the European biomaterials-, pharmaceutical- and food industry by developing unique and novel materials and related production technologies" (Proposal #013469; see Fig. 1.1).

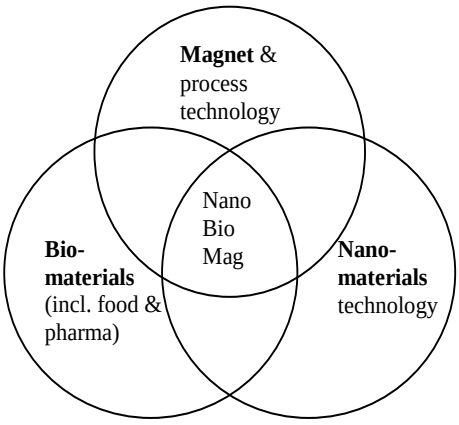

Figure 1.1 Schematic diagram of the NanoBioMag principles integration (Proposal #013469).

This Ph.D research project was part of Work Package 1 (WP1), with the primary objective to create various new and highly robust 'Smart Polymer Magnetic Adsorbent Phases' or SP-MAPs, for future production technologies of biomaterials, as well as bioseparation objectives, such as High-Gradient Magnetic Fishing (HGMF). SP-MAPs' magnetic properties will enable their external manipulation and separation through a combination of magnetic and other forces, whereas highly selective particle coatings will allow the capture of target biomaterials

out of complex environments. Size and surface properties provide new breakthroughs in adsorption characteristics and reduced processing time, so that such 'smart' materials may ultimately revolutionize the way in which future magnetic phases are designed, fabricated and employed, as well as further enable the manufacture of new and even 'smarter' products to be realized.

1.2 Downstream processing

Downstream processing, or DSP, can be defined as "the various stages of processing that occur after the completion of the fermentation or bioconversion stage, including separation, purification, and packaging of the product" (http://www.biology-online.org/dictionary). Broadly speaking there are four sequential steps involved, namely: clarification; primary isolation; intermediate purification; and polishing or final purification.

(a) **Clarification** entails the separation of cells from the fermentation liquor and is usually carried out by centrifugation, mechanical filtration or flocculation (Lightfoot and Moscariello, 2004).

(b) During **Primary isolation** a variety of non-selective techniques are used (e.g. adsorption, liquid-liquid extraction, flocculation and precipitation), which aim to remove the product from the cells or the cell-free broth and increase its quality and concentration.

(c) **Intermediate purification** is considered one of the most challenging stages of DSP, since it involves processes that aim to separate the target molecule from chemically and physically

similar impurities. Typical large scale operations include fractional precipitation, ultrafiltration and fixed bed chromatography.

(d) **Polishing** usually aims to remove traces of harmful impurities but also for solvent exchange prior to final formulation. Membrane filtrations as well as crystallisation and size exclusion chromatography are used extensively at this stage.

1.2.1 Current status and challenges of downstream processing

During a recent study[1] on the socio-economic impact of biotechnology in Europe (http://www.bionity.com/news/e/63927) it was revealed that:

"the number of biopharmaceuticals on the market has more than doubled in the last 10 years and the number of biopharmaceutical companies rose from 37 (1996) to 143 (2005)"; and

"revenues for biotech vaccines jumped from €65 million in 1996 to €259 million".

Clearly this exponential growth puts considerable pressure on both biopharmaceutical manufacturers and contract manufacturing organisations to increase production capacity within the next few years (http://www.contractpharma.com/articles/2008/05/biocapacity-in-2012). Upstream processing is already improving dramatically, with typical product expression levels in mammalian cell cultures of >1 g L^{-1}, a figure which is predicted will rise to 10 g L^{-1} within the next 10 years (Langer E.S., 2007a). Unfortunately, downstream processing has not yet managed to match the upstream success, and since it accounts for 75%

[1] the Joint Research Centre study 'Consequences, Opportunities and Challenges of Modern Biotechnology for Europe' also known as the Biotechn for Europe or Bio4EU

of the total manufacturing costs (Aldridge, 2006) it is considered by almost 50% of the European Biomanufacturers to be a bottleneck on production capacity (Langer, 2007 b).

Downstream processing employs a long sequence of technologies and unit operations to achieve the desirable product purity requirements. For example, a typical flow sheet for the production of a monoclonal antibody involves ten purification steps (see Fig. 1.2), out of which three are chromatography. In a similar manner, chromatography is the dominating purification technology in the separation of the majority of biopharmaceuticals, making it "the workhorse of the industry" (Curling and Gottschalk, 2007) for the last 30 years[2], and therefore, is discussed in further detail in the following section.

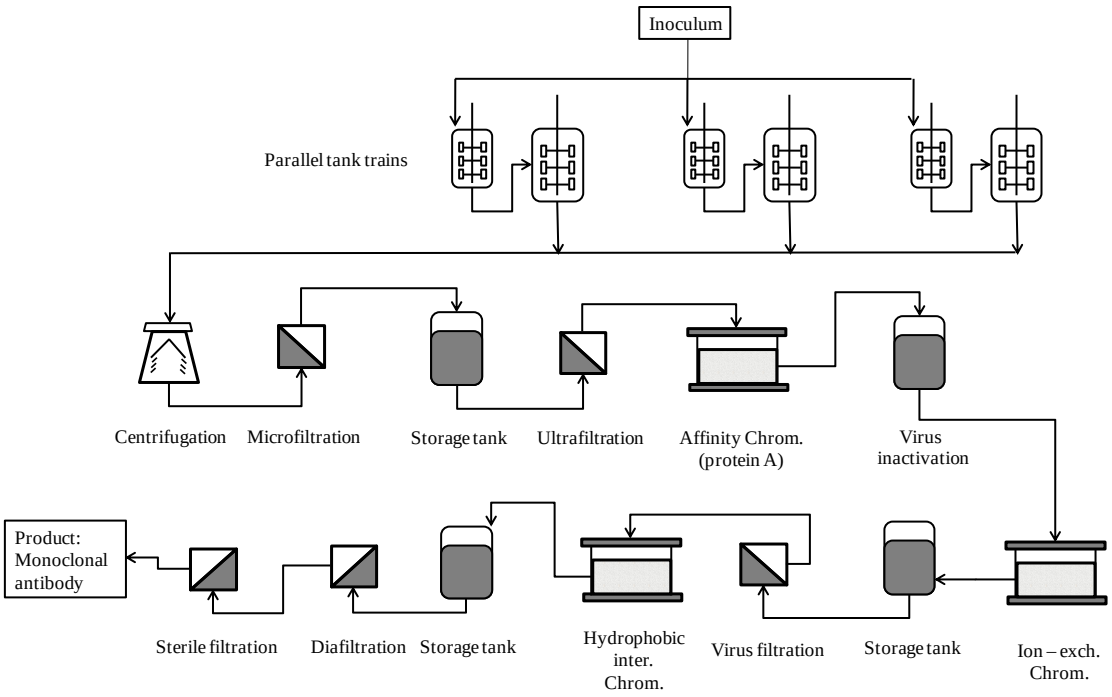

Figure 1.2 Flowsheet for monoclonal antibody production (reproduced from Sommerfeld and Strube, 2005).

[2] a statement that is further supported by the fact that the GE Healthcare's Life Science Division increased its bioprocess revenues from $36 million in 1986 to $461 million in 2006 (Ehrenheim P. GE, Healthcare presentation, 2006; Curling and Gottschalk, 2007)

1.2.2 Process chromatography

Chromatography[3] is a separation method based on the partitioning of the components of a mixture between a stationary and a mobile phase. In its most common form, chromatography is carried out within a column, which contains a solid stationary phase and a liquid or gas mobile phase. The general principle of the technique is that various molecules move through the system at different velocities dependent on their tendency to stay in the stationary or the mobile phase (Janson and Jönsson, 1998). In the field of protein separation the mobile phase is liquid (usually an aqueous buffer) whereas the solid phase is a porous matrix, with defined pore size distribution, composed of a hydrophilic polymer with various ligands immobilised onto it (apart from size exclusion matrices). Table 1.1 summarises the separation principles behind the most popular types of protein chromatography, which are then discussed in further detail in the following paragraphs.

Table 1.1 Types of protein liquid chromatography and their separation principles (re-drawn from Janson and Jönsson, 1998).

Type of chromatography	Separation principle
Size exclusion or Gel filtration	Size & shape
Ion exchange	Net charge
Hydrophobic Interaction	Hydrophobicity
Reverse Phase	Hydrophobicity
Affinity	Biological function
Immobilised Metal Ion Affinity	Metal binding

Size exclusion chromatography (SEC): SEC separates the molecules according to their size and shape; larger species have limited diffusivity or are even unable to enter the pores of the

[3] from Greek: 'χρώμα' (*chroma*) meaning 'colour', and 'γράφειν' (*graphein*) meaning 'to write'

support so they come out of the column first, whereas smaller ones diffuse further into the pores and therefore it takes longer to pass down the column. Commercial SEC gels are made of cross-linked dextran, agarose and polyacrylamide and more recently silica, hydrophilized vinyl polymers and highly cross-linked agarose (Hagel, 1998). Whilst SEC is a simple and straightforward technique, with low running costs, it is not used very widely in the manufacturing process of new biotechnology products, because of its low throughput and efficiency and it is normally replaced by ultrafiltration/diafiltration for buffer exchange or adsorptive chromatography for other separations (Shukla and Yigzaw, 2007).

Ion exchange chromatography (IEC): IEC relies on reversible electrostatic interactions between charged molecules and oppositely charged groups immobilised on the stationary phase. These interactions depend on the net charge and the surface charge distribution of the species to be separated, the ionic strength and the pH of the medium, as well as the nature of the particular ions of the solvent and additives (Karlsson *et al*., 1998). There are two types of ion exchange chromatography, depending on the charge of their functional groups: anion exchange (AEC) containing positive groups; and cation exchange (CEC) containing negative groups (see Table 1.2). Quaternary aminoethyl (Q) and sulfopropyl (SP) groups remain charged over a wide pH range and are therefore classed as strong ion exchangers. In contrast, moieties such as diethyl aminoethyl (DEAE) and carboxymethyl (CM) exhibit pH limits beyond which they become deionised; and are referred to as weak ion exchangers.

Ion exchange is the most widely used type of chromatography, and features in ~75% of purification protocols (Karlsson *et al.*, 1998). This is due to its versatility (it can be used at all stages of the purification process from the initial capture right through to intermediate

purification and polishing), simple principle of operation, high capacity, and high resolving power.

Table 1.2 Ion exchange groups used in protein chromatography (taken from Shukla and Yigzaw, 2007).

Name & abbreviation	**pK**
Anion exchangers	
Diethyl aminoethyl (DEAE)	9-9.5
Quaternary aminoethyl (Q)	>9.5
Dimethyl aminoethyl (DMAE)	9
Trimethyl aminoethyl (TMAE)	>13
Cation exchangers	
Carboxymethyl (CM)	3-5
Sulfonate (S)	2
Sulfoethyl (SE)	2
Sulfopropyl (SP)	<1

Hydrophobic interaction chromatography (HIC) and Reversed phase chromatography (RPC): Both types operate on the same physicochemical principles, i.e. interactions between non-polar groups on the surface of biomolecules and hydrophobic ligands attached to the stationary phase. In the HIC adsorbents, the ligand chain length is shorter (alkyl or aryl groups) and the ligand density is lower than those used in RPC. As a consequence HIC is a 'milder' and more prevalent mode of chromatography compared to PRC, the latter leading to protein denaturation and therefore used in preference for the separation of peptides and small proteins (Eriksson, 1998).

Affinity chromatography (AC): In its broad term, affinity chromatography exploits reversible specific interactions[4] occurring between an immobilised ligand and the target biomolecule. It enables purification on the basis of a molecule's biological function or individual chemical structure, which makes it highly selective and therefore ideally suited for the isolation of the product of interest from relatively crude mixtures (Carlsson *et al*., 1998). Commercially available activated matrices consist of a chemically and physically inert base matrix (e.g. agarose), a biospecific ligand (e.g. hormones, enzyme co-factors, dyes, immunoadsorbents, lectins etc.), and in cases of steric hindrance effects, a spacer arm to improve binding between ligand and target molecule.

Affinity chromatography's main disadvantage is the high cost, due to the need of highly purified ligands, which may pose significant hurdles when there is a need to be implemented at large production scale.

Immobilised metal ion affinity chromatography (IMAC): The affinity of certain compounds for heavy metal ions was first explored for protein fractionation and purification by Porath *et al.* (1975), though even the principle of the technique was introduced much earlier by Hellferich (Hellferich, 1961). Most proteins can form complexes with metal ions bound to a metal chelating substance, which in turn is attached to a solid support (see Fig. 1.3; Kågedal, 1998). These complexes are based on the interaction of metal binding amino acid residues on the protein surface with the divalent metal ions Co^{2+}, Zn^{2+}, Cu^{2+} and Ni^{2+}. The metal ion is held on the stationary phase with the aid of a chelating substance, the most common being iminodiacetic acid (IDA) and nitrilotriacetic acid (NTA). Histidine, tryptophan and cysteine are the amino acids with the strongest metal affinity and it is common practise

[4] Some of the biological interactions used in AC are: antibody–antigen/virus/cell; inhibitor–enzyme; nucleic acid–nucleic acid binding protein; hormone–receptor, etc.

nowadays to introduce histidine-rich (His-tag) stretches at either terminus of a protein or a peptide to achieve high purity and yield during both laboratory and large scale protein purification processes. Furthermore, IMAC has been used for the removal and inactivation of viruses (Kågedal, 1998), protein characterisation and refolding and biosensors (Ueda *et al.*, 2003).

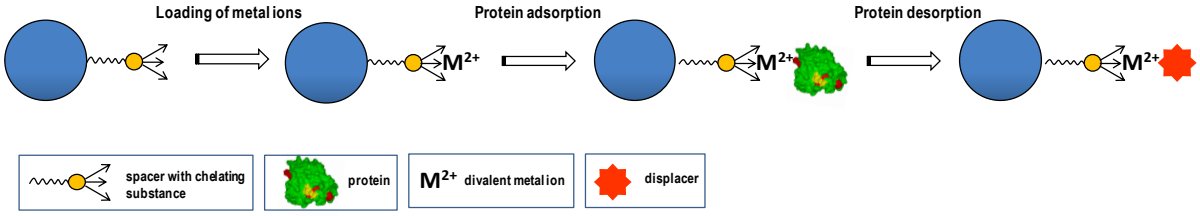

Figure 1.3 Principle of IMAC (reproduced from Ueda *et al.*, 2003).

The IMAC supports (and other chromatographic media), should ideal have the following characteristics: (a) be easy to derivatise; (b) do not exhibit non-specific adsorption; (c) be good physical, mechanical and chemical stability; (d) provide easy ligand accessibility (e.g. high porosity); (e) promote high flow rates; (f) be stable to eluants (e.g. denaturative agents); (g) permit easy regeneration of the column without degradation of the matrix; and (h) provide stable gel without any shrinking/swelling during the chromatographic process.

Protein binding in IMAC was first studied in agarose beads such as Sepharose 6B (Maisano *et al.*, 1989). In these procedures, IDA was coupled onto the resin, using the methods described previously by Porath and Olin (1983). Today, commercial available IMAC adsorbents are mainly cellulose, silica, cross-linked agarose and hydrophilised beads (Ueda *et al.*, 2003).

In IMAC, there are many factors that can influence the adsorption and desorption of proteins, such as the chelate structure, the type of metal ions, and the composition of the mobile phase

(buffers, pH, ionic strength) (Arnold, 1991; Kågedal, 1998). The number of linkages of metal ion with the metal chelator, the affinity of the chelator for the metal ion and the stability of the chelator- metal complex, play a major role for the selectivity and affinity of the target protein (Ueda *et al*., 2003). During the binding of proteins, undesired electrostatic interactions are developed between the proteins and the matrix (or between the proteins), which can be suppressed by increasing the ionic strength of the buffer (e.g. by adding salt in high concentrations (Kågedal, 1998). For protein retention, normally the pH is kept between 7 and 8. For protein elution, a wide range of conditions can be employed such as changing the pH, the ionic strength, the polarity or adding a competitive ligand, e.g. imidazole (Porath *et al*., 1975: Sulkowski, 1996; Amersham Biosciences, 2007).

IMAC offers several advantages over other chromatographic affinity techniques such as: (a) the variety of metal ions that can be immobilised onto the same matrix after successive stripping, where regeneration can be achieved mainly by using a strong chelator, such as EDTA while the base matrix retains its chelating properties; (b) after the elution, the proteins are recovered uncharged (unless enzymes remove a metal ion); (c) depletion of bacterial growth as the solution passes from the metal free column (very low concentration of metal ions); and (d) high reproducibility (Porath, 1988). However, the main disadvantage of this technique is the metal ion leakage from the matrix which can contaminate the product (Porath, 1988).

Apart from IMAC, there are also other operations that utilise the concept of metal affinity for protein separation. As an example, is the Expanded Bed Adsorption (EBA) employing chelator metal complexes on resins packed in a column, which has been successfully used for the purification of his-tagged proteins or naturally occurring proteins (Willoughby, 1999; Clemmitt and Chase, 2000). Other systems based on metal affinity interactions of proteins is

the metal chelate affinity precipitation (MCAP) (Galaev *et al.,* 1997; Kumar *et al.,* 1998) and the IMA-partitioning in aqueous two phase polymer systems (ATPS[5]) (Birkenmeier *et al.,* 1991; Pietruszka *et al*., 2000; Sivars *et al*., 2000), which are now being widely applied in protein purification, especially when dealing with recombinant proteins (Ueda *et al.,* 2003).

1.3 Alternatives to chromatography

Although chromatography is considered as the 'workhorse' of bioseparations, being a key unit operation in the purification of biotherapeutics for the last 50 years, intensive research is performed not only in the optimisation of the existing processes, but also in its substitution by other more cost effective operations (Przybycien *et al.,* 2004). Chromatographic alternatives have been broadly categorised by Przybycien and co-workers (2004) as bulk, field based, and adsorptive separation techniques and are summarised briefly in Table 1.3.

In parallel, late advances in product engineering (new fusion tags), host engineering (alternative hosts, genetic engineering of contaminant composition, etc.), novel approaches to integration (upstream/downstream coupling, upstream formulation) and the development of new materials ('smart' polymers, new ligands, etc.) are considered possible alternative pathways (Przybycien *et al.*, 2004). It has been demonstrated, for example, that target molecules can be separated in a simple and cost-effective way by incorporating 'smart' polymers in aqueous two-phase polymer systems (ATPs) (Pietruszka *et al.*, 2000; Kumar e*t al.,* 2001), affinity precipitation (Galaev *et al.* 1997; Kumar *et al.* 1998a, 1988b and 1999) or

[5] An aqueous two-phase system (ATP) is an aqueous, liquid–liquid, biphasic system which is obtained either by a mixture of aqueous solution of two polymers (e.g. polyethylene glycol & dextran), or a polymer and a salt (e.g. polyethylene glycol & sodium sulphate) (Albertsson, 1986 and 1996)

thermoresponsive chromatography (Kanazawa *at al.* 1996; Lakhiari *et al.*, 1998; Kobayashi *et al.*, 2003; Ayano *et al.*, 2006). In this work, this type of 'smart' polymer materials (SP) were also employed, in an attempt to modify and improve the current mono-functional magnetic adsorbents employed in a new technique called High Gradient Magnetic Fishing (HGMF), and an introduction to both the technique and the materials is presented in the following sections.

Table 1.3 Summary of chromatographic alternatives according to Przybycien *et al*. (2004).

Chromatography alternatives		
Bulk separations	***Advantages***	***Separation examples***
Aqueous two-phase extraction	easy to use/process, cheap reagents	cells, virus, plasmid DNA
Three-phase partitioning	significant purification at initial steps of isolation	GFP, xylanase, antigenic proteins, alginate
Precipitation	variety of precipitation agents	removal of nucleic acids during cell lysis, separation of lactase from corn protein, separation of DNA-binding protein and his-tagged proteins
Crystallization	low cost	from industrial enzymes to approved pharmaceuticals like insulin
Field based separations		
Membrane filtration	flexibility to modulate selectivity	whey protein fractionation, lysozyme purification from egg-white, RNA/DNA separation
Adsorptive separations:		
Monoliths	fast, minimal losses in resolution, reduction of product degradability, high throughputs	myoglobin, conalbumin, soybean trypsin inhibitor, clotting factor IX from human plasma
Expanded Bed Adsorption (EBA)	single capture operation fusing clarification, concentration & initial purification into one single step	proteins from crude feedstocks
Membrane chromatography	dynamic capacities for large particles	therapeutic proteins, antibodies, fusion proteins

1.4 Magnetic systems for protein recovery

1.4.1 Magnetic units and definitions (Purcell, 1984; Gerber and Birss, 1983)

Magnetic fields are generated when electric charge carriers such as electrons move (through space or within electrical conductors). A magnetic field can be defined by either its cause (e.g. an electric current within a wire), or by its effect (e.g. the measured force acting on a small permanent magnet). The effect of a magnetic field is defined by the theoretical force acting on a 1 m length of wire (located within the field) carrying a current of 1 Ampere. The ratio between the force, *F*, and the product of the current, *I*, and the wire length, *l*, is a measure of the field intensity and is called the magnetic *flux density*, *B*:

$$B = \frac{F}{I \cdot l} \qquad \text{Eq. (1.1)}$$

The flux density (a vector pointing into the direction of the magnetic field) is measured in units of Tesla:

$$1\frac{\mathrm{N}}{\mathrm{A}\cdot\mathrm{m}} = 1\frac{\mathrm{W}\cdot\mathrm{s}}{\mathrm{A}\cdot\mathrm{m}^2} = 1\frac{\mathrm{V}\cdot\mathrm{s}}{\mathrm{m}^2} = 1\,\mathrm{Tesla}$$

If the wire is coiled into a long cylindrical shape, then the flux density inside the coil is proportional to (i) the current, *I*, in the wire and (ii) the ratio between the number of windings, *n*, and the length of the coil, *l*:

$$B = \mu_0 \cdot \mu_r \cdot I \cdot \frac{n}{l} \qquad \text{Eq. (1.2)}$$

In Eq. (1.2), μ_r is a dimensionless number characterizing the influence of the matter inside the coil and is called the *permeability*. In a vacuum, μ_r is equal to 1; in air, it is approximately 1.

The proportionality factor, μ_0, is the *magnetic field constant* or *permeability of free space.* In the cgs system of units, μ_0 is dimensionless, with a value of 1; in the SI system, it has a value of $4\pi \times \cdot 10^{-7}$ V s A^{-1} m^{-1}.

To quantify the magnetic field intensity, which is independent of the constants μ_r and μ_0, another physical variable is introduced, the so-called *magnetic field strength, H*. In the case of a long coil, *H* is defined as follows:

$$H = I \cdot \frac{n}{l} \qquad \text{Eq. (1.3)}$$

Substitution of eq. (1.3) into eq. (1.2) yields the following relationship between magnetic flux density and magnetic field strength:

$$B = \mu_0 \cdot \mu_r \cdot H \qquad \text{Eq. (1.4)}$$

1.4.2 Forms of magnetism

When a magnetic field is applied on a body, the field influences the movement of the electrons around the nuclei developing magnetic dipoles. The *magnetisation, M*, for the body is defined as the volumetric average magnetic dipole moment with units A m^{-1}, or as the difference between the apparent magnetic field strength inside the body (H_{inside}) and that outside of the body ($H_{outside}$):

$$M = \Delta H = H_{inside} - H_{outside} \qquad \text{Eq. (1.5)}$$

The dependence of the magnetisation on the external magnetic field strength, H_0, can also be expressed by a dimensionless proportionality constant, known as the *magnetic susceptibility*, χ:

$$M = \chi \cdot H_{outside} = \chi \cdot H_0 \qquad \text{Eq. (1.6)}$$

Materials are magnetically characterized by their *magnetic susceptibility* and fall into three main categories: ferromagnetic, paramagnetic and diamagnetic. The hysteresis loops or magnetisation curves of the above materials are illustrated in Fig. 1.4.

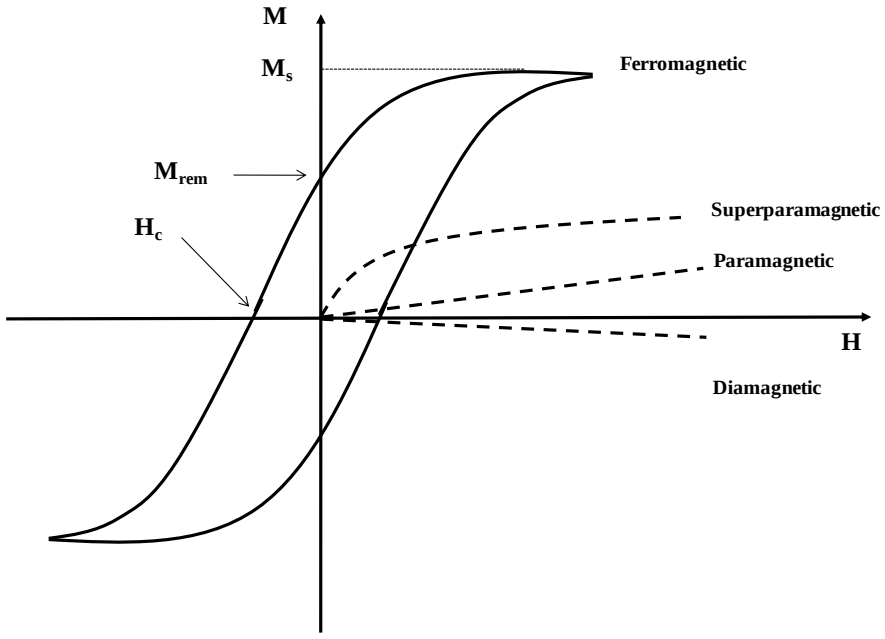

Figure 1.4 Magnetisation curves (the magnetization *M* is plotted as a function of magnetic field strength H) of ferro-, para-, superpara- and diamagnetic materials. *M*: magnetization; M_s: saturation magnetization; M_{rem}: remanent magnetisation; *H*: magnetic field strength; H_c: magnetic coercivity.

For paramagnetic (e.g. manganese, hematite) or diamagnetic (e.g. gold, bismuth) materials, the magnetisation curve is linear (χ is constant). Ferromagnetic (e.g. iron, cobalt, nickel) materials are characterized by high magnetisation and by saturation behavior at high field strengths (Heebøll-Nielsen, 2002). When a magnetic field is applied on these materials, the

magnetization does not return to zero and a hysteresis behavior is observed (the intercept of the magnetization curve with the *M* axis gives the remanent magnetization M_{rem}, while the intercept with the *H* axis gives the coercivity H_c). Paramagnetic materials have small positive magnetic susceptibility, while diamagnetic materials have small and negative one (Heebøll-Nielsen, 2002). When ferro- or ferromagnetic materials become very small (e.g nanoparticles) they behave as superparamagnetic being an intermediate between ferromagnetism and paramagnetism. These materials are easily magnetised while keep no remanent magnetization in the absence of the field (Hubbuch, 2001).

1.4.3 Historical development

Although the phenomenon of magnetism has been observed since 550 BC from ancient Greeks, it was until the middle of 19th century that was started to applied for magnetic separation purposes. The separation of coarse iron ores from 'non-magnetic' impurities surrounding the minerals was shown from Ball, Norton and Edison (Svoboda and Fujita, 2003). The recent progress in theoretical aspects of magnetism allow the even broader application of magnetic separation to materials of decreasing dimensions (i.e. from coarse to colloidal species) and to that required weaker magnetic fields (i.e. from magnetic to diamagnetic species) (Svoboda and Fujita, 2003). In 1940's and for the first time, the use of magnetic adsorbents for the separation of biological materials for wastewater treatment applications was addressed (Pieters *et al.*, 1991). The use of magnetic adsorbents for the selective separation of biomolecules was first reported by Peter Dunnill and Malcolm Lilly at the University College London (UCL) in the early 1970's. They described the immobilisation of enzymes onto iron oxide particles and the application of such particles as bioaffinity

adsorbents (Dunnill and Lilly 1974; Halling and Dunnill 1980; Robinson *et al.*, 1973; Franzreb *et al.*, 2006). Today, various magnetic separation techniques are employed throughout the bioscience field, such as in molecular biology, cell biology, microbiology, biochemistry and analytical chemistry (Safaric *et al*., 2001). For example, new developed magnetic adsorbents serve towards separation of nucleic acids and oligonucleotides, target cells and cell organelles, enzymes, lectins and antibodies as well as the concentration of microorganisms and target analytes (Safaricova and Safaric, 1999; Safaric *et al*., 1995; Safaric *et al.*, 2001). During these separations/concentrations, the handling of samples takes place in very small volumes. The basic concept is to selectively bind the biomaterial of interest (e.g., a specific cell, protein etc.) to a magnetic particle and then separate it from its surrounding matrix using a magnetic field. The idea is quite simple and provides advantages such as: few handling steps, no need for expensive equipment (such as liquid chromatography systems, centrifuges), direct application in crude samples containing suspended solid material, shortening of total separation time, and easy removal/recovery from the sample (Safaric and Safaricova, 2004). The magnetic particles used for these separations are derivatised with basic ligands that normally used in chromatographic methods such as affinity, pseudo affinity, ion exchange, hydrophobic etc. (Franzreb *et al*., 2006).

The magnetic separation techniques are also the basis of various automated procedures, especially magnetic-particle based immunoassay systems for the determination of a variety of analytes, among them proteins and peptides. Several automated systems for the separation of proteins or nucleic acids have become available recently. However nowadays, it is also essential to employ magnetic adsorption in much larger volumes of feedstocks for biotechnological mainly purposes. As an example, the integration of high-gradient magnetic

separation with functionalised magnetic carriers named as high-gradient magnetic fishing (HGMF) was developed by Hubbuch *et al.* in 2001 for this purpose (see section 1.4.4).

The magnetic separation techniques (for laboratory and industrial applications) are quite new, and further development is required. The high cost of magnetic carriers must be diminished, by preparing these materials with more simple and affordable methods (Franzreb *et al.*, 2006). These adsorbents must be also easy towards cleaning and reusability, while providing high adsorption capacities (improvement of functionalisation techniques) and scaleability. The design and manufacturing of new process equipment for large scale operations, needs also further development and optimisation procedures (Franzreb *et al.*, 2006).

1.4.4 High Gradient Magnetic Fishing (HGMF)

A High Gradient Magnetic Separator (HGMS) consists of a canister packed with a magnetisable matrix (steel wool or wire meshes) which is introduced inside an electromagnet (Fig. 1.5). In the presence of a magnetic field, the wires bundle the magnetic field lines (generating large field gradients) that strongly attract paramagnetic or ferromagnetic materials (Gerber and Birss, 1983; Dunlop *et al.*, 1984).

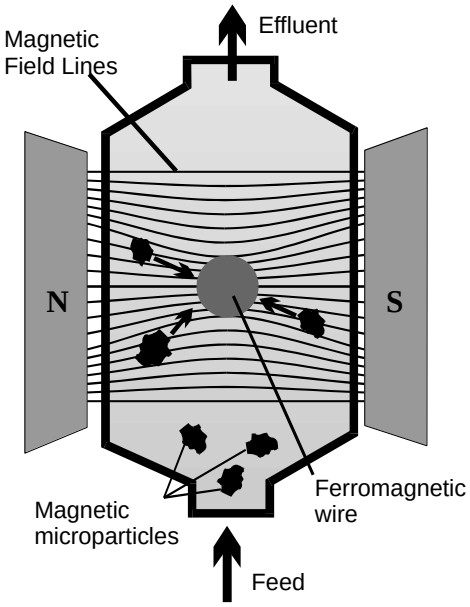

Figure 1.5 Schematic cross-sectional view of a HGMS (Thomas and Franzreb, 2007).

High Gradient Magnetic Separation has been used in clay, mineral and power industries as well as wastewater treatment (Gerber and Birss, 1983; Svoboda, 1987). Lately, this method has been also applied for the separation of biological species employing functionalised particles (Safarikova and Safaric 1999; Hubbuch and Thomas 2002; Franzreb *et al.*, 2006).

High-Gradient Magnetic Fishing (HGMF) relies on the combined use of submicron-sized superparamagnetic adsorbent particles and a High-Gradient Magnetic Separation (HGMS) unit for protein purification purposes. In contrast to barely the collection of particles in HGMS, HGMF is an integrated process. It consists of coupling an adsorption step to magnetic particles handling (capture, washing and elution) with the aid of a high-gradient magnetic filter, so that the product is recovered in a clarified and partially purified form (Hubbuch *et al.*, 2001; Heebøll-Nielsen, 2002). The main steps that are followed during the process are: (a) protein adsorption onto sub-micron and micron sized superparamagnetic adsorbent particles; (b) rapid collection of the target-loaded adsorbents in a strongly

magnetised filter; and (c) subsequent desorption and recovery of the bound protein from the adsorbent. The HGMF rig, which is equipped with a recycle loop for washing the loaded particles and subsequent product desorption, is shown in Figure 1.6 below.

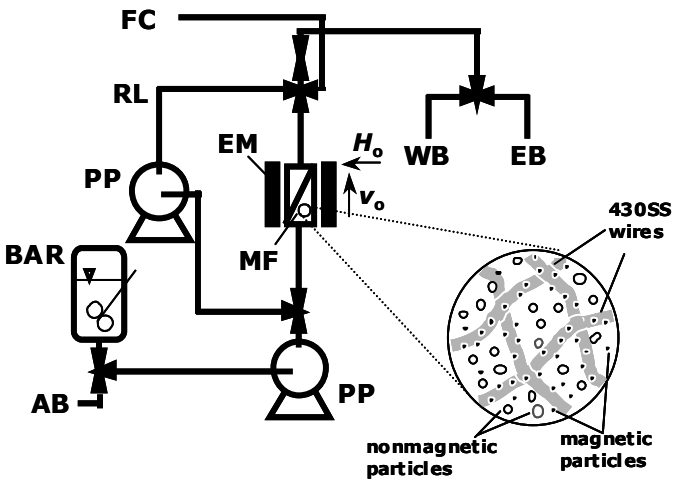

Figure 1.6 Schematic diagram of a HGMF system, taken from Hubbuch and Thomas (2002). AB- Adsortpion Buffer; BAR- Batch Adsorption Reactor; EB- Elution Buffer; EM-Electromagnet; FC- Fraction Collector; MF- Magnetic Filter; PP- Peristaltic Pump; RL- Recycle Loop; WB- Wash Buffer; H_0- Magnetic Field; v_0- Fluid flow.

HGMF offers several advantages over the use of chromatographic techniques for truly large-scale recovery of proteins from high volumes of crude liquors, mainly in terms of scale-flexibility, speed, and compatibility with suspended solids and other fouling components present is such feedstocks. A first principle comparison of HGMF and EBA has been given by Hubbuch and co-workers (2001). HGMF allows faster purification, it utilizes non-porous superparamagnetic beads, the product capture and separation are carried out in two steps so they can be optimized independently, and the high voidage of filters enable the handling of very dirty feed streams. In HGMF, the property of superparamagnetism, i.e. responsiveness to an applied magnetic field without any permanent magnetisation, is essential as the adsorbents

can be employed repeatedly for product recovery from dirty process liquors. Without this property, permanent particle agglomeration would be inevitable, leading to severely compromised product desorption, support cleaning and reuse.

1.4.5 Magnetic adsorbents

There is a plethora of commercially available magnetic particles, as well as standard protocols to prepare them in the laboratory. They are made from various synthetic polymers, biopolymers or porous glass, or surface modified magnetite (Safarik and Safarikova, 2004), while their surface is functionalised with ligands for the selective binding of species. In Fig. 1.7, the designs of various magnetic adsorbents prepared by different methods are presented.

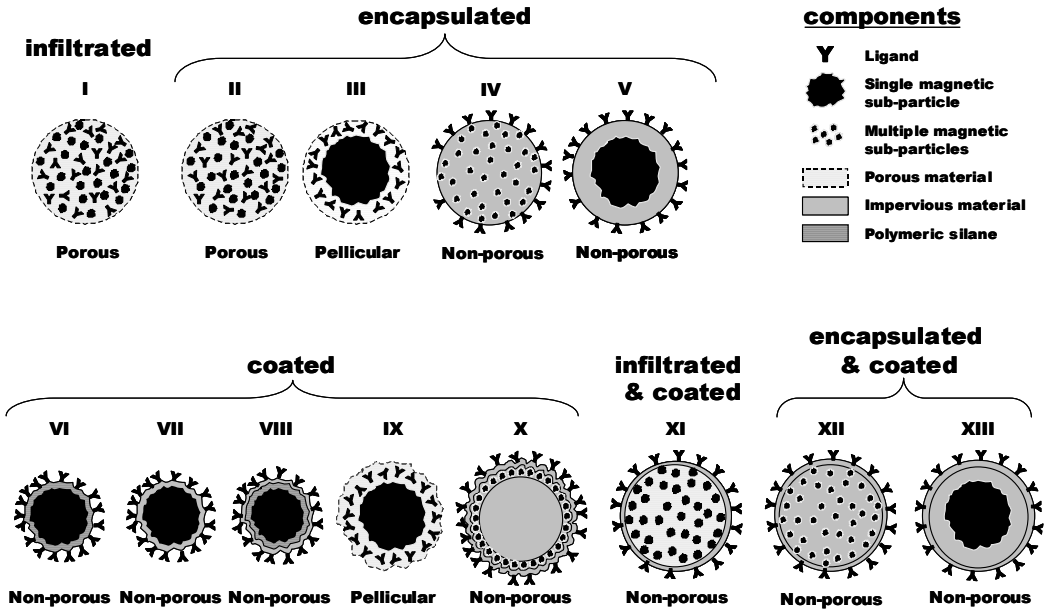

Figure 1.7 Designs of magnetic adsorbent made by infiltration, encapsulation and coating techniques. For simplicity, only the primary location of ligands is depicted (Courtesy of O.R.T. Thomas, University of Birmingham, UK).

The selection and the design of a magnetic support depend upon the method and the scale of the separation which they are intended for. Properties such as specific surface area, superparamagnetism, porosity, magnetite content, dispersity, diameter size distribution, corrosion resistance, re-usability and functionalization possibilities, are quite important. As mentioned above, superparamagnetism is necessary to prevent permanent, magnetic agglomeration of the supports (ability to re-disperse the magnetically captured adsorbents). In most of the cases the specific surface area must be sufficiently large to reach high protein binding capacities, yet the size of the adsorbents is important for the magnetic capture in high gradient magnetic filters. Porosity is undesirable adsorbents designed for use in unclarified feedstreams, as there is a risk of pore clogging from particulate contaminants that can be difficult to remove (Anspach *et al.,* 1999). In contrast, non-porous adsorbents are resistant to such fouling, and are also easier to regenerate (Hubbuch and Thomas, 2002). Thus the ideal base matrix should have a rough, non-porous surface, creating the sufficient specific area needed for the capture of large enough particles by HGMF. Furthermore, as iron oxides are commonly used to introduce magnetism, the particles must be coated to prevent any undesirable leaching of iron ions to the environment (Heebøll-Nielsen, 2002).

Commercially available magnetic particles can be obtained from a variety of companies for example Enzacryl FEO-(M) (Sigma, USA), Magarose (Whatman, UK), MPG® (CPG Inc., USA), Estapor® (Merck Chemie, F) and M-PVA (Chemagen Biopolymer-Technologie AG, D). Polymer matrices such as polystyrene, cellulose, agarose, silica, porous glass or silanized magnetic particles are available.

Ligands (e.g. affinity ligands, such as Streptavidin, antibodies, protein A and G, nitrilotriacetic acid, glutathione, trypsin, trypsin inhibitor, gelatine, etc.) are already

immobilized to some commercially available magnetic beads. Immobilisation of other ligands to the particles can be achieved by employing standard methods used in chromatography. Magnetic carriers normally are functionalised with groups such as -COOH, -OH or $-NH_2$ or in some cases are available already activated (e.g. tosylactivated, epoxyactivated, etc.) (Safarikova, 2004).

1.5 Surfaces with adaptive and responsive properties

Since we entered the nanotech age of 'shrinking dimensions', the surface properties of a material become increasingly important, and not surprisingly, the demand for new ever more sophisticated surface materials continues to grow apace. Furthermore, the ultimate performance of a material is, regardless of the application, determined not only by its bulk properties, but also by the nature (both physical and chemical) of its surface. In fact, the surface microstructure and interfacial behaviour of materials define their functions at applications, such as friction, shearing, lubrication, wetting, adhesion, adsorption and abrasion (Tsukruk, 1997; Luzinov *et al.,* 2004). In addition, further progress in materials science creates the need for different and most of the time opposite surface properties for a given material: depending on the conditions under which is utilized, has to be hydrophobic and hydrophilic, acidic and basic, conductive or non-conductive, adhesive or repellent, and be able to release or to adsorb some species (Luzinov *et al.,* 2004).

Pristine polymeric materials have the tendency to respond to external stimuli or environmental changes. As a consequence, for several decades the research has focused on the relationship between the bulk properties with surface properties of these materials. With time,

the research moved towards to the development and design of synthetic polymers to obtain materials with “smart” or “intelligent” surface behaviour. Significant efforts have also been made to prepare, characterize and understand the structure/properties relationships of adaptive/responsive surface layers attached to or deposited on the materials surface (Luzinov *et al*., 2004).

Synthetic polymers offer a wealth of opportunities to design sophisticated materials with responsive surfaces by variation of the length, chemical composition, architecture, and topology of the chains (Russel, 2002). As a result, the design of ‘smart’ or ‘intelligent’ surfaces includes the synthesis of functional polymers with specific composition and architecture and their attachment onto the surfaces of interest. The polymer chains can be attached to a surface by different ways (tethered or anchored polymers). According to reorganizations of these polymer layers due to changes in the surrounding environment (pH, temperature, solvent quality), useful physical properties (lubrication adjustment, friction, adhesion and wettablity, colloid stabilisation) can be achieved on surfaces, which are important in many applications today (Luzinov *et al*., 2004).

1.5.1 Polymer brushes

The latest progress in the theory, physics and engineering of macromolecules in conjunction with the discovery of reliable polymerisation reactions has lead to the synthesis of new well-defined co-polymers and the design and of nano-patterned polymer brushes. These structures not only can be self-assemble, but also pre-assemble to materials at precise nano-structured morphologies with desired properties. The molecular structure of polymer chains define the final macroscopic properties of the new materials, thus macromolecular engineering should

include: (a) rational design of final structure (chain size, topology, uniformity, microstructure, composition and functionality), (b) accurate synthesis and reasonable cost, (c) assembly to supramolecular structures via controlled processing (d) detailed characterisation at both molecularly and macroscopically level, (e) further modelling for optimisation of the entire process (Matyjaszewski, 2005).

1.5.1.1 Polymer brushes in nanotechnology

Polymer brushes have been described as the ideal building blocks to create 'smart' surfaces (Zhou and Huck, 2006). Generally, polymer brushes refer to an assembly of 'tethered polymer chains', i.e. polymer chains end grafted to a supporting surface or interface (Zhao and Brittain, 2000). However, most of the times, this term is associated when under specific conditions, the strong interactions of densely grafted polymer chains, dictate the behaviour of the tethered layer (Brittain and Minko, 2007). The behaviour of a polymer brush cannot be found in unconfined systems. The attaching of chain ends to a surface at high density, stretch away the macromolecules with respect to their isolated state, independently of the solvating strength of the surrounding fluid. As an example, the tethered coils in a good solvent[6] stretch in semi-dilute conditions, whereas the free coils contract (Toomey and Tirrell, 2008). The repulsive force between the brushes is a result from the high osmotic pressure inside the layer. As a consequence, the use of polymer brushes is found in applications such as: adhesive materials, protein-resistant surfaces, lubricants, chromatographic devices, surfactants and polymer compatibilizers (Zhao and Brittain, 2000).

[6] A good solvent is one which polymer-solvent contacts are favoured (tends to increase coil dimensions); a poor solvent is one in which polymer-polymer contacts are favoured (Hiemenz and Rajagopalan, 1997)

Recently, two main approaches have been reported to fabricate polymer layers composed of two components (polymers). The first refers to grafting block copolymers to a solid substrate, whereas the second involves the attachment of two incompatible polymers grafted to the same substrate. Their study in selective and non selective solvents, show how the properties of the polymer coating responds to changes of the surrounding media (Soga *et al.*, 1996; Zhao and Brittain, 1999 and 2000; Sidorenko *et al.*, 1999; Draper *et al.*, 2002; Minko *et al.*, 2001; Minko *et al.*, 2002). When two polymers are attached to the surface in polymer brush regime, their chains are stretched away and perpendicular to the substrate. If a solvent selective for only one of the polymers is applied onto the layer, then some of the polymer chains will be distributed in a swollen conformation (top of the layer) while the rest in a collapsed conformation (bottom of the layer) according to their selectivity towards that solvent. Depending on the selective or non selective solvents (good or poor) applied onto the polymer film, the balance between favourable chain-chain and chain-solvent interactions will determine the final morphology of the layer (Minko *et al.*, 2001); the two possible morphologies are illustrated in Fig. 1.8. The smart materials provided with this mechanism can be used for several applications and solve various industrial problems due to: (a) the variety of brush morphologies obtained; (b) the restricted lateral mobility of the (end grafted) chains demonstrating pronounced response to external stimuli; (c) their reversibility between the different states; and (d) the choice to control the transitions by change of solvent quality, temperature and asymmetry of the mixed brush (Minko *et al.*, 2003). Until now, the development of surfaces with adjusted properties can be accomplished either by controlling the architecture of the layer or its chemical composition within the brush. In the case of homopolymer brushes only the first can be achieved i.e. to control the thickness of the brush. However, for a mixed (binary) brush, there are more possible alterations that can be made

(structure, surface chemistry) providing more possible morphologies (depending the chemistry used) allowing for more diverse applications (Sidorenko *et al.*, 1999; Zhao and Brittain, 2000).

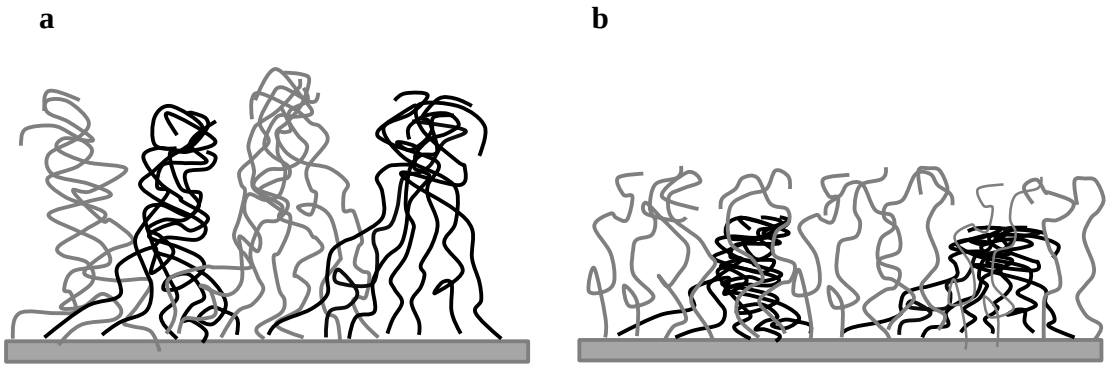

Figure 1.8 Illustration of mixed brushes possible morphologies grafted on solid substrates (Minko *et al*., 2003): (a) Ripple morphology in a non-selective solvent, and (b) Dimple morphology in a solvent poor for the chains in black.

Generally, in terms of their chemical composition, polymer brushes can be divided into the following categories (Zhao and Brittain, 2000):

(a) Homopolymer brushes: composed of tethered polymer chains consisting of one type of repeat unit (these can be neutral or charged).

(b) Mixed homopolymer brushes: composed of two or more types of homopolymer random copolymer brushes and block copolymer brushes.

(c) Random copolymer brushes: composed of polymer chains consisting of two different repeat units which are randomly distributed along the polymer chain.

(d) Block copolymer brushes: composed of polymer chains consisting of two or more homopolymer chains covalently connected to each other at one end.

1.5.1.2 Theoretical and experimental characteristic parameters of polymer brushes

The most important and distinctive characteristic of polymer brushes derived from theoretical models, is that the equilibrium thickness varies linearly with the degree of polymerization. It has been also demonstrated that the densely tethered polymer chains are deformed. The relationship between the equilibrium thickness and degree of polymerization of polymer chains is linear. This is the origin of the novel behaviour of tethered polymer brushes (Zhao and Brittain, 2000).

As the area of neutral tethered polymer chains has attracted much attention, further theoretical and experimental approaches have revealed that depending on the grafting density of the polymers at the solution/substrate interface (σ), the anchored chains form either mushroom or brush regimes. The grafted chains overlap, as soon as their size approaches the distance between grafting points. This point is a transition point between a single grafted chain (mushroom) regime and brush regime. (Wu *et al.*, 2002; Brittain and Minko, 2007).

The Grafting density (σ) is defined as:

$$\sigma = (\mathrm{h} \cdot \rho \cdot \mathrm{NA})/\mathrm{Mn} \qquad \text{Eq. (1.7)}$$

In Eq. 1.7, h is the brush thickness, ρ is bulk density of the brush composition, A is the Avogadro's number and Mn is the number average molecular weight of the species.

The distance between the graft sites, which is denoted as D, is used to evaluate the structure of a surface-immobilized polymer. In this case, the grafting density (σ) can be determined as:

$$\sigma = 1/\mathrm{D}^2 \qquad \text{Eq. (1.8)}$$

For the quantitative characterisation of the transition from mushroom to brush regime, a commonly used parameter is the reduced tethered density (Σ), which describes the number of chains that occupy an area that a free non-overlapping polymer chain would normally fill under the same experimental conditions. Σ can be determined as:

$$\Sigma = \sigma \pi Rg^2 \qquad \text{Eq. (1.9)}$$

In Eq. 1.9, Rg is radius of gyration of a tethered chain at specific experimental conditions of solvent and temperature. Theoretically, three regimes exist in brush formation (Fig. 1.9), according to the degree of stretching between the grafted chains:

(a) the 'mushroom' or weakly interacting regime, where $\Sigma < 1$;

(b) the crossover regime, where $\Sigma \sim 1$; and

(c) the highly stretched regime, where $\Sigma > 1$.

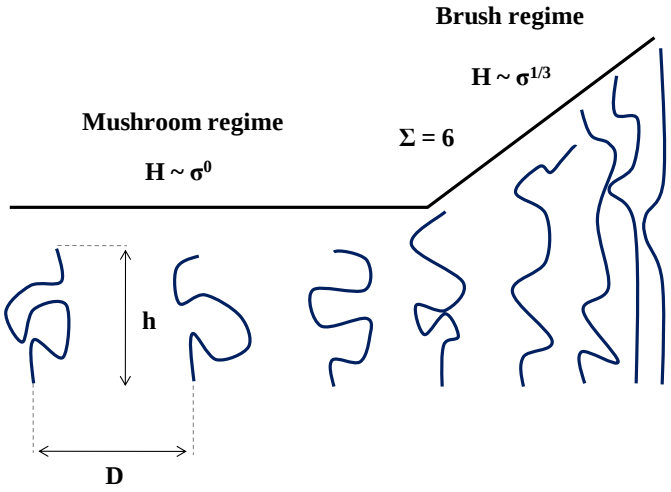

Figure 1.9 Characteristic parameters of the polymer brush: h-height and D-distance between grafting points (Britain and Minko, 2007). Experimental observations of the transition between the 'mushroom' regime and 'true brush' regime of polyacrylamide brushes (Wu *et al.*, 2002). In good solvents, the thickness of the anchored polymer, *H*, in the low grafting density or 'mushroom' regime locates around $H \sim N\sigma^0$, where *N* is the degree of polymerization of the polymer; in the brush regime the chains become more crowded and the brush height locates around $H \sim N\sigma^{1/3}$.

However, in reality, the density and composition fluctuations of the grafting points (polydispersity, i.e. non-homogeneous distribution of Σ) promote the formation of irregular structures, and randomness prevents the formation of a long-range order. Even very small fluctuations of the grafting sites are sufficient to change the lateral structures of the brush (Wenning *et al*., 2005). In practise, the 'true brush' regime can be approached at a significantly high stretching of polymer chains that is typically characterized by $\Sigma > 5$, but this value can vary from system to system.

Experimental studies revealed that, the tethered polymer chains can be characterized by three major regimes in terms of grafting density: the mushroom regime at $\Sigma < 1$, mushroom-to-brush transition regime at $1 < \Sigma < 5$, and brush regime at $\Sigma > 5$ (note that this categorisation defers than the one mentioned before, as it is based on experimental studies rather than theoretical ones).

In the brush regime, the average thickness H of the tethered layer is proportional with the grafting density (σ) (Milner, 1991; Halperin *et al*., 1992):

$$H \sim N \sigma^{\alpha} \qquad \text{Eq. (1.10)}$$

In Eq. 1.10, the exponent α specifies the driving force for the chain stretch.

In a good solvent, repulsive excluded volume interactions govern and α=1/3. In a poor solvent, attractive excluded volume interactions govern and α approaches unity. According to this equation, the tethering density, independently of environmental conditions, rules the arrangement and the degree of polymer layer contraction. For example, polymer brushes of increased density (high degree of overlapping) contract less, as steric crowding of the chains hinder the collapse (Kilbey *et al.*, 2001).

Other groups use theoretical predictions for terminally grafted polymer chains, based on Alexander-de Gennes (A-dG) polymer brush theory (Plunkett *et al*., 2006; Zhu *et al.*, 2007). According to this model, the three different chain configurations can be also defined according to the ratio of the Flory radius (R_F) to the average distance between the polymer chains, *s*.

The Flory radius R_F, is defined as

$$R_F = ln^{3/5} \qquad \text{Eq. (1.11)}$$

In Eq. 1.11, *l* is the effective segment length and *n* is the number of segments in the chain (Israelachvili, 1991).

Under the assumption that the polymer chains are swollen at 25 °C, then:

- At $s/2R_F > 1$, the polymer chains are in the non-overlapping mushroom regime
- At $s/2R_F < 1$, the polymer chains are in the weak overlap regime
- At $s/2R_F << 1$, the polymer chains form brushes

Using the above denotations, the brush thickness *L*, can be described from the equation below:

$$L = s(\frac{R_F}{s})^{5/3} \qquad \text{Eq. (1.12)}$$

The complexity involved in the design of a polymer brush with specific responses towards its surroundings depends on the system and its specific components. For example, the description or the predictability of a brush's behaviour is different for classical or non-classical systems, as described by Toomey and Tirrell (2008). In classical systems, (e.g. neutral brushes) the

interactions within the brush are more general and can be described by van der Waals potentials. Their behaviour at different conditions can be predicted using few global parameters. On the contrary, in non-classical systems (e.g. stimuli responsive brushes, see section *1.5.2.2.1*), several parameters have to be considered (e.g. structuring effects in hydrogen bonding solvents, interactions dependent on compositions, correlation between polyions and counterions), so that the model-depended potentials may not necessarily lead to universal scaling laws. In non-classical systems, such that of water soluble molecules, the role of the solvent and density is very crucial. The water molecules create a hydration layer around the polymer which in turn is dependent on the concentration (polymer volume fraction).

1.5.1.3 Protein adsorption/desorption behaviour onto polymer brushes

Depending on the type and polymer composition of a brush, it can be employed either for the selective immobilization of target molecules, or to prevent adverse fouling on a substrate surface. An example of the former, is the use of poly(acrylic acid) chains to functionalise ultrafiltration (UF) membranes made of polysulfones (PSf) followed by successful covalent immobilization of bovine serum albumin, γ-globulin and alkaline phosphatase (Ulbricht and Riedel, 1998). Additionally, polymer brushes serve as non-fouling surfaces by repelling the proteins (and cells). As an example, water-soluble polymers are used to enhance the biocompatibility of materials utilised in bioengineering and biotechnology and solve the problems associated with blood-contacting biomaterials and filtration membranes (Halperin and Leckband, 2000; Kato *et al*., 2003). Hydrophilic polymers, such as poly(ethylene oxide) (PEO) and poly(ethylene glycol) (PEG), have been extensively studied for these purposes (Halperin, 1999; Halperin and Leckband, 2000; Sheth and Leckband, 2005). In these

approaches, the kinetics of protein adsorption/desorption, as well as the design parameters for protein repression are analysed. In conclusion, there are three distinctive interactions between a protein and a polymer brush differing in range and charge: (a) a contact attraction between the protein and the surface; (b) the van der Waals attraction between the protein and the surface which is long-ranged; and (c) a repulsive interaction, of osmotic origin, between the protein and the brush. Considering the above interactions, there are two different adsorption modes during protein contaction with a polymer layer: (a) the primary adsorption at the grafting surface due to contact interaction, and (b) the secondary adsorption at the outer edge of the brush due to long-ranged attractions (van der Waals). During primary adsorption, there are two different mechanisms, depending on the size of the protein. Small proteins may penetrate the brush layer without affecting considerably the structure of the later (insertion mechanism). Large proteins cannot penetrate the brush, but compress it in the intermediate region (compressive mechanism) (Fig. 1.10) (Halperin, 1999). If the polymer chains are very crowded, the protein cannot contact with the surface as the compression makes the layer even denser. So they preferably undergo secondary adsorption at the edge of the brush. However, this is possible if the van der Waals attraction at the edge is sufficient, and this can be satisfied mainly for the rod like proteins.

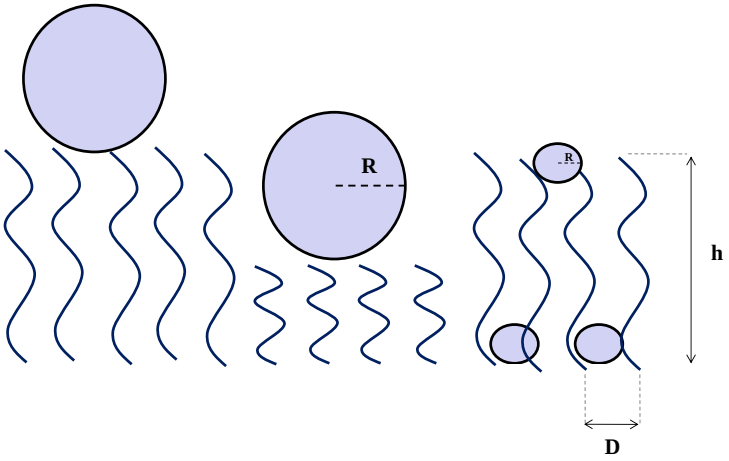

Figure 1.10 Interactions of proteins with a polymer brush, (Halperin, 1999): Large proteins compared to brush thickness, compress the brush without penetrating the layer (compressive mechanism). Small proteins can penetrate the layer (insertion mechanism).

As explained in previous paragraph, the thickness and the grafting density of a polymer layer on a surface, determines the efficacy of a polymer brush. Moreover, the optimal design characteristics of the brush depend on the protein composition profile (size, concentration, structure, adsorption free energy etc.) of the target environment.

1.5.2 Smart polymers and smart polymer brushes

'Smart'[7] or stimulus-responsive polymers (also known as 'intelligent' or 'environmental') undergo strong fast reversible changes in microstructure from a hydrophilic to a hydrophobic state when only small variations in the environment (e.g. pH, temperature, ionic strength, electric or magnetic field, etc.) occur. These changes are apparent at the macroscopic level as precipitate formation from a solution or order-of-magnitude changes in the size and water

[7] The name 'smart polymers' was given because of the similarity of the stimuli-responsive polymers to biopolymers **(**Dagani, 1995**).**

content of hydrogels, and are reversible, as the system returns to its initial state when the trigger is removed (Galaev *et al*., 1996; Galaev and Mattiason, 1999).

Smart polymers can be categorised according to the three common physical forms in which they exist: (a) *linear free chains in solution*, where the polymers collapse reversibly under an environmental change; (b) *covalently cross-linked gels and reversible or physical gels*, being either macroscopic or microscopic networks with swelling behaviour under an external stimulus; and (c) *chain adsorbed or surface-grafted*, in which the polymer chain reversibly swells or collapses on a surface, thereby modifying the interface with hydrophilic or hydrophobic behaviour (Kumar *et al.*, 2007). As the stimulus-responsive behaviour occurs in aqueous solutions, these polymers can be employed in numerous applications; for example, in bioseparation and drug delivery; for the development of new biocatalysts; as biomimetic actuators; and, as surfaces with switchable hydrophobic–hydrophilic properties (Galaev and Mattiasson, 1999).

The main classes of polymers that are used for the creation of responsive surfaces are: photoresponsive, dendritic, polyelectrolyte, block copolymers, and thermoresponsive (Luzinov *et al.*, 2004). Figure 1.11 below summarises the physical forms, properties and applications of SPs.

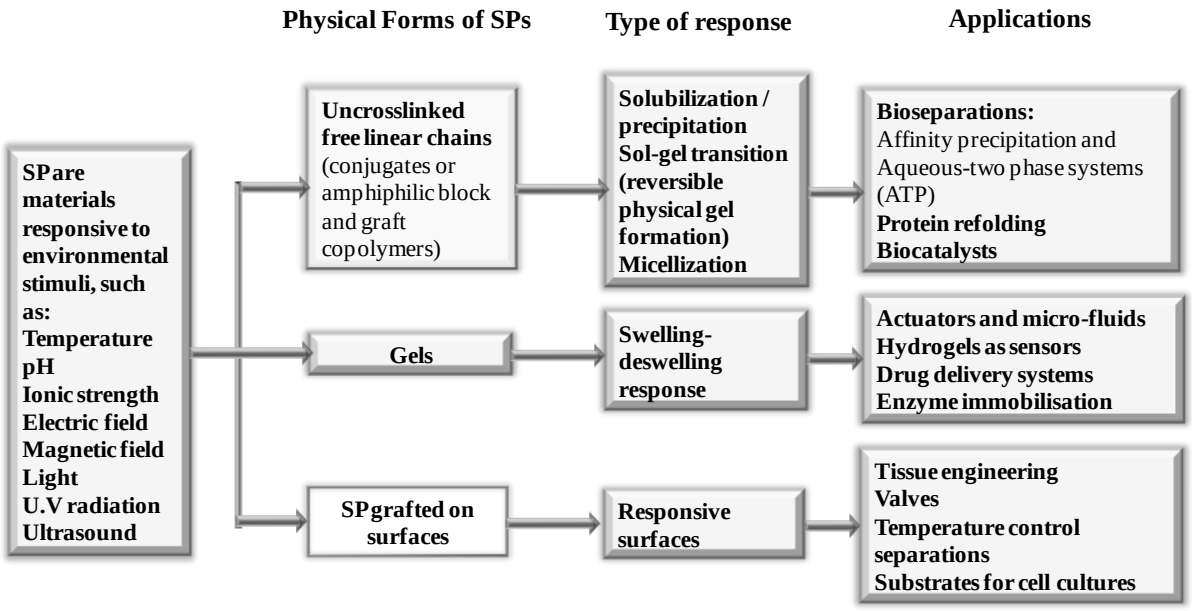

Figure 1.11 Summary of Smart Polymers (SP) and their use in bioseparations and medicine.

1.5.2.1 Thermoresponsive polymers and the phase transition phenomenon

Temperature-sensitive polymers exhibit a critical solution temperature (CST) behaviour, where phase separation is induced by surpassing a certain temperature. There are two types of thermoresponsive behaviour: polymers are either water-soluble at high temperature but insoluble at low temperature, i.e. an upper critical solution temperature – UCST exists; or water-soluble at low temperature but insoluble at high temperature, i.e. the systems exhibit a lower critical solution temperature – LCST (Taylor and Gerankowski, 1975).

The liquid-liquid phase diagram of binary polymer solutions at constant temperature is usually determined by plotting the temperature of the incipient phase separation as a function of the overall polymer concentration (Fig. 1.12). This diagram defines the potential working area for a two-phase system and is unique to that under specific conditions of temperature and

polymer concentration. The minimum in the phase diagram, also known as cloud point curve, is called the precipitation threshold (or LCST), since it denotes the extreme temperature at which phase separation occurs (Boutris *et al.*, 1997). This phase phenomenon, which is common for polymer systems, is caused by the presence of a high concentration of hydrogen-bond forming chemical groups in the polymer backbone (Fig. 1.12). The change in the Gibbs free energy of mixing (ΔG_m) that occurs when a polymer dissolves in a solvent is:

$$\Delta G_m = \Delta H_m - T\Delta S_m \qquad \text{Eq. (1.13)}$$

In Eq. (1.13), ΔH_m is the enthalpy change of mixing and ΔS_m is the change in entropy that occurs from the mixing process (Prigogine and Defay, 1954). At temperatures where $\Delta G_m > 0$, dissolution is not possible, and phase separation occurs (the positive entropy term overcompensates the heat term). At the LCST, the enthalpy contribution of water that is hydrogen-bonded to the polymer is less than the total entropic gain of the system (Netopilík *et al.*, 1997) and thus the phase separation depends on the hydrogen-bonding abilities of the monomer units. Below the LCST, the hydrophilic and completely miscible with water polymer develops a highly swollen coiled chain conformation. When the temperature increases above the LCST, the polymer is hydrophobic and becomes incompatible with water, i.e. the polymer–water homogeneous mixture encounters phase separation where the polymer becomes globular and separates from the water-enriched phase (Luzinov *et al.*, 2004). Thus, a sudden shift in temperature away from the LCST point, can cause reversible and dramatic changes in the state of the polymer from hydrophilic to hydrophobic and back (Fig. 1.12).

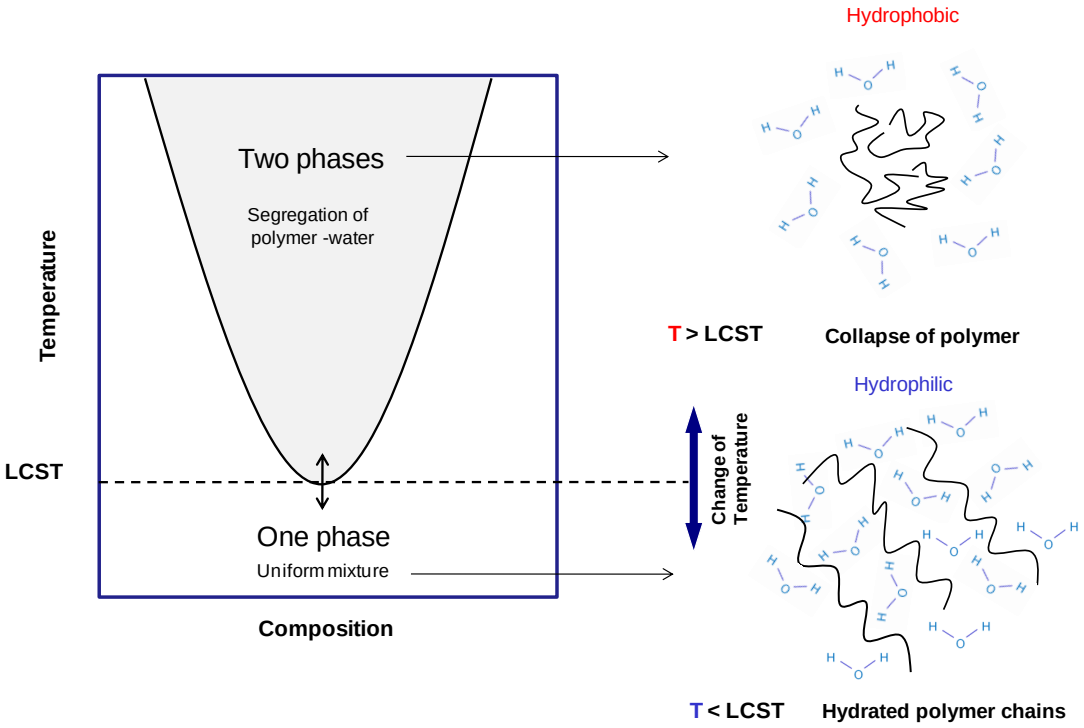

Figure 1.12 Left hand side: Phase diagram for polymer-water system with LCST and illustration of transition across the phase line (reproduced from Afroze *et al.*, 2000). Right hand side: Inverse temperature solubility behaviour of thermoresponsive polymers at the (LCST), i.e. hydrated polymer below the LCST and entropic loss of water and chain collapse above LCST.

Thermoresponise polymers can be categorised into different groups depending on their chemistry and the mechanism of reaction to temperature variations, and these are: (a) poly(*N*-alkyl substituted acrylamides), e.g. poly(*N*-isopropyl acrylamide) or NIPAAm, with transition temperature at 32 ºC; and (b) poly(*N*-vinylalkylamides), such as poly(*N*-vinylisobutyramide) with transition temperature of 39 ºC (Suwa *et al.*, 1996), or poly(*N*-vinylcaprolactam) with transition temperature of 32-33 ºC (Tager *et al.*, 1993). There are also other types, for example Pluronic® F127[8] and (PLLA)/PEG/PLLA[9] triblock copolymer and a class of

[8] poly(ethylene oxide)106-poly(propylene oxide)70-poly (ethylene oxide)106

[9] poly lactic acid-co–poly ethylene glycol–poly lactic acid

temperature-responsive polymers which involves elastin like polymers (ELPs) (Kumar *et al*., 2007).

1.5.2.2 Thermoresponsive behaviour of poly(N-alkyl substituted acrylamides)

Among the thermoresponsive polymers, which are distinguished from other polymers by associating with solubility changes with heating, poly (*N*-isopropylacrylamide) is the most popular. Its phase transition from a hydrophilic to a hydrophobic structure occurs suddenly at the LCST, which experimentally lies between ca. 30 and 35 ºC, depending on the exact microstructure of the macromolecule (Schild, 1992).

The very first report of the LCST of poly (*N*-isopropylacrylamide) in the literature was reported in 1967 by Scarpa and co-workers (Scarpa *et al*., 1967), who reported inverse temperature solubility and subsequent precipitation of a 2% solution near 31 ºC. After a while, Heskins and Guillet (1968) described this macroscopic phase separation upon heating after a simple visual observation. This simple method was used to determining the LCST and is commonly known as the cloud point method. Using the phase diagram, these authors studied the thermodynamic properties of the system attributing the phenomenon to an entropy effect.

Many theories have been proposed to explain the LCST phenomenon in pNIPAAm single chains and gels. From studies of pNIPAAm in dilute aqueous solutions, it appears that below the LCST, the polymer exists as isolated, flexible but extended coils. Although this is not obvious with the light scattering technique, Winnik (1990) managed to obtain more information using viscometry and UV absorption of labelled pNIPAAm chains. At the LCST,

he observed that the individual polymer chains collapsed prior to aggregation as scattering was increased. This was the cloud point which was coincident with a calorimetric endotherm. Then, a second phase of lower polarity was formed which was suspended in the water-rich phase.

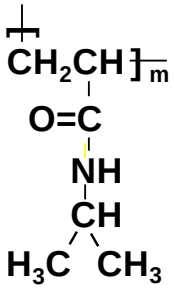

Figure 1.13 Chemical structure of pNIPAAm repeat unit.

As shown in Fig. 1.13, pNIPAAm is composed of amide groups that are hydrophilic and isopropyl groups that are hydrophobic (Kubota *et al*., 1990; Schild, 1992). Below the LCST, the water molecules cover the hydrophobic groups and the hydrogen bonds between the amide groups and water stabilise the solution, whereas above the LCST the hydrogen bonds become so weak that the attractions between the hydrophobic groups become bigger (de-mixing of polymer chains). As the water molecules destabilise around the isopropyl group, there is no available energy for mixing as the heat absorbed by the system is lower than the change in enthalpy (Eq. 2.1) and ultimately the chains demix.

1.5.2.2.1 Behaviour of pNIPAAm polymer brushes

In classical systems of polymer brushes, there is always an upper critical solution temperature (UCST) at very low concentrations. The collapse (shrinkage) of the layer is always

continuous and can be described by the classical Flory-Huggins model. However in non classical systems, the water-soluble polymers (as explained in section *1.5.2.2.1*), can have a critical point in any given concentration and commonly exhibit a lower critical solution temperature (LCST). In such cases, the shape of the two-phase diagram and the critical point may shift (Toomey and Tirrell 2008, and references therein). An extended phase diagram for a water soluble polymer (e.g. pNPAAm) consists of two distinctive curves: when the system requires activation energy for the initiation of a new phase, the phase separation proceeds by a nucleation and growth mechanism. This process takes place under the binodal curve in the metastable portion of the diagram. Alternatively, when separation occurs without an activation barrier, the separation occurs under the spinodal curve. In this case, the nature of the process changes, following a spinodal decomposition mechanism. In Fig. 1.14, the coexistence curve (binodal) of pNIPAAm, represents the boundary of the unstable region where phase separation occurs (Afroze *et al*., 2000). Inside is the spinodal, which is a two regions boundary with different materials composition. The two curves coincide at the LCST. At high tethering densities, the system cannot enter the miscibility cap and collapse happens in a continuous way. However, at a given polymer fraction an interference with the miscibility cap (i.e. at T > LCST) occurs and the phase transition becomes discontinuous. For example, in some cases, during phase separation of pNIPAAm brushes, the polymer segments near the surface enter the miscibility gap ahead the outer segments resulting in bilayer-type profiles (Baulin *et al*., 2003; Yim *et al.*, 2005; Toomey and Tirrell, 2008). The shape and the location of the coexistence curve define the transition characteristics. Depending on the structure of the polymer brush (molecular weight and surface coverage), different hydrophobic-hydrophilic balances may developed, and it can thus collapse continuously or discontinuously (Toomey and Tirrell, 2008).

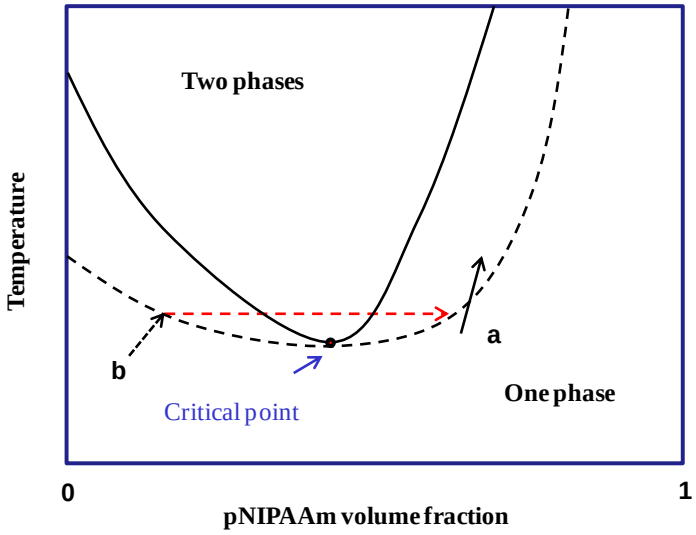

Figure 1.14 Phase diagram for the demixing of linear pNIPAAm, presenting the predicted binodal (– – –) and spinodal (——) curves and the critical point (•), (Reproduced from Afroze et *al*., 2000; and Toomey and Tirrell, 2008). There are two possible routes: (a) (——→) there is no interference with the miscibility cap, i.e. continuous phase transition; and (b) (– – →) discontinuous phase transition, as the polymer volume fraction interferes with the miscibility cap.

As a consequence, for these systems, the development of prediction models, as well as the control of polymerisation degree and tethering density present many challenges due to their promising application in a broad range of scientific fields.

1.5.2.3 Control of Transition Temperature using additives

The LCST of pNIPAAm (32-34 ºC) in aqueous solutions can change by the addition of other polymers (co-polymerisation), salt and surfactants. For example, by introducing hydrophilic, hydrophobic and/or charged monomers, such as acrylic acid, methacrylic acid, acrylamide, n-butyl acrylamide or *N,N'*-dimethylaminopropylacrylamide (Kobayashi *et al.* 2003; Ayano *et al*., 2006; Maharjan *et al.*, 2008), co-polymers with a desired thermosensitivity or temperature tunable hydrophilicity/hydrophobicity and charge density can be produced. Instead of linear

pNIPAAm chains some authors use comb-type structures. These are crosslinked hydrogels where the polymer chains contain grafted chains, enhancing the exclusion of water from the network during collapse. This is attributed to the grafted side chains that create hydrophobic regions able to promote rapid de-swelling upon temperature change. (Yoshida *et al*., 1995; Maharjan *et al.*, 2008). The lowering of the transition temperature when adding salt was observed by Shild and Tirrell (1990). The same effect (lower LCST) due to interactions of pNIPAAm with a series of n-alkyl sulphates in solution has been also reported (Schild and Tirrell, 1991).

Studies related to the effect of salts on non-anionic *N*-isopropylacrylamide gels, have shown that the transition temperature depends on the type of salt and type of ions (i.e. anions rather than cations) (Inomata *et al.*, 1992; Dhara and Chatterji, 2000). Among other salts, sodium chloride is a very strong salting out agent, lowering the LCST of pNIPAAm gels with increasing concentration. The latter observation was primarily explained as inter- and intramolecular hydrophobic interactions (Park and Hoffman, 1993).

The Hofmeister series were proposed in 1888 as a qualitative scale of ions with respect their salting-out effect on proteins from solutions (Hofmeister, 1888; Gurau *et al.*, 2004; Zhang and Cremer, 2006). Their typical ordering is presented in Fig. 1.15. The anions to the left of Cl^- are called kosmotropes and those to the right chaotropes, according to their ability to change the hydrogen bonding network of the water. Kosmotropes are strongly hydrated and have salting-out effects on proteins and macromolecules, whereas chaotropes can destabilize folded proteins and promote salting in effects.

Kosmotropes ← → Chaotropes

CO_3^{2-} SO_4^{2-} $S_2O_3^{2-}$ $H_2PO_4^-$ F^- Cl^- Br^- NO_3^- I^- ClO_4^- SCN^-

Figure 1.15 The Hofmeister series for typical anions.

When sodium salts of 11 anions were studied, it was found that their ability to lower the LCST of pNIPAAm followed the Hofmeister series. Three direct interactions of the anions with the polymer and its adjacent hydration shell were identified (Zhang and Cremer, 2006; Fig. 1.16):

(a) Both chaotropes and kosmotropes can increase hydrophobic hydration (i.e. raise the surface tension of the cavity that surrounds the molecule (salting-out effect is induced and the LCST is lowered with the salt concentration).

(b) The water molecules form hydrogen bonds with the amide groups of the polymer as can be polarised by anions (salting-out effect is induced and the LCST is lowered with salt concentration).

(c) Anions bind directly to the side-chain amide moieties (salting-in effect is induced).

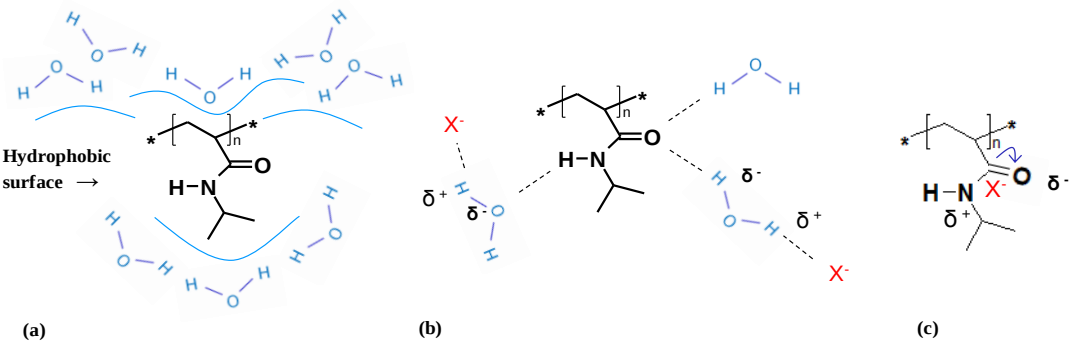

Figure 1.16 Interactions amongst anions, pNIPAAm, and water. (a) Hydrophobic hydration of the macromolecule with surface tension dependence; (b) Hydrogen bonding of the amide and its destabilization through polarization by the anion, X^-; (c) Binding of the anion to the amide group of pNIPAAm. Reproduced from Zhang and Cremer (2006).

1.5.2.4 Applications of thermoresponsive polymers in bioseparations

The thermoresponsive polymers in bioseparations are used to overcome problems and improve existing techniques. For example, in process chromatography the use of large volumes of solvents and buffers, results in rocketing processing costs and creates safety and environmental disposal issues. Smart polymers have the advantage that they operate under mild aqueous conditions, providing a novel and cost effective way to isolate 'smartly' valuable biomolecules from raw materials (Maharjan, 2008). In the following sections the most important applications of thermoresponsive polymers in bioseparations are presented.

1.5.2.4.1 Smart bioconjugates in affinity separations

The IMA technique offers a number of important advantages over other biospecific affinity techniques for protein purification, particularly with respect to ligand stability, binding capacity, protein recovery, and matrix regeneration (Arnold, 1991). However, in affinity

chromatography there are many problems related to column operations, such as difficult scale up, clogging of the column and low flow rates due to impurities (Arnold *et al.*, 1985). Affinity precipitation and affinity aqueous two-phase extractions are recommended to overcome these problems (Kumar *et al*., 2003). On the other hand, the use of smart polymers as bioconjugates, have been applied to all the above techniques.

In IMAC, the elution of target protein is usually achieved using imidazole, which competes with the protein bound to metal ions via histidines and finally displace it (displacement mode) (Vunnum *et al*., 1996). A copolymer of vinyl imidazole and vinyl caprolactam [poly(VI-VCL)] was synthesized and found that could be used as a displacer of protein or enzyme from Cu^{2+} loaded supports (Arvidsson *et al*., 2001; Ivanov *et al*., 2001). The use of the thermosponsive co-monomer enhanced the thermosensitivity of the copolymer which was precipitated with increasing the temperature.

In affinity precipitation, a 'smart' bioconjugate has been also synthesized by coupling a ligand to a water soluble polymer. The ligand-polymer conjugate selectively binds the target protein from the crude extract and the protein-polymer complex is precipitated from the solution by a simple change in the environment (pH, temperature, ionic strength or addition of some reagents). Finally, the desired protein is dissociated from the polymer and the latter can be recovered and re-used for another cycle. Various ligands like protease inhibitors, antibodies, nucleotides, carbohydrates, and triazine dyes have been successfully used in affinity precipitation (Galaev *et al.*, 1997).). However, chelated metal ions offer many advantages over classical biological affinity types, as they are small molecules, inexpensive, chemically and physically stable, easily coupled to matrices at high density resulting in high capacity adsorbents. The metal chelating ligand, vinylimidazole (VI) has been mostly used for the

metal chelate affinity precipitation of proteins (Galaev *et al.,* 1997). When copolymerized with NIPAAm, the copolymer of p(VI-NIPAAm) forms a complex with metal ions in such a way that two to three imidazole residues coordinated with a single metal ion (Kumar *et al.,* 1999). Through these studies, it was shown that the thermoprecipitation of pNIPAAm was pH-independent because the hydrophobic interactions responsible for the polymer precipitation are unaffected by the acidity of the medium over a wide range of pH. In contrast, the precipitation of the copolymer with vinylimidazole was highly pH-dependent.

Thermoresponsive polymers have been also used in ATPS, where the polymer-ligand complex is partitioned to the top phase and recovered by an external stimulus (Pietruszka *et al.,* 2000; Kumar *et al.,* 2001). In the traditional ATP systems, the selective partitioning of the protein between the two phases is based on their charge, size, hydrophobicity, and can be also promoted with the addition of salt or coupling an affinity ligand to one of the polymer phases (Albertsson, 1972). However, the separation of the target protein from the phase forming polymer still remains the major problem of this method (Galev and Mattiasson, 1999). To overcome this, thermoresponsive polymers such as poly(ethylene oxide-*co*-propylene oxide) and poly(*N*-vinyl caprolactam-*co*-vinyl imidazole) forming two-phase systems with dextran have been used (Farkas *et al.,* 1996; Franco 1997; Galaev and Mattiasson, 1999). During this procedure, the protein partitions into the thermoresponsive polymer phase, then the polymer phases are separated, and finally the protein is precipitated in an aqueous supernatant phase by heating. Another interesting approach for animal cells separation has been reported where the smart polymer is coupled with an antibody (Kumar 2002, Roy and Gupta, 2003).

1.5.2.4.2 Temperature controlled separations with smart polymers on solid supports

A novel chromatography concept (called temperature-responsive chromatography), in which the surface properties and functions of an HPLC stationary phase are regulated via external temperature changes whereas the mobile phase composition remains unaltered, has been described by Kanazawa and co-workers (Kanazawa *et al*, 1996 and 1998). The approach was based on the modification of silica beads with pNIPAAm, in order to render them with hydrophilic-hydrophobic properties. The beads were subsequently packed into HPLC columns and used for the separation of steroids, in the presence of water as a mobile phase. Elution was achieved simply by increasing the temperature of the column above the LCST of pNIPAAm (32 °C) with maximum resolution at 50 °C. Porous silica beads coated with hydrophilic polymer gels (dextrans of different molecular weights) carrying diethylaminoethyl (DEAE) groups have been employed as stationary phases for the High Performance Size-Exclusion Chromatography (HPSEC) of protein. Introduction of pNIPAAm chains into the surface of DEAE was used to such beads to change their pore size in response to temperature (Lakhiari *et al*., 1998). Modified silica beads with co-polymers of pNIPAAm have been evaluated as anionic (Kobayashi *et al*., 2003) and cationic (Ayano *et a*l., 2006) temperature-responsive chromatography media in ion-exchange chromatography. Finally, silica monoliths have been modified with pNIPAAm and evaluated for the separation of steroids using the thermoresponsive alterations of surface properties in aqueous media (Roohi, 2008).

Another potential application of pNIPAAm is on the control of bacterial fouling. The accumulation of microorganisms at solid-liquid interfaces, results in the formation of biofilms, which are quite undesirable at human operations. The natural occurring or cultured

microorganisms can be attached at pNIPAAm chains and removed by means of temperature change (Ista *et al.*, 1999). The change of the physical state of the polymer chains can result in switching the surface wettability that is favourable for attachment (hydrophobic) to a wettability that is less favourable (hydrophilic). On the other hand, the phase transition can be used for the detachment (removal) of the organisms. Thermoresponsive polymers have found use as switchable substrates for temperature-controlled cell harvesting (Kikuchi *et al.*, 1998), as well as for the recovery of cells from tissue culture substrata without the need for enzymes (Takezawa *et al*., 1990; Okano *et al*., 1993).

1.5.2.4.3 Combination of magnetic field and thermoreponsive properties in 'complex fluids'

The design of 'stimuli-responsive' gels is restricted by the slow rates of swelling and de-swelling making the development of these materials difficult in terms of optimisation. However, electric and magnetic fields may provide a fast and reliable signal control system. For this reason, the combination of solid-like and fluid-like behaviour in colloidal solutions named as 'complex fluids' is currently investigated. During these developments, colloidal particles are incorporated into a gel network allowing faster response to an external stimulus (Dimitrov *et al.*, 2007). Lately, there are some attempts to manufacture thermosensitive microgel particles. Ding *et al.* (1998) prepared multifunctional Fe_3O_4/poly(styrene-NIPAAm) [P(St-NIPAAm)] particles exhibiting thermosensitive behaviour and afterwards Ding and co-workers (2000), characterised these particles and tested them for their protein Human Serum Albumin (HSA) adsorption/desorption behaviour. Elaissari *et al.* (2001), prepared core-shell magnetic latex particles bearing pNIPAAm in the shell, investigating their cationic character in terms of nucleic acid adsorption/desorption by controlling the pH and salinity of the

medium. The same year, Elaissari and Bourrel (2001), examined the adsorption and desorption of HSA onto the prepared thermosensitive magnetic latex particles as a function of temperature, incubation time, pH and ionic strength. More recently, Shamim *et al.* (2006) manufactured surface-modified magnetic nanoparticles investigating the adsorption/desorption of bovine serum albumin (BSA) from these materials.

1.6 Aims of the thesis

The aim of this thesis was the synthesis and characterisation of polymer brushes as 'smart' surfaces onto magnetic adsorbents to improve their performance in terms of protein binding and release. When unlike polymers are combined in the same surface it is expected that this surface will adapt a combination of different properties. By alternating environmental parameters such as temperature of the polymer phase, switching of different properties can be achieved onto the surface. By integrating this concept to magnetic field assisted bioseparation process, improved adsorbents with temperature-controlled functions (such as protein self-elution) can be employed. In this work, patterning of magnetic phases by pre-assembling affinity ligand polymers and thermoresponsive polymers at various 2D structures, different types of Smart Polymer Adsorbent Phases (SP-APs) are proposed (see description in Fig.1.17).

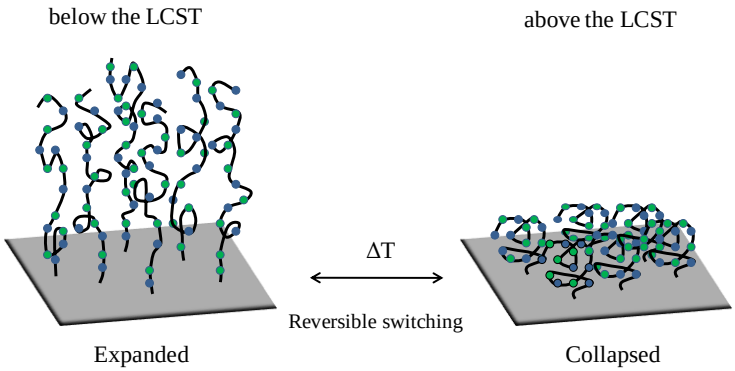

a. Alternating (co)polymer brush

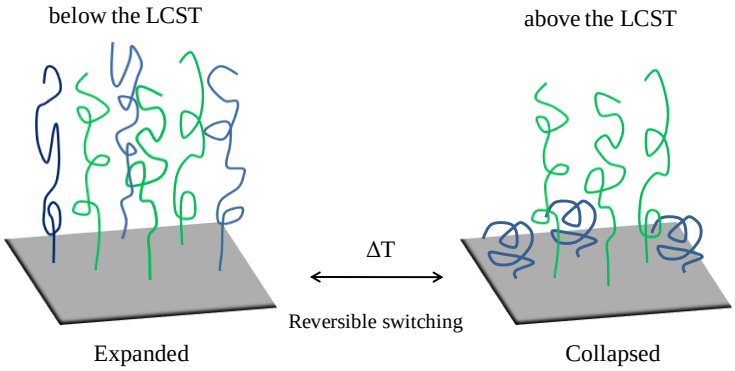

b. Mixed polymer brush

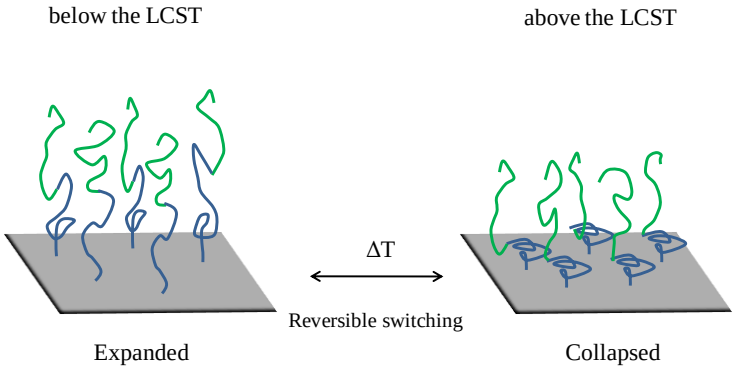

c. Di-block polymer brush

Figure 1.17 Proposed designs of Smart Polymer Adsorbent Phases (SP-APs) composed of affinity ligands (green) and smart (thermorsponsive) (blue) polymers: (**a**) Alternating (co)polymer brush– composed of the two monomer units which alternate sequential along the polymer backbone; (**b**) Mixed functionality polymer brush- composed of adjacent smart and affinity ligand polymer chains; (**c**) Di-block polymer brush- composed of an affinity ligand polymer chain end-capped with smart polymer graft (note: the order of polymers can change, i.e. the smart polymer chain end-capped with an affinity ligand polymer).

The specific objectives of the project were to:

1. Identify possible Smart Polymer Adsorbent Phases (SP-APs) combining thermoresponsive with affinity ligand polymers (as illustrated in Fig 1.17).

2. Explore the 'graft from' approach employing two different chemistries (cerium (IV) initiated polymerisation and ATRP) and investigate the possibilities / designs that can be achieved following each route.

3. Demonstrate and evaluate protein binding and release via temperature transition cycles on the mixed brush supports. These studies are mainly focus on forced thermoresponsive desorption in assisting the cleaning of adsorbed difficult to remove materials from supports (e.g. haemoglobin protein).

Magnetic carriers used in both small (laboratory) and large (e.g. HGMF) scales need further development to isolate, concentrate or purify valuable biomolecules such as recombinant proteins, in cost effective ways. Smart polymers have the advantage that they operate under mild aqueous conditions, making their integration in magnetic separations very attractive. Two different synthetic routes for the proposed SP-APs have been identified and further analysed in Chapter 2. In Chapter 3, cerium (IV) grafting has been employed to prepare magnetic supports grafted either with homopolymers or copolymer brush supports. Characterisation of these materials in terms of brush composition and protein binding/elution behaviour is used as a precursor to Chapter 4.

Mixed functionality polymer brushes composed of two different polymers can be used to deliver dual properties onto a surface while having the ability to respond to environmental stimuli. In Chapter 4, using the sequential cerium (IV) initiated polymerisation, mixed

brushes composed of affinity and thermoresponsive polymers aside to each other were created, characterised and applied for protein binding and release (via temperature shifts above and below the LCST) purposes.

Recent advances in polymer science propose the use of controlled/living radical polymerization like ATRP, for the construction of well defined (co)polymer structures in a controllable fashion. In Chapter 5, the patterning of polymer chains at various configurations and controlled densities is explored. The system is evaluated for polymer brushes (mixed and block) attachment onto magnetic particles. Its efficiency for protein binding/release in comparison with those materials obtained in Chapter 4 is also presented.

Finally, in Chapter 6 the main conclusions obtained from this work are briefly summarised while future study is proposed upon further smart magnetic adsorbents development and optimisation.

2. Surface ‘graft from’ approaches employed in this thesis

2.1 Introduction

Generally, there are two ways to attach polymer brushes onto surfaces: via physisorption and covalent attachment (Boyes *et al.*, 2004). In the first case, block copolymers adsorb onto a substrate as one of the blocks interacts strong enough with the surface, while the other block interacts weakly. Covalent attachment provides more stable bonds and can be performed by either ‘grafting to’ or ‘grafting from’ approach. In a ‘grafting to’ approach, preformed end-functionalized polymer molecules react with an appropriate substrate to form polymer brushes. In ‘grafting from’ approach an initiator is immobilised onto the surface and polymerisation reaction follows. This method (in-situ polymerisation) is more promising for polymer brushes preparation where high grafting density is essential (Zhao and Brittain, 2000).

Polymerization methods that have been used to synthesize polymer brushes include conventional free radical polymerisation reaction (CFRP), anionic and cationic polymerisation, ring opening polymerization, TEMPO-mediated radical, and atom transfer radical polymerization (ATRP). Generally, anionic polymerisation requires harsh reaction conditions and cationic polymerisation is complex. Additionally, ring opening and cationic polymerisation is suitable only for few monomers. On the other hand, CFRP has been used for polymer brushes preparation but only in cases where there are no requirements for multi-blocks. There are many reported systems describing CFRP methods to create polymer brushes. For example, Sugawara and Matsuda (1994) grafted polystyrene (PS) and

polyacrylamide onto poly(vinyl alcohol) and poly(ethylene terephthalate) (PET) films respectively. Minko *et al*., (1999) bound azo initiators onto silicon wafer followed by the reaction. The main difficulties during some CFRP are mainly: the several steps required for the immobilisation of the initiator on the surface, the side reactions producing undesirable structures on the surface, and the significant polydispersity of the brushes grown making the quantitative comparisons difficult. However depending on the system, it is possible to obtain thick polymer films, a variety of vinyl monomers can polymerised, and the grafting density can be controlled via a good choice of initiator and polymerization conditions (Toomey and Tirrell, 2008, Zhao and Brittain, 2000). Due to better control over chain length distribution as well as the prospect of block copolymers synthesis, ATRP has been far the current trend for polymer brushes preparation. Although this reaction demonstrates living characteristics, has not being yet successfully with all the monomers (e.g. strongly coordinating basic, acidic or nucleophilic acidic monomers deactivate the catalyst or kill the living ends). However, there are many efforts to study the effects of solvents, monomers, ligands and catalysts onto equilibrium of the reaction.

In this work, free radical polymerisation (using the Ce(IV) redox polymerisation) and ATRP have been employed, which are discussed below.

2.2 Cerium (IV) initiated 'graft from' polymerisation

It has been found that the redox system of Ce(IV)-alcohol is very effective for grafting polymers onto hydroxy-groups (Mino and Kaizerman 1958; Mino *et al*., 1959). This type of initiator has been widely used for grafting vinyl monomers on cellulose, starch as well as Poly

(vinyl alcohol) (Gonen and Kohn, 1981). For example, the method to prepare grafted polymers (tentacle-type ion exchangers) onto PVA was developed by Muller (Muller, 1990). Additionally, graft polymerization of anionic monomers (cation exchangers) onto PVA chromatographic supports has been performed by Pitfield (1992).

Generation of free radicals, reaction mechanism and initiation ability of free radicals in these systems have been studied extensively (Sarac, 1996 and 1999).

The following general scheme (Eq. 2.1-2.4) has been proposed for cerium (IV) reducing agent redox system:

$$Ce(IV) + R \leftrightarrows [Ce(IV) - R] \quad \text{Eq. (2.1)}$$

complex

$$[Ce(IV) - R] \xrightarrow{kd} R^{\cdot} + Ce(III) + H^{+} \text{ (decomposition)} \quad \text{Eq. (2.2)}$$

Primary radical

$$R^{\cdot} + M \xrightarrow{ki} R M^{\cdot} \quad \text{Eq. (2.3)}$$

$$RM^{\cdot} + nM \xrightarrow{kp} R(Mn) M^{\cdot} \quad \text{Eq. (2.4)}$$

Complex formation and generation of the primary radical (reaction of ceric ion with the reducing agent R) is described by Eq. 2.1 and Eq. 2.2. In the presence of monomer M, the polymerisation is initiated by the reaction of the free radical with the monomer (Eq. 2.3). The

reaction propagates following Eq. 2.4 scheme and depending on cerium (IV) concentration and other factors there are two possible termination reactions (Eq. 2.5-2.6) (Sarac, 1996 and 1999; Ozturk and Cakmak, 2007):

$$\mathrm{R(Mn)M} + \mathrm{Ce(IV)} \xrightarrow{\mathrm{kt}} \mathrm{polymer} + \mathrm{Ce(III)} + \mathrm{H^+} \qquad \text{Eq. (2.5)}$$

Termination by cerium (IV)

$$\mathrm{R(Mn)\,M^{\cdot}} + \mathrm{M^{\cdot}(Mn)}R \xrightarrow{\mathrm{kt}} \mathrm{R-Mn-M-M-Mn-R} \qquad \text{Eq. (2.6)}$$

Mutual termination

The cerium (IV) initiated polymerisation can be adapted to grow polymer tentacles onto magnetic particles. Various vinyl monomers of interest can be polymerized onto hydroxy containing supports using cerium (IV) redox system. For example, in this work, homo-polymer brushes of smart polymers (pNIPAAm and pVCL), affinity ligand polymers (pVI and pVBIDA) and/or the combination of these two different functionality polymers were grafted onto the M-PVA matrix. The polymerization scheme is illustrated in Fig. 2.1, where *N*-isopropylacrylamide (NIPAAm) is grafted onto M-PVA hydroxyl containing surface:

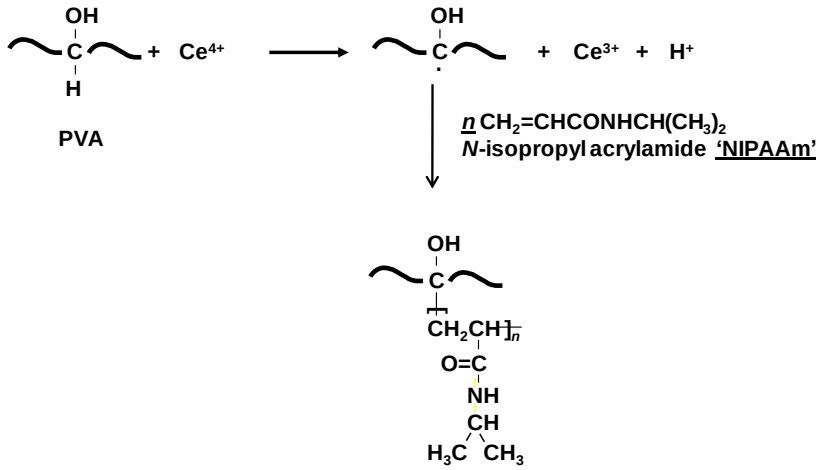

Figure 2.1 Cerium (IV) initiated grafting of *N*-isopropylacrylamide onto M-PVA supports.

2.3 Atom Transfer Polymerisation Reaction (ATRP)

The term 'living polymer' first appeared in the work of Szwarc in 1956, and since then, living anionic polymerization has played a significant role in polymer and materials science. Living anionic polymerization[10] and subsequently other controlled/living reactions (in which chain-breaking does occur but allows formation of well-defined co-polymers) have contribute to major developments as it enabled the preparation of well-defined (co)polymers of accurately designed molecular and nano-structured architectures (Matyjaszewski and Müller, 2006).

Some recent advances in the control over various polymerization systems (including ionic, radical, coordination and even polycondensation) have enabled synthesis of many new well-defined (co)polymers (Matyjaszewski, 2005). Precise controlled living radical polymerisations (CPRs) may take place not only under homogenous conditions, but also in heterogeneous polymerisation systems. These systems refer mainly to dispersion, suspension,

[10] defined as a polymerisation without chain-breaking reactions

emulsion and mini-emulsion polymerisations and are applicable to a wide range of monomers (Qiu *et al*., 2001). An advantage of CPR is that can be employed for the pre-assembling of materials, i.e. facilitate the controlled growth over pattern substrates (eg. flat surfaces, particles, polymer chains) (Luzinov *et al*., 2004; Matyjaszewski, 2005).

2.3.1 Fundamentals and mechanism of ATRP

In the early 1940's, Atom transfer radical addition (ATRA), or Kharasch addition, was developed, based on a simple free-radical mechanism**.** Afterwards, it was found rather limited due to unavoidable telomerisation reactions (Pintauer and Matyjaszewski, 2005). The research was thus moved towards of finding ways to control more precisely the polymers growth, and in the 1960's, researchers began to investigate the use of transition metal complexes to catalyze the ATRA. This was achieved by recognizing that the transition metal complexes are much more effective halogen transfer agents than alkyl halides. Similarly to transition metal catalyzed ATRA, Atom Transfer Polymerisation Reactions (ATRP) also employs transition metal complexes as halogen transfer agents (Pintauer and Matyjaszewski, 2005). The general mechanism for ATRP is shown in Fig. 2.2.

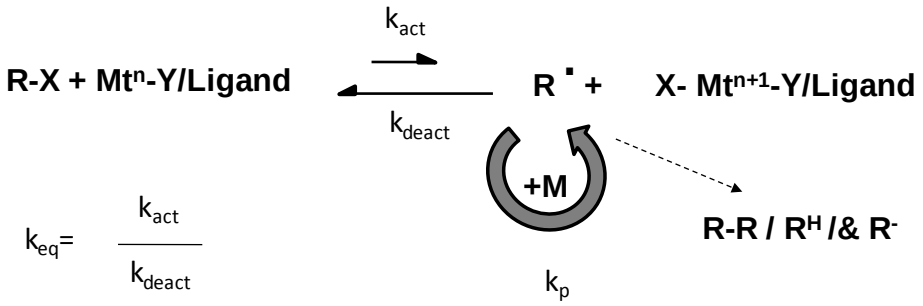

Figure 2.2 Transition metal catalysed ATRP (reproduced from Matyjaszewski and Xia, 2001). Note: **Mt^n** can be a metal such as Cu, Ru, Fe, Ni, etc. in the oxidation state n, **Y**: counterion (or another complexing ligand), **X**: (pseudo)halogen, **M**: vinyl monomer.

In this reaction, the catalyst consists of a transition metal (**Mt^n)** combined with a complexing ligand (**L)** and a counterion (**Y**) which can form a bond with the metal centre. Homolytic cleavage of the alkyl (pseudo)halogen bond (**R-X**) by the transition metal complex in the lower oxidation state (**Mt^n Y/ligand**) generates an alkyl radical (**R$^{\bullet}$**) and a transition metal complex in the higher oxidation state (**X-Mt^{n+1}-Y/ligand**). The formed radicals can initiate the polymerization by adding across the double bond of a vinyl monomer, propagate, and terminate. Termination happens by either coupling or disproportionation[11], or be reversibly deactivated by the transition metal complex in the higher oxidation state (Pintauer and Matyjaszewski, 2005). During coupling, radicals from separate chains react with each other, and a covalent C-C bond is generated between the chains terminating the polymerisation. During disproportionation, a hydrogen atom from one radical chain is transferred to the other and as a consequence, an allyl group is generated on one chain while both radicals are lost.

[11] defined as a reaction in which the same element is both oxidized and reduced (http://www.britannica.com/EBchecked/topic/165892/disproportionation).

2.3.2 ATRP components

2.3.2.1 Monomers

Plenty of monomers, such as styrenes, methacrylates, acrylates, styrenes, acrylamides, vinylpiridines and acrylonitrile, have been successfully polymerized using ATRP (Kamigaito, 2001). However, under the same conditions and using the same catalyst, each monomer has its own atom transfer equilibrium constant for its active and dormant species. Since ATRP is a catalytic process, the overall position of the equilibrium not only depends on the radical (monomer) and the dormant species, but also can be adjusted by the amount and reactivity of the transition-metal catalyst added (Matyjaszewski and Xia, 2001). The polymerisation rate is determined by the equilibrium constant (K_{eq}), which is the ratio k_{act}/k_{deact}. If the equilibrium constant is very small, ATRP will not proceed, whereas if it is too large, the radical concentration increases and an extended termination occur slowing down the polymerisation rate (shift of the equilibrium towards dormant species and subsequent deactivation of higher oxidation state of metal complex).

2.3.2.2 Initiators

Alkyl halides (R-X) are commonly used as initiators in ATRP. For these species the rate of the polymerization is considered as first order with respect to the concentration of R-X. The group X (halide) is must be such as can move fast between the chain and the metal complex, delivering well-defined polymers (increased monodipersity of the system). For this reason, either bromine or chlorine is preferred. The initiator determines the number of polymer chains that are going to be grown (concentration of initiator equals the number of chains), if there is

no transfer or termination (Matyjaszewski and Xia, 2001). On the other hand, the allyl radical is relatively stable due to the conjugation of a vinyl group with the carbon-centred radical.

2.3.2.3 Catalysts – transition metal complexes – Copper

The equilibrium of the ATRP and the dynamics between the dormant and active species depends on the type of catalyst. There are parameters that have to be considered for the selection of an efficient transition metal catalyst such as: The metal centre of the catalyst must have an affinity toward a halogen and at least two readily accessible oxidation states separated by one electron. The coordination sphere around the metal should be able to selectively accommodate a (pseudo)-halogen, whereas the ligand should complex the metal relatively strongly (Pintauer and Matyjaszewski, 2005). Eventually, the position and dynamics of the ATRP equilibrium should be appropriate for the specific system. A variety of transition-metal complexes have been studied and Copper has proven by far to be the transition metal of choice as determined by the successful application of its complexes as catalysts for a broad range of monomers in different media by many research groups (Queffelec *et al*., 2000; Braunecker and Matyjaszewski, 2007).

3. Preparation and characterisation of polymer brushes on magnetic supports by cerium (IV) initiated 'graft from' polymerisation reaction

3.1 Abstract

In this work the approaches for preparation and characterisation of polymer brushes via cerium (IV) initiated 'graft from' polymerisation reaction onto M-PVA supports are described. The optimum conditions and the kinetics of the employed reactions were examined by characterising homopolymer brushes of pNIPAAm, pVI and pVBIDA. The results indicate that the polymerisation reactions were fast and terminate prematurely. The degree of grafting was strongly related to: monomer concentration, monomer solubility, solvent selection (i.e. water preferably than DMSO), and spacing between the graft sites. As an attempt to construct alternating copolymer brushes, one pot cerium (IV) initiated reactions were employed to mixtures of monomers. Characterisation of the resulting materials revealed that polymerisation delivered homopolymers or di-block copolymers (i.e. either pVI or pVI end grafted with short pNIPAAm cap). The thermoresponsive behaviour of pNIPAAm and block copolymer supports was studied, and their LCST was detected. Estimations of the s/(2RF) ratios (<<1 in most of the cases) showed that the polymer chains are configured at the 'true' brush regime. The homopolymer (affinity or thermoresponsive) and di-block polymer brushes were tested for haemoglobin sorption/desorption at temperatures below and above the LCST. Above the LCST, the elution of protein was lower due to stronger interactions and the partial unfolding of the protein onto the polymer film.

3.2 Introduction

In downstream processing the purification of proteins using magnetic adsorbent particles has become very popular during the last years. The development of magnetic separation techniques is such, that scientists are searching ways to be realised into industrial practice (Franzreb *et al.*, 2006). Current magnetic adsorbents employed in magnetic separations, share several common features, e.g. they lie in the 'few tens of nanometers to few microns' size range, are classed as superparamagnetic, possess high specific surface areas, and are functionalised to endow just a single and relatively simple function: It has been demonstrated how very fast recovery of a given target protein product from crude bioprocess feedstocks can be achieved in the process termed High-Gradient Magnetic Fishing (HGMF) (Franzreb *et al.*, 2006 and references therein). The superparamagnetic adsorbents employed in HGMF can combine one ability, i.e. to sorb/desorb target species, with another, namely to respond reversibly to the influence of an externally applied magnetic field (Hubbuch, 2000; Hubbuch *et al*., 2001; Hubbuch and Thomas, 2002). However, current superparamagnetic adsorbents can be improved to provide predetermined functions.

Commercial available adsorbents are available from many companies as mentioned in Chapter 1 (section 1.4.5). Among them, Chemagen Biopolymer-Technologie AG, supplies magnetic beads under the trade name M-PVA. These beads are developed by an innovative suspension-based production process, which is patented worldwide, and allows a very economical production of biocompatible magnetic beads based on polyvinyl alcohol. The main advantages of these magnetic beads are: (a) the hydrophilicity of the PVA surface (inert-protein friendly surface); (b) the degree of magnetisation; (c) the individually tunable sizes of the beads, depending on the application; (d) the chemical functionality of the matrix

(functionalized with –OH groups), which can be used for many different modifications; and (e) the potential of high ligand binding capacity due to high surface area (www.chemagen.de).

In affinity separations, the ligands used are classified as biospecific (antibodies) and pseudo affinity ligands (immobilised metal ion complexes, hydrophobic amino acids, synthetic dyes) (Hage, 1999; Kawai *et al.*, 2003). There are several affinity chromatographic methods which success relies to the type of the immobilised ligand. Depending on the protein of interest and feedstock, the literature indicates which ligand should be used. In addition, several functionalisation techniques that can be easily adapted to coat magnetic adsorbents are described by Hermanson *et al.* (1992), which are based mainly on activation and coupling. The magnetic adsorbents can be functionalised with a vast of ligands that are used in chromatography, including affinity and pseudo affinity ones (Franzreb *et al.*, 2006). Preferably, the magnetic adsorbents should be of high adsorbance capacity, easy to clean, reusable and have low cost, so not only appropriate equipment but also new functionalisation routes are required in magnetic separations (Franzreb *et al*., 2006). A magnetic adsorbent should have a high surface area (higher maximum binding capacities can be achieved), as well as high ligand density. The latter is quite important especially for the metal chelate affinity adsorbents, where the ligand can bind the protein at many sites (surface exposed histidines) (Hubbuch and Thomas, 2002; Heebøll-Nielsen *et al*., 2004).

The research in the field of adaptive/responsive materials which has started several years ago has establish many advantages where it is possible to design surfaces able to respond to external stimuli in a controlled manner. Additionally, there is a considerable interest to modify surfaces with materials that have dual properties, for example thermoresponsive polymers such as pNIPAAm that depending on the temperature can be either hydrophilic or

hydrophobic. Incorporating such polymers onto a given surface can be very useful where the ultimate performance of the material is improved by obtaining desired properties (Luzinov, 2004). For example, in thermoresponsive chromatography field it has been demonstrated that by modifying materials with pNIPAAm, the surfaces gain hydrophilic-hydrophobic properties, and elution of the target species is achieved as the temperature gradients are analogous to that of solvents in reverse-phase HPLC (hydrophobic interaction chromatography) (Kanazawa *et al.*, 1996 and 1998; Maharjan *et al*., 2008). Additionally, in affinity thermopercipitation, bioconjugates containing VI and NIPAAm selectively bind the target protein from the crude extract and the protein-polymer complex is precipitated from the solution by a simple change in the temperature (Gupta and Mattiasson 1994; Gupta *et al*., 1996). The use of the thermoresponsive property for the separation of biomolecules can be very advantageous by minimising buffer consumption. This is of paramount importance as protein separation processes nowadays require large volumes of buffers and regeneration solutions, where significant costs arise to produce, store and dispose these solutions (Kawai *et al.*, 2003).

Recently, surface-initiated polymer brushes have received considerable attention as means to modify surfaces with chemically and mechanically robust thin polymer films. The unique properties of polymer brushes arise from the fact that polymers as small molecules are attached to a surface in very high grafting densities (Brittain and Minko, 2007). Polymer brushes can be attached onto surfaces using various 'grafting from' methods, as mentioned in Chapter 2. Free radical polymerisation onto substrates using redox systems is an important synthetic route as it is applicable to a plethora of vinyl monomers, suppress side reactions such as branching, and it is easy and inexpensive in comparison with other ionic methods. In these systems, the oxidant reacts with the organic molecule, forms a complex and then

decomposes producing free radicals that can initiate polymerisation (Mahadevaiah, 2007). Among other initiators, cerium (IV) ion is considered suitable for graft copolymerisation in terms of industrial applicability (low temperature) and ending up with scarce amounts of homopolymers most of the times (Simon and Bajpai, 2003). It has been used in various forms such as cerium (IV) ammonium nitrate, cerium (IV) ammonium sulphate, cerium (IV) sulphate, and ceric perchlorate (Sarac, 1999; Mahadevaiah, 2007). Generally, graft polymerization onto surfaces is a useful tool to tailor surface properties since a wide variety of monomers is readily available. Mino *et al.* (1959) found that the redox system of Ce (IV)-alcohol is very effective for grafting polymers onto hydroxy-groups. This type of initiator has been widely used for grafting vinyl monomers on cellulose, starch as well as Poly (vinyl alcohol) (Gonen and Kohn, 1981). For example, the method to prepare grafted polymers (tentacle-type ion exchangers) onto PVA was developed by Müller (1990). Additionally, graft polymerization of anionic monomers (cation exchangers) onto PVA chromatographic supports has been performed by Pitfield (1992).

Utilising the cerium (IV) grafting from approach, it is possible to graft polymer chains at defined length and spacing (by regulating the amount of initiator and monomer) onto magnetic particles containing hydroxyls such as M-PVA as shown in Fig. 3.1 below:

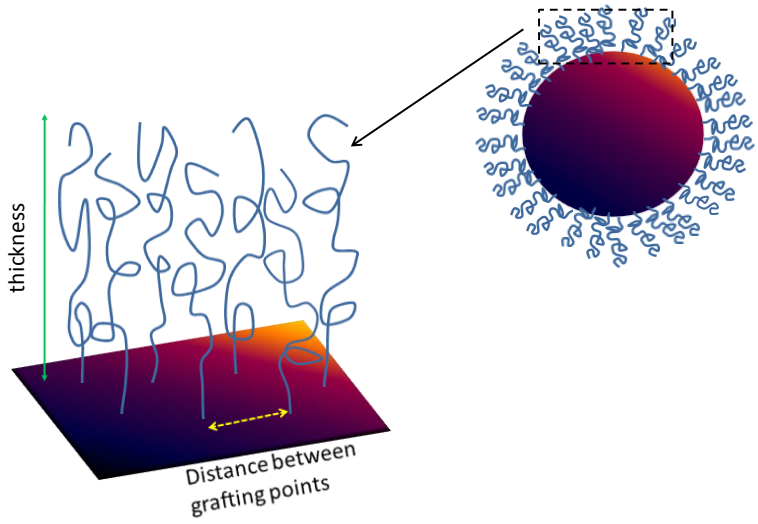

Figure 3.1 Grafted polymer chains attached to M-PVA surface at fixed positions.

In Chapter 1, various designs of Smart Polymer Affinity Phases were proposed, composed of both thermoresponsive and affinity polymers in different combinations (e.g. alternating and mixed polymer brushes). In this Chapter, cerium (IV) initiated polymerisation is employed to graft homopolymer brushes of either affinity ligand or thermoresponsive polymers (e.g. Fig. 3.3), and polymer brushes composed of thermoresponsive and affinity monomer units in an alternating fashion (Fig. 3.2).

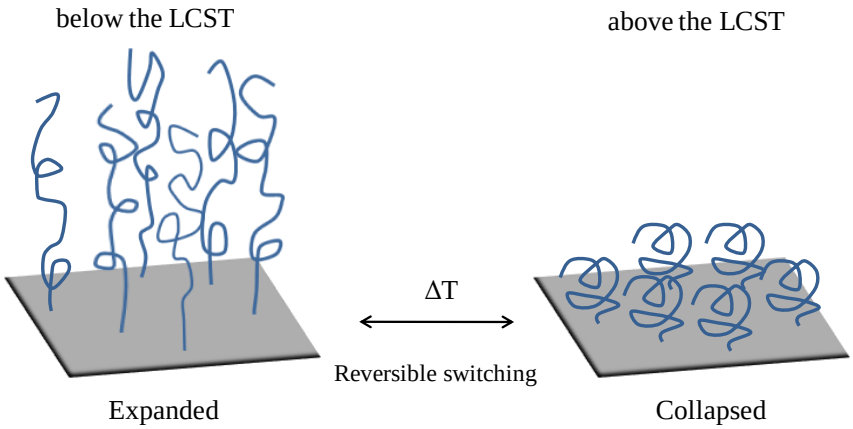

Figure 3.2 Homopolymer brush of smart polymer (pNIPAAm).

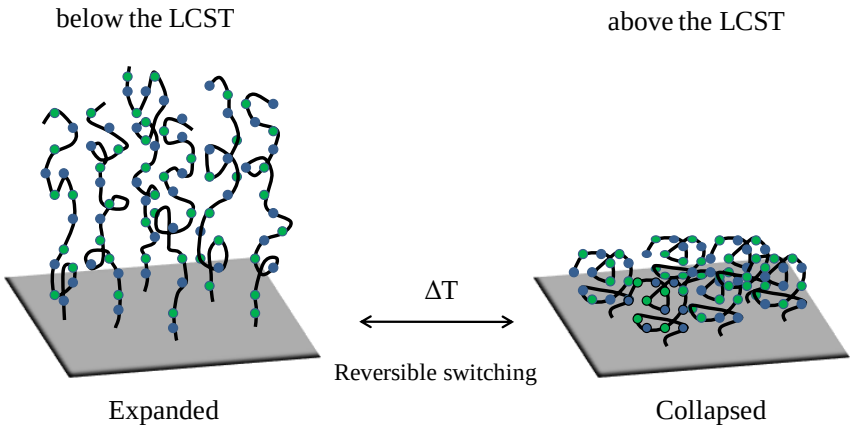

Figure 3.3 Schematic diagram of an alternating brush composed of thermoresponsive (blue) and affinity (green) monomer units in an alternating fashion along the polymer backbone.

By manufacturing the above materials, the concepts mentioned before can been exploited by grafting magnetic adsorbents with polymer brushes composed of: (a) affinity ligands at very high densities and (b) thermoresponsive polymers for protein elution via temperature and no other means (i.e. elution buffers).

The work in this chapter is a necessary precursor to subsequent chapters (Chapter 4 and 5) dealing with the fabrication and testing of mixed functionality polymer brush derivatised M-PVA supports. As a consequence, the main objectives of this work is to: (a) explore cerium (IV) chemistry by grafting different polymers onto the M-PVA surface and characterise the resulting materials (spacing of grafting and chain length); (b) perform one-pot cerium (IV) reactions of a mixture of monomers and find out if it is possible to construct alternating copolymers via this route; (c) investigate the thermoresponsive behaviour of supports grafted with pNIPAAm; (d) test most of the supports for protein adsorption and desorption characteristics. In these studies haemoglobin was selected as a model protein, which is generally a material difficult to elute from surfaces.

3.3 Materials and methods

3.3.1 Materials

Five batches of M-PVA particles (M_r 130,000; acetyl content: 10.0-11.6 %; degree of hydrolysis: 86.8-88.7 %; 2 µm mean diameter) were used (batch 1: U2-3236; batch 2: R2-1606; batch 3: R2-0105096; batch 4: R2-0109027; and batch 5: R2-0126067). Batches 1 and 3 were supplied by Chemagen Biopolymer-Technologie AG (Baesweiler, Germany), whereas batches 2, 4 and 5 were received as gifts from the same company. *N*-isopropylacrylamide (NIPAAm), *N*-vinylcaprolactam (VCL), *1*-vinylimidazole (VI), Iminodiacetic acid, 4-vinylbenzyl chloride, ammonium cerium (IV) nitrate and haemoglobin from bovine blood (lyophilized powder) were purchased from Sigma-Aldrich Company Ltd. (Gillingham, UK). All other chemicals used were of analytical grade unless otherwise stated. MilliQ water was used in all experiments.

3.3.2 Recovery, washing and density measurements of M-PVA supports before and after functionalisation

During all the washing and functionalisation steps, the magnetic supports were separated from their solvent using side-pull magnetic racks (~0.15 Tesla; Chemagic Stand 50k Type A and Chemagic Stand 2x12; Chemagen Biopolymer-Technologie AG, Baesweiler, Germany).

Before any polymerisation reaction, 25 mg M-PVA particles were transferred to a 50 mL tube and then washed sequentially with 3 mL portions of the following solutions: twice with water; once with 50 % (v/v) acetone in water; once with 100 % acetone; once with 50 % (v/v) acetone in methanol; once with 100 % methanol; once with 50 % (v/v) methanol in water;

twice with water; once with 1 M NaCl; and finally, three times with water. During each step, the particles were mixed for 30 s into the solvent using a vortex mixer (VM20, Chiltern Scientific Instrumentation Ltd., Wendover, UK).

After functionalisation, the polymer grafted supports were washed sequentially with 3 mL portions of the following solutions: once with 0.2 M Na_2SO_3 in 10 % (v/v) acetic acid; twice with water; once with 1 M NaCl; and finally three times with water. Finally, the polymer grafted supports were stored in 3 mL distilled deionised water at 4 ºC until further use.

Following each washing step, the exact concentration of the M-PVA in solution was determined by the following procedure: an HPLC vial was labelled and placed in a pyrex dish in the oven to dry at 60 ºC for 2 h, and then weighted using a Mettler AT261 balance (Delta range, Leicester, UK)**.** A fully suspended particle solution (0.2 mL) was transferred into the vial and let to dry in the oven for 16 h, before it was weighted once again. The weight of the sample content was calculated from the difference in weight before and after sample addition, allowing the determination of the initial concentration of the particles in the suspension.

3.3.3 Preparation of polymer grafted M-PVA supports by cerium (IV) 'graft from' initiated reactions

3.3.3.1 Preparation of poly (N-isopropylacrylamide) thermoresponsive homopolymer brushes

N-Isopropylacrylamide (NIPAAm) was polymerized onto hydroxy containing M-PVA supports using the cerium (IV) redox system. The polymerization scheme is illustrated in Fig. 3.4:

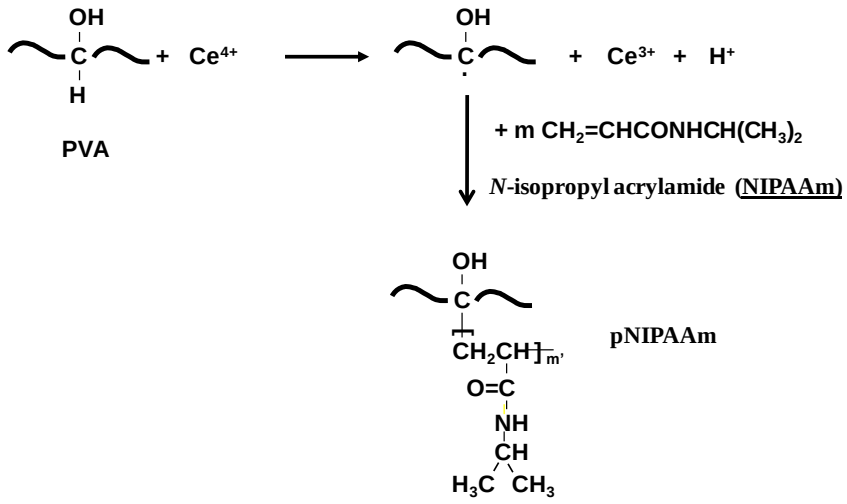

Figure 3.4 Cerium (IV) initiated grafting of *N*-isopropylacrylamide (NIPAAm) onto M-PVA support.

A volume of water (25 mL) was degassed in a clean 50 mL plastic screw cap tube by purging with a stream of nitrogen gas (N_2) for 0.5 h. For each sample, 25 mg of washed M-PVA particles were transferred into a 2 mL clean plastic screw cap tube. The particles were separated from the supernatant using a magnetic rack and mixed thoroughly with 1.5 mL of degassed water using the vortex mixer. This procedure was repeated once more, and the suspensions were purged with nitrogen gas for 600 s at 22 ºC. NIPAAm was dissolved into

water at a final concentration of 311 g L^{-1} and degassed with nitrogen for 600 s. From this solution, different volumes of NIPAAm were added to each sample corresponding to a final concentration of 4.4; 8.8; 44.0; and 110.0 mmol g^{-1} of monomer to M-PVA support respectively. Appropriate amounts of degassed distilled deionised water were added to each tube to keep the same reaction volumes, and then the tubes were tightly sealed and mixed in an orbital shaker (IKA®-Werke GmbH, Staufen, Germany) for 300 s at room temperature. Meanwhile, 60 mg of ammonium cerium (IV) nitrate (ACN) was dissolved into 750 μL solution of 2 M HNO_3 and again degassed separately for another 600 s. Then still under exclusion of air, 75 μL (6 mg or 11 μmol ACN) from this stock solution were added to each sample and the mixtures were stirred under nitrogen for 3 h at an orbital shaker (IKA®-Werke GmbH, Staufen, Germany) at 2000 rpm.

The amount of Ce(IV) added to the M-PVA support (0.44 mmol g^{-1}) was such that the resulting spacing between the initiation graft sites would be approximately 4.0 Å, taking into account that the specific surface area of the first batch of M-PVA particles supplied was 43 m^2 g^{-1}. By keeping the amount of ACN constant and altering the molar ratio of the monomer added (relative to the Ce(IV)), the same spacing with different chain lengths will be theoretically achieved during grafting, if the reaction goes to completion (Pitfield, 1992). Molar ratios of monomer: Ce(IV) of 10:1, 20:1, 100:1 and 250:1 were selected so that the target chain length would be of 10, 20, 100 and 250 monomer units. The reaction was also performed by adding 0.044 mmol of Ce (IV) per g of M-PVA support and 100:1 monomer to Ce (IV) ratio.

Finally, the reaction was also performed in 95.6 % DMSO to investigate the effect this solvent on polymerisation.

3.3.3.2 Preparation of poly (N-vinylimidazole) or poly (N-(4-vinyl)-benzyl Iminodiacetic acid) affinity ligand homopolymer grafted M-PVA supports

N-(4-vinyl)-benzyl Iminodiacetic acid (VBIDA) was prepared in-house as follows: 10.6 g Iminodiacetic acid (IDA) and 5.3 g NaOH were dissolved with 160 mL water/methanol mixture (volume: 1/1) in a 250 mL round bottom flask. The mixture was gently agitated using a glass stirrer and heated at 60 °C in a water bath. During the first 0.5 h, 5.7 g of 4-(vinylbenzyl) chloride were added drop wise (0.044 mL per 60 s) in the flask and during the following 0.5 h, 5.3 g of NaOH (3.4 M) were added in the same drop wise manner (4.0 mL per 180 s). At the end of the reaction, the colour of the liquid changed from orange to salmon pink. Half of this volume was removed using vacuum evaporation, and the resulting mixture was extracted (twice) in a separation funnel using diethyl ether to remove the thick oil (co-product impurity) formed during the reaction. The pH of the final liquid was adjusted to 2.0 by adding 37 % concentrated HCl, and the colour changed from salmon pink to light yellow, while a white precipitate was formed. The mixture was allowed to stand overnight, washed with a small amount of water (at pH 2.0) to remove any residual NaCl, and then placed in a vacuum desiccator for 24 h to re-crystallise and dry. The structure of the final product was confirmed by NMR (Appendix, section 7.1, Fig. 7.1). Before any reaction, VBIDA was completely dissolved in NaOH at a molar ratio of 1:2.

M-PVA supports functionalised with *N*-vinylimidazole (VI) or *N*-(4-vinyl)-benzyl Iminodiacetic acid (VBIDA) (polymerization scheme is illustrated in Fig. 3.5), were prepared by following the same procedure as described in section *3.3.3.1*. The spacing between the graft sites was again kept constant by adding the same amount of Ce(IV) onto M-PVA support (0.44 mmol g^{-1}). The target lengths were 20 and 100 monomer units for pVI and 100

monomer units for pVBIDA. The above reactions of 100 monomer units target length were repeated in 95.6 % DMSO, to investigate the effect of the solvent on polymerisation.

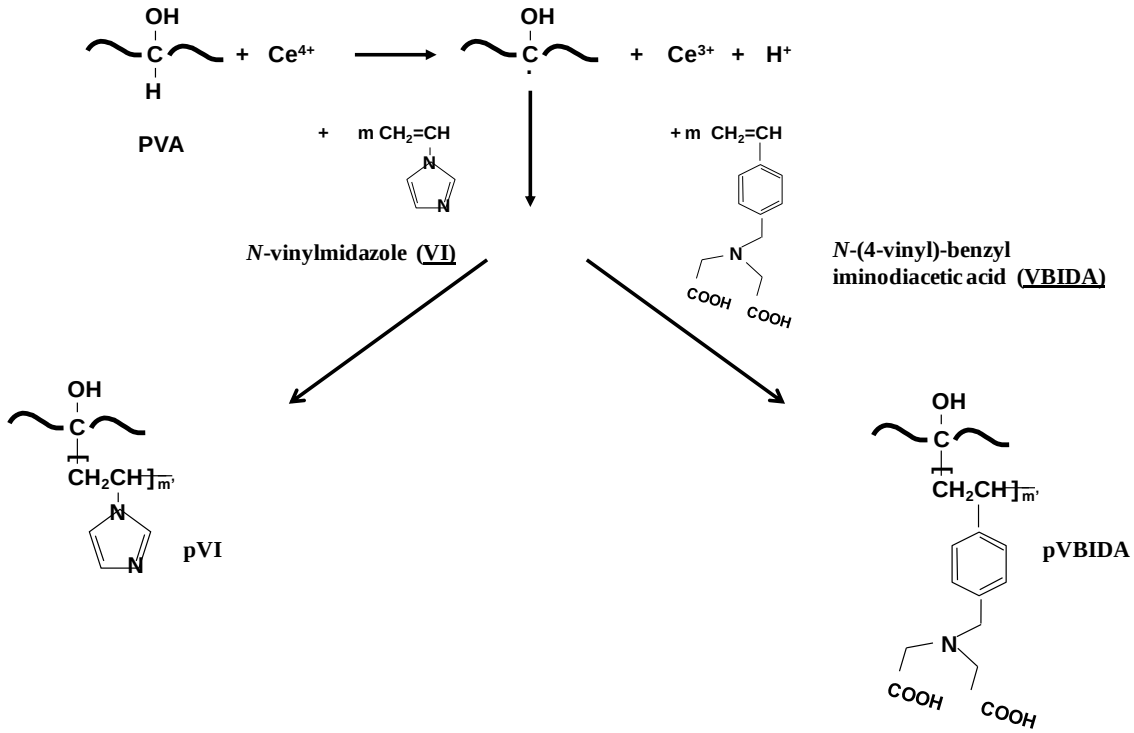

Figure 3.5 Cerium (IV) initiated grafting of affinity ligands *N*-vinylimidazole (VI) or *N*-(4-vinyl)-benzyl Iminodiacetic acid (VBIDA) onto M-PVA supports.

3.3.3.3 Preparation of copolymer grafted M-PVA supports by combining a thermoresponsive monomer (N-isopropylacrylamide or N-vinylcaprolactam) with an affinity ligand monomer (N-Vinylimidazole) in one-pot cerium (IV) reaction

A mixture of two monomers with different properties (thermoresponsiveness and affinity) was reacted in one-pot cerium (IV) initiated reaction onto M-PVA supports (Fig. 3.6) at different combinations. By keeping the same chain length, but altering the composition

between the two monomers as well as the spacing between the grafted chains, it was possible to examine how a mixture of two monomers may polymerise via cerium (IV) grafting.

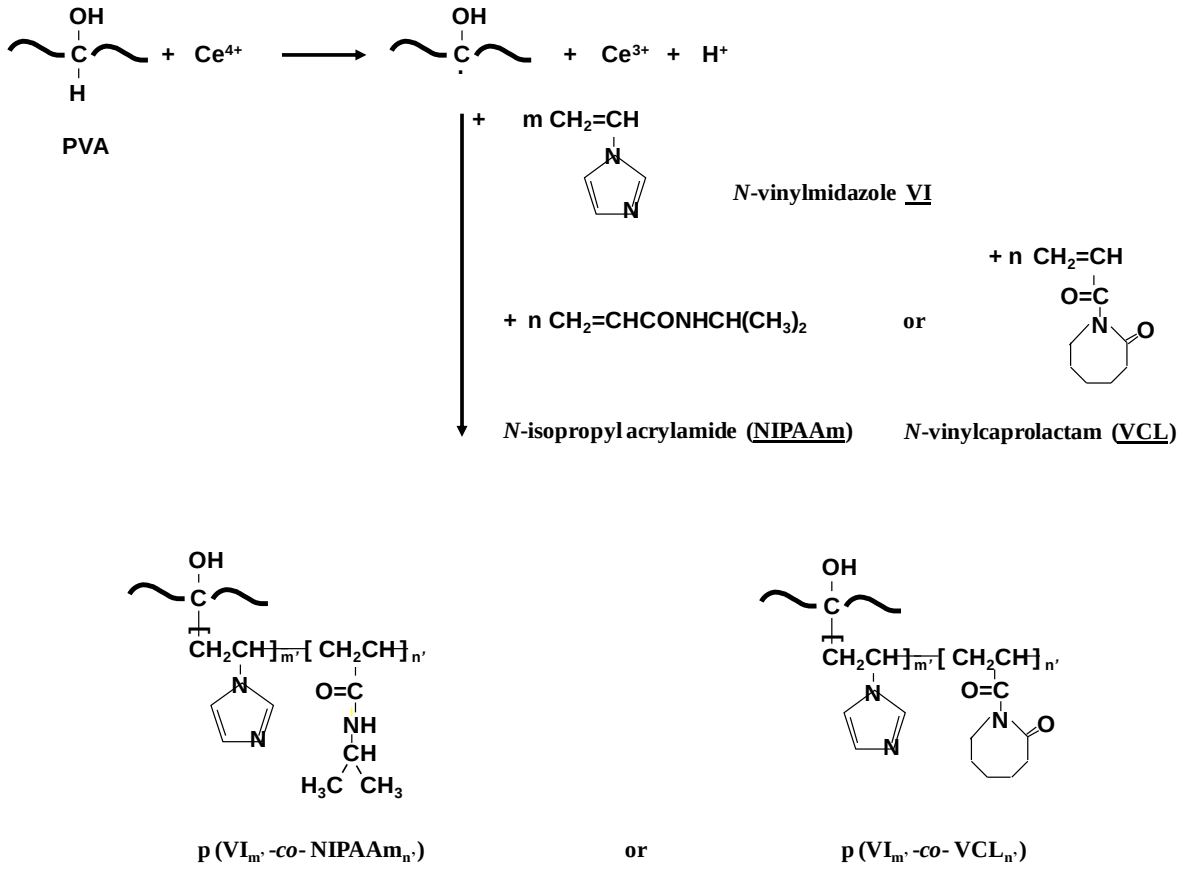

Figure 3.6 Cerium (IV) initiated grafting of *N*-isopropylacrylamide (NIPAAm) and *N*-vinylcaprolactam (VCL) or *N*-vinylimidazole (VI) onto M-PVA supports.

In these experiments, 0.44 mmol or 0.044 mmol of Ce(IV) per g of M-PVA support was utilised, while the amount of total monomer added was such as 20 or 100 monomer units length was targeted. Different feed composition was used by regulating the molar ratio of NIPAAm (or VCL) to VI, i.e. 4:1, 2:1, or 1:1.

3.3.4 Thermoresponsive assay for the detection of LCST

Samples of magnetic supports (unmodified and pNIPAAm modified) were diluted in 1.0 mM Sodium Phosphate buffer, pH 7.0 to a final concentration of 0.2 g L^{-1}, transferred to plastic disposable cuvettes and left to settle at different temperatures while absorbance readings were taken at 500 nm at regular intervals (every 300 s) using a UVICON 922 spectrophotometer (Kontron Instruments, Bletchley, UK). The spectrophotometer was connected to an OLS 200 water bath (Grant Instruments, Shepreth, UK) equipped with an in-house made thermocouple directly immersed at the reference cuvette, in order to continuously monitor, adjust and maintain the temperature at the desired levels. For the two sets of experiments, two different cuvettes were used: (a) a semi-micro (10 x 4 mm) acrylic 1.5 mL capacity and 10 mm light pathway (Sarstedt, Leicester, UK); and (b) a macro (10 x 10 mm) polystyrene 4.0 mL capacity and 10 mm light path (Fisher Scientific UK Ltd., Loughborough, UK).

3.3.5 Protein binding and elution studies

The functionalised supports (3 mg) were charged with Cu^{2+} ions by suspending them in 1.5 mL of 50 mM $CuCl_2$. The solution was incubated with shaking using an orbital shaker (IKA®-Werke GmbH, Staufen, Germany) at 1800 rpm for 0.3 h, and the procedure was repeated again. The supports were then equilibrated and washed from any unbound Cu^{2+} ions with 1.5 mL binding buffer for 0.3 h twice. Meanwhile, haemoglobin solutions of increasing concentrations (0.02 – 1.00 g L^{-1}) in binding buffer were prepared. The charged supports were re-suspended with 1.5 mL of the lowest concentration haemoglobin binding solution, and then mixed and incubated on the shaking plate at room temperature. After 0.5 h, the supernatant was magnetically removed from the support and the concentration of the unbound protein was

determined by using the analysis described in section *3.3.6.7*. The above procedure was repeated sequentially by adding haemoglobin of higher concentrations. At the end of the protein binding procedure, the protein loaded supports were washed with 1.5 mL of an elution buffer composed of 200 mM imidazole at pH 7.0. The supports were incubated for 30 min and then magnetically separated. The elution procedure was repeated until no further haemoglobin was desorbed judging from absorbance measurements.

The binding isotherms of the supports tested, were fitted to the Langmuir model using the Sigma Plot version 9.0 software (Systat Software Inc, CA, USA).

$$Q^* = \frac{Q_{max} K_d C^*}{1 + K_d C^*} \qquad \text{Eq. (3.1)}$$

In Eq. 3.1, Q* is the amount of protein adsorbed per gram of support and C* is the liquid-phase protein concentration at equilibrium. In this model, binding is described by the terms of dissociation constant K_d and the maximum capacity for adsorbed protein Q_{max}. These parameters were predicted using the nonlinear least squares fitting function of the said software. The estimation of the initial slope of the binding isotherms (Q_{max} /K_d) allowed easy comparisons of the performance of the different adsorbents.

3.3.6 Analytical techniques

3.3.6.1 Surface area measurements

Surface area measurements of the different M-PVA batches were performed using the method of Brunauer, Emmett and Teller (BET) based on the physical adsorption of an organic vapour

(octane) onto the surface of the beads. The dried samples were analysed using an automated gravimetric Advantage 1 Dynamic Vapour Sorption analyser (Surface Measurement System Ltd., Alperton, UK).

3.3.6.2 Magnetic properties

The magnetic properties of the M-PVA materials were examined by a Vibrating Sample Magnetometer (7300 series, Lakeshore Ltd, Harpender, UK). When a material is placed within a uniform magnetic field and is made to undergo sinusoidal motion (i.e. is mechanically vibrated), a change in magnetic flux occurs. This induces a voltage in the pick-up coils, which is proportional to the magnetic moment of the sample. The output measurement displays the magnetic moment M as a function of the field H. For the measurements, the samples were completely dried in an oven at 60 °C overnight and then placed in a Perspex holder. The holder was then attached to the end of a rod and aligned with the magnetic field along the x, y and z-axis. The magnetic field was increased gradually to 2.1 T, before being decreased to –2.1 T and then increased back up to 2.1 T to give a complete hysteresis loop for the sample.

3.3.6.3 Reduction of cerium (IV) concentration during the reactions

The reduction of cerium concentration in the supernatant solution was monitored, to get a timeline analysis of its consumption and the speed of the activation reaction during cerium (IV) initiation polymerisation. A simple, non-destructive method of analysis was employed by taking absorbance measurements at 353 nm (Ce(IV) peak wavelength) at different time

intervals (0.0, 0.25, 0.5, 1.0, 2.0, 3.0, 4.0 and 6.0 h) with the aid of a UVICON 922 spectrophotometer (Kontron Instruments, Bletchley, UK).

3.3.6.4 Detection of polymers grafted onto M-PVA supports using Fourier Transform Infrared Spectroscopy (FT-IR)

After each reaction, the functionalized supports were subsequently washed, completely dried and 1 or 2 mg of each was mixed and crushed with 300 mg potassium bromide (KBr) to form a very thin powder. These mixtures were then pressed between pellets at 10 tons, and the resulting discs were tested with a Nicolet 380 FT-IR spectrometer (Thermo Fisher Scientific, Waltham, MA, USA). The FT-IR spectra of both unmodified and modified beads were compared in order to detect the appearance of new bands corresponding to the species grafted on the support surface.

3.3.6.5 Analysis of monomer consumption using Attenuated Total Reflection Fourier Transform Infrared Spectroscopy (ATR FT-IR)

A method for the quantification of the monomer consumption during the reactions employed in this work was developed using the ATR FT-IR technique. In order to analyse the concentration of the unreacted monomer present in the supernatants, solutions of known concentration were prepared, a suitable band was chosen, the area at this wavelength was measured, and standard curves were plotted. This method was adapted to calibrate all of the monomers used at Ce(IV) initiated reactions and at different solvents (water and DMSO) as

described above. The main procedure followed for the construction of calibration curves is described bellow:

Routinely, 5-10 μL of each solution was transferred onto the surface of the smart orbit diamond accessory of the FT-IR instrument (Nicolet 380, Thermo Fischer Scientific, Waltham, MA, USA) and scanned 32 times at a resolution of 4 cm^{-1} in Attenuated Total Reflection (ATR) mode. A measurement without any sample in the beam was used as background to keep a relative scale for the adsorption intensity. Background measurements were taken every 0.5 h during sample measurements. The ATR spectrum of each standard was obtained by subtracting the spectrum of pure water from the aqueous solutions spectra. The Version 7.3 OMNIC ™ DS (Data Security) software (Thermo Fischer Scientific, Waltham, MA, USA), was used as the interface for data collection and processing (interpretations of interferograms and peak area measurements). Peak areas of the same region and baseline from each spectrum were chosen and measured, and linear relationships between the peak area and the concentration were obtained (see Fig. 3.7 as an example for NIPAAm calibration). The slopes of the calibration curves (peak area units per g L^{-1} or % substance) were used to determine the amount of unreacted monomers present in the supernatants after each reaction with high accuracy (correlation factors >0.99; Appendix section, Fig. 7.2 - 7.7).

Example of NIPAAm calibration in the reaction mixture

ACN was dissolved in Nitric Acid solution at 80 g L^{-1} concentration. Then 4.48 mL of this solution was diluted into 95.52 mL water (i.e. 4.48% of ACN in water). From that a 100 g L^{-1} NIPAAm solution was prepared by dissolving 1 g of NIPAAm into 10 mL of the above solution. Serial dilutions of this solution were carried out to prepare solutions of various

concentrations. The area under the peak of N-H bend (1550 cm^{-1}) of each standard's spectrum was calculated, keeping the same region and baseline at 1625-1500 cm^{-1} during all the readings. In Fig. 3.7, the FT-IR spectra obtained and the resulting calibration curve are shown.

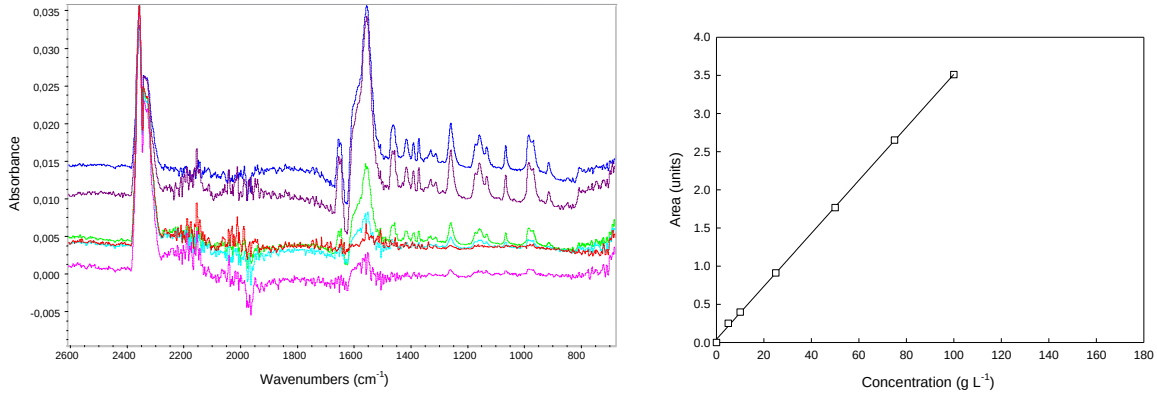

Figure 3.7 ATR FT-IR calibration of NIPAAm in the reaction mixture: **a-** FT-IR spectra of NIPAAm at different concentrations; **b-** NIPAAm concentration vs area of peak at 1500 cm^{-1}. The slope of this line was found 0.0353 peak area units per g L^{-1} with a correlation factor of 0.9992.

3.3.6.6 Scanning Electron Microscopy (SEM) and Energy Dispersive X-Ray (EDX) analysis

SEM technique under different modes was used for M-PVA surface topography studies. The method was employed to obtain images of the beads and examine their surface due to the high magnification and resolution that can be achieved with the electron microscope. In parallel, as the EM beam machine produces X-rays, Energy Dispersive X-Ray (EDX) microanalysis was performed, where a spectrum was generated, with peaks corresponding to specific X-ray lines and the elements could be then identified. In this work, two microscopes were used, that of SEM JSM-7000F (JEOL Ltd., Tokyo, Japan) and Philips XL-30 ESEM-FEG (FEI, Hillsboro, OR, USA), both linked with Oxford Inca EDS equipment (Oxford Instruments, Abingdon, UK). The samples were either tested wet (ESEM mode), or dried and sputter coated with

platinum. For cryo-SEM imaging the Philips XL-30 ESEM-FEG was used operating on SEM mode. The bead suspension was transferred on a metallic disc which was placed at the tip of the SEM rod, on a brass stage, which was then submerged into nitrogen slush at -140 °C. In this way, the beads were frozen while ice crystal formation was prevented. The rod was then quickly transferred into the SEM sample preparation chamber. Etching of the sample took place for 540 s at -90 °C. During etching, part of the intra-particle water was evaporated and hence the bead surface was visible. After etching and cooling back to -140 °C, the frozen sample was sputtered under the Au/Pt cathode for 30 seconds thus preventing subsequent sample damage by the electron beam. The sample was then transferred to the SEM chamber for examination. A beam intensity of 10 eV was selected in order to obtain clear images of the particles.

3.3.6.7 Assay for protein content

The concentration of protein bound on the supports was defined by estimating the protein remained in the supernatants. For this purpose a calibration curve of haemoglobin concentration in binding buffer was prepared (Appendix, section 7.3, Fig. 7.8) by measuring the absorbance of different concentrations of protein at 405 nm. For the measurements a UVICON 922 Spectrophotometer (Kontron Instruments, Bletchley, UK) was employed.

3.4 Results and discussion

3.4.1 Physical and magnetic characterisation of M-PVA base support materials

Five different batches of M-PVA, supplied by Chemagen Biopolymer-Technologie AG, were employed in this work. According to manufacturer specifications these particles are composed of a polyvinyl alcohol matrix with a high magnetite content (50-60 %) permitting rapid separation processes. These beads are superparamagnetic and have a polydisperse size distribution between 1-3 μm. In Fig. 3.8, the surface area (a) and the magnetic properties (b) of the supports supplied are given. In Fig. 3.9, the beads morphology is illustrated by the SEM images taken.

a

M-PVA supports		**Surface area**
Batch #	Lot #	(m^2 g^{-1})
Batch 1	(U2-3236)	43
Batch 2	(R2-16066)	50
Batch 3	(R2-0105096)	55
Batch 4	(R2-0109027)	55
Batch 5	(R2-0126067)	51

b

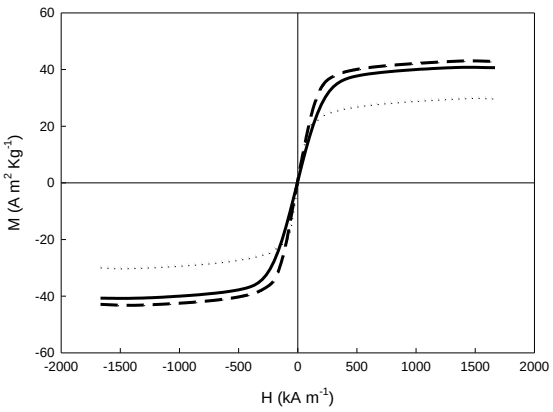

Figure 3.8 a- Surface area of the M-PVA batches used in this work; **b-** Magnetic hysteresis curves from VSM measurements (batch 1; dotted line, batch 4; dashed line, batch 5; solid line).

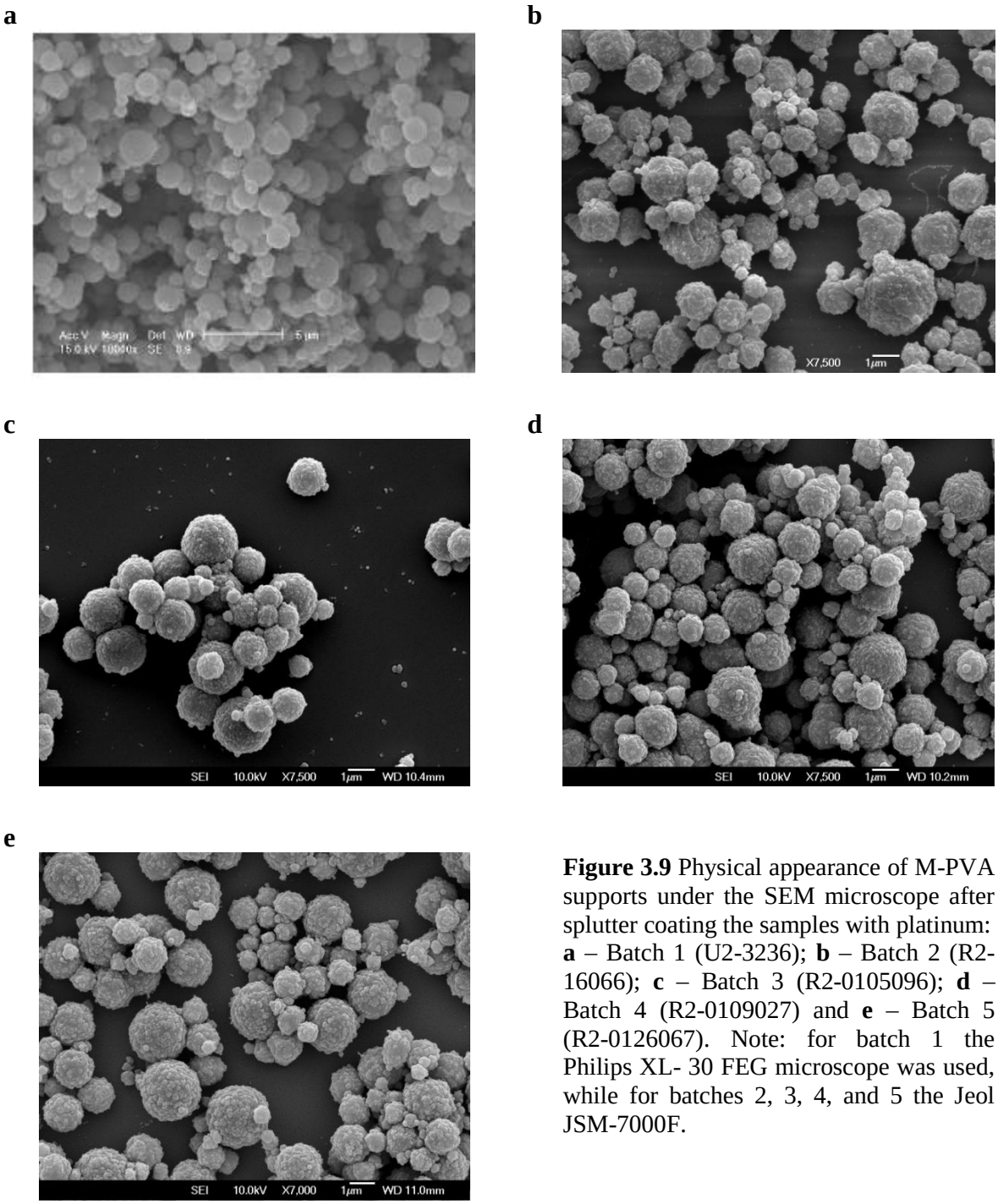

Figure 3.9 Physical appearance of M-PVA supports under the SEM microscope after splutter coating the samples with platinum: **a** – Batch 1 (U2-3236); **b** – Batch 2 (R2-16066); **c** – Batch 3 (R2-0105096); **d** – Batch 4 (R2-0109027) and **e** – Batch 5 (R2-0126067). Note: for batch 1 the Philips XL- 30 FEG microscope was used, while for batches 2, 3, 4, and 5 the Jeol JSM-7000F.

The SEM images obtained from M-PVA batches indicated no significant differences between the materials. However, among the batches, batch 2 seems to have the most heterogenous surface of increased roughness. Differences in surface area and magnetic properties between

the batches are more noticeable. According to the VSM shapes interpretation (Chapter 1, section 1.4.2), the particles are superparamagnetic in terms of remanence and magnetic coercivity. The maximum magnetisation values for batches 4 and 5 were close (42 and 40 $Am^2 Kg^{-1}$ respectively), however for batch 1 this value was much lower (29 A $m^2 Kg^{-1}$). This indicates that batches 4 and 5 had at least 1.45 fold more content of entrapped magnetite crystals than batch 1. The higher magnetite content of batches 4 and 5 in comparison with batch 1 is also reflected by the increased surface area (i.e. 55 and 51 $m^2 g^{-1}$ *cf.* 43 $m^2 g^{-1}$). The correlation of surface area with magnetite content is based on the possibility that the increased amount of magnetite crystals may contribute on surface heterogeneity and roughness and as a consequence to higher specific surface area (Brown, 2008).

3.4.2 Ce(IV) initiated 'graft from' polymerization onto M-PVA supports

Ce(IV) initiated graft from polymerization has been utilised since 1958 for grafting polymers onto hydroxyl-groups (Mino and Kaizerman 1958; Mino *et al.*, 1959). This type of reaction has been used for grafting a number of vinyl monomers onto cellulose, starch, wool, *Cassia tora* gum, and poly vinyl alcohol (Gonen and Kohn, 1981; Müller, 1990; Pitfield, 1992; Sharma *et al.*, 2002; Ma *et al.*, 2005). For example, *N*-isopropylacrylamide has been successfully grafted onto cellulose by Gupta and Khandekar (2003) demonstrating an LCST at 32 °C.

The graft polymerization reaction is initiated by Ce(IV), (ammonium cerium nitrate in a nitrogen environment): a hydrogen atom (H^+ ion) from the carbon bearing the hydroxy group of the polymer (PVA) is abstracted and oxidised in a reversible redox reaction. In the reaction, Ce(IV) is converted to Ce(III) where nitric acid is produced and free radicals are generated on

the polymer backbone. After the initiation stage, the monomer present in solution reacts with the activated surface and the polymerisation reaction proceeds until termination takes place (Mino and Kaizerman, 1958; Müller, 1990).

The same chemistry has been also used to graft two monomers from their binary mixtures onto substrates. For example, the graft copolymerization of acrylonitrile and methyl methacrylate onto carboxymethyl cellulose was demonstrated by Okieimen and Ogbeifun (1996). Based on that work, Gupta and Sahoo (2001) investigated the effect of monomer-monomer interactions on grafting when introducing two different monomer units (acrylonitrile and methyl methacrylate) into the reaction mixture. The authors estimated the average sequence lengths of the monomers that were found to be dependent on feed composition while being arranged in an alternating fashion in the grafted chains (Gupta and Sahoo, 2001). In this work, one-pot cerium (IV) initiated reactions of NIPAAm (or VCL) and VI mixtures were performed in an attempt to construct alternating copolymers (the polymerisation scheme is illustrated in Fig. 3.6).

3.4.3 Homopolymer grafted supports

The cerium (IV) redox system was utilised in this work for the graft polymerisation of three different monomers such as NIPAAm, VI and VBIDA in order to construct homopolymer brushes at defined spacing (the polymerisation schemes are illustrated in Fig. 3.4 and 3.5). The distance between the growing chains was adjusted by the addition of certain amounts of Ce(IV) onto the M-PVA surface. For example, for a specific surface area of 40 m^2 g^{-1} M-PVA the required amount of cerium (IV) for 4 Å spacing is estimated to 0.44 mmol g^{-1}. The target chain length was adjusted by the amount of monomer concentration to that of cerium (IV).

For example, 44 mmol g^{-1} of monomer concentration corresponds to 100 monomer unit length (i.e. 100:1 ratio monomer: initiator).

3.4.3.1 Ce(IV) consumption

The consumption of cerium (IV) after the polymerisations was specified by measuring the absorbance at its λmax of 353 nm. Essentially over 95-98 % of cerium (IV) converted to cerium (III) during the reactions. The resulting estimated spacing for each support is based on the assumption of 100 % consumption and utilisation of cerium (IV) as initiator.

3.4.3.2 Fourier Transform Infrared Spectroscopy (FT-IR)

In this work, FT-IR was used both qualitative and quantitative. Solid samples of functionalised M-PVA supports were analysed in KBr discs to identify new peaks appearance due to polymers addition on surfaces (the method is described in section *3.3.6.4*). As the Bee-Lambert law (see Appendix section 7.2.1) is applicable to the ATR FT-IR (the liquid sample has a fixed path length), the technique was used quantitative to determine the amount of polymers grafted onto the supports (the method is described in section *3.3.6.5*). In this work, the quantification employed can be considered confident due to the following reasons and observations: a. the high accuracy of the FT-IR accessories that are insensitive to the sample volume and thickness; b. the selection of an appropriate peak for area calculations while keeping always the same baseline and region throughout all quantifications; c. the non-complexity of the reaction mixture (ACN reagent cannot contribute to any spectra changes) during the standard reactions and when appropriate new calibrations were constructed if other

solvents apart from water were used (e.g. incorporation of DMSO contribution); d. the high accuracy obtained from calibration graphs, i.e. correlation factors where above 0.99; e. The confirmation that no polymerisation took place in the reaction mixture by observing the resulting spectra (i.e. the obtained scans corresponded only to characteristic peaks of monomers) and f. all the monomer solutions were highly homogenous due to the hydrophilic character of these species.

3.4.3.2.1 Monomers consumption after cerium (IV) initiated polymerisation and modification of supports

A series of cerium (IV) initiated reactions onto M-PVA particles were performed, in order to grow homopolymer brushes composed of pNIPAAm, pVI or pVBIDA chains. The polymerisations took place at five different M-PVA batches which physical characteristics were given in section 3.4.1. All reactions took place at Room Temperature (22 ºC), as low temperature redox polymerisation is more attractive both in an industrially (economical advantages) and scientifically manner. It has been reported that at elevated temperatures, there is a decrease of the percent of grafting (chain transfer termination due to increase of diffusion of monomer) as well as chain branching (Mahadevaiah, 2007). The reactions took place in water and in organic solvent (DMSO) in an attempt to investigate and compare the efficiency of these solvents. Additionally, the ACN solution was introduced into the reaction mixture, either before adding the monomer or afterwards, to test if the order of addition plays a crucial role. The percentage (%) of reacted monomers was estimated under all the conditions employed as described above, by quantifying the amount of unreacted products in supernatants using the FT-IR calibration curves.

In Table 3.1, the estimated mass of polymer attached on the supports is shown. Depending on the amount of monomer presented in the reaction, NIPAAm grafted between 0.242-0.4983 g/g support (for 100 monomers target length) and 0.508-0.6539 g/g support (for 250 monomers target length), VI between 0.486-0.605 g/g support (for 100 monomers target length), and VBIDA between 0.547-0.640 g/g support (for 100 monomers target length). Based on the size of the monomers and the degree of polymerisation, the resulting extended length of polymer chains will be between 1.9-6.0 nm (for 100 monomers target length) or 9.1-11.4 nm (for 250 monomers target length) for NIPAAm, between 17.7-29.6 nm for VI and 7.3-10.7 nm for VBIDA.

The high amount of polymer introduced onto M-PVA can be explained by the high density of the polymer film as the chains are grafted at very narrow spacing, i.e. very close to each other. As mentioned before, the estimation of spacing was based on 100 % consumption of the initiator by colorimetrically observing the disappearance of cerium (IV) from the reaction mixture. The disappearance of cerium (IV) from the supernatants was estimated at 96.1 ± 0.6 %. However the possibility that not all of the cerium (IV) has been utilised in the reaction cannot be excluded. For this reason in section 3.4.6 different levels of cerium consumption are assumed based on findings of other groups that used cerium (IV) grafting, whereas the estimated R_F values are given (Table 3.6). It has to be noted that in this work, the most important aspect is the configuration of the polymer chains, which define the behaviour of a polymer brush. In section 3.4.6, it is shown that independently the initiator consumption in all cases the polymer chains are configured at the 'true' brush regime. These outcomes are mainly based on the amounts of monomer consumed according to the FT-IR analysis. Observations on the supports after the reaction revealed that the grafted materials were much

heavier than the same materials before grafting (considerable increased settling at the same solvent volume). Performing a gravimetric analysis could also provide further confirmation.

In parallel, the modified solid supports were tested with FT-IR technique in KBr discs to detect the grafted polymers after the reactions by identifying the appearance of new bands on the spectra in comparison with those of unmodified M-PVA supports, if possible (Fig. 3.10). Grafting of pNIPAAm onto M-PVA support was confirmed with the appearance of N-H bend at 1550 cm^{-1}. For pVI, the spectrum of PVA interferes with that of pVI in such a way making the comparison more difficult, however modification is detected due to the following observations: (a) the increase of peak area and height at 1633 cm^{-1} due to C=C stretch vibration of imidazole ring (Hummel and Scholl, 1990); and (b) the increase of peak height at 1380 cm^{-1}, as peaks in the range of 1475-1250 cm^{-1} overlap in an enhanced form assigned to various bending vibrations of C-H bonds and C-N vibrations of PVA and pVI (Caner *et. al.*, 2007). The same modification trends are observed for the VBIDA, due to its similarity with the pVI backbone structure.

Table 3.1 Cerium (IV) grafted homo-brush supports.

Support #	M-PVA starting material		Ce(IV) grafting parameters				Support characterization								Polymer brush description on finished support
	Batch	SA (m^2/g)	Monomer employed	Order of addition/ reaction solvent	Ce(IV) (mmol/g M-PVA)	Monomer presented (mmol/g M-PVA)	Target DP (units)	React^n (%)	DP (units)	Spacing (Å)	Monomer installed (mmol/g M-PVA)	Polymer (g/g M-PVA)	Polymer (g/g support)	Monomer installed (mmol/g support)	
Homo-1.1	1	43	NIPAAm	Std/H_2O	0.44	8.8	20	40.0	8.0	4.04	3.52	0.3978	0.2846	2.52	$pNIPAAm_8$ – 4.0 Å
Homo-1.2	1	43	NIPAAm	Std/H_2O	0.44	44	100	20.0	20.0	4.04	8.79	0.9933	0.4983	4.41	$pNIPAAm_{20}$ – 4.0 Å
Homo-1.3	1	43	NIPAAm	Std/H_2O	0.44	110	250	15.2	38.0	4.04	16.72	1.8894	0.6539	5.79	$pNIPAAm_{38}$ – 4.0 Å
Homo-1.4	1	43	VI	Std/H_2O	0.44	44	100	38.2	38.2	4.04	16.81	1.5800	0.6124	6.51	$pVI_{38.2}$ – 4.0 Å
Homo-2.1	2	50	NIPAAm	Std/H_2O	0.44	8.8	20	nd	nd	4.35	nd	nd	nd	nd	$pNIPAAm_{\underline{20}}$ – 4.4 Å
Homo-2.2	2	50	NIPAAm	Std/H_2O	0.44	44	100	nd	nd	4.35	nd	nd	nd	nd	$pNIPAAm_{\underline{100}}$ – 4.4 Å
Homo-2.3	2	50	VI	Std/H_2O	0.44	8.8	20	nd	nd	4.35	nd	nd	nd	nd	$pVI_{\underline{20}}$ – 4.4 Å
Homo-2.4	2	50	VI	Std/H_2O	0.44	44	100	nd	nd	4.35	nd	nd	nd	nd	$pVI_{\underline{100}}$ – 4.4 Å
Homo-3.1	3	55	NIPAAm	Std/H_2O	0.44	4.4	10	3.7	0.37	4.56	0.16	0.0181	0.0178	0.16	$pNIPAAm_{0.4}$ – 4.6Å
Homo-3.2	3	55	NIPAAm	Std/H_2O	0.44	8.8	20	7.2	1.44	4.56	0.63	0.0712	0.067	0.59	$pNIPAAm_{1.4}$ – 4.6 Å
Homo-3.3	3	55	NIPAAm	Std/H_2O	0.44	44	100	14.3	14.3	4.56	6.29	0.711	0.416	3.68	$pNIPAAm_{14}$ – 4.6 Å
Homo-3.4	3	55	NIPAAm	Std/H_2O	0.44	110	250	12.1	30.3	4.56	13.31	1.504	0.601	5.32	$pNIPAAm_{30.3}$ – 4.6 Å
Homo-3.5	3	55	VI	Std/H_2O	0.44	44	100	37.0	37.0	4.56	16.3	1.532	0.605	6.44	pVI_{37} – 4.6 Å
Homo-4.1	4	55	NIPAAm	Std/H_2O	0.44	8.8	20	8.1	1.62	4.56	0.71	0.080	0.074	0.66	$pNIPAAm_{1.6}$ – 4.6 Å
Homo-4.2	4	55	NIPAAm	Std/H_2O	0.44	44	100	10.3	10.3	4.56	4.53	0.512	0.339	3.00	$pNIPAAm_{10.3}$ – 4.6 Å
Homo-4.3	4	55	NIPAAm	Std/H_2O	0.44	44	100	13.2	13.2	4.56	5.81	0.656	0.396	3.51	$pNIPAAm_{13.2}$ – 4.6 Å
Homo-4.4	4	55	NIPAAm	Std/H_2O	0.44	110	250	8.3	20.8	4.56	9.13	1.032	0.508	4.49	$pNIPAAm_{20.8}$ – 4.6Å
Homo-4.5	4	55	NIPAAm	Std/H_2O	0.044	4.4	100	11.9	11.9	14.43	0.52	0.060	0.056	0.50	$pNIPAAm_{21}$ – 4.6Å
Homo-4.6	4	55	VI	Std/H_2O	0.44	8.8	20	100	20.0	4.56	8.80	0.827	0.453	4.82	pVI_{20} – 4.6 Å
Homo-4.7	4	55	VI	Std/H_2O	0.44	44	100	36.7	36.7	4.56	16.15	1.518	0.603	6.41	$pVI_{36.7}$ – 4.6 Å
Homo-4.8	4	55	VI	Std/H_2O	0.44	44	100	30.9	30.9	4.56	13.60	1.278	0.561	5.97	$pVI_{30.9}$– 4.6 Å
Homo-4.9	4	55	VBIDA	Std/DMSO	0.44	44	100	16.0	16.0	4.56	7.04	1.760	0.640	2.55	$pVBIDA_{16}$– 4.6 Å
Homo-5.1	5	55	NIPAAm	Std/H_2O	0.44	44	100	6.4	6.4	4.56	2.82	0.319	0.242	2.14	$pNIPAAm_{6.4}$ – 4.6 Å
Homo-5.2	5	55	NIPAAm	Std/DMSO	0.44	44	100	0.0	0.0	-	0.0	0.0	0.0	0.0	-
Homo-5.3	5	55	NIPAAm	Reverse/ H_2O	0.44	44	100	4.1	4.1	4.56	1.80	0.203	0.169	1.50	$pNIPAAm_{4.1}$ – 4.6 Å
Homo-5.4	5	55	VI	Std/H_2O	0.44	44	100	22.9	22.9	4.56	10.08	0.947	0.486	5.18	$pVI_{22.9}$ – 4.6 Å
Homo-5.5	5	55	VI	Std/DMSO	0.44	44	100	6.7	6.7	4.56	2.95	0.277	0.217	2.31	$pVI_{6.7}$ – 4.6 Å
Homo-5.6	5	55	VBIDA	Std/H_2O	0.44	44	100	10.9	10.9	4.56	4.80	1.207	0.547	2.17	$pVBIDA_{10.9}$ – 4.6 Å
Homo-5.7	5	55	VBIDA	Std/DMSO	0.44	44	100	7.0	7.0	4.56	3.08	0.774	0.436	1.74	$pVBIDA_7$ – 4.6 Å
Homo-5.8	5	55	VBIDA	Reverse/ H_2O	0.44	44	100	2.4	2.4	4.56	1.06	0.266	0.210	0.84	$pVBIDA_{2.4}$ – 4.6 Å

a

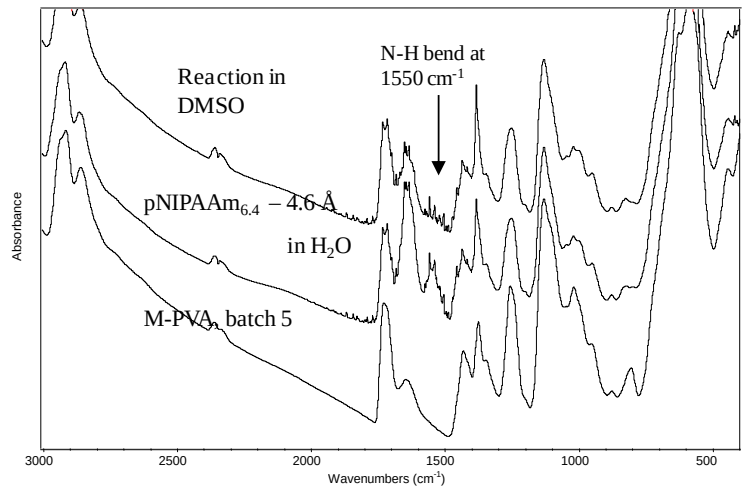

b

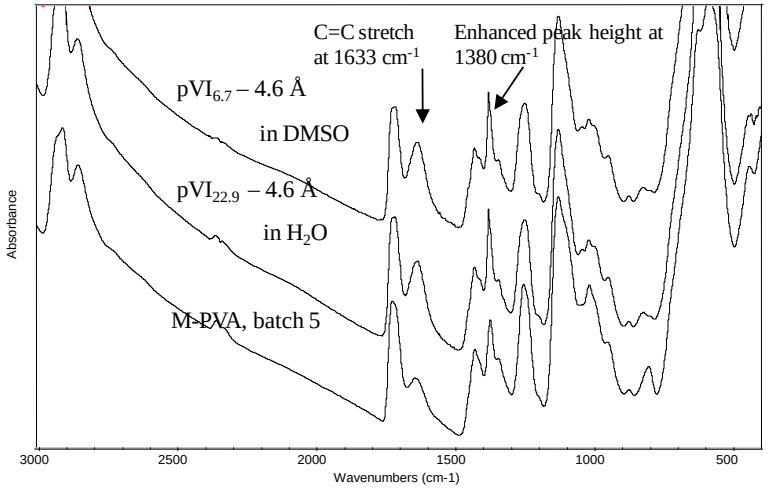

c

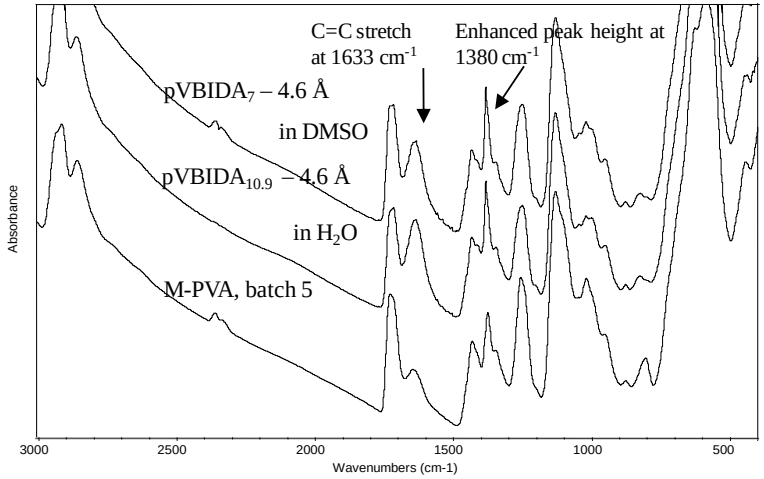

Figure 3.10 FT-IR spectra of unmodified and modified M-PVA supports: **a**- Modification of M-PVA batch 5 with pNIPAAm in water and DMSO, **b**- Modification of M-PVA batch 5 with pVI in water and DMSO, **c**- Modification of batch 5 M-PVA with pVBIDA in water and DMSO.

3.4.3.3.1 Effect of reaction solvent in cerium (IV) initiated polymerisation

According to Table 3.1, the use of DMSO instead of water as solvent resulted in considerable decrease of the polymerisation degree for all the monomers. This is also clear from spectra at image (a) of Fig. 3.10, where pNIPAAm peak at 1550 cm^{-1} is much sharper/broader when the reaction takes place in water. Previous reports related to redox initiation system, have shown that the reaction is not much successful in a variety of organic solvents. The first attempt to initiate polymerisation by cerium (IV) in organic solvents (toluene) was performed by Singh *et al.* (1979) who observed the inhibition of the polymerisation process. Other authors, have also shown that tertiary amine, hydro-peroxide-cobalt octate, methanol, ethanol and DMF are either not applicable to vinyl polymerisations or decrease the polymerisation (Mahadevaiah, 2007). According to Schulz *et al.* (1954), the solvent molecules interrupt the strong hydration layer in the aqueous medium, resulting in the termination of the radical ends, while in some cases the production of primary radicals renders the termination rate fast as compared to the growth rate of the polymer chains.

3.4.3.3.2 Effect of monomer and batch variation in cerium (IV) initiated polymerisation

Under the same reaction conditions, there are clear differences between the reactivity of the monomers. From a first observation, the extent of monomer consumption follows the trend VI > VBIDA > NIPAAm. From previous studies of graft polymerisation of vinyl monomers initiated by ceric ammonium nitrate, it has been reported that the degree of grafting is related to the polarity and solubility of the monomer (Reyes *et al.,* 1966).

The polymerisation reaction was investigated over increasing concentrations of monomer (NIPAAm and VI). NIPAAm concentrations of 4.4, 8.8, 44.0 and 110.0 mmol g^{-1} were reacted to the magnetic support, aiming for target chain lengths of 10, 20, 100 and 250 monomer units respectively. All the other parameters (ACN concentration, nitric acid concentration and reaction time) were kept constant. With respect to quantification of % monomer reacted, the percentage conversions were found to increase with monomer concentration up to 44.0 mmol g^{-1} and then start to decrease at 110.0 mmol g^{-1} (Fig. 3.11).

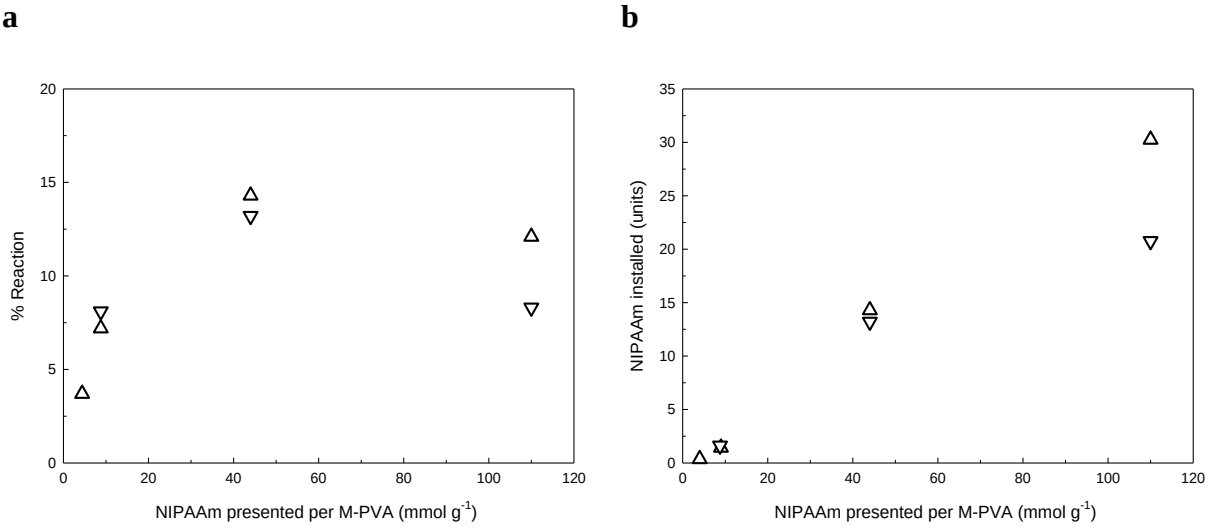

Figure 3.11 Effect of monomer (NIPAAm) concentration at cerium (IV) reaction onto M-PVA supports: batch 3 (up triangles) and batch 4 (down triangles): **a**- Percent of monomer conversion with amount of monomer presented during cerium (IV) grafting; **b**- Monomer units installed with amount of monomer presented during cerium (IV) grafting.

This has been attributed to the increased availability of monomer in the propagation step which obviously increases the rate of polymerisation (Rai *et al.*, 2000). However at further increase of monomer concentration, the grafted polymer chains become longer come closer to each other and so mutual radical termination is promoted. Compared to similar studies by others where NIPAAm has been grafted onto cellulose matrix via cerium (IV) initiation, as

the monomer concentration increases there is a deviation from linearity with polymer grafting at higher concentrations (Gupta and Khandekar, 2003).

For VI reactions, two different concentrations were examined where a decreased % of conversion at higher monomer concentrations was observed. However, for 8.8 mmol g^{-1}, a total conversion was achieved, i.e. 20 monomer unit length chains were grown, indicating again that each monomer has different reactivity during the polymerisation.

VI is grafted more efficiently than NIPAAm, but there are clear differences in the relative reactivity of VI to NIPAAm for the different batches (Fig. 3.12). Although the highest levels of NIPAAm that could be installed were observed with batch 1, VI installed was essential constant between (31-38 %) for all the batches.

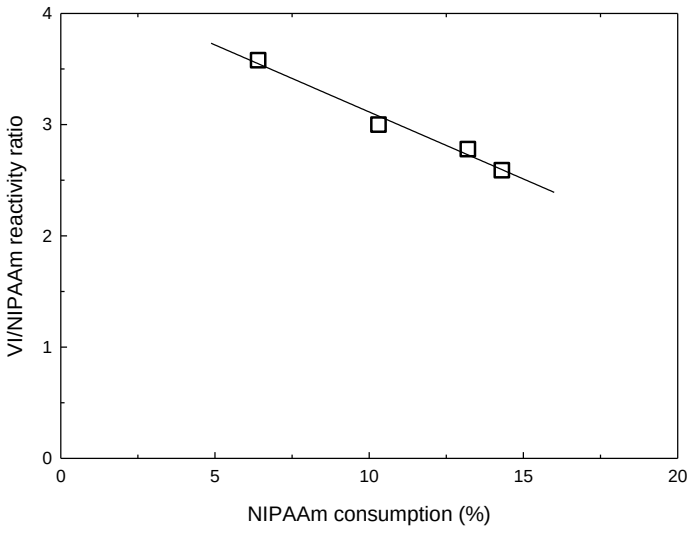

Figure 3.12 VI/NIPAAM reactivity ratio for NIPAAm reactions in water (44.0 mmol presented per g M-PVA) for batches 1, 3, 4 and 5. The linear regression gave a correlation factor of 0.9823.

Between the batches employed such as batch 1, 3, 4 and 5, batch 1 delivered the highest polymerisation yields. There were not significant differences in the extent of polymerisation between the batches 3 and 4. However, batch 5 delivered materials of much less polymer

weight grafted on its surface. The variation between the batches may be attributed to the differences in specific surface areas, the surface homogeneity as well as the possibility of impurities (eg. unwashed surfactants, mineral oils, PVA and magnetite crystals) remained after their production in large scale affecting the functionalisation reactions.

3.4.3.3.3 Effect of cerium (IV) order of addition

By adding the monomer (NIPAAm or VBIDA) before introducing the cerium into the reaction mixture, the percent of polymerisation is increased (Table 3.1 and Fig. 3.13).

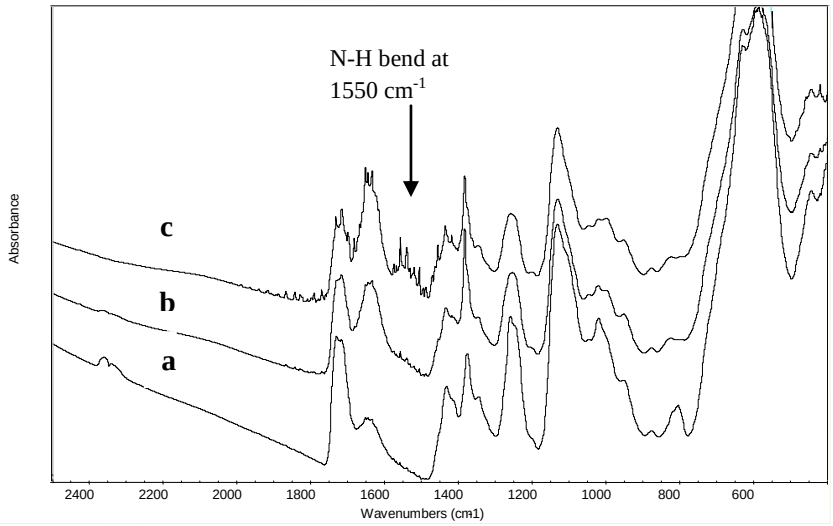

Figure 3.13 FT-IR spectra of: **a**- Unmodified M-PVA support (batch 5); **b**- M-PVA grafted with pNIPAAm by adding first the cerium (IV) and **c**- M-PVA grafted with pNIPAAm by adding first the monomer. Note the appearance of N-H bend at 1550 cm^{-1} due to pNIPAAm backbone.

Adding the cerium first in the reaction, initiation sites are instantly formed at high concentrations and as a prossible consequence the polymerisation rate changes while termination takes place faster (i.e. termination predominates over propagation). Hritsu *et al.* (1999) also observed that incremental addition of the initiator and monomer delivered higher

polymer yield during cerium (IV) grafting. These findings suggest that further investigation of the mechanism taking place in such cases is required.

3.4.3.3.4 Kinetic studies of cerium (IV) initiated graft polymerisation of NIPAAm

Kinetic measurements were performed, by determining the monomer and cerium (IV) consumption simultaneously at different time periods. The monomer consumption was determined by quantifying the amount the unreacted substance (NIPAAm) using ATR FT-IR, while the percentage of cerium (IV) disappearance was followed spectrophotometrically at its λ_{max} (353 nm). In Fig. 3.14, it is shown that cerium (IV) has almost completely consumed before the first 15 min of the reaction. Within the same time period the maximum amount of monomer consumed has been reached. These results indicate that the polymerisation reaction terminates fast and reaches completion in less than a few minutes, as the percent grafting does not change appreciably during the rest course of reaction. The same trend is observed when cerium (IV) is added into the reaction mixture before the monomer, however the percent conversion is lower.

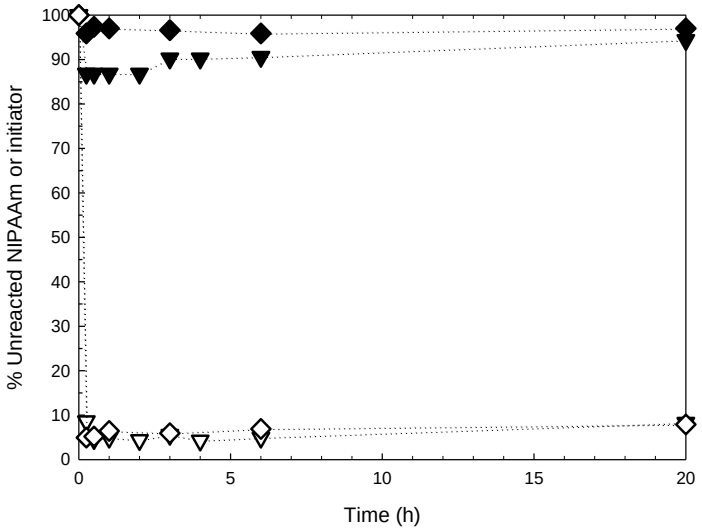

Figure 3.14 Kinetic studies of cerium (IV) initiated polymerisation reactions of 0.44 mmol g^{-1} NIPAAm reacted per M-PVA (target chain length of 100 monomer units). NIPAAm (black down triangles) and cerium (IV) (white down triangles) consumption for standard order of addition using batch 4; NIPAAm (black diamonds) and cerium (IV) (white diamonds) consumption for reverse order of addition using batch 5.

It has been reported that in some cases, and especially at high cerium (IV) concentrations, the formation of homopolymer chains in solution competes with grafting on the surface (Sharma *et al.*, 2002). Gupta and Khandekar (2003), observed that when grafting NIPAAm on cellulose via cerium (IV) initiated polymerization, however at insignificant amounts. In this work, no such indication was noticed by examination of the reactions supernatants: no increase in viscosity due to polymerization in solution and the FT-IR spectra exhibited peaks only for the relevant monomers and not their polymers. Generally, in cerium (IV) initiated polymerization reactions two different termination mechanisms have been proposed, i.e. that of linear termination by cerium (IV) and that by mutual termination (Chapter 2, Section 2.2, Eq. 2.5 and 2.6) (Sarac 1996 and 1999; Ozturk and Cakmak, 2007). In bimolecular termination either combination or disproportionation of two growing polymer radicals may occur. The combination reaction (i.e. $\dot{M}_x+\dot{M}_y \rightarrow M_{x+y}$) results in the formation of one dead

polymer chain, while termination by disproportionation (i.e. $\dot{M}_x+\dot{M}_y \rightarrow M_x + M_y$) results in the formation of two polymer chains (Misra and Bajpai, 1982). In this system, where high concentrations of initiator are introduced to grow the chains very close to each other, premature termination of the reactions by the said mechanisms is unavoidable.

3.4.3.4 SEM analysis and EDX characterization

In this section, the physical characteristics of unmodified and polymer modified M-PVA supports were examined by obtaining images under different modes of the SEM microscope. In addition, EDX analysis was performed to a numerous beads at different conditions and modifications.

3.4.3.4.1 SEM imaging analysis

The images of beads before and after functionalisation with pNIPAAm are presented at wet state (a and b, Fig. 3.15, ESEM mode), dry state (c and d, Fig. 3.15, SEM mode) and cryo-fixation state (a-d, Fig. 3.16, cryo-SEM mode). In ESEM and SEM mode no significant size differences between the modified and unmodified supports are observed. This can be attributed to the very low thickness of the added pNIPAAm nano-film in comparison with that of PVA. It is also noticeable, that under the ESEM mode (image b, Fig. 3.15) the surface of pNIPAAm grafted supports becomes smoother and more homogenous than the unmodified one due to the film coverage. Under the SEM mode (image d, Fig. 3.15) this is not observable as the particles are at dry state.

a **b**

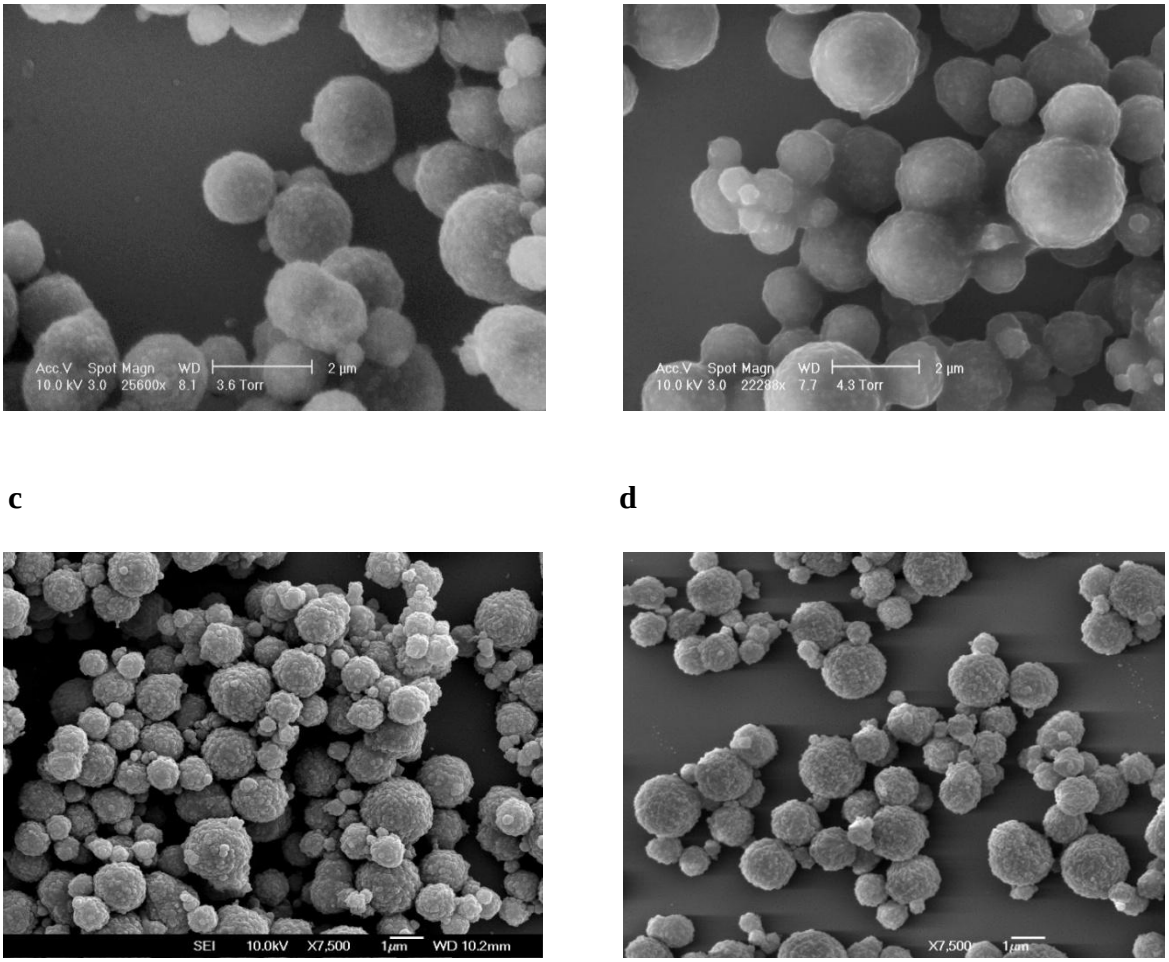

c **d**

Figure 3.15 ESEM and SEM images: **a** and **b-** M-PVA (batch 3) and pNIPAAm$_{30.3}$ – 4.6 Å respectively under the ESEM mode; **c** and **d-** M-PVA (batch 4) and pNIPAAm$_{21.3}$ – 4.6 Å respectively under the SEM mode.

In images b and d in Fig. 3.16 of cryo-SEM mode, the pNIPAAm modified supports have gained a swollen morphology. This can be attributed mainly to the method which allows the sample to be preserved and recorded in its fully hydrated and unmodified state. However, part of the sample was not in such a swollen condition indicating that some of the pNIPAAm particles were remained more hydrated than others.

a

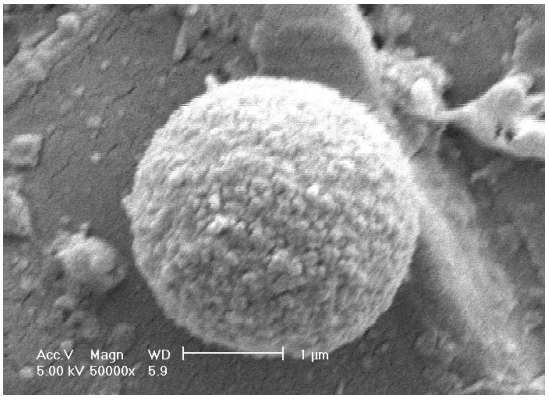

b

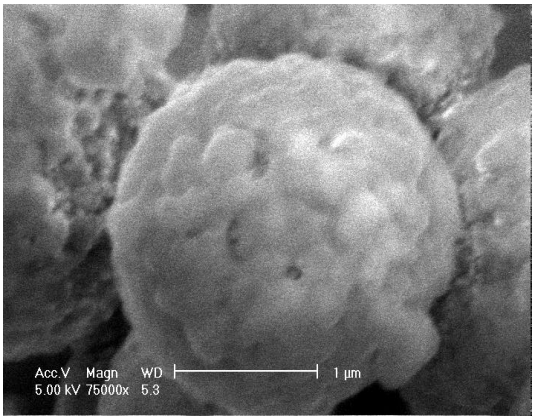

c

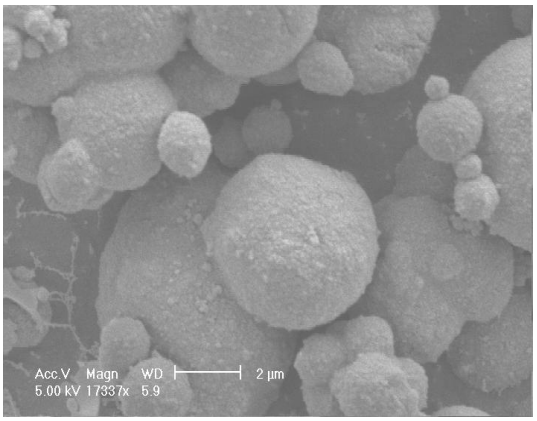

d

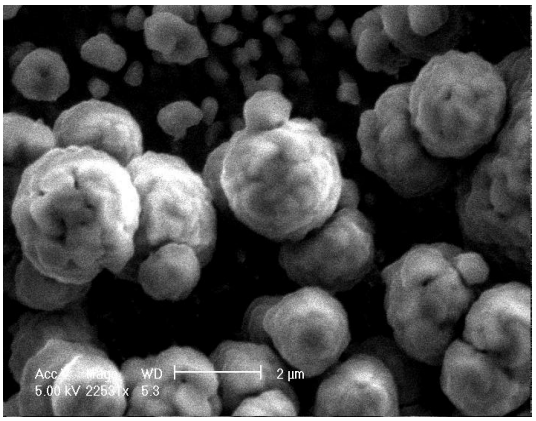

Figure 3.16 Cryo-SEM images: **a** and **c**- M-PVA (batch 3); **b** and **d**- pNIPAAm$_{30.3}$ – 4.6 Å under the cryo-SEM mode.

3.4.3.4.2 SEM and Energy Dispersive X-Ray (EDX) analysis of M-PVA supports at various stages of cerium (IV) initiated polymerisation reaction and under different buffer conditions

SEM in combination of EDX analysis was used for imaging and elemental analysis of M-PVA supports at different conditions and modifications. Primarily, this method was used semi-quantitative and exploited as a qualitative measure indicating the presence or the absence of specific elements, if possible.

All the samples analysed, were placed beforehand onto a sample holder covered with circular slides composed mainly by SiO_2 and Platinum. The EDX spectrum and the total elemental composition of a scan of this slide is given in the Appendix section 7.6.1 (Fig. 7.15), so that the possible contribution to other samples introduced from this surface could be taken account. Due to the depth of the EDX beam which penetrates the surface of the bead at high extend (it was not possible to see any differences on modified supports introduced into water or buffer (i.e. that of pNIPAAm, pVI and pVBIDA, Appendix section Fig. 7.30, 7.25 and 7.22 respectively). At 10 kV, the beam will penetrate into Ni about 250 nm (closest element to Fe) and Si (similar density to the PVA) about 1 micron. In addition, due to peak interferences it was not possible to identify cerium on activated samples (Appendix section 7.6.4, Fig. 7.28 and 7.29). However, the analysis was found efficient to identify the Cu^{+2} ions bound onto the charged supports as show in the next paragraph.

3.4.3.4.2.1 Elemental analysis of uncharged or charged with Cu^{2+} ions M-PVA supports in buffers of different ionic strength

Two different batches of M-PVA support were analysed unwashed (as supplied form Chemagen Biopolymer-Technologie AG) as well as after being washed with the standard washing regime used (section 3.3.2) before any functionalisation. According to Fig. 3.17, the magnetic particles exhibited peaks for carbon (C) at 0.2774 keV (at Kα principal line), oxygen (O) at 0.5249 keV (at Kα principal line), and iron (Fe) at 6.3896 and 0.7048 keV (at Kα and Lα principal lines respectively for different oxidation states i.e., 2 or 3). The oxygen and iron peaks correspond to the magnetite (Iron(II,III) oxide or $FeO{\cdot}Fe_2O_3$) content of the particles, while the carbon peak correspond to the backbone of poly vinyl alcohol accommodating the iron oxide. The results were similar for batches 4 and 5, washed and unwashed, indicating the presence of the same elements (Appendix section 7.6.1, Fig. 7.16-7.18).

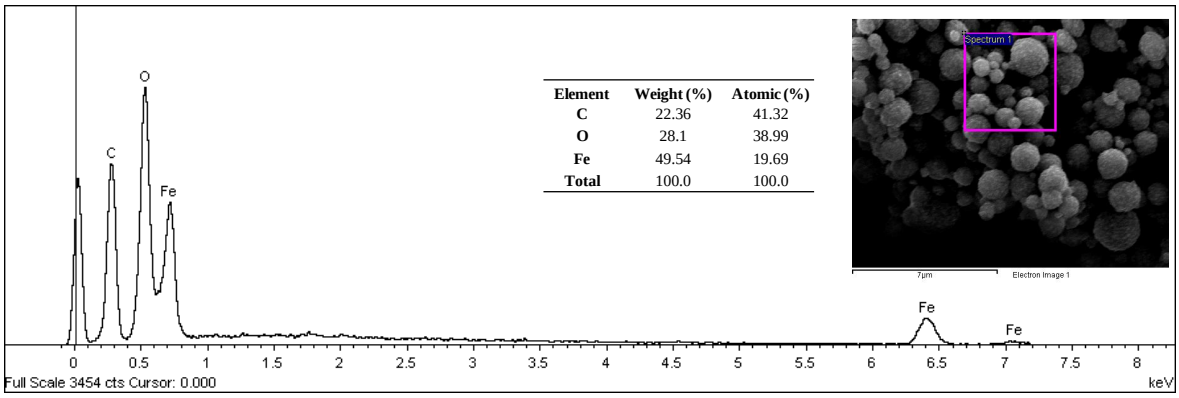

Figure 3.17 EDX spectrum, SEM image and elemental analysis of M-PVA (batch 4) as supplied (unwashed).

M-PVA support (batch 4) was introduced into 100 mM Sodium Phosphate and 1 M NaCl buffer (Appendix section 7.6.2, Fig. 7.19). The new peaks at 1.0410 keV and 2.0134 keV (for Na and P respectively) appearing at these spectra corresponded to the elements of buffer

introduced. However for all the samples, peaks of oxygen and Na might be contributed from the sample stub. Peaks of Pt (at 2.0485 keV), Si (at 1.7398 keV) and K (at 3.3129 keV) have been omitted during quantification as they can be only provided from the stub.

The same support was charged with Cu^{2+} ions, washed twice and analysed with the above procedure in the same buffer (Fig. 3.18). The relative X-Ray intensities for Kα and Lα lines of Cupper (Cu) are at 8.0413 and 0.9297 keV respectively. The peak at Lα line for Cu is very near with that of Na. Although this interference, when the sample is charged, the said peak becomes broader i.e. at 0.9000 to 1.0000 keV. This indicates the possibility of small amount of ions still remained after washing onto the particles after charging. Probably a small amount of Cu^{2+} ions may be adsorbed forming a weak complex with the –OH groups of PVA as has been mentioned by Pitfield (1992).

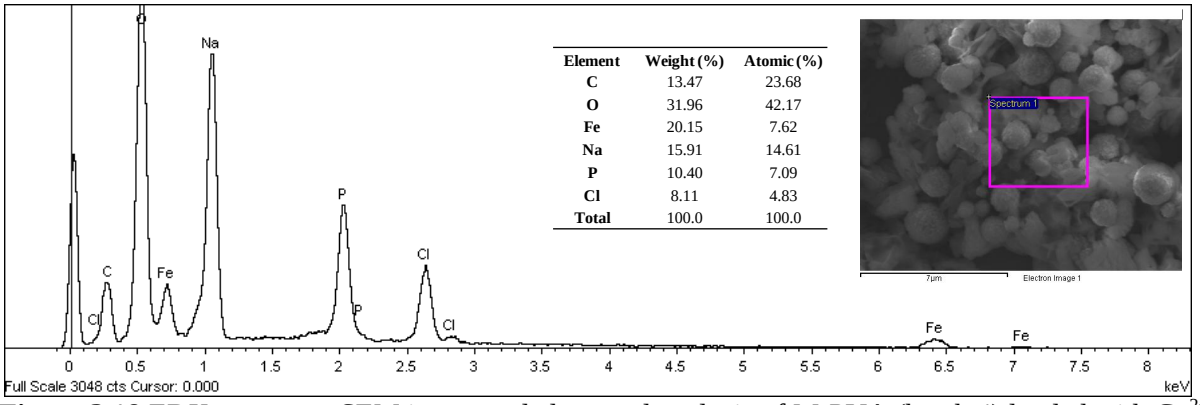

Element	Weight (%)	Atomic (%)
C	13.47	23.68
O	31.96	42.17
Fe	20.15	7.62
Na	15.91	14.61
P	10.40	7.09
Cl	8.11	4.83
Total	100.0	100.0

Figure 3.18 EDX spectrum, SEM image and elemental analysis of M-PVA (batch 4) loaded with Cu^{2+} ions, washed and introduced into 100mM Sodium Phosphate and 1 M NaCl buffer.

M-PVA supports (batch 4) modified with affinity ligands (VBIDA and VI) were also introduced to 100 mM Sodium Phosphate and 1 M NaCl buffer (uncharged) and analysed with EDX (Appendix section 7.6.3, Fig. 7.22 and Fig. 7.25). The same supports were charged with Cu^{2+} ions, washed twice with the same buffers and analysed with the same method described before (Fig. 3.19 and Fig. 3.20).

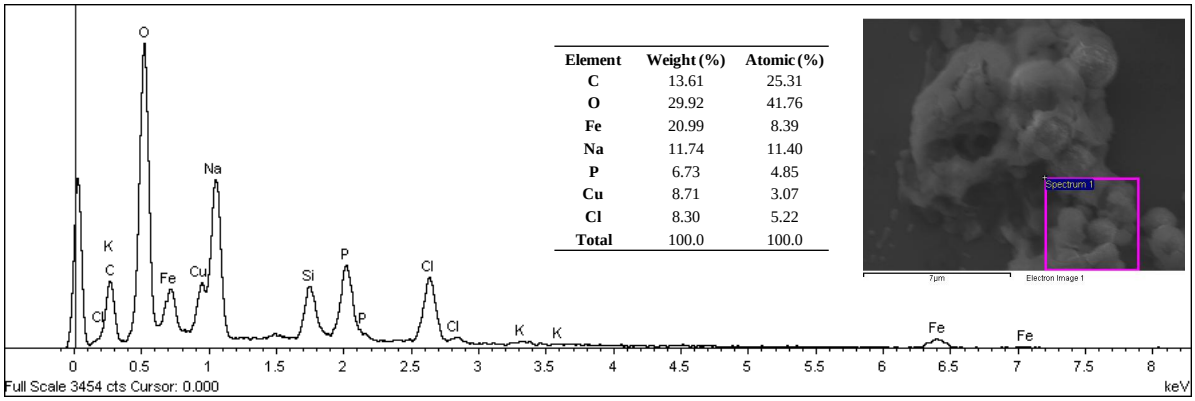

Element	Weight (%)	Atomic (%)
C	13.61	25.31
O	29.92	41.76
Fe	20.99	8.39
Na	11.74	11.40
P	6.73	4.85
Cu	8.71	3.07
Cl	8.30	5.22
Total	100.0	100.0

Figure 3.19 EDX spectrum, SEM image and elemental analysis of M-PVA (batch 4) installed with pVBIDA and loaded with Cu^{2+} ions (Cu^{2+} - $p(VBIDA)_{16}$ - 4.6 Å), washed and introduced into 100mM Sodium Phosphate and 1 M NaCl buffer.

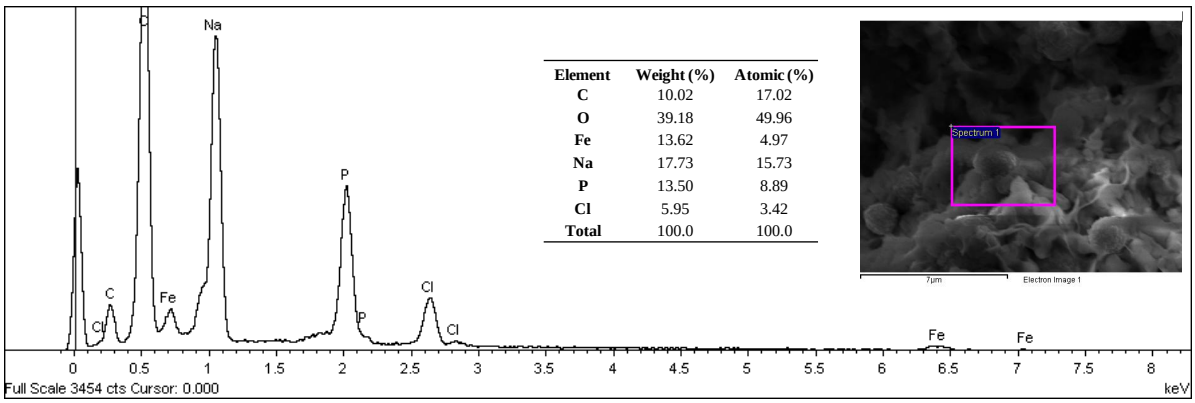

Element	Weight (%)	Atomic (%)
C	10.02	17.02
O	39.18	49.96
Fe	13.62	4.97
Na	17.73	15.73
P	13.50	8.89
Cl	5.95	3.42
Total	100.0	100.0

Figure 3.20 EDX spectrum, SEM image and elemental analysis of M-PVA (batch 4) installed with pVI and loaded with Cu^{2+} ions (Cu^{2+} - $pVI_{36.7}$ - 4.6 Å), washed and introduced into 100 mM Sodium Phosphate buffer and 1 M NaCl.

The relative X-Ray intensities for Kα and Lα lines of Cupper (Cu) are at 8.0413 and 0.9297 keV respectively for the different oxidation states. For the M-PVA support modified with pVBIDA and then charged with metal ions, the peak at 0.9297 keV for Cu is quite clear (Fig. 3.22). The same peak appears also for the pVI modified M-PVA support, however at lower extent. Although the molecular weight of VBIDA introduced during cerium (IV) grafting was less than that of pVI, this result does not come as a surprise. Generally, IDA moieties coordinate better and form stronger complexes with Cu^{2+} ions (1 Cu^{2+} ion is shared by 1-2 IDA groups) than other ligands such as VI (1 Cu^{2+} ion is shared by 2-3 VIs) (Kumar *et al.*, 1998a; Kumar *et al.*, 1999; Ivanov *et al.*, 2001; Porath, 1992).

The sane experiment for unfunctionalised and functionalised M-PVA supports was repeated in Sodium Phosphate buffer without salt (Appendix section 7.6.2 and 7.6.3), however due to peak interferences not any pronounced peak differences were identified.

Although the EDX analysis could not be used quantitatively, it helped to confirm qualitative the metal chelating interactions of affinity ligands introduced onto modified M-PVA supports.

3.4.4 Towards the manufacturing of alternating copolymers: Smart and affinity monomers arranged in an alternating fashion in the grafted chain

Although preparation of copolymers using cerium (IV) initiation is a common approach, attempts to graft vinyl monomers from their mixtures on synthetic and natural polymers is rarer (Gupta and Sahoo, 2001). Graft copolymerisation of acrylonitrile and methyl methacrylate onto cellulose by the use of ceric ion initiator in aqueous medium has been reported from Okieimen and Ogbeifun (1996), and Gupta and Sahoo (2001). The later estimated the reactivity ratios and average sequence lengths of the monomers installed in the grafted chains, indicating the importance of the feed composition to the monomer-monomer interactions and the final composition of the grafted chains.

As an attempt to graft on a magnetic support an alternating copolymer combining two different functionalities, one-pot cerium (IV) initiated reactions were utilised. Initially, the one-pot reactions were performed at batches 1 and 2. However, the reactions were not quantified as at that stage the FT-IR technique was not developed quantitatively. In Table 3.2, the supports that prepared with these batches are given in parallel with the conditions

employed (feed ratio, target total length of chains and spacing). Most of these supports were tested for protein binding and elution and the results are presented later on (section *3.4.6.6*).

When the quantitative FT-IR method was developed a number of new supports were prepared using batch 4 and fully characterised in terms of initiator and monomer consumptions. Taking account the results obtained during the homopolymer brush construction, such as the fast kinetics, the reactivity variation between monomers, the percentages of conversion, and the adjacent packing of polymer chains, cerium (IV) reactions took place under specific considerations. Not only the ratio between the two monomers (NIPAAm:VI) in the reaction was varied, but also the spacing between the graft sites (by decreasing the cerium concentration onto M-PVA support).

Different materials were prepared by: (a) varying the feed ratio (NIPAAm:VI) between the two monomers added (4:1, 2:1 and 1:1) for a fixed ACN concentration onto support (0.44 mmol g^{-1}), and (b) reducing the ACN concentration (0.044 mmol g^{-1}) for a 4:1 ratio between NIPAAm and VI. For all the reactions, the total amount of monomer added was such that a target length of 100 monomer units was aimed. In Table 3.3, the reactivities in terms of monomer (NIPAAm and VI) installed (in monomer units and mmol g^{-1}) after performing the above set of reactions on M-PVA batch 4 are given.

Table 3.2 Attempts at manufacturing alternating copolymer brush supports in one pot Ce(IV) initiated graft from polymerisation reactions (with batches 1 & 2).

Support #	M-PVA starting material		Ce (IV) grafting parameters				Support characterization								Attempted alternating co-polymer brush layer on finished support
	Batch	SA (m^2/g)	Monomers employed *(ratio)*	Order of addition/ reaction solvent	Ce(IV) (mmol/g M-PVA)	Monomer presented (mmol/g M-PVA)	Target DP (units)	React^n (%)	DP (units)	Spacing (Å)	Monomer installed (mmol/g M-PVA)	Polymer (g/g M-PVA)	Polymer (g/g support)	Monomer installed (mmol/g support)	
Co-1.1	1	43	NIPAAm VI *(2:1)*	Std/H_2O	0.44	29.3 14.7 44	66.7 33.3 100	nd nd	nd nd	4.04	nd nd	nd nd	nd nd	nd nd	p(NIPAAm$_{\underline{2}}$-*co*-VI)$_{\underline{100}}$ – 4.0 Å
Co-1.2	1	43	VCL VI *(2:1)*	Std/H_2O	0.44	29.3 14.7 44	66.7 33.3 100	nd nd	nd nd	4.04	nd nd	nd nd	nd nd	nd nd	p(VCL$_{\underline{2}}$-*co*-VI)$_{\underline{100}}$ – 4.0
Co-1.3	1	43	NIPAAm VI *(4:1)*	Std/H_2O	0.044	3.52 0.88 4.4	80 20 100	nd nd	nd nd	12.76	nd nd	nd nd	nd nd	nd nd	p(NIPAAm$_{\underline{4}}$-*co*-VI)$_{\underline{100}}$–12.8 Å
Co-1.4	1	43	VCL VI *(4:1)*	Std/H_2O	0.044	3.52 0.88 4.4	80 20 100	nd nd	nd nd	12.76	nd nd	nd nd	nd nd	nd nd	p(VCL$_{\underline{4}}$-*co*-VI)$_{\underline{100}}$ – 12.8 Å
Co-2.1	2	50	NIPAAm VI *(2:1)*	Std/H_2O	0.44	5.87 2.93 8.8	13.3 6.7 20	nd nd	nd nd	4.35	nd nd	nd nd	nd nd	nd nd	p(NIPAAm$_{\underline{2}}$-*co*-VI)$_{\underline{20}}$ – 4.4 Å
Co-2.2	2	50	NIPAAm VI *(2:1)*	Std/H_2O	0.44	29.3 14.7 44	66.7 33.3 100	nd nd	nd nd	4.35	nd nd	nd nd	nd nd	nd nd	p(NIPAAm$_{\underline{2}}$-*co*-VI)$_{\underline{100}}$ – 4.4 Å
Co-2.3	2	50	NIPAAm VI *(4:1)*	Std/H_2O	0.044	7.04 1.76 8.8	15 5 20	nd nd	nd nd	13.76	nd nd	nd nd	nd nd	nd nd	p(NIPAAm$_{\underline{4}}$-*co*-VI)$_{\underline{20}}$ – 13.8 Å
Co-2.4	2	50	NIPAAm VI *(4:1)*	Std/H_2O	0.044	35.2 8.8 44	80 20 100	nd nd	nd nd	13.76	nd nd	nd nd	nd nd	nd nd	p(NIPAAm$_{\underline{4}}$-*co*-VI)$_{\underline{100}}$ – 13.8 Å

Table 3.3 Attempts at manufacturing alternating copolymer brush supports in one pot Ce(IV) initiated graft from polymerisation reactions with batch 4**.**

Support #	M-PVA starting material		Ce (IV) grafting parameters				Support characterization								Polymer brush description on finished support
	Batch	SA (m^2/g)	Monomers employed *(ratio)*	Order of addition/ reaction solvent	Ce(IV) (mmol/g M-PVA)	Monomer presented (mmol/g M-PVA)	Target DP (units)	React^n (%)	DP (units)	Spacing (Å)	Monomer installed (mmol/g M-PVA)	Polymer (g/g M-PVA)	Polymer (g/g support)	Monomer installed (mmol/g support)	
Co-4.1	4	55	NIPAAm VI *(1:1)*	Std/H_2O	0.44	22 22	50 50 100	11.8 43.4	5.9 21.7 27.6	4.56	2.60 9.55 12.15	0.294 0.898 1.192	0.134 0.410 0.544	1.19 4.36 5.55	Copolymer brush with av. of 21.7 VI and 5.9 NIPAAm units per chain. p($VI_{21.7}$-*co*-$NIPAAm_{5.9}$) – 4.6 Å
Co-4.2	4	55	NIPAAm VI *(1:1)*	Std/H_2O	0.44	22 22	50 50 100	6.0 44.6	3.0 22.3 25.3	4.56	1.32 9.82 11.14	0.149 0.923 1.072	0.072 0.446 0.518	0.64 4.74 5.38	Copolymer brush with av. of 22.3 VI and 3 NIPAAm units per chain. p($VI_{22.3}$-*co*-$NIPAAm_3$) – 4.6 Å
Co-4.3	4	55	NIPAAm VI *(2:1)*	Std/H_2O	0.44	29.3 14.7	66.7 33.3 100	0 52.6	0 17.5 17.5	4.56	0 7.71 7.71	0 0.725 0.725	0 0.420 0.420	0 4.39 4.39	No NIPAAm incorporated. p($VI)_{17.5}$ – 4.6 Å
Co-4.4	4	55	NIPAAm VI *(2:1)*	Std/H_2O	0.44	29.3 14.7	66.7 33.3 100	0 57.7	0 19.2 19.2	4.56	0 8.47 8.47	0 0.796 0.796	0 0.443 0.443	0 4.16 4.16	No NIPAAm incorporated. p($VI)_{19.2}$ – 4.6 Å
Co-4.5	4	55	NIPAAm VI *(4:1)*	Std/H_2O	0.44	35.2 8.8	80 20 100	0 91.2	0 18.2 18.2	4.56	0 8.03 8.03	0 0.755 0.755	0 0.430 0.430	0 4.04 4.04	No NIPAAm incorporated. p($VI)_{18.2}$ – 4.6 Å
Co-4.6	4	55	NIPAAm VI *(4:1)*	Std/H_2O	0.44	35.2 8.8	80 20 100	0 91.2	0 18.2 18.2	4.56	0 8.03 8.03	0 0.755 0.755	0 0.430 0.430	0 4.04 4.04	No NIPAAm incorporated. p($VI)_{18.2}$ – 4.6 Å
Co-4.7	4	55	NIPAAm VI *(4:1)*	Std/H_2O	0.044	3.52 0.88	80 20 100	9.7 100	7.8 20.0 37.8	14.43	0.341 0.880 1.221	0.038 0.083 0.121	0.034 0.074 0.108	0.30 0.79 1.09	Copolymer brush with av. of 20 VI and 7.8 NIPAAm units per chain. p(VI_{20}-*co*-$NIPAAm_{7.8}$) – 14.4 Å

At higher concentrations of cerium (IV) (i.e. 0.44 mmol g^{-1}) in the reaction mixture, the percentages of conversions were found less than that of reduced concentration of cerium (0.044 mmol g^{-1}). This can be explained as by increasing the concentration of the initiator there is more chance for premature termination of growing chain radicals, which in turn reduces the degree of polymerisation (Behari *et al*., 1993; Gupta and Khandekar, 2003). Additionally, there is a preference for VI polymerisation instead of NIPAAm. This corresponds to previous results, where there are higher degrees of VI conversions in comparison with that of NIPAAm. So as there is competition between the two monomers for cerium grafting, there is more chance for VI to react during these fast polymerisation reactions. By decreasing the concentration of cerium, there is a total (100%) conversion of VI and polymerisation may proceed further, where NIPAAm also starts to participate into the reaction (Table 3.3, support Co-4.7). As a consequence, instead of alternating copolymers, either pVI homopolymers or pVI with short pNIPAAm cap block copolymers were formed depending on the amount of initiator and feed composition (the illustration of block copolymers is given in Fig. 3.21).

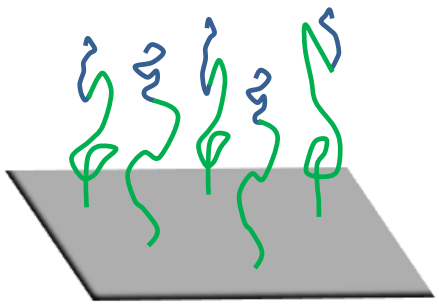

Figure 3.21 Di-block polymer brush; pVI block (green) is attached onto the M-PVA surface while end grafted with pNIPAAm block (blue).

Observation on the supernatants of the above reactions, indicated almost complete consumption of cerium (IV) (no colour detection) and no homo-polymerisation taking place

in the aqueous solution according to their resulting ATR FT-IR spectra (initiation takes place onto the M-PVA surface as in the case of homopolymer brushes). Additionally, the modified particles grafted with pVI were still soluble after the reaction indicating no cross linking.

From these results, it can be said, that by increasing the amount of initiator, the polymerisation rate is also increased and so the reaction terminates faster. So by increasing the spacing between the graft sites (i.e. decreasing the amount of initiator), brushes with longer chains can be created.

3.4.5 Thermoresponsive properties of NIPAAm modified supports

The thermo-responsive behaviour of two different M-PVA batches (batch 1; U2-3236 and batch 3; R2-0105096) modified with pNIPAAm (of increasing content or copolymerised with VI) was examined by investigating their settling behaviour in 1.0 mM Sodium Phosphate buffer, pH 7.0. Initially, the optical density of the modified supports was measured at 500 nm and their corresponding apparent extinction coefficient was correlated with the amount of NIPAAm grafted on the supports (Fig. 3.22). The extinction coefficients of the supports were calculated using their optical density at given concentrations. However, the optical density of the supports was dependent not only on the batch morphology and optical properties, but also on the amount of NIPAAm grafted on them. In Fig. 3.23 the apparent particle extinction coefficients have been normalised and correlated with the NIPAAm content of the supports. For both batches, the coefficients decreased with NIPAAm content in a linear fashion.

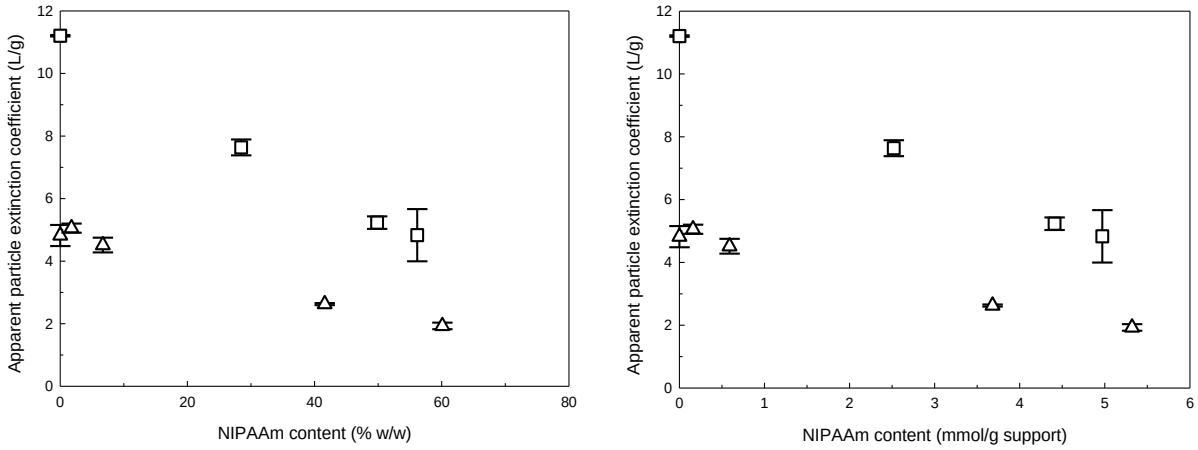

Figure 3.22 Apparent particle extinction coefficient versus NIPAAm content: batch 1; squares and batch 2; up triangles.

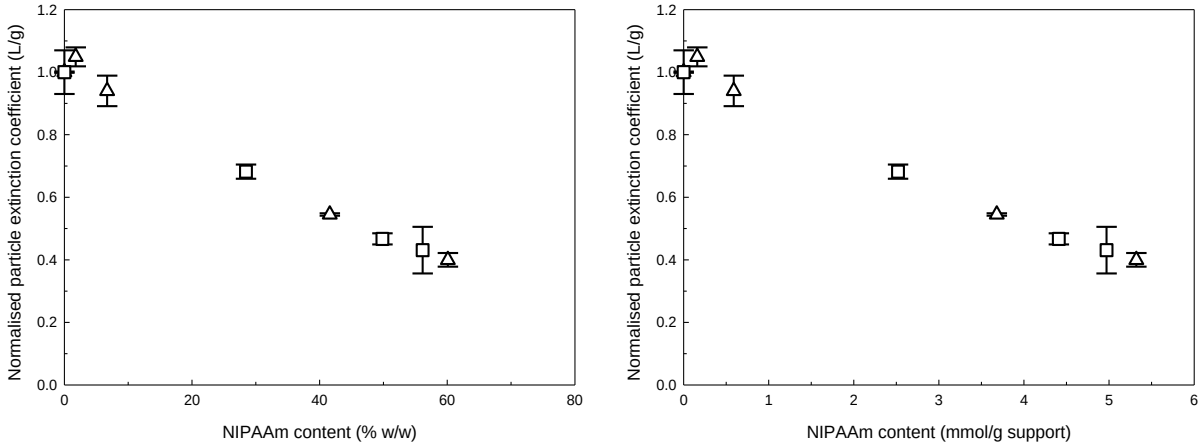

Figure 3.23 Normalised particle extinction coefficient versus NIPAAm content: batch 1; squares and batch 2; up triangles.

The settling experiments for both batches were performed at a particle concentration of ca. 0.2 g/L modified supports, however at different cuvette configuration. For batch 1, the restricted type of semi-micro (pathway 10 mm) acrylic cuvettes was used. For batch 3, the non-restricted type of polystyrene cuvettes (optical pathway 10 mm) was used. In Fig 3.24-3.28, the settling profiles of M-PVA (batch 1), $pNIPAAm_8$ – 4.0 Å, $pNIPAAm_{20}$ – 4.0 Å, $pNIPAAm_{38}$ – 4.0 Å and $p(NIPAAm_{\underline{4}}\text{-}co\text{-}VI)_{\underline{100}}$ – 12.8 Å supports are presented by following the OD_{500} remaining (%) versus time at different temperatures. Although the $p(NIPAAm_{\underline{4}}\text{-}co\text{-}$

VI)$_{\underline{100}}$ – 12.8 Å (co-1.3, Table 3.2) support was not characterised with FT-IR in terms of monomer consumption, it is expected that will be of similar composition with p(VI_{20}-*co*-$NIPAAm_{7.8}$) – 13.8 Å support (co-4.7, Table 3.3) prepared using batch 4 under exactly the same conditions. Based on that, the extinction coefficient of that support was estimated at 9.8 L/g by extrapolating the assumed polymer amount grafted on the support using Fig. 3.22 (i.e. the particle extinction coefficient versus NIPAAm content graph). In Fig 3.29-3.33, the settling profiles of M-PVA (batch 3), $pNIPAAm_{0.4}$ – 4.6 Å, $pNIPAAm_{1.4}$ – 4.6 Å, $pNIPAAm_{14}$ – 4.6 Å and $pNIPAAm_{30.3}$ – 4.6 Å supports are presented.

Batch 1

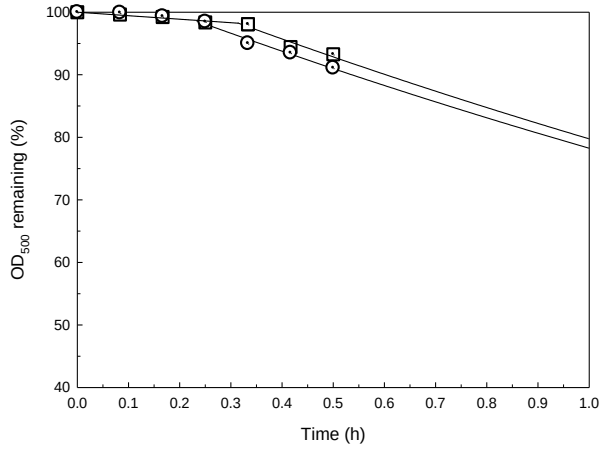

Figure 3.24 OD_{500} remaining (%) versus time for M-PVA (batch 1): 28 ° C (squares), 32 °C (circles).
Mean starting OD: 1.0415± 0.0021, (n=2)

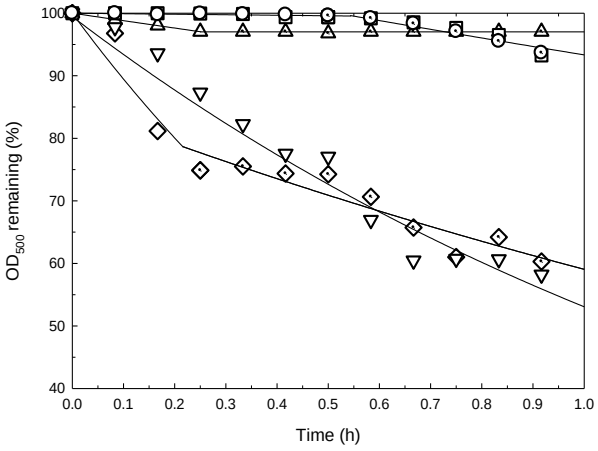

Figure 3.25 OD_{500} remaining (%) versus time for $pNIPAAm_8$ – 4.0 Å (Homo-1.1): 24 °C (squares), 27 °C (circles), 30 °C (up triangles), 34 °C (down triangles), 37 °C (diamonds).
Mean starting OD: 1.5274± 0.0508, (n=5)

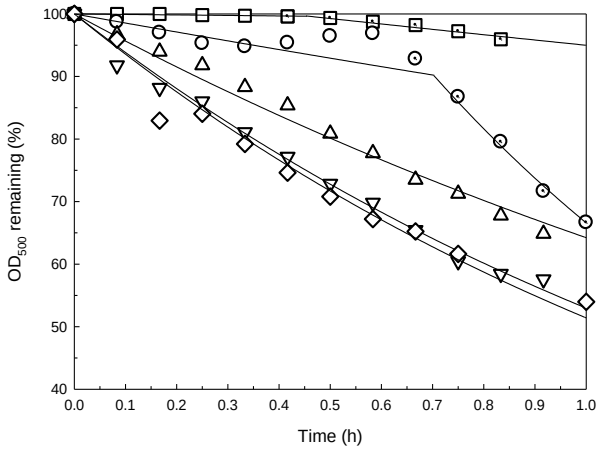

Figure 3.26 OD_{500} remaining (%) versus time for $pNIPAAm_{20}$ – 4.0 Å (Homo-1.2): 27 ° C (squares), 31 °C (circles), 33 °C (up triangles) 40 °C (down triangles), 52 °C (diamonds).
Mean starting OD: 1.3605± 0.05187, (n=6)

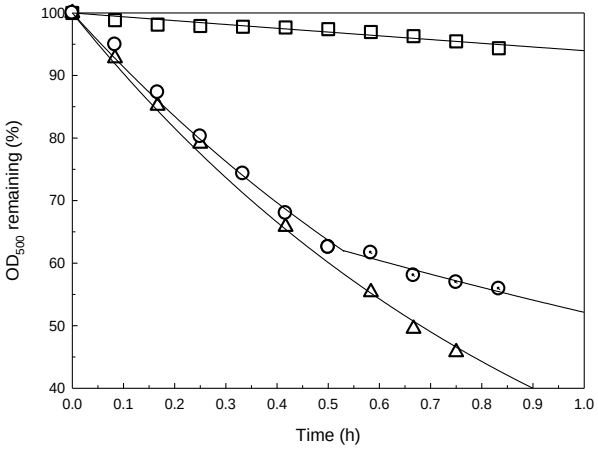

Figure 3.27 OD_{500} remaining (%) versus time for $pNIPAAm_{38}$ – 4.0 Å (Homo-1.3): 23 ° C (squares), 35 °C (circles) , 40 °C (up triangles).
Mean starting OD: 1.1129± 0.192, (n=3)

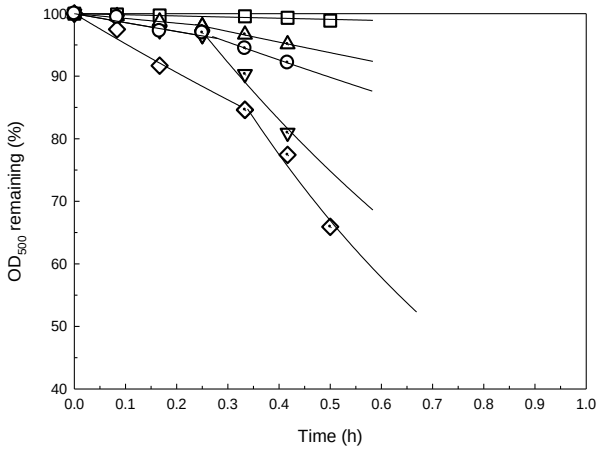

Figure 3.28 OD_{500} remaining (%) versus time for $p(NIPAAm_{\underline{4}}\text{-}co\text{-}VI)_{\underline{100}}$ – 12.8 Å (co-1.3): 24 ° C (squares), 28 °C (circles), 30 °C (up triangles) 32 °C (down triangles), 35 °C (diamonds).
Mean starting OD: 1.1393± 0.132, (n=5)

Batch 3

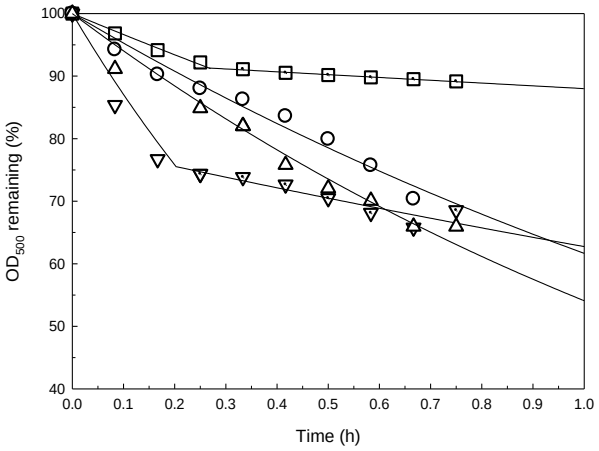

Figure 3.29 OD_{500} remaining (%) versus time for M-PVA (batch 3): 25.7 ° C (squares), 32.6 °C (circles), 35 °C (up triangles), 40.5 °C (down triangles).
Starting OD: 1.3270± 0.0927, (n=4)

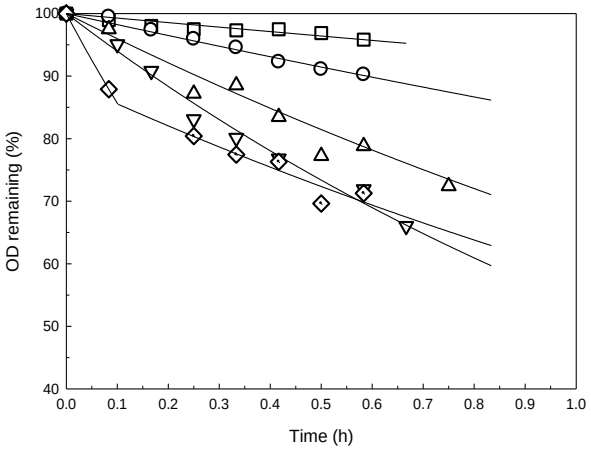

Figure 3.30 OD_{500} remaining (%) versus time for): $pNIPAAm_{0.4}$ – 4.6 Å (Homo-3.1): 25 ° C (squares), 28 °C (circles), 30 °C (up triangles), 32 °C (down triangles), 35 °C (diamonds).
Starting OD: 1.198± 0.0347, (n=5)

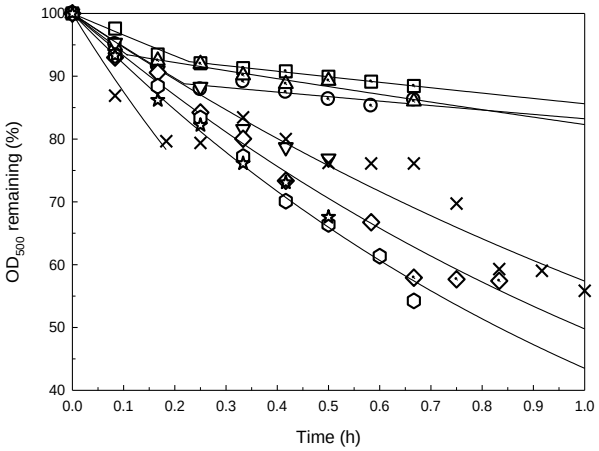

Figure 3.31 OD_{500} remaining (%) versus time for $pNIPAAm_{1.4}$ – 4.6 Å (Homo-3.2): 25 ° C (squares), 28 °C (circles), 30 °C (up triangles), 31 °C (down triangles), 32 °C (diamonds), 33 °C (hexagons), 35 ° (stars), 40 °C (X).
Starting OD: 1.1258± 0.05853, (n=8)

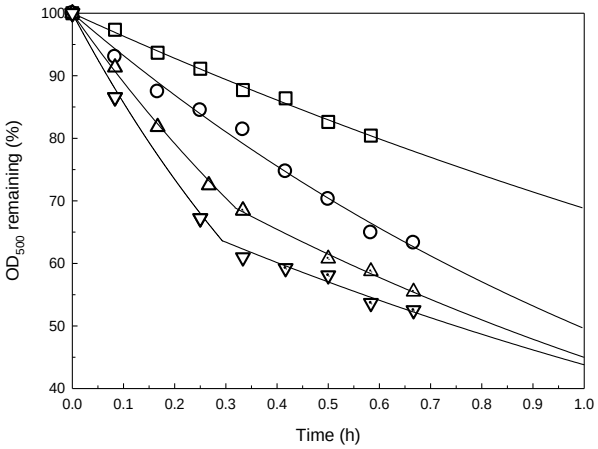

Figure 3.32 OD_{500} remaining (%) versus time for $pNIPAAm_{14}$ – 4.6 Å (Homo-3.3): 30 ° C (squares), 31 °C (circles), 32 °C (up triangles), 33 °C (down triangles).
Starting OD: 1.045± 0.0075, (n=5)

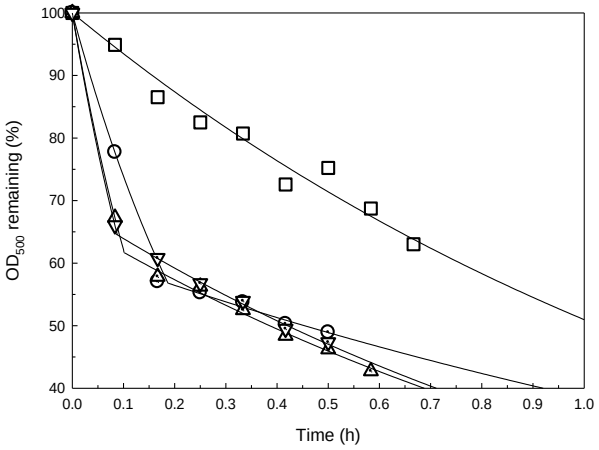

Figure 3.33 OD_{500} remaining (%) versus time for $pNIPAAm_{30.3}$ – 4.6 Å (Homo-3.4): 31 ° C (squares), 32 °C (circles), 33 °C (up triangles), 35 °C (down triangles).
Starting OD: 1.125± 0.06113, (n=6)

For batch 1, on reaching a sufficiently high temperature an appreciable lag phase is observed before the settling rate increases in a roughly linear fashion ($pNIPAAm_{20}$ – 4.0 Å at 31 °C for example in Fig. 3.26). This lag phase tends to be reduced as the temperature is further increased, and also appears to be related to the NIPAAm content. The lag phase probably represents a slow transformation (collapse) of the tethered hydrophilic polymer chains to the hydrophobic state, and that only once the particle exterior surfaces are sufficiently hydrophobic, particle-particle aggregation and enhanced settling will occur. For batch 3, this lag phase is absent ($pNIPAAm_{14}$ – 4.6 Å at 31 °C for example in Fig. 3.32), however this can be attributed to the morphology differences between the batches and the enhanced settling of the particles in the non-restricted cuvettes.

The data obtained from the settling profiles of the supports was fitted to the following exponential decay function:

$$OD(t) = OD(0)\, e^{-bt} \qquad \text{Eq. (3.2)}$$

In Eq. 3.2, b is the decay constant in h^{-1} and OD(0) is the initial (starting) OD in %. At Table 3.4 and 3.5, the estimated decay constant(s) and decay rate(s) for batch 1 and batch 3 supports are given in h^{-1} and OD/ h. Using the apparent extinction coefficients (L/g), the above decay rates were also expressed as settling rates in mg/Lh. As observed before, the settling behaviour of batch 3 M-PVA is different than that that of batch 1 (i.e. 0.005 mg/Lh for M-PVA batch 1 *cf.* 0.978 mg/Lh for that of batch 3 at 25.7-32 °C region).

Table 3.4 Summary of estimated settling rates at different temperatures for batch 1 supports.

Support description	Temp. (°C)	Time interval (h)	Decay constant (h^{-1})	Decay rate (OD/h)	Initial settling rate (mg/Lh)
M-PVA (batch 1)	28	0-0.33	0.056	0.0006	0.052
		0.33-0.5	0.304	0.0031	0.277
	32	0-0.33	0.056	0.0006	0.052
		0.33-0.5	0.253	0.0025	0.223
Homo-1.1 $pNIPAAm_8$ – 4.0 Å	24	0-0.5	0.008	0.0001	0.017
		0.5-0.92	0.143	0.0022	0.292
	27	0-0.5	0.008	0.0001	0.016
		0.5-0.92	0.143	0.0021	0.279
	30	0-0.92	0.047	0.0007	0.097
	34	0-0.92	0.623	0.0091	1.196
	37	0-0.25	1.112	0.0169	2.210
Homo-1.2 $pNIPAAm_{20}$ – 4.0 Å	27	0-0.42	0.008	0.0001	0.021
		0.42-0.83	0.088	0.0012	0.231
	31	0-0.42	0.147	0.0019	0.371
		0.42-1.0	1.018	0.0128	2.449
	33	0-0.92	0.443	0.0060	1.143
	40	0-0.92	0.635	0.0093	1.770
	52	0-1.0	0.665	0.0089	1.706
Homo-1.3 $pNIPAAm_{38}$ – 4.0 Å	23	0-0.92	0.062	0.0006	0.129
	35	0-0.5	0.904	0.0088	1.823
		0.5-0.83	0.369	0.0036	0.744
	40	0-0.75	1.018	0.0136	2.808
Co-1.3 $p(NIPAAm_{\underline{4}}\text{-}co\text{-}VI)_{\underline{100}}$ – 4.0 Å	24	0-0.5	0.0185	0.0002	0.024
	28	0-0.25	0.0768	0.0008	0.082
		0.25-0.42	0.1783	0.1095	11.176
	30	0-0.25	0.1333	0.0014	0.0142
		0.25-0.42	0.3041	0.1847	18.844
	32	0-0.25	0.1451	0.0015	0.155
		0.25-0.42	1.0434	0.6310	64.392
	35	0-0.33	0.4941	0.0064	0.650
		0.33-0.67	1.4628	0.9576	97.718

Table 3.5 Summary of estimated settling rates at different temperatures for batch 3 supports.

Support description	Temp. (°C)	Time interval (h)	Decay constant (h^{-1})	Decay rate (OD/h)	Initial settling rate (mg/Lh)
M-PVA (batch3)	25.7	0-0.25	0.341	0.0047	0.978
		0.33-0.75	0.050	0.0006	0.131
	32.6	0-0.75	0.483	0.0067	1.383
	35	0-0.75	0.614	0.0083	1.730
	40.5	0-0.25	1.384	0.0165	3.413
		0.25-0.75	0.233	0.0021	0.427
Homo-3.1 $pNIPAAm_{0.4}$ – 4.6 Å	25	0-0.58	0.073	0.0008	0.167
	28	0-0.58	0.179	0.0021	0.417
	30	0-0.75	0.410	0.0049	0.977
	32	0-0.67	0.619	0.0077	1.521
	35	0-0.08	1.547	0.0188	3.719
		0.25-0.58	0.419	0.0041	0.810
Homo-3.2 $pNIPAAm_{1.4}$ – 4.6 Å	25	0-0.25	0.350	0.0041	0.899
		0.33-0.67	0.098	0.0010	0.229
	28	0-0.25	0.526	0.0061	1.353
		0.25-0.67	0.111	0.0011	0.246
	30	0-0.08	0.638	0.0074	1.638
		0.25-0.67	0.146	0.0016	0.345
	31	0-0.5	0.555	0.0058	1.282
	32	0-0.58	0.697	0.0081	1.802
		0.67-0.83	0.461	0.0031	0.690
	33	0-0.67	0.832	0.0086	1.893
	35	0-0.58	0.790	0.0093	2.066
	40	0-0.17	1.334	0.0151	3.339
		0.25-1.0	0.498	0.0045	0.989
Homo-3.3 $pNIPAAm_{14}$ – 4.6 Å	30	0-35	0.374	0.0040	1.507
	31	0-40	0.701	0.0073	2.786
	32	0-20	1.168	0.0122	4.626
		0.33-0.67	0.625	0.0045	1.694
	33	0-20	1.612	0.0168	6.385
		0.42-0.67	0.529	0.0033	1.240
Homo-3.4 $pNIPAAm_{30}$ – 4.6 Å	31	0-67	0.674	0.0069	3.546
	32	0-0.17	3.263	0.0366	18.955
		0.17-0.67	0.479	0.0031	1.587
	33	0-0.17	3.562	0.0427	22.086
		0.17-0.67	0.739	0.0051	2.654
	35	0-0.17	3.726	0.0435	22.490
		0.17-0.67	0.883	0.0054	2.819

In Fig. 3.34, the initial settling rates of each support have been plotted against Temperature (°C). For batch 1, it appears that, the settling rates for the pNIPAAm modified supports increase within the temperature range of 31-33 °C, while that of M-PVA does not. It is known that within this temperature range, the NIPAAm polymer becomes hydrophobic as crosses its LCST and collapse (Heskins and Guillet, 1968; Schild, 1992). So the settling rates are temperature dependent as a result of the transition from the hydrophilic to hydrophobic character of the pNIPAM modified supports above and below the LCST. The same trend is observed for the p(NIPAAm$_{\underline{4}}$-*co*-VI)$_{\underline{100}}$ – 12.8 Å support, however at less extend and few degrees of higher temperature (i.e. settling starts to increase within the range 32-35 °C) due to the following reasons: (a) the lower molecular weight of the polymer grafted; and (b) the incorporation of VI block rendering the copolymer more hydrophilic (Kumar *et al.* 1998a; Kumar *et al.,* 1998b). As above, for batch 3, the settling rates of highly modified pNIPAAm supports were considerably increased within the 31-32 °C range. However, the pNIPAAm$_{0.4}$ – 4.6 Å and pNIPAAm$_{1.4}$ – 4.6 Å did not reveal any thermoresponsive behaviour as the settling rates did not increase with temperature increase. This was expected due to the very low molecular weight of pNIPAAm grafted onto these supports.

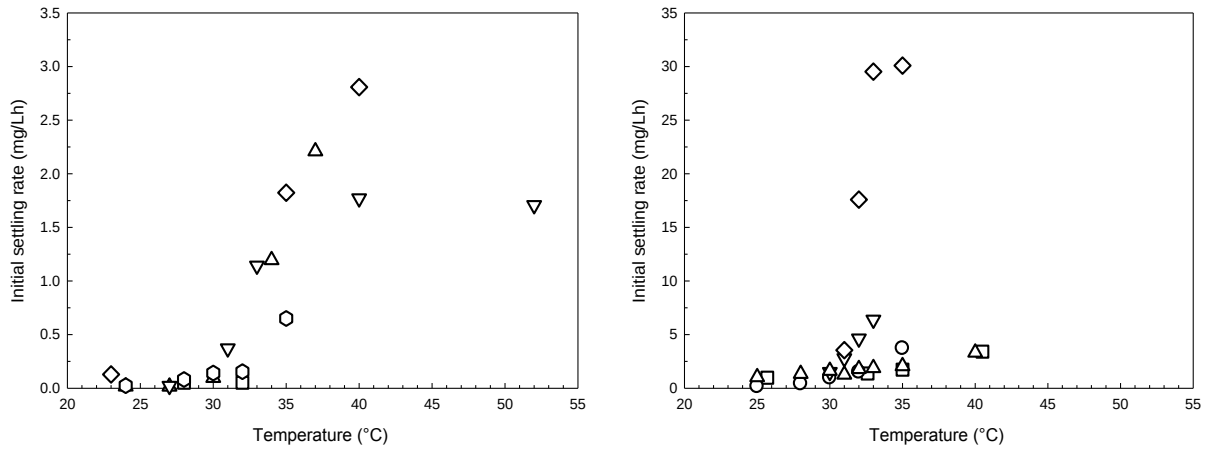

Figure 3.34 Initial settling rate versus temperature for batch 1 (Left Hand Side) and batch 3 (Right Hand Side). **LHS:** M-PVA (squares), $pNIPAAm_8$ – 4.0 Å (up triangles), $pNIPAAm_{20}$ – 4.0 Å (down triangles), $pNIPAAm_{38}$ – 4.0 Å (diamonds) and $p(NIPAAm_{\underline{4}}\text{-}co\text{-}VI)_{\underline{100}}$ – 12.8 Å (hex). **RHS:** M-PVA (squares), $pNIPAAm_{0.4}$ – 4.6 Å (circles), $pNIPAAm_{1.4}$ – 4.6 Å (up triangles), $pNIPAAm_{14}$ – 4.6 Å (down triangles), $pNIPAAm_{30.3}$ – 4.6 Å (diamonds).

Despite the different configuration and base supports used between the two experiments, the developed assay was found capable to demonstrate the thermoresponsive behaviour of the pNIPAAm functionalised beads and detect their LCST at high sensitivity. In addition, for both batches, at increasing degree of modification the transition becomes more obvious. It is clear that the lower transition temperature for pNIPAAm chains tethered on M-PVA surfaces is within the reported range of 32-34 ºC (Heskins and Guillet, 1968; Schild, 1992). However, the LCST of the pNIPAAm modified materials can be shifted under certain conditions. For example, the introduction of hydrophilic affinity moieties such as vinylimidazole and their charging with Cu^{2+} ions it is expected to increase the LCST (Kumar *et al*., 1998a). On the other hand, the addition of salt will decrease the LCST with increasing concentration (Schild and Tirrell, 1991; Inomata *et al.*, 1992; Park and Hoffman, 1993; Dhara and Chatterji, 2000; Zhang and Cremer, 2006). For these reasons, further examination could be useful to investigate the effect of such parameters on pNIPAAm collapse and its thermorsponsive behaviour.

It has been both predicted and observed, that the phase behaviour is influenced by the grafting density, architecture and molecular weight of the tethered pNIPAAm chains (Baulin and Halperin, 2003; Yim *et al*., 2004; Plunkett, 2006). Chain collapse above the LCST, takes place at high grafting density and molecular weight, while at low molecular weights pNIPAAm does not collapse (Zhu *et al*., 2007). Generally, the chain collapse behaviour of pNIPAAm tethered on a surface is quite different than that of free pNIPAAm in solution (Zhulina *et al.,* 1991; Wu *et al*., 2008). Some authors suggest that in tethered polymer brushes the chains are configured in a dense inner phase and a more dilute compressible outer phase (Halperin 1998; Baulin and Halperin 2003; Plunkett, 2006; Wu *et al*., 2008). As a consequence, the inner region demonstrates a lower transition temperature than that of the outer region (Shan *et al*., 2004 in Wu *et a*l., 2008). In contrast, other authors argue that the pNIPAAm transition on planar surfaces occurs in a wider range in relation with that of coil to globule transition in aqueous solutions (Hu *et al*., 2002; Balamurugan *et al*., 2003; Kizhakkedathu *et al*., 2004; Zhu and Napper, 1994; Zhu and Napper 1997). In such cases, the transition is of second order and the collapse begins from the outer more dilute layer (Zhulina *et al.,* 1991). As in brush regime the chains are highly packed on the surface, inter-chain interactions deduce their weaker collapse on increasing temperature than that in their isolated three-dimensional chain (Zhulina *et al.,* 1991 in Kizhakkedathu *et al.,* 2004). Apart from inter-chain interactions, the transition of the chains depends on solvent quality and curvature of the surface (Zhulina *et al.,* 1991). Lately, Toomey and Tirrell (2008) based on coexistence curve of Afroze *et al.* (2000) and the above observations, concluded that the structure of the polymer brush (molecular weight and surface density), defines the developed hydrophobic-hydrophilic balances and as a consequence, it can either collapse continuously or discontinuously (Chapter 1, section *1.5.2.2.1*).

In these results, the phase transition (LCST) for all the pNIPAAm modified supports is observed within the reported range of 31-34 ºC. This suggests that although the polymer chains are close to each other, they are at such configuration which allows their 'free' collapse and expansion above and below their LCST respectively. Due to the nature of the thermoresponsive assay the phase transition is observable as the exterior surface of the particles becomes hydrophobic (settling behaviour is influences by the chain collapse of the outer phase). Same observations have been reported by Gupta and Khandekar (2003) who grafted NIPAAm onto cellulose via cerium (IV) grafting and the LCST of pNIPAAm modified cellulose was detected at 32 °C. In the next section, the regime of the polymer chains grafted on the M-PVAs is investigated to provide a clearer picture of their configuration.

3.4.6 Flory radii and regime of homopolymer chains

The Flory radii (R_F) (Chapter 1, section *1.5.1.2*) of the homopolymer chains grafted on the supports were estimated under three different considerations: (a) assuming 100 % consumption of cerium (IV) as over 95-98 % of that disappeared from the mixtures after the reactions; (b) assuming 70 % of cerium (IV) consumption based on findings of Gupta and Sahoo (2001); and (c) assuming 2 % of cerium (IV) consumption based on findings of Hritcu *et al*. (1999).

The configuration of chains depends on the ratio of density *s* to that of twice the Flory Radius (R_F) as described in Fig. 3.35:

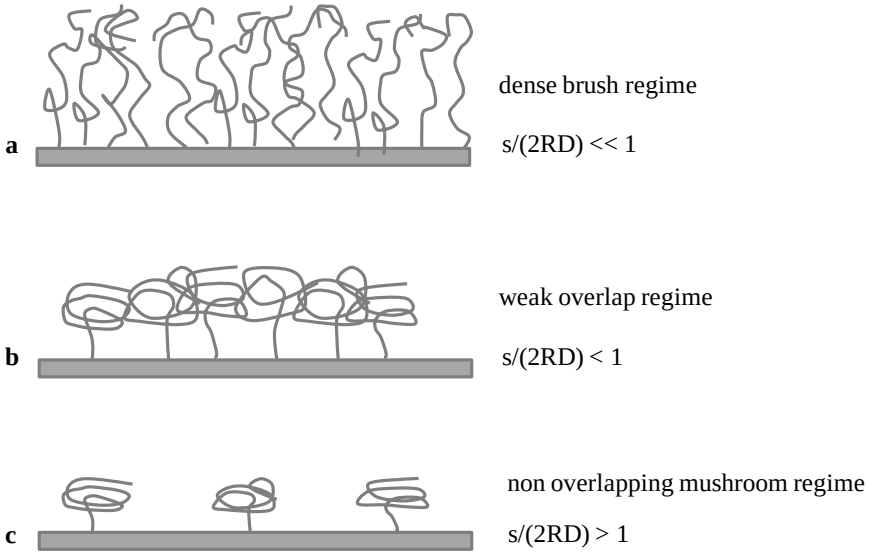

Figure 3.35 Different regimes of grafted chains (reproduced from Zhu *et al*., 2007): **a-** At $s/2R_F$ <<1, the polymer chains form bushes, **b-** At $s/2R_F$ <1, the polymer chains are in the weak overlap regime and **c-** At $s/2R_F$ >1, the polymer chains are in the non overlapping mushroom regime (Israelachvili, 1991; Plunkett *et al*., 2006; Zhu *et al*., 2007).

As shown in Table 3.6, the values of ratio *s*/(2*R*F) in most of the cases (100, 70 and 2 % cerium (IV) consumption) was much smaller than 1 (i.e. the distance between the chains is smaller than twice the RF), indicating that the polymer chains were in the dense brush regime. However, with decreasing cerium (IV) consumption both the spacing and the final length of the polymer chains increase. From the assumptions made, the range of values obtained for 2 % consumption is rather unlikely. Same authors contributed the low grafting efficiency to the homopolymerisation taken place in solution (observed by high molecular weights in solutions and high viscosities of supernatants) instead on the grafting surface (polystyrene latex) (Hritcu *et al*., 1999). In this work, no such observations transpired and no polymerisation was detected in supernatants, indicating that grafting was initiated from the PVA surface and no other site.

Considering the thermoresponsive behaviour of pNIPAAm modified supports in the previous section and the obtained $s/2R_F$ ratios (e.g. ranged from 0.08 – 0.33 for 100 % cerium (IV)

consumption and 100 to 250 monomer units target length), it is expected that the polymers chains are at the brush regime and at length at which the resulting final composition allows their ‘freely’ collapse in solution upon heating at 31-32 °C and above. The phase separation is discontinuous, as the bush architecture is such that hydrophobic forces are favoured above the LCST. Due to higher reactivities and sizes of VI and VBIDA monomers, lower s/(2RF) ratios were obtained, indicating that their grafting delivered polymer chains of even denser brush regime (i.e. $s/2R_F$ ratios ranged between 0.03 – 0.2 for 100 % cerium (IV) consumption).

Table 3.6 Grafting parameters such as density, degree of polymerisation, R_F and $s/(2R_F)$ ratio under different assumptions of % cerium (IV) consumption.

Support #	Monomer employed	100 % cerium (IV) consumption					70 % cerium (IV) consumption					2 % cerium (IV) consumption				
		s (Å)	DP (units)	Segment length *l* (Å)[a]	R_F (Å)	$s/(2R_F)$[b]	s, (Å)	DP (units)	Segment length *l* (Å)[a]	R_F (Å)	$s/(2R_F)$[b]	s (Å)	DP (units)	Segment length *l* (Å)[a]	R_F (Å)	$s/(2R_F)$[b]
Homo-	NIPAAm	4.04	8.0	3.0	10.45	0.19	4.82	11.4	3.0	12.94	0.19	28.54	400.0	3.0	109.23	0.13
Homo-	NIPAAm	4.04	20.0	3.0	18.10	0.11	4.82	28.5	3.0	22.41	0.11	28.54	998.9	3.0	189.16	0.08
Homo-	NIPAAm	4.04	38.0	3.0	26.61	0.08	4.82	54.3	3.0	32.96	0.07	28.54	1900.0	3.0	278.21	0.05
Homo-	VI	4.04	38.2	7.74	68.86	0.03	4.82	54.6	7.74	85.30	0.03	28.54	1910.2	7.74	720.10	0.02
Homo-	NIPAAm	4.56	0.37	3.0	1.65	1.38	5.46	0.5	3.0	2.03	1.35	32.27	18.2	3.0	17.10	0.94
Homo-	NIPAAm	4.56	1.44	3.0	3.73	0.61	5.46	2.0	3.0	4.61	0.59	32.27	71.6	3.0	38.91	0.41
Homo-	NIPAAm	4.56	14.3	3.0	14.80	0.15	5.46	20.4	3.0	18.33	0.15	32.27	714.8	3.0	154.75	0.10
Homo-	NIPAAm	4.56	30.3	3.0	23.23	0.10	5.46	43.2	3.0	28.74	0.09	32.27	1512.5	3.0	242.63	0.07
Homo-	VI	4.56	37	7.74	67.56	0.03	5.46	52.9	7.74	83.74	0.03	32.27	1852.3	7.74	706.91	0.02
Homo-	NIPAAm	4.56	1.62	3.0	4.01	0.57	5.46	2.3	3.0	4.95	0.55	32.27	80.7	3.0	41.80	0.39
Homo-	NIPAAm	4.56	10.3	3.0	12.16	0.19	5.46	14.7	3.0	15.05	0.18	32.27	514.8	3.0	127.08	0.13
Homo-	NIPAAm	4.56	13.2	3.0	14.11	0.16	5.46	18.9	3.0	17.48	0.16	32.27	660.2	3.0	147.55	0.11
Homo-	NIPAAm	4.56	20.8	3.0	18.53	0.12	5.46	29.6	3.0	22.92	0.12	32.27	1037.5	3.0	193.51	0.08
Homo-	NIPAAm	14.43	11.9	3.0	13.26	0.54	17.25	16.9	3.0	16.35	0.53	102.06	590.9	3.0	138.05	0.37
Homo-	VI	4.56	20.0	7.74	46.70	0.05	5.46	28.6	7.74	57.85	0.05	32.27	1000.0	7.74	488.36	0.03
Homo-	VI	4.56	36.7	7.74	67.23	0.03	5.46	52.4	7.74	83.27	0.03	32.27	1835.2	7.74	703.00	0.02
Homo-	VI	4.56	30.9	7.74	60.63	0.04	5.46	44.2	7.74	75.12	0.04	32.27	1545.5	7.74	634.12	0.03
Homo-	VBIDA	4.56	16.0	6.70	35.36	0.06	5.46	22.9	6.70	43.85	0.06	32.27	800.0	6.70	369.77	0.04
Homo-	NIPAAm	4.56	6.4	3.0	9.14	0.25	5.46	9.2	3.0	11.33	0.24	32.27	320.5	3.0	95.63	0.17
Homo-	NIPAAm	4.56	4.1	3.0	7.00	0.33	5.46	5.8	3.0	8.65	0.32	32.27	204.5	3.0	73.05	0.22
Homo-	VI	4.56	22.9	7.74	50.66	0.05	5.46	32.7	7.74	62.76	0.04	32.27	1145.5	7.74	529.82	0.03
Homo-	VI	4.56	6.7	7.74	24.23	0.09	5.46	9.6	7.74	30.03	0.09	32.27	335.2	7.74	253.48	0.06
Homo-	VBIDA	4.56	10.9	6.70	28.09	0.08	5.46	15.6	6.70	34.81	0.08	32.27	545.5	6.70	293.85	0.05
Homo-	VBIDA	4.56	7.0	6.70	21.53	0.11	5.46	10.0	6.70	26.67	0.10	32.27	350.0	6.70	225.17	0.07
Homo-	VBIDA	4.56	2.4	6.70	11.33	0.20	5.46	3.4	6.70	14.06	0.19	32.27	120.5	6.70	118.73	0.14

[a] the size of NIPAAm monomer unit was assumed to be 3 Å (Carey, 1992; Plunkett *et al*., 2006; Zhu *et al*., 2007); the size of VI monomer unit was assumed to be 7.74 Å (Brandrup *et al*., 1989) and the size of VBIDA monomer unit was assumed to be 6.7 Å as that of styrene due to structure similarity (Brandrup *et al*., 1989).
[b] s/(2RF) values < 0.5 are at brush regime, s/(2RF) values between 0.5 – 1.0 are at weak overlap regime and s/(2RF) >1.0 are at non overlapping mushroom regime according to Zhu *et al.* (2007).

3.4.7 Binding and elution studies with haemoglobin

The supports characterised previously were tested for protein binding and elution using haemoglobin as a model protein. Haemoglobin belongs to the group of multimeric proteins, i.e. is a tetramer of two α-chains and two β-chains composed of 141 and 146 amino acid residues respectively (Lukin *et al.,* 2002; Michnik *et al.,* 2005). In these experiments haemoglobin from bovine was used which has 20 exposed histidines able to interact with metal chelating ions and expected to have high strength of binding (Van Dam *et al*., 1989; O' Brien *et al*., 1996). Figueroa *et al.* (1986) noticed that it was difficult to elute haemoglobin from IMAC columns under mild conditions and could not show elution even under relatively strong elution conditions (Figueroa *et al.*, 1986 in Plomer *et al.,* 1996). In this work, this type of protein was selected for subsequent studies of forced thermoresponsive desorption in assisting the cleaning of adsorbed difficult to remove materials from supports. In addition, this protein has strong spectroscopic signals making its quantification easy. The M-PVA supports as well as the homopolymer and co-polymer brushes constructed with cerium (IV) were tested while being charged with Cu^{2+} ions or uncharged, to investigate the adsorption of protein via metal chelating affinity interactions. In addition, the protein binding was investigated under different conditions, such as salinity and temperature. The pH was kept constant near neutrality at which the surface histidines are unprotonated and free to co-ordinate bound metal ions (Todd *et al.,* 1994; O' Brien *et al.,* 1996).

3.4.6.1 Haemoglobin binding onto M-PVA supports

The affinity of M-PVA for haemoglobin binding was examined by performing protein binding on three different batches (batch 3, 4 and 5) of unmodified supports. All of these materials were tested while being charged with Cu^{2+} ions or uncharged, as well as in the presence or absence of 1 M NaCL. The Langmuir isotherms are shown in Fig. 3.36 and the corresponding characteristic parameters are summarised in Table 3.7.

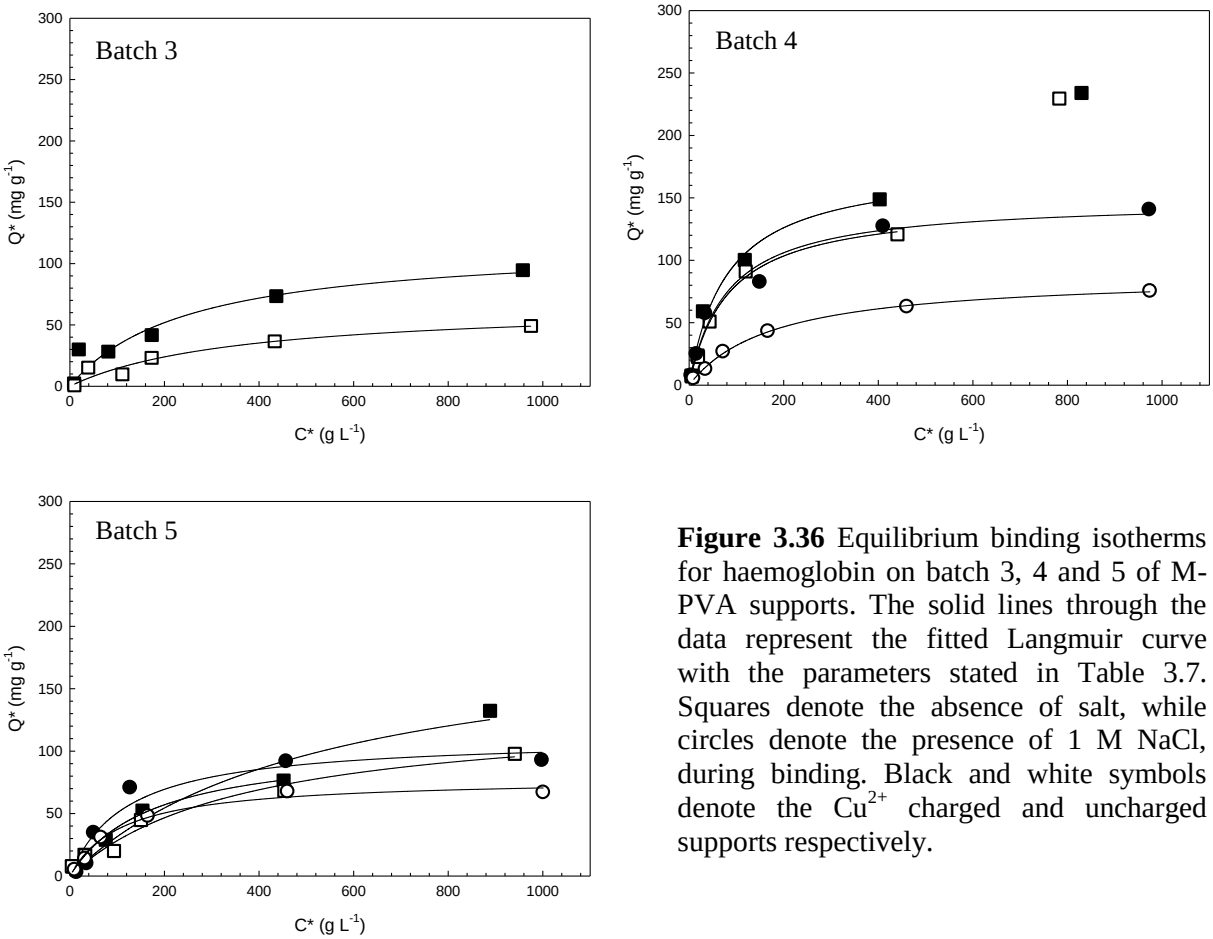

Figure 3.36 Equilibrium binding isotherms for haemoglobin on batch 3, 4 and 5 of M-PVA supports. The solid lines through the data represent the fitted Langmuir curve with the parameters stated in Table 3.7. Squares denote the absence of salt, while circles denote the presence of 1 M NaCl, during binding. Black and white symbols denote the Cu^{2+} charged and uncharged supports respectively.

Table 3.7 Langmuir predicted parameters for the curves fitted in Fig. 3.36.

M-PVA starting material	Support	NaCl conc^{n} in binding buffer (M)	Q_{max} (mg/g)	K_d (μM)	Initial slope (L/g)
Batch 3, lot R2-0105096	M-PVA	0	66	5.6	0.18
	Cu^{2+}- M-PVA	0	121	4.4	0.49
Batch 4, lot R2-0109027	M-PVA	0	146	1.3	1.78
	M-PVA	1.0	86	2.6	0.51
	Cu^{2+}- M-PVA	0	176	1.2	2.21
	Cu^{2+}- M-PVA	1.0	140	1.1	2.03
Batch 5, lot R2-0126067	M-PVA	0	133	5.8	0.36
	M-PVA	1.0	78	1.7	0.71
	Cu^{2+}- M-PVA	0	106	2.7	0.62
	Cu^{2+}- M-PVA	1.0	111	1.9	0.93

Surprisingly, the unmodified M-PVA supports delivered protein binding capacities between 66-146 mg g^{-1} while being uncharged which increased to 106-176 mg g^{-1} when was charged with Cu^{2+} ions (and in the absence of salt). The considerable amount of protein adsorbed onto the base matrix can be attributed to the structure of haemoglobin and the base matrix morphology. It has been reported that, the haemoglobin molecule can be easily adsorbed even on 'neutral' hydrophilic surfaces (Matsui, 2008) as observed here where the M-PVA surface is considered hydrophilic. The increased binding on the charged matrices can be attributed to the affinity of the materials for Cu^{2+} ions (Pitfield, 1992). Although the ions are loosely bound onto –OH groups, even after washing (twice with binding buffer), some still remained on the surface where protein could interact with them. This was observed previously with the EDX analysis (section *3.4.3.4.2.3*), where the possibility for affinity of Cu^{2+} towards the M-PVA matrix was not excluded. The introduction of salt during binding decreased the capacities of the supports (the effect was more pronounced on the uncharged M-PVAs). When the ionic strength of the solvent increases, the charge is shielded by the counterions and as a result the ionic interactions are weakened (Marshak, 1996; Amersham, 2007). As a consequence, in the presence of salt the ion exchange effects are eliminated.

Among the batches, batch 3 delivered the lowest background binding, while batch 4 the higher. This variation could be due to the differences of the exterior surface morphology of the supports, e.g. roughness, however it is expected that after functionalisation the background binding will be of second concern as the polymer brushes will cover the surfaces.

3.4.6.2 Haemoglobin binding onto pVI grafted supports

It is known, that copolymers containing vinyl imidazole can be used for the recovery of proteins and enzymes, as are able to form a complex with metal ions in such a way that two to three imidazole residues coordinate with a single metal ion (Galaev *et al.,* 1997; Kumar *et al*., 1998a, Kumar *et al.,* 1999; Ivanov *et al*., 2001). In this section the haemoglobin binding on the pVI grafted M-PVA supports is examined. The Langmuir isotherms for the batches 1, 2, 3, 4 and 5 are presented in Fig. 3.37, while the predicted parameters of the characterised supports are given in Table 3.8.

In respect with the amount of pVI grafted onto the supports as well as the binding characteristics, batches 1, 3 and 4 performed very similar. The charged brushes, delivered a maximum capacity of 135 mg g^{-1} with a K_d value of 1.9. For batch 3, the incorporation of VI improved the binding characteristics of the supports (the charged unmodified matrix delivered a capacity of 122 mg g^{-1} with a K_d value at 4.4). The affinity ligand (VI) favoured the adsorption of copper ions with its chelating groups and the binding performance was great influenced by the chemistry and the introduced terminal groups as expected (Kato *et al*., 2003).

The maximum binding of the uncharged brushes for both batches 3 and 4 was decreased to 46 mg g^{-1} in comparison with that of unmodified M-PVA (66-146 mg g^{-1}) due to the coverage of the M–PVA surface with the hydrophilic chains of vinyl imidazole moieties. Although the addition of salt during protein binding on the M-PVA lowered the capacities not such an effect is observed for the pVI supports.

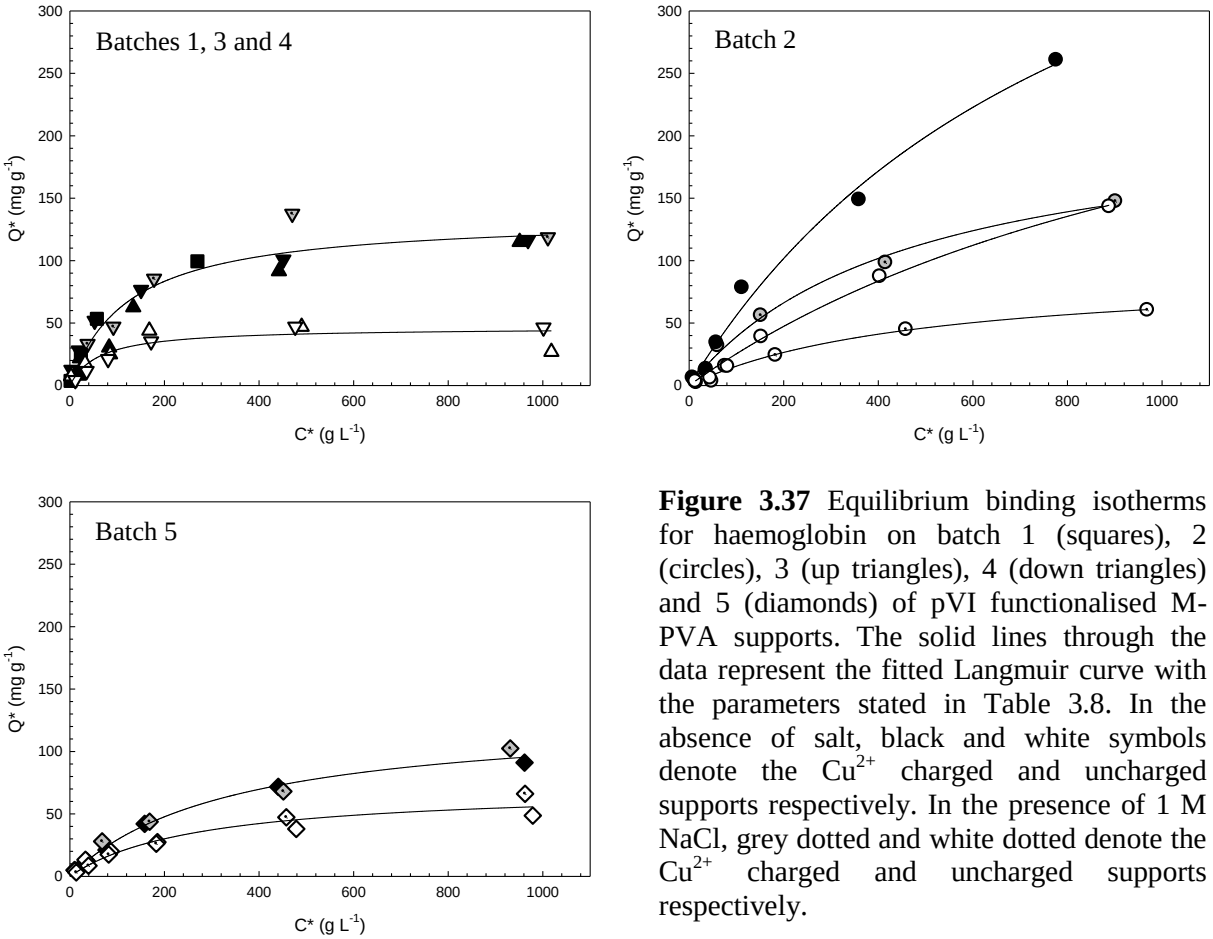

Figure 3.37 Equilibrium binding isotherms for haemoglobin on batch 1 (squares), 2 (circles), 3 (up triangles), 4 (down triangles) and 5 (diamonds) of pVI functionalised M-PVA supports. The solid lines through the data represent the fitted Langmuir curve with the parameters stated in Table 3.8. In the absence of salt, black and white symbols denote the Cu^{2+} charged and uncharged supports respectively. In the presence of 1 M NaCl, grey dotted and white dotted denote the Cu^{2+} charged and uncharged supports respectively.

Table 3.8 Langmuir predicted parameters for the curves fitted in Fig. 3.37.

Support #	Batch # and description	NaCl conc^{n} in binding buffer (M)	Q_{max} (mg/g)	K_d (μM)	Initial slope (L/g)
	Batches 1, 3 and 4:				
Homo-3.5	pVI_{37} – 4.6 Å	0	46	1.0	0.75
Homo-4.8	$pVI_{36.7}$ – 4.6 Å				
Homo-1.4	Cu^{2+} -pVI_{100} – 4.0 Å	0	135	1.9	1.10
Homo-3.5	Cu^{2+} -pVI_{37} – 4.6 Å	0			
Homo-4.8	Cu^{2+} -$pVI_{36.7}$ – 4.6 Å	0			
Homo-4.8	Cu^{2+} -$pVI_{36.7}$ – 4.6 Å	1			
	Batch 2:				
Homo-2.3	pVI_{20} – 4.4 Å	0	92	7.6	0.2
Homo-2.4	pVI_{100} – 4.4 Å	0	357	20.3	0.3
Homo-2.3	Cu^{2+} - $p(VI)_{20}$ – 4.4 Å	0	219	7.1	0.5
Homo-2.4	Cu^{2+} - $p(VI)_{100}$ – 4.4 Å	0	550	13.6	0.6
	Batch 5:				
Homo-5.4	$pVI_{22.9}$ – 4.6 Å	0	71	4.3	0.26
Homo-5.4	$pVI_{22.9}$ – 4.6 Å	1.0			
Homo-5.4	Cu^{2+} -$pVI_{22.9}$ – 4.6 Å	0	129	5.3	0.38
Homo-5.4	Cu^{2+} -$p(VI)_{22.9}$ – 4.6 Å	1.0			

Among all the batches, batch 1, 3 and 4 delivered the most satisfactory materials, while batch 2 and 5 the worst. Batch 5 delivered lower binding performance than batches 1, 3 and 4, which also grafted with less VI content. Similarly and at higher extend, batch 2 delivered very high dissociation constants (7-10 folds difference) and low initial slopes, indicating the supply of low quality M-PVA materials may affect both the functionalisation and the protein binding behaviour.

3.4.6.3 Haemoglobin binding onto pVBIDA grafted supports

Two different batches (batch 4 and 5) of M-PVA particles were employed in the construction pVBIDA modified supports. These supports were characterised in terms of the cerium (IV) grafting extend of as well as of haemoglobin binding behaviour at different buffers (see Fig. 3.38 and Table 3.9). The pVBIDA supports were manufactured with the intention of replacing

pVI with it especially for the construction of mixed polymer brushes. The previously made supports of pVI although delivered satisfactory haemoglobin binding capacities, were relative weak in binding strength. So the chelating monomer VBIDA was synthesized for the improvement of Cu^{2+} ions coordination versus that of imidazole. IDA is a polydentate carboxy-containing ligands, which is considered very useful in IMAC due to its very strong binding to the metal ions (Porath, 1992; Kumar *et al*., 1998a).

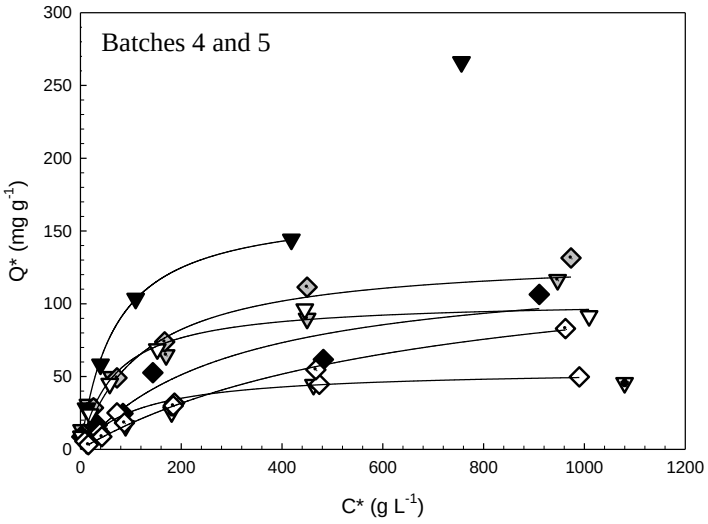

Figure 3.38 Equilibrium binding isotherms for haemoglobin on batch 4 (down triangles) and 5 (diamonds) of p(VBIDA) functionalised M-PVA supports. The solid lines through the data represent the fitted Langmuir curve with the parameters stated in Table 3.9. In the absence of salt, black and white symbols denote the Cu^{2+} charged and uncharged supports respectively. In the presence of 1 M NaCl, grey dotted and white dotted denote the Cu^{2+} charged and uncharged supports respectively.

Table 3.9 Langmuir predicted parameters for the curves fitted in Fig. 3.38.

Support #	Batch # and description	NaCl conc^{n} in binding buffer (M)	Q_{max} (mg/g)	K_d (μM)	Initial slope (L/g)
	Batches 4 and 5:				
Homo-4.9	$pVBIDA_{16}$ – 4.6 Å	0	103	1.1	1.51
Homo-5.6	$pVBIDA_{10.9}$ – 4.6 Å	0	55	1.8	0.48
Homo-4.9	$pVBIDA_{16}$ – 4.6 Å	1.0	56	2.9	0.30
Homo-5.6	$pVBIDA_{10.9}$ – 4.6 Å	1.0	141	10.7	0.20
Homo-4.9	Cu^{2+}-$pVBIDA_{16}$ – 4.6 Å	0	167	1.1	2.45
Homo-5.6	Cu^{2+}-$pVBIDA_{10.9}$ – 4.6 Å	0	129	4.7	0.42
Homo-4.9	Cu^{2+}-$pVBIDA_{16}$ – 4.6 Å	1.0	133	1.9	1.07
Homo-5.6	Cu^{2+}-$pVBIDA_{10.9}$ – 4.6 Å	1.0			

In view of the argumentation above concerning IDA greater coordinating power *cf*. Imidazole, this result may come as a surprise. It should be noted that shorter chains (and therefore lower ligand densities) were achieved in reactions involving the VBIDA monomer *cf*. VI (Table 3.9). On the other hand, the effect of affinity chain length is not expected to be tremendous (especially beyond reaching a sufficient spacing and high chain length), as the metal chelating interactions are of short range and protein interacts with the groups exposed at the exterior of the brush.

Generally, the functionalised supports prepared with batch 4 delivered better binding characteristics in terms of dissociation constants (K_d) and initial slopes (Q_{max}/K_d) with that prepared with batch 5 material. This accounts mainly to better cerium (IV) grafting of brushes (longer chain lengths). Finally, for all the supports the addition of salt lowered the binding, as ionic interactions were eliminated.

3.4.6.4 Haemoglobin binding onto pNIPAAm grafted supports

In these sets of experiments, batch 2 and 3 functionalised with pNIPAAm were tested for protein binding, while being charged and uncharged with Cu^{2+} ions (see Fig. 3.39 and Table 3.10). Introducing pNIPAAm onto the batch 3 support, the protein binding decreased dramatically (i.e. Q_{max} = 5.3 mg g^{-1}), indicating that the incorporation of this type of polymer (experiments performed below the LCST at 22 °C) can contribute to protein binding inhibition. Research in the area of biofouling indicates that water soluble proteins are repelled by hydrophilic surfaces, while these proteins stick to hydrophobic surfaces (Prime and Whitesides, 1991). It has been also demonstrated, that proteins interact more strongly above the LCST of pNIPAAm modified surfaces, while below the LCST the non-specific

interactions are minimised (Kanazawa *et al*., 1996; Lakhiari *et al.,* 1998; Ding *et al*. 1999). However, the hydrophilicity and so the protein interaction with pNIPAAm introduced surfaces strongly depends on the surface coverage such as the density of grafted chains and the chain length (Kidoaki *et al*., 2001). This effect was not observed for batch 2 modified supports, however from previous studies on this batch it is known that their bad quality (heterogeneous and dirty surfaces) rendered the efficiency of cerium (IV) grafting.

Another interesting observation here is that when the pNIPAAm modified support was loaded with Cu^{2+} ions, a considerable amount of protein was bound on it (Q_{max} = 86 mg g^{-1}). The affinity of this support for haemoglobin indicates that the pNIPAAm chains may interact and form complex with the metal ions. However, as indicated by the increased dissociation constant (K_d =11.3), theses interactions are weak. The coordination of Cu^{2+} ions at the N-terminal amino nitrogen of pNIPAAm has been indicated by Mu and Fang (2006). Same authors suggest also that the binding of copper ions onto pNIPAAm backbone can influence the phase transition of pNIPAAm (i.e. shift of the polymer LCST).

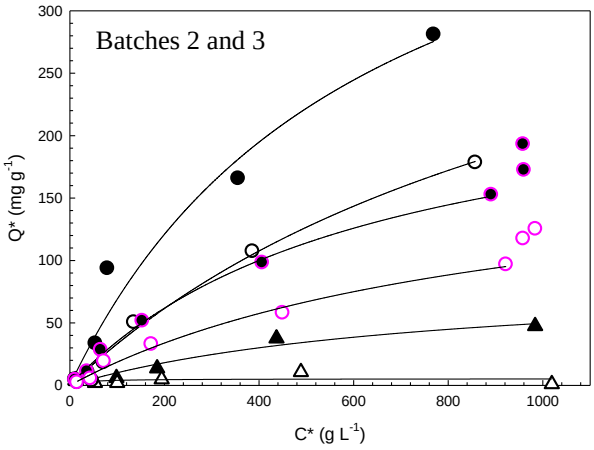

Figure 3.39 Equilibrium binding isotherms for haemoglobin on batch 2 (circles) and 3 (up triangles) of pNIPAAm functionalised M-PVA supports. The solid lines through the data represent the fitted Langmuir curve with the parameters stated in Table 3.10. In the absence of salt, black and white symbols denote the Cu^{2+} charged and uncharged supports respectively. Note: For batch 2, $p(NIPAAm)_{\underline{20}}$ – 4.4 Å is denoted with circles of pink edges, while $p(NIPAAm)_{\underline{100}}$ – 4.4 Å with black edges.

Table 3.10 Langmuir predicted parameters for the curves fitted in Fig. 3.39.

Support #	Batch # and description	NaCl conc^{n} in binding buffer (M)	Q_{max} (mg/g)	K_d (μM)	Initial slope (L/g)
	Batch 2:				
Homo-2.1	$pNIPAAm_{\underline{20}}$ – 4.4 Å	0	191	14.2	0.2
Homo-2.2	$pNIPAAm_{\underline{100}}$ – 4.4 Å	0	430	18.6	0.4
Homo-2.1	Cu^{2+} - $pNIPAAm_{\underline{20}}$ – 4.4 Å	0	261	9.9	0.4
Homo-2.2	Cu^{2+} - $pNIPAAm_{\underline{100}}$ – 4.4 Å	0	499	9.6	0.8
	Batch 3:				
Homo-3.3	$pNIPAAm_{14}$ – 4.6 Å	0	5.3	0.5	0.18
Homo-3.3	Cu^{2+}-$pNIPAAm_{14}$ – 4.6 Å	0	86	11.3	0.12

3.4.6.5 Haemoglobin binding and elution studies below and above the Lower Critical Solution Temperature (LCST) of pNIPAAm

The polymer brushes of pVI and pNIPAAm made with batch 2 were not characterized in terms of modification/actual lengths as at that time the FT-IR technique was not developed.

However, the above materials were tested for protein (haemoglobin) adsorption and desorption, at 22 ºC and 42 ºC (i.e. above and below their LCST at 32 ºC). The metal affinity interactions were further exploited by performing the above experiments in the presence and absence of Cu^{2+} ions. Finally, some of these supports were washed twice with the binding buffer to remove any loosely bound protein and three further sequential imidazole (0.2 M, pH 7.0) washes were performed.

The resulting Langmuir isotherms for the $pVI_{\underline{20}}$ – 4.4 Å, $pVI_{\underline{100}}$ – 4.4 Å, $pNIPAAm_{\underline{20}}$ – 4.4 Å and $pNIPAAm_{\underline{100}}$ – 4.4 Å supports are presented in Fig. 3.40, while the predicted parameters obtained (Q_{max}, K_d, initial slopes) are given in Table 3.11. From this data, it is again clear that this batch material behaved quite differently than the other batches employed in this work in terms of haemoglobin binding performance. For example, weak protein binding onto the Cu^{2+} -$p(VI)_{\underline{100}}$ – 4.5 Å support is observed according to the high k_d value obtained (i.e. 10 folds difference from those obtained with batch 1 and 3 similar Cu^{2+} -$p(VI)_{\underline{100}}$ supports).

Switching the temperature across the LCST (from 22 to 42 °C), the binding characteristics for both series (VI and NIPAAm) of supports changed. In the case of 100 monomer units target length supports (Table 3.11), switching the temperature of binding from 22 to 42 °C exerted no significant effect for the pVI homopolymer brush. However for the pNIPAAm homo-brushes the same increase in temperature was accompanied by increasing binding capacities and of reduced selectivity. By shifting the temperature above the LCST, the affinity for protein adsorption increases as the surface changes from hydrophilic to hydrophobic, resulting in higher amounts of protein being adsorbed (Ding *et al*., 1999). When these interactions are taking place, the protein unfolds to expose its hydrophobic

amino acid residues to the hydrophobic surface while the bound water is released to the surroundings and some denaturation of protein is expected (Uenouama and Hoffman, 1988).

The same trends are followed for the 20 monomer units length support series (Table 3.11) apart from pVI homo-brush where the binding capacity is increased considerably at 42 °C. Below the LCST (at 22°C), the $p(VI)_{\underline{20}}$ material maintained relatively high selectivity, however this effect was lost at 42 °C. The general trend followed by both Cu^{2+}- pNIPAAm support sets is that the binding increases with increasing temperature. When pNIPAAm is grafted onto a surface, it is expected protein binding elimination due to the increased hydrophilicity. As mentioned before (section *3.4.6.4*), the pNIPAAm modified M-PVA supports, have an apparent affinity for protein binding when charged with Cu^{2+} ions. However, the high amounts of protein bound on these supports (in comparison with the previous made ones) can be attributed to the bad quality of this M-PVA batch (heterogeneous and dirty PVA surfaces). On the other hand, the uncharged pNIPAAm supports, delivered less protein binding due to the absence of metal ions. In addition, the possibility of interactions of protein molecules and pNIPAAm chains even below the LCST cannot be neglected. As mentioned before, the protein interaction with pNIPAAm depends on the density and lengths of polymer chains (Kidoaki *et al*., 2001). From previous experiments on different M-PVA materials (batch 3), the elimination of haemoglobin binding was observed below the LCST, indicating that denser and of higher length polymer chains of pNIPAAm were grafted on that batch.

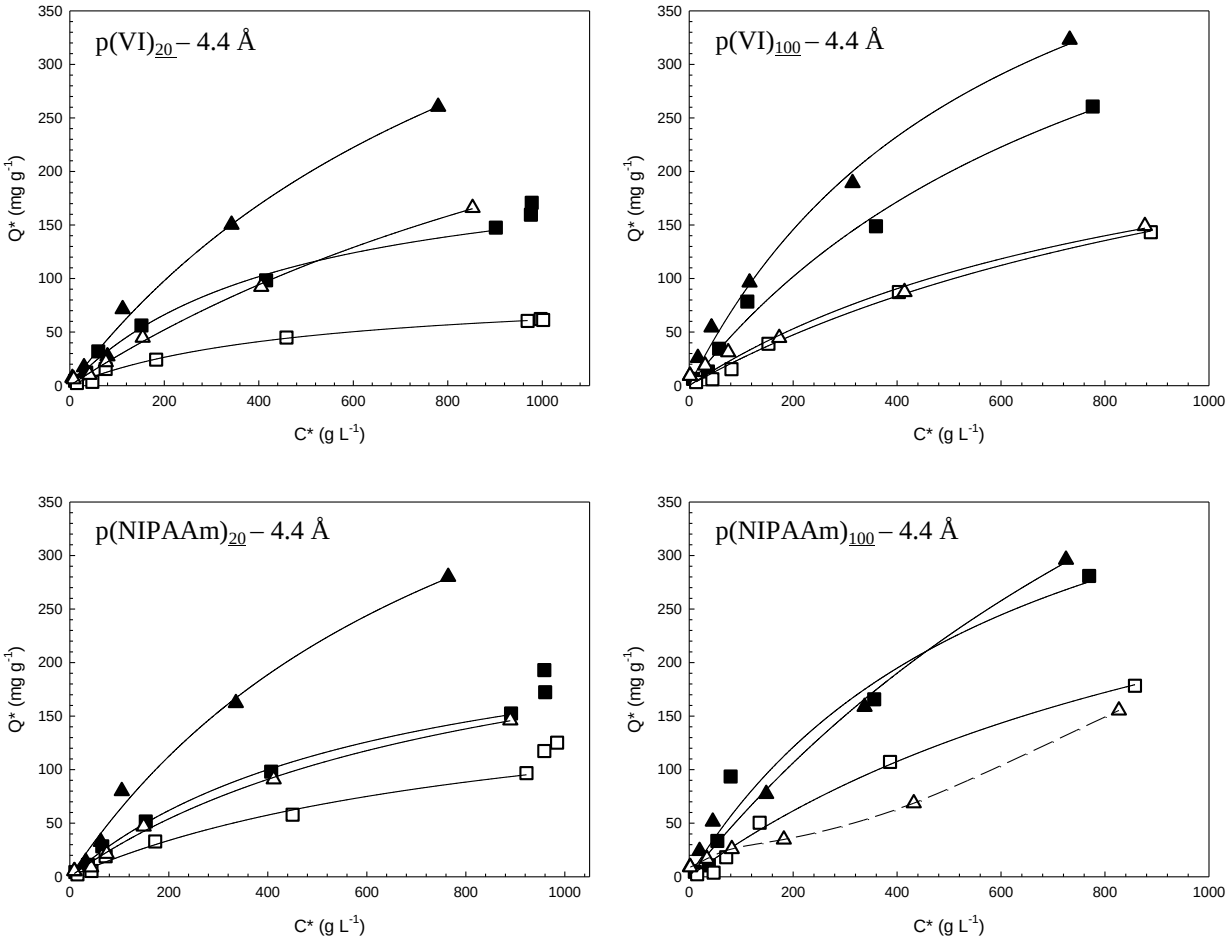

Figure 3.40 Equilibrium adsorption isotherms for haemoglobin on functionalised M-PVA (batch 2, R2-16066) support with 20 and 100 monomers target length at 4.4 Å spacing. The solid lines through the data represent the fitted Langmuir curves with the parameter values stated in Table 3.11. The dashed line indicates that data failed to fit in the model. Black and white symbols denote Cu^{2+} charged and uncharged supports respectively; squares and up triangles denote binding at 22 ºC and 42 ºC respectively.

Table 3.11 Langmuir predicted parameters for the curves fitted in Fig. 3.40.

Support description	Binding Temp.	Q_{max}	K_d	*Initial slope*
	(°C)	(mg/g)	(μM)	(L/g)
$p(VI)_{\underline{20}}$ – 4.4 Å	22	92	7.6	0.2
$p(VI)_{\underline{20}}$ – 4.4 Å	42	496	26.2	0.3
Cu^{2+} - $p(VI)_{\underline{20}}$ – 4.4 Å	22	219	7.1	0.5
Cu^{2+} - $p(VI)_{\underline{20}}$ – 4.4 Å	42	610	16	0.6
$p(VI)_{100}$ – 4.4 Å	22	357	20.3	0.3
$p(VI)_{100}$ – 4.4 Å	42	309	14.8	0.3
Cu^{2+} - $p(VI)_{100}$ – 4.4 Å	22	550	13.6	0.6
Cu^{2+} - $p(VI)_{100}$ – 4.4 Å	42	579	9.2	1.0
$p(NIPAAm)_{20}$ - 4.4 Å	22	191	14.2	0.2
$p(NIPAAm)_{20}$ - 4.4 Å	42	287	13.2	0.4
Cu^{2+} - $p(NIPAAm)_{20}$ - 4.4 Å	22	261	9.9	0.4
Cu^{2+} - $p(NIPAAm)_{20}$ - 4.4 Å	42	588	13	0.7
$p(NIPAAm)_{100}$ - 4.4 Å	22	430	18.6	0.4
$p(NIPAAm)_{100}$ - 4.4 Å	42	296[a]	nd	nd
Cu^{2+} - $p(NIPAAm)_{100}$ – 4.4 Å	22	499	9.6	0.8
Cu^{2+} - $p(NIPAAm)_{\underline{100}}$ - 4.4 Å	42	894	22.7	0.6

[a]data could not be fitted to Langmuir model. The capacity indicated is the maximum value Q* obtained.

At Table 3.12, the amount of protein eluted after binding at 22 °C and 42 °C is given. In terms of protein elution characteristics with imidazole (0.2 M, pH 7.0), the DP = 20 support series showed better behaviour than the DP=100 series (higher amount of eluted protein). From the supports tested, the elution was considerably decreased by rising the temperature at 42 °C. This observation can be attributed to the effect of heating on both the surface properties and protein structure. Thermal studies on bovine haemoglobin show that the protein denatures by a two-stage thermal transition: the initial perturbation stage starts between 30-40 °C, then thermal unfolding stage happens between 44-54 °C and finally the thermal aggregation takes place at 54-70 °C (Yan *et al.*, 2004; Digel *et al.*, 2006). At 42 °C structural changes take place, where the helical structures and hydrophobic parts of haemoglobin become more

solvent exposed. As a consequence, at high temperatures the binding may increased due to partial protein unfolding.

It has also been demonstrated that by increasing the temperature, the retention of transition metal ions (under specific eluent conditions) also increases on chelate columns. This effect is more pronounced at increased ionic strength (limitation of ionic exchange interactions) and pH (increase stationary phase complexation) (Bashir *et al*., 2002; Bashir and Paull, 2002). In addition, the nature of the stationary phase plays al very crucial role on this effect.

The temperature effect on the retention of solutes during chromatographic separations is expressed by the following relation (Elefterov *et al*. 1997, Kolpachnikova *et al*. 1998; Paull and Bashir, 2003).

$$\ln k' = -\frac{\Delta H}{RT} + \frac{\Delta S}{R} + \ln \varphi \qquad \text{Eq. (3.3)}$$

In Eq. 3.3, k' is the solute retention factor, ΔH is the enthalpy of sorption, ΔS is the change in entropy due to sorption, and φ is the phase ratio (characteristic constant for a given column). A van't Hoff plot (i.e. $\ln k'$ versus $1/T$) should be linear and will have a slope value equal to $-\Delta H/R$ (Paull and Bashir, 2003). For pure ion exchange interactions and under the assumption that ΔS is constant, the sorption exhibits exothermic behaviour (negative ΔH), the slope is positive and the retention is decreased with temperature**.** However the ΔH values are very small, and in ion exchange separations the effect of temperature is insignificant (Paull and Bashir, 2003). Elefterov *et al*. (1997) and Kolpachnikova *et al*. (1998) reported that when the exothermic behaviour changes to endothermic then the retention mechanism changes from ion exchange to complexation. In parallel, Jones and Nesterenko in 1997 (Paull and Bashir,

2003), proposed that in cases of chelate complex formation, changes in entropy (ΔS) are more significant than those of enthalpy (ΔH). As ΔS is positively large, the Gibbs free energy ΔG will be negative (ΔG = ΔH – TΔS). With increasing temperature, ΔG becomes negative and the stability constant (*K*) is increased (ΔG = –RT ln *K).* As a consequence, if complexation is the dominant retention mechanism, retention will always increase with increasing column temperature according to the following relation:

$$- \Delta G = - \Delta H + \Delta ST \qquad \text{Eq. (3.4)}$$

On charging the VI-NIPAAm copolymers with Cu^{2+} ions, Kumar *et al*. (1998a and 1998b) observed that the conjugate could not precipitated even at very high temperatures as its LCST was increased. To overcome this problem the authors managed to precipitate the copolymer by promoting hydrophobic interactions (lowering the LCST) with the addition of salt (NaCl). Other authors also note that pNIPAAm surfaces at high temperatures become hydrophobic promoting higher amounts of protein to be adsorbed on it (Kanazawa *et al*., 1996; Lakhiari *et al.*, 1998; Ding *et al*. 1999).

Based on the above observations, subsequent studies of haemoglobin binding (and release via temperature changes) onto mixed brushes of pNIPAAm and VI will take place below the LCST and in the presence of salt.

Table 3.12 Elution characteristics of pVI and pNIPAAm modified supports.

Support description	Temp.	Hb firmly bound, (Q_{ads})	Hb eluted (%) of Qads at 22 °C or 42 °C, using 0.2M imidazole, pH7.0			
	(°C)	(mg/g)	1st elution	2nd elution	3rd elution	Total eluted
$p(VI)_{\underline{20}}$ - 4.4 Å	22	36	12.8	3.6	6.0	22.4
$p(VI)_{\underline{20}}$ - 4.4 Å	42	145	3.1	1.5	1.6	6.2
Cu^{2+} - $p(VI)_{\underline{20}}$ - 4.4 Å	22	152	14.6	3.2	1.7	19.5
Cu^{2+} - $p(VI)_{\underline{20}}$ - 4.4 Å	42	259	0.4	0.5	0.3	1.1
$p(VI)_{\underline{100}}$ - 4.4 Å	22	124	2.2	1.7	2.1	6.0
$p(VI)_{\underline{100}}$ - 4.4 Å	42	nd	nd	nd	nd	nd
Cu^{2+} - $p(VI)_{\underline{100}}$ - 4.4 Å	22	259	8.1	1.8	0.9	10.8
Cu^{2+} - $p(VI)_{\underline{100}}$ - 4.4 Å	42	nd	nd	nd	nd	nd
$p(NIPAAm)_{\underline{20}}$ - 4.4 Å	22	125	nd	nd	nd	nd
$p(NIPAAm)_{\underline{20}}$ - 4.4 Å	42	128	3.8	3.3	3	10.1
Cu^{2+} - $p(NIPAAm)_{\underline{20}}$ - 4.4 Å	22	177	10.7	2.1	1.6	14.5
Cu^{2+} - $p(NIPAAm)_{\underline{20}}$ - 4.4 Å	42	280	nd	nd	nd	nd
$p(NIPAAm)_{\underline{100}}$ - 4.4Å	22	161	1.1	0.8	0.4	2.3
$p(NIPAAm)_{\underline{100}}$ - 4.4 Å	42	nd	nd	nd	nd	nd
Cu^{2+} - $p(NIPAAm)_{\underline{100}}$ - 4.4 Å	22	272	5.5	0.9	0.9	7.3
Cu^{2+} - $p(NIPAAm)_{\underline{100}}$ - 4.4 Å	42	296	nd	nd	nd	nd

3.4.6.6 Haemoglobin binding onto copolymer grafted supports

The copolymers constructed with batch 1 (see Table 3.2), in parallel with a pVI support were tested for haemoglobin adsorption. In Fig. 3.41, the Langmuir adsorption isotherms are presented while in Table 3.13 the adsorption parameters are given.

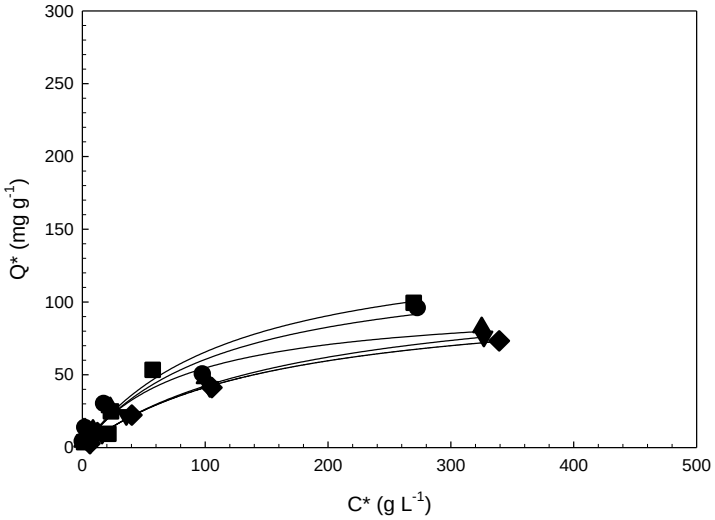

Figure 3.41 Equilibrium binding isotherms for haemoglobin on charged $pVI_{38.2}$ – 4.0 Å (squares), p(NIPAAm$_{\underline{2}}$-*co*-VI)$_{\underline{100}}$ – 4.0 Å (circles), p(VCL$_{\underline{2}}$-*co*-VI)$_{\underline{100}}$ – 4.0 (up triangles), p(NIPAAm$_{\underline{4}}$-*co*-VI)$_{\underline{100}}$ –12.8 Å (down triangles), p(VCL$_{\underline{4}}$-*co*-VI)$_{\underline{100}}$ – 12.8 Å (diamonds) of batch 1 functionalised M-PVA supports. The solid lines through the data represent the fitted Langmuir curve with the parameters stated in Table 3.13.

Table 3.13 Langmuir predicted parameters for the curves fitted in Fig. 3.41.

Support #	Batch # and description	NaCl conc^{n} in binding buffer (M)	Q_{max} (mg/g)	K_d (μM)	Initial slope (L/g)
	Batch 1:				
Homo-1.4	Cu^{2+} - $pVI_{38.2}$ – 4.0 Å	0	146	1.9	1.19
Co-1.1	Cu^{2+} - p(NIPAAm$_{\underline{2}}$-*co*-VI)$_{\underline{100}}$ – 4.0 Å	0	130	1.8	1.13
Co-1.2	Cu^{2+} - p(VCL$_{\underline{2}}$-*co*-VI)$_{\underline{100}}$ – 4.0 Å	0	100	1.3	1.20
Co-1.3	Cu^{2+} - p(NIPAAm$_{\underline{4}}$-*co*-VI)$_{\underline{100}}$ –12.8 Å	0	117	2.7	0.66
Co-1.4	Cu^{2+} - p(VCL$_{\underline{4}}$-*co*-VI)$_{\underline{100}}$ – 12.8 Å	0	107	2.5	0.67

From the above supports, the pVI homobrush support delivered the highest haemoglobin binding capacity. The copolymer supports made at 4.0 Å spacing (and utilising NIPAAm) demonstrated better performance than those made at 12.8 Å. From characterisation of the copolymers composition using batch 4, we know that at 4.0 Å spacing, mostly pVI homo-brushes may result. As a consequence, the introduced pNIPAAm content at wider spacing supports decreased considerably the haemoglobin binding performance (higher K_d values and

lower slopes). As the supports were charged, Cu^{2+}-NIPAAm residues are also expected to contribute to protein binding as explained in section *3.4.6.4*.

In Table 3.14, the elution characteristics of a copolymer brush support prepared using batch 2 are shown. For the reasons explained in section *3.4.6.5*, the elution efficiency was reduced with increasing temperature.

Table 3.14 Elution characteristics of copolymer modified support (co-2.1).

Support description	Temp.	Hb firmly bound, (Q_{ads})	Hb eluted (%) of Qads at 22 °C or 42 °C, using 0.2M imidazole, pH 7.			
	(°C)	(mg/g)	1st elution	2nd elution	3rd elution	Total eluted
Cu^{2+}-p(NIPAAm$_2$:VI)$_{20}$–4.4 Å	22	178	9.1	2.0	1.1	12.2
	42	269	0.2	0.3	0.3	0.8

3.5 Conclusions

Initially, cerium (IV) initiated 'graft from' polymerisation was employed to manufacture polymer brushes composed of either affinity or thermoresponsive polymers (homopolymers). FT-IR analysis on solid products and ATR FT-IR on liquid supernatants were employed to confirm the modification of M-PVA supports and characterise these materials in terms of the amount of polymer installed. The effect of different solvents, monomer and cerium (IV) concentration, time of reaction, order of cerium (IV) addition and M-PVA batch onto monomers polymerisation was investigated extensively.

From the sets of conditions used, reactivity was favoured when using water and adding the monomer first into the mixtures. Comparison of % monomer consumption during polymerisations showed that VI proceeds much further towards polymerisation than VBIDA and NIPAAm monomers, due to differences in solubility/polarity (i.e. the extent of monomer

consumption followed the trend VI > VBIDA > NIPAAm). Kinetic studies were performed by following the monomer (NIPAAm) and cerium (IV) consumption with time of polymerisation. Both of the reactions employed by adding either the cerium (IV) or the monomer first terminated in less than few minutes. Premature termination of cerium (IV) initiated reactions onto M-PVA supports can be attributed to the very high polymerisation rates and unavoidable termination reactions between the growing polymer chains.

Thermoresponive studies onto modified supports with pNIPAAm were employed by observing their settling behaviour in solution. These studies revealed that all the supports modified with sufficient amounts of polymer (in terms of length extend) demonstrated thermoresponsive behaviour with a sharp phase transition within the range of 31-33 °C. The degree of the thermoresponsiveness was related to pNIPAAm chain length, VI copolymerisation and spacing. However, further experimentation is required to investigate the influence of salt and Cu^{2+} addition on chain collapse. The same implies for testing the settling behaviour of mixed functionality polymer brush supports constructed in the next Chapter.

Characterisation of modified magnetic supports with one-pot cerium (IV) reactions employing a mixture of NIPAAm and VI monomers showed that the resulting brushes are not alternating copolymers. Instead, homopolymer pVI or co-polymer pVI end grafted with short pNIPAAm caps (di-block copolymers) were grown from the PVA surfaces depending on the amount of initiator added on the support and feed composition.

In conclusion, by exploring the cerium (IV) grafting, the outcomes obtained utilising this chemistry were: (**a**) the thickness of each polymer chain can be partially controlled by adjusting the concentration of the monomer in relation to initiator added; (**b**) the density between the homopolymer chains can be controlled by the amount of initiator added; (**c**) the

final chemical composition of the brush within the two components added in the one-pot initiation reactions can be partially controlled by adjusting the amount of initiator and feed composition. However, some limitations have been identified using this chemical route, such as: Firstly, after any reaction, no more polymerisation can take place from a grafted chain (the reaction 'dies'). Secondly, high grafting density promotes termination as the chains grow very close to each other. However, knowing the reactivity of each monomer, the chain length can be predicted and/or regulated at some degree.

Estimation of Flory Radius (R_F) of homopolymer bushes indicated that the polymer chains were configured at the 'true' brush regime (i.e. at such density and length so they can be stretched away from the M-PVA surface).

Further characterisation of the polymer brushes, was performed by testing the supports in terms of protein binding and elution behaviour. The binding characteristics were dependent on type of polymer grafted, the degree of polymerisation and the M-PVA batch utilised. PNIPAAm homopolymer brushes eliminated haemoglobin adsorption below the LCST and when charged could from weak complexes with Cu^{2+} ions able to bind protein. The incorporation of affinity ligands increased the efficiency of binding especially in terms of selectivity. In addition, the impact of binding temperature (below or above the LCST), polymer composition, and ionic strength onto the capacity of various supports was investigated. The general trend followed by the pNIPAAm modified supports was that higher haemoglobin binding capacities were obtained at higher temperatures due to hydrophobic properties developed on the M-PVA surface, the increased retention of metal ions, and the partial unfolding of the protein. As a consequence, the elution was favoured below the LCST. Finally, elimination of ionic interactions was achieved by the addition of salt during binding.

4. Synthesis of mixed functionality polymer brushes using sequential cerium (IV) 'grafting from' approach on M-PVA supports and their application for protein binding and subsequent desorption via temperature transitions

4.1 Abstract

A method to manufacture mixed polymer brushes of dual functionality, i.e. that to adsorb and desorb protein on magnetic supports is presented. Sequential cerium (IV) initiated polymerisation was employed onto M-PVA surface to incorporate pNIPAAm aside to pVI or pVBIDA chains. The supports were manufactured at fixed density and characterised in terms of chain lengths/composition of polymers grafted. The effect of order of polymer addition was examined to make sure that a brush was constructed by grafting both of its components from the PVA surface and no other site. The mixed polymer supports were in 'true' brush regime as the estimated s/(2RF) ratios were between 0.05-0.08, i.e. much less than unity. The Hb binding characteristics of these materials were correlated to their final composition (i.e. affinity and thermoresponsive polymer content). Finally, protein (Hb and GFP) batch binding and subsequent desorption with temperature shift cycles across the LCST was performed to the supports. The GFP desorption was much higher than that of Hb, as each protein interacts different with the polymer film, subject of their stability and conformational changes. Desorption was dependent on the type of affinity ligand (i.e. due to stronger interactions of protein with VBIDA, the efficiency of desorption dropped considerably).

4.2 Introduction

Lately, there is much interest in 'smart' polymers and hydrogels, able to undergo fast and reversible changes in response to environmental changes (Galaev and Mattiasson, 1999). Among other smart materials, the thermoresponsive polymers in aqueous environment may exist in two states depending on the medium temperature: below the Lower Critical Solution Temperature (LCST) the polymer chains are miscible with water obtaining a highly swollen coiled conformation, whereas above that temperature become incompatible with water forming globular structures (Luzinov *et al.*, 2004). Poly (*N-i*sopropylacrylamide), which is the most well studied thermo-responsive polymer has been used in many biological applications such as that of enzyme immobilisation, cell sorting and temperature-controlled cell harvesting, drug release and protein purification (Kikuchi *et al*., 1998; Shamim *et al*., 2006; Xu *et al.*, 2007).

The use of switching between the hydrophilic and hydrophobic state of pNIPAAm polymer, has been studied and used in cell attachment/detachment control as well as protein adsorption/release (Okano *et al*., 1995; Elaïssari and Bourrel, 2001; Elaïssari *et al*., 2001; Garipcan *et al*., 2004). It has been shown that cultured cells adhere to hydrophobic surfaces (above the LCST of pNIPAAm, 32 °C) while are prone to detach after changing the hydration state of pNIPAAm (decreasing the temperatures below the LCST) (Ista *et al.*, 1999; Luzinov *et al.*, 2004; Kim *et al.*, 2004; Selezneva *et al*., 2006). The same mechanism has been utilised for protein adsorption/desorption purposes. For example, in biomedical research, thermoresponsive microgels have been used to control protein adsorption/release via the pH, temperature and salinity (Elaïssari *et al*., 2001).

In protein purification, the use of thermoresponsive polymers has attracted a lot of attention by providing mild operating conditions for proteins (Kanazawa *et al*., 1996, 1997 and 1998;

Teal *et al.* 2000; Kikutchi and Okano 2002; Shamim *et al*., 2006). In addition, these materials may serve as cost-effective means for target product isolation in downstream processing of many raw materials. In process chromatography, where there is plenty room for improvement in terms of capacity, throughput, scalability and optimisation, the use of smart polymers is promising as it can provide improved materials as well as reduce costs (e.g. by reducing the large quantities of buffers required) (Maharjan, 2008).

The thermoresponsive polymers in the bioseparation field, have been employed as bioconjugates, stimuli responsive gels or as materials attached onto surfaces. Their potential use in immobilised affinity chromatography (IMAC), metal chelate affinity precipitation, IMA-partitioning in aqueous two phase polymer systems (ATPs) and temperature-responsive chromatography has been demonstrated (Kanazawa *et al*., 1996 and 1998; Galaev *et al.*, 1997; Galaev and Mattiasson, 1999; Kumar *et al.*, 1999 and 2001; Pietruszka *et al.*, 2000; Ivanov *et al*., 2001; Elaïssari *et al*., 2001; Kobayashi *et al*., 2003; Ayano *et al*., 2006).

Copolymers of thermoresponsive polymers (eg. NIPAAm, vinyl caprolactam) and vinyl imidazole are capable to form complexes with metal ions such as Cu^{2+} and proteins containing residues such as histidines (Ivanov *et al*., 2001). This kind of synthetic copolymers which combine thermoresponsive and binding to metal ions properties have been proven very effective means in both metal chelating affinity precipitation of proteins and in displacement chromatography (Galaev *et al.* 1997; Kumar *et al.*, 1999; Ivanov *et al.* 2001). In addition, copolymerisation of vinyl imidazole with acidic units (eg. acrylic and methacrylic acid) has been utilised to synthesize intelligent materials such as polyampholytes (more pH dependent than polyelectrolytes), combining basic and acidic properties (Annenkov *et al*., 2004). The above systems are designed to combine different properties and are based on the synthesis of water-soluble copolymers. Thermorsponsive polymers, such as pNIPAAm, have also been employed as means to modify surfaces of beads used in column chromatography to promote

protein elution by simply changing the temperature without the need of solvent addition (Kanazawa *et al.*, 1996 and 1998; Maharjan *et al*., 2008).

There are several approaches to create stimuli-responsive surfaces and interfaces. Tethering of polymer layers onto substrates has been found useful in many applications to control adhesion, wettability, lubrication, biocompatibility adsoprtion, roughness and other properties (Luzinov, 2004; Minko *et al.*, 2001). In addition, surfaces with controllable functions can be made by changing the polymer layer morphology and/or composition. As mentioned in Chapter 1, there are different types of polymer brushes. Depending on their chemical composition, they are broadly divided in homopolymer brushes, mixed homopolymer brushes, random copolymer brushes and block copolymer brushes (Zhao, 2003). In the case of a homopolymer brush it is possible to change only the thickness (and density) of the layer. On the other hand, in the case of a mixed brush (composed of two different polymers) it is possible to make more alternations (structure, morphology, surface chemistry, incorporation of more properties etc.) allowing more functions and applications (Sidorenko *et al.*, 1999; Zhao and Brittain, 2000).

The synthesis of mixed polymer brushes is considered difficult in terms of preparation of well-defined polymer systems. Initially, their construction was based on conventional radical polymerisations from azo-initiators immobilised on surfaces, lacking control of molecular weight distribution and grafting density (Zhao, 2003 and references therein). Lately, most of the attempts to fabricate two polymers on the same surface are based on controlled living polymerisation reactions; for example using ATRP in two sequential steps (Zhou *et al.*, 2004). However, in literature no efforts have been reported utilising conventional free radical polymerisation reactions, such as that of cerium (IV) initiation system.

By exploring the cerium (IV) grafting in previous Chapter, it was found that the grafting density of the polymer brushes can be adjusted by the amount of initiator added and that the length of the polymer chains can be predicted and regulated at some degree by knowing the reactivity of each monomer. In addition, the properties of polymers added (i.e. that of affinity and thermoresponsiveness) were retained after grafting. In this work, we try to tether mixed functionality polymer brushes composed of thermoresponsive polymers and affinity polymers adjacent to each other onto magnetic particles for protein binding and release purposes, using sequential cerium (IV) grafting as illustrated in Fig. 4.1.

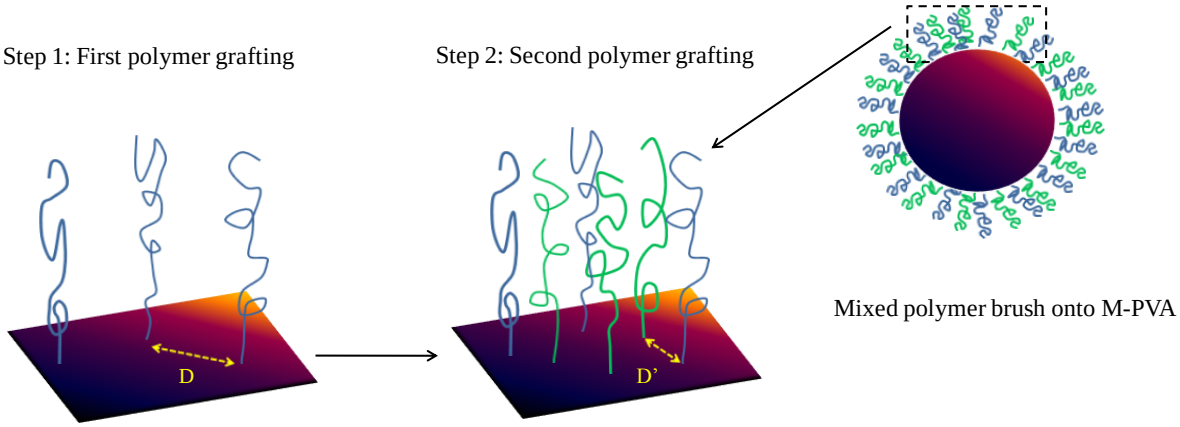

Figure 4.1 Mixed functionality polymer brush synthesis onto M-PVA support using sequential cerium (IV) initiated polymerisation reaction at two steps: **Step 1**- first polymer (blue) grafting at spacing D; **Step 2**- second polymer (green) grafting at same spacing D, delivering a mixed brush of fixed and narrower spacing at D'.

The mixed functionality brushes are mainly manufactured to incorporate onto the surface of the M-PVA support two different properties, i.e. that of protein binding and elution. In Fig. 4.2, the structure and the behaviour of the system across the LCST of pNIPAAm is presented.

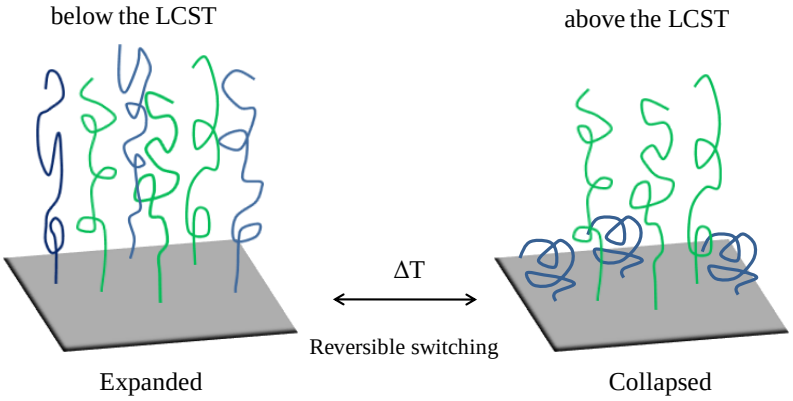

Figure 4.2 Mixed functionality brush switching behaviour by temperature transition across the LCST; below the LCST the thermoresponsive polymer chains (pNIPAAm; blue) and the affinity ligand polymer chains (pVI or pVBIDA; green) are fully extended (hydrophilic state); above the LCST the affinity ligand polymer chains are still in hydrophilic state and in extended form while the thermoresponsive polymer chains collapse (hydrophobic state).

The main objectives of the work described in this Chapter are: (a) to construct mixed brushes composed of thermoresponsive and affinity ligand polymers at fixed positions, utilising sequential cerium (IV) grafting; (b) to characterise these materials in terms of resulting chain lengths and positions; (c) to perform protein haemoglobin binding studies and (d) to evaluate the performance of the mixed brushes for release of different proteins (haemoglobin and green fluorescent protein) via temperature changes.

4.3 Materials and Methods

4.3.1 Materials

M-PVA 012 particles (M_r 130,000; acetyl content: 10.0-11.6 %; degree of hydrolysis: 86.8-88.7 %; 2 µm mean diameter) were used (batch 4, R2-0109027). This batch of M-PVA was supplied by Chemagen Biopolymer-Technologie AG (Baesweiler, Germany). *N*-isopropylacrylamide (NIPAAm), *1*-vinylimidazole (VI), Iminodiacetic acid, 4-vinylbenzyl chloride, poly (*N*-isopropylacrylamide), imidazole, ammonium cerium (IV) nitrate and

haemoglobin from bovine blood (lyophilized powder) were purchased from Sigma-Aldrich Company Ltd. (Gillingham, UK). *N*-vinyl benzyl Iminodiacetic acid was prepared in-house as described in Chapter 3, section *3.3.3.2*. Poly (*N*-vinylimidazole) was purchased from Polymer Source Inc. (Quebec, Canada). Green fluorescence protein (GFP) was supplied by Joerg Becker from Karlsruhe Institute of Technology and purified as described in section *4.3.1.1*. The Coomassie Plus (Better Bradford assay reagent) was purchased by Piercenet (Thermo Fisher Scientific, Perbio Science UK Ltd, Cramlington, UK). All other chemicals used were of analytical grade unless otherwise stated. MilliQ water was used in all experiments.

4.3.1.1. Purification of supplied Green Fluorescent Protein (GFP)

GFP with 6 x His-tag at the N terminus was received with a purity degree of ~95% at a concentration 3 g L^{-1}. The GFP was previously bound to IDA-coupled M-PVA particles and eluted with 1 M imidazole, 0.2 M NaCl, pH 6.8. Before using the protein in binding studies, the eluted copper and the imidazole was removed by the following buffer exchange procedure: centrifugal filter units (Amicon Ultra-15, 10 kDA) supplied by Millipore (U.K.) Ltd. (Watford, UK) were rinsed with distilled deionized water. Then 1 mL of sample was transferred to each of the filter units and mixed by aspiration with 9 mL of fresh buffer (20 mM Sodium Phosphate, 200 mM NaCl). The tubes were spun in a Jouan C 4 22 centrifuge (Jouan, Nantes, France) at 4000 rpm for 0.5 h. The permeate (had light blue color due to copper) was discarded and the centrifugation was repeated for another 5 times. The purified GFP was diluted in the same buffer at 0.6 g L^{-1} and stored at 4 °C.

4.3.2 Preparation of mixed functionality polymer brushes - Sequential grafting of brushes consisting of poly (*N*-isopropylacrylamide) and poly (*N*-vinylimidazole) or poly (*N*-vinyl benzyl Iminodiacetic acid) onto M-PVA supports using cerium (IV) initiated polymerisation reaction

PVA coated magnetic particles were activated with Ce(IV) and grafted with two different polymers in a two step reaction as illustrated in Fig.4.3.

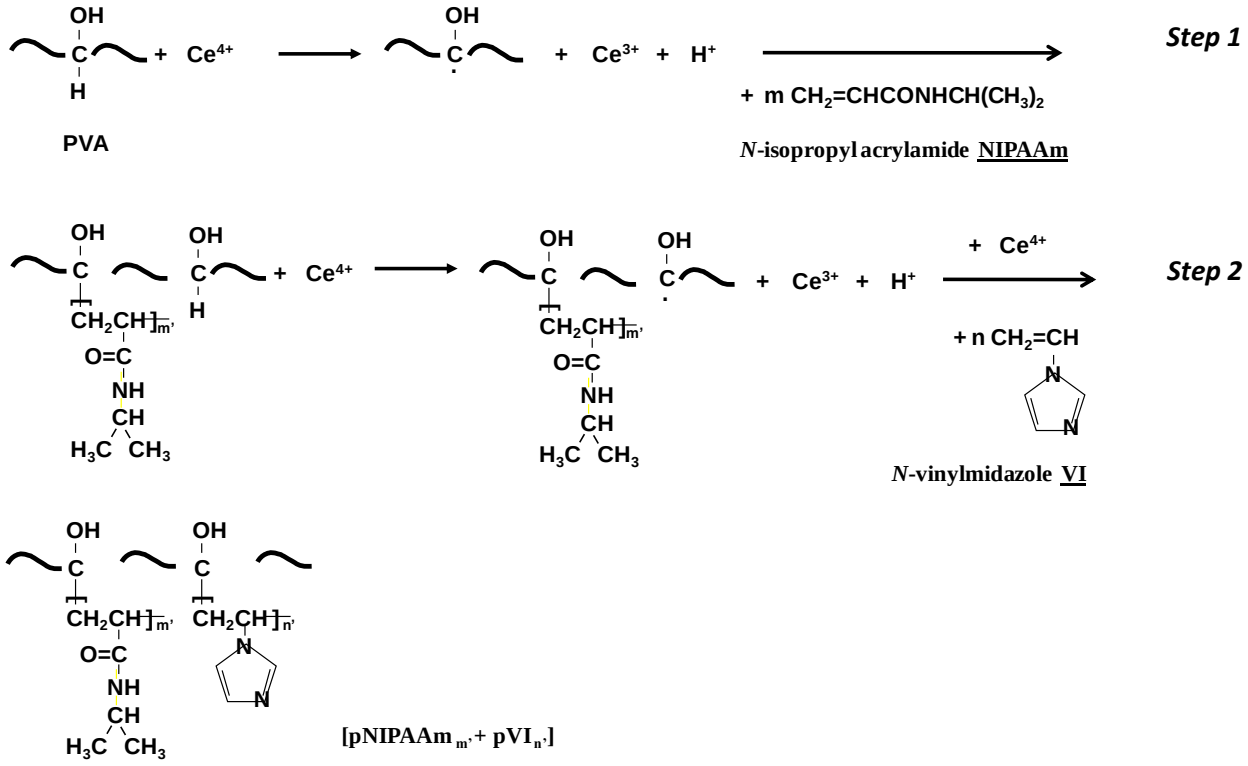

Figure 4.3 Scheme of sequential cerium (IV) initiated grafting of mixed polymer brushes composed of poly (*N*-isopropylacrylamide) (pNIPAAm) and poly (*N*-vinylimidazole) (pVI) onto M-PVA supports. Note: the same scheme was used for grafting poly (*N*-vinyl Iminodiacetic acid) (pVBIDA) aside to pNIPAAm.

At *Step 1*, 50 mg of particles were reacted with 6 mg of Ammonium Ce(IV) Nitrate (ACN), corresponding to a 6.5 Å spacing between the graft sites (based on surface area of 55 m^2 g^{-1} of batch 4), and then the first monomer was added allowing the reaction to proceed for 3 h. The radical polymerization reaction was quenched to remove any radicals which could interfere with subsequent reactions performed on the grafted support, by adding 4-

ethoxyphenol as an inhibitor (10 mg, 10 molar excess to ACN) to the reaction mixture under nitrogen after *Step 1* (Fig. 4.4).

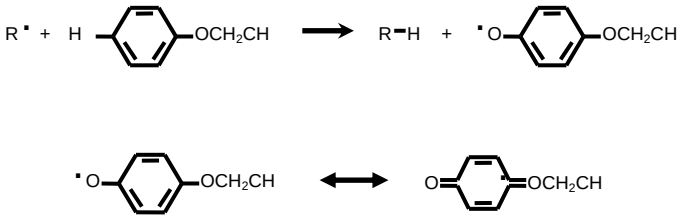

Figure 4.4 Mechanism of radical quenching, using 4-ethoxyphenol as inhibitor.

Following washing of the beads, the particles were reacted again with 6 mg of cerium (IV), and then the second monomer (pVI or pVBIDA) was added to the mixture (Fig. 4.3, *Step 2*). As overall 0.44 mmol g^{-1} of ACN applied onto the support, the final density between the graft sites of the two polymers is estimated to 4.6 Å.

Four different functionalised supports were prepared, by altering the type of affinity ligand as well as the order of the monomer addition. The first support was prepared by reacting NIPAAm at the first instant and then the affinity ligand VI, while for the second support VI was polymerised before NIPAAm. Another two supports were prepared using VBIDA instead of VI, by inverting again the order of monomer addition.

4.3.3 Cerium (IV) reaction of poly (*N*-isopropylacrylamide) and *N*-vinylimidazole in solution, to test if *N*-vinylimidazole can be grafted onto poly (*N*-isopropylacrylamide)

In order to examine the possibility that VI can be grafted onto pNIPAAm via cerium (VI) initiated grafting, the following reaction took place: 56.58 mg of pNIPAAm (corresponding mass to 0.5 mmol NIPAAm monomer), 0.5 mmol of VI, 0.05 mmol of ACN in 0.342 mL of 2 M Nitric Acid and 0.8 mL of H_2O were degassed under Nitrogen for 0.25 h, sealed and

mixed for 3 h. The product was heated at 200 °C, so that the remaining VI could evaporate (bp. of VI is 192-194°C). An amount of 3 mg from the remaining material was mixed and crushed with 300 mg of KBr, and tested with FT-IR.

4.3.4 Cerium (IV) reaction of poly-vinylimidazole and *N*-isopropylacrylamide in solution, to test if *N*-isopropylacrylamide can be grafted onto poly (*N*-vinylimidazole)

In order to investigate the case that NIPAAm can be grafted onto pVI via cerium (VI) reaction in solution, the following reaction took place: 47.05 mg (0.5 mmol) of pVI and 56.58 mg (0.5 mmol) of NIPAAm were dissolved into 0.4 mL H_2O each, and degassed for 30 min under Nitrogen. A mass of 27.41 mg (0.05 mmol) ACN were dissolved into 0.8 mL H_2O and degassed also for 30 min. ACN was finally mixed with pVI and NIPAAm for over 12 h. The product was dried in the oven for 2 h at 100°C so that to allow evaporation of any remaining NIPAAm (bp. of NIPAAm is 89-92°C). An amount of 3 mg from the remaining material was mixed with 300 mg of KBr, and tested with FT-IR.

4.3.5 Protein (haemoglobin) binding and elution studies

The functionalised supports (3 mg) were charged with Cu^{2+} ions by suspending them in 1.5 mL of 50 mM $CuCl_2$. The solution was incubated with shaking using an orbital shaker (IKA®-Werke GmbH, Staufen, Germany) at 1800 rpm for 0.3 h, and the procedure was repeated again. The supports were then washed with 1.5 mL binding buffer for 0.3 h twice. The charged supports were re-suspending with 1.5 mL of the lowest concentration haemoglobin binding solution, and then mixed and incubated on the shaking plate at room temperature. After 0.5 h, the supernatant was magnetically removed from the support and the

concentration of protein unbound on the support was determined by using the analysis described in section *4.3.7.3*. The above procedure was repeated sequentially by adding haemoglobin of higher concentrations.

The binding isotherms of the supports tested, were fitted to the Langmuir model (Eq. 4.1) using the Sigma Plot version 9.0 software (Systat Software Inc, CA, USA).

$$Q^* = \frac{Q_{max} K_d C^*}{1 + K_d C^*} \qquad \text{Eq. (4.1)}$$

In Eq. 4.1, Q* is the amount of protein adsorbed per gram of support and C* is the liquid-phase protein concentration at equilibrium. In this model binding is described by the terms of dissociation constant K_d and the maximum capacity for adsorbed protein Q_{max}. The initial slope of the binding isotherms (Q_{max} /K_d) allow easy comparisons of the performance of the different adsorbents.

4.3.6 Protein (haemoglobin and green fluorescence protein) batch binding and release studies with temperature

The functionalised supports (2 mg) were charged with Cu^{2+} ions by suspending them in 1.0 mL of 50 mM $CuCl_2$. The solutions were mixed with shaking using an orbital shaker (IKA®-Werke GmbH, Staufen, Germany) at 1800 rpm for 0.3 h. The supports were then equilibrated and washed from any unbound Cu^{2+} ions with 1.5 mL binding buffer for 0.3 h twice. The supports were then incubated for 1 h with protein (haemoglobin or GFP) solution at 300 mg g^{-1} in an OLS 200 water bath (Grant Instruments, Shepreth, UK) at 20 ºC. After protein binding, the samples were washed twice with 1.0 mL of binding buffer at 20 ºC to remove any loosely bound protein from the matrix. These materials were washed with the same

binding buffer at temperatures above and below the LCST, i.e. at 42 ºC and 20 ºC, to investigate any protein elution via phase transition of polymers. Each sample was introduced in eight temperature shifting cycles for at least 360 s. The same procedure was repeated for each sample (homo-polymer or mixed brush) but under the following conditions: (a) without any addition of Cu^{2+} ions (uncharged supports); and (b) charging the supports and replacing the binding buffer with elution buffer. In the later case, the supports were introduced in only four temperature shifting cycles. The charged and uncharged supports were afterwards eluted with 1.0 mL of 0.2 M imidazole at pH 7.0. Finally, the remaining protein was stripped off the support with 1.0 mL of 0.5 M NaOH by incubation for 1 h in the orbital shaker.

4.3.7 Analytical techniques

4.3.7.1 Solid based detection of polymers grafted onto M-PVA supports using Fourier Transform Infrared Spectroscopy (FT-IR) in solids

After each reaction, the functionalized supports were subsequently washed, dried in the oven and 1 or 2 mg of each was mixed and crushed with 300 mg potassium bromide (KBr) to form a very thin powder. These mixtures were then pressed between pellets at 10 tons, and the resulting discs were tested with the Nicolet 380 FT-IR spectrometer (Thermo Fisher Scientific, Waltham, MA, USA). The FT-IR spectra of both unmodified and modified beads were compared in order to detect the appearance of new bands corresponding to the polymers grafted on the support surface.

4.3.7.2 Liquid based analysis of monomer consumption using Attenuated Total Reflection Fourier Transform Infrared Spectroscopy (ATR FT-IR) in liquids

The concentration of the monomers remained in the supernatants after each step of the reaction was measured using the same method described in section *3.3.6.5* in Chapter 3. The same calibrations constructed before (Appendix section, Fig. 7.2 - 7.7) were used as the type of reactants and the reaction mixture remained the same in these experiments.

4.3.7.3 Analytical assays for protein content

The concentration of protein bound and released/eluted onto/from the supports was defined by estimating the protein remained in the supernatants. For this purpose a calibration curve of Hb in binding buffer measuring the absorbance of different concentrations of protein at 405 nm was used. The same calibration curve was employed to estimate the Hb washed and released from the supports. The Hb stripped with the addition of NaOH was estimated by constructing a calibration graph of protein in NaOH and measuring the absorbance at 210 nm. The GFP bound/washed onto/from the support and stripped in NaOH was determined by using the standard Better Bradford Assay of the tube protocol in the corresponding solvents. The GFP eluted from the support was determined using the Better Bradford assay of micro-test protocol. For the measurements a UVICON 922 Spectrophotometer (Kontron Instruments, Bletchley, UK) was employed. All the above curves are given in the Appendix, section 7.3, Fig. 7.8 - 7.11.

4.4 Results

4.4.1 Mixed functionality polymer brushes composed of smart polymer and affinity ligand polymers: manufacturing and characterisation

Sequential cerium (IV) grafting was used to create mixed brushes composed of two different functionality polymers grafted adjacent to each other on the same M-PVA particles surface (Fig. 4.5). For all the experiments in this work, the same M-PVA support (batch 4) was used, due to availability in large amount and its behaviour in comparison with other available materials (i.e. higher polymerisation degree and better binding characteristics in comparison with that of batch 5 M-PVA).

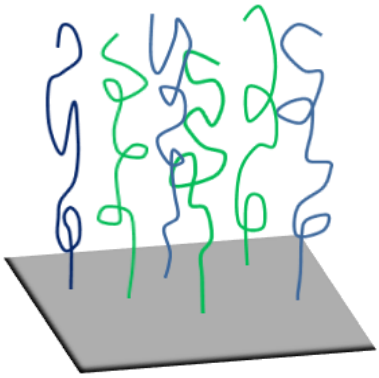

Figure 4.5 Mixed polymer brushes composed of smart polymer (blue) and affinity ligand polymer (green).

In graft copolymerisation a common used method for chemical initiation of vinyl monomers is the reaction of ceric ions with a polymer backbone (eg. wool, silk, pulp, cellulose collagen etc.) (Misra and Bajpai, 1982; Simon and Bajpai, 2003). Mino and Kaizerman (1958) managed to graft acrylamide, acrylonitrile and methyl methacrylate onto poly vinyl alcohol, where the grafting occurred only on the substrate backbone without any homopolymers formation (free radicals were generated directly onto the polymer backbone). Cerium (IV) initiated polymerisation has been employed in this work to graft two vinyl polymers onto the same PVA backbone at two steps. The manufacturing of mixed brushes material was

achieved by employing two cerium (IV) sequential polymerisation reactions steps as described and illustrated before (section 4.3.2). Between the two steps, a termination procedure was performed to eliminate any active sites remained after the first cerium (IV) reaction. During each step, 0.22 mmol g^{-1} of ACN was added to the support, so the resulting mixed brushes were composed of two polymers grafted at final spacing of 4.6 Å. In addition, in every step, the initiator to monomer ratio was such as 1:250 and 1:100 ratio for the thermoresponsive monomer (NIPAAm) and the affinity ligand monomer (VI or VBIDA) respectively. The initiator to monomer ratio utilised for NIPAAm was higher than that of VI, having in mind its lower reactivity according to results in the previous chapter.

For all the above experiments the density between the graft sites (of each component and each brush) was kept constant. Based on Monte Carlo simulations, it has been shown that any density and composition fluctuations of the grafting points can 'promote' the structure formation in both one-component and mixed polymer brushes. The (lateral) structures of a mixed brush can be influenced/changed even from tiny fluctuations of the grafting points. Although the lack of periodicity will not inhibit the reversibly switching average surface properties, it can hamper the degree of phase transition sharpness by temperature or solvent quality (only a gradual crossover from one phase to the other can be observed), (Wenning *et al.*, 2005). So for more accurate comparison between the four different materials constructed any changes in density were avoided as possible. During the mixed brushes manufacturing, the amounts of pNIPAAm and initiator were kept constant during each step while cerium (IV) disappearance was recorded (97.07 ± 1.9 %). In addition efficient mixing was applied during the course of reactions. By this way the thermoresponsive behaviour of the brushes should be retained similarly with those examined in the previous chapter.

The reactions employed by combining two different monomers (e.g. NIPAAm and then VI or NIPAAm and then VBIDA) on the same M-PVA support, were repeated by inverting the

order of addition of monomers (e.g. VI and then NIPAAm or VBIDA and then NIPAAm). This was followed as depending on the structure of a polymer it might be possible to end graft the second polymer onto the backbone of the first one.

In summary, the above polymer supports were characterised by: (a) detecting the polymers grafted onto the M-PVA surface using FT-IR in KBr discs, if possible (section *4.4.4.1*); (b) quantifying the monomer consumed after each step using the method employed in Chapter 3 (section *4.4.4.1*); (c) investigating the possibility of end grafting the second polymer onto the backbone of the first one (section *4.4.1.2*); (d) estimating the Flory radii (R_F) to predict the configuration of polymer chains and their regime (section *4.4.1.3*); (e) performing haemoglobin binding studies at buffers of low ionic strength by introducing salt (section 4.4.2); (f) carry out protein binding and release studies using two different proteins (haemoglobin and GFP) (section 4.4.3).

4.4.1.1 FI-IR characterisation of mixed polymer brushes

The amount of monomer reacted during each step reaction was estimated by quantifying the concentration of the unreacted monomer remained in supernatants using the ATR FT-IR calibration curves constructed before. In Table 4.1, all the reactions performed during each step of mixed type polymer supports construction, incorporating the amount of reactants (initiator, monomers) presented and finally installed are summarised. The target spacing between the graft sites is given by assuming almost complete consumption of the initiator utilised accordingly to studies performed before (Chapter 3, section *3.4.3.3.4*) and observations of supernatants (disappearance of cerium color). Associating this with the amount of monomers consumed, the final chain length of each installed polymer was approximately determined. For the above estimations, it has been assumed that no end

grafting took place during the second step polymerisation reaction to simplify the comparison between the supports.

The considerable increase of mass of supports after grafting, may explained by the resulting density of the introduced polymer layers. Information on this can be obtained mainly by calculating the dimensions of layers introduced using the 'grafting to' approach. Based on the resulting mixed brushes composed of poly(2-vinyl pyridine) (P2VP) and poly(methacrylic acid) (PMMA) (Willett, 2009), the increase of volume brush and weight of support is estimated as follows: Following P2VP of 95 nm length 'grafting to' at 3.2 nm spacing, the volume of the particle increase by 31.3 % and the weight by 14.2 %, i.e. the density of the layer is roughly half of that of the M-PVA. After 'grafting to' PMMA of 55 nm length at 3.26 nm spacing, the volume and weight increases by 17.4 % and 15.5 % respectively. In the case of double polymer formation and assuming that the volume increase is determined by the P2VP polymer which grafted at higher degree, then the volume and weight increase by 31.3 % and 29.7 % respectively. As the double polymer layers cannot pack more than 1.9 nm close during 'grafting to', the corresponding volume and weight increase lies between 30-35 %. This increase in weight with the proposed dimensions of polymer layers implies that the brushes are extremely dense (densities of layers range from half to the same of that of M-PVA).

FT-IR spectroscopy was also employed to obtain spectra of modified beads for comparison with that of the unmodified ones. The resulting spectra of samples in KBr discs were used qualitative in order to detect new bands and/or height peak changes indicating any modification after each step reaction. In Fig. 4.6, the spectra of the four mixed brushes composed of pNIPAAm and pVI or pVBIDA in different polymer order of addition are shown.

For the [$pNIPAAm_{26.8}$ + $pVI_{26.4}$] – 4.6 Å support (Fig. 4.6), spectrum (b) represents the M-PVA support grafted with pNIPAAm at the first step while spectrum (c) represents the same support grafted with pVI at the second step. By comparing, the unmodified M-PVA support (a) with spectrum (b), we can note the appearance of N-H bend at 1550 cm^{-1} wavelength due to pNIPAAm backbone addition. After the second reaction, at spectrum (c), the modification of the support is observed by the increased height of peak at 1380 cm^{-1} wavelength (overlapping of pVI and PVA peaks in an enhanced form within the range of 1475-1250 cm^{-1} assigned to various bending vibrations of C-H bonds and C-N vibrations). Additionally, there is an increase of peak area and height at 1633 cm^{-1} due to C=C stretch vibration of imidazole ring (similar observations were noted for pVI homo-polymer brush grafted onto PVA backbone in Chapter 3, section *3.4.3.2.1*). The above changes (increased heights) are much smaller than those observed during homopolymer brushes characterisation as the amount of monomer presented and final installed onto the support is much less (i.e. less ACN applied: 0.22 mmol g^{-1} *cf.* 0.44 mmol g^{-1} for same initiator to monomer ratio).

By comparing the unmodified M-PVA support (a) with spectrum (b) of [$pVI_{17.7}$ + $pNIPAAm_{26.3}$] – 4.6 Å support, we can note again as above the increased height of peak at 1380 cm^{-1}. When introducing the second polymer at the second step, the appearance of N-H bend at 1550 cm^{-1} wavelength due to pNIPAAm backbone appears, while the peak at 1380 cm^{-1} is decreased.

Comparing the unmodified M-PVA support (a) with spectrum (b) of [$pNIPAAm_{21.3}$ + $pVBIDA_{17}$] – 4.6 Å support, we can note the appearance of N-H bend at 1550 cm^{-1} wavelength due to pNIPAAm backbone addition after the first step. After the second reaction, at spectrum (c), there is a considerably increase of peak at 1633 cm^{-1} due to the additional C=C bonds introduced from pVBIDA addition onto the support.

Comparing the unmodified M-PVA support (a) with spectrum (b) of [$pVBIDA_{17.9}$ + $pNIPAAm_{19.5}$] – 4.6 Å support, we can note again as before the increased height of the peak at 1380 cm^{-1}. According to spectrum (c) when introducing pNIPAAm at second step, the appearance of N-H bend at 1550 cm^{-1} wavelength due to pNIPAAm backbone appears, while the peak at 1380 cm^{-1} is decreased (the same trend was noted before for the [$pVI_{17.7}$ + $pNIPAAm_{26.3}$] – 4.6 Å support). Due to these observations where pNIPAAm is introduced during the second step and the peaks at 1380 cm^{-1} for both pVI and pVBIDA (introduced during the first step) decrease, investigation of the possibility of end grafting the second polymer onto the backbone of the first one as well as quantification of all the reactions has been carried out.

Table 4.1 Cerium (IV) grafted mixed brush supports (batch 4 supports).

Support #	M-PVA starting material		Sequential Ce(IV) grafting parameters				Support characterization								Polymer brush description on finished support
	Batch	SA (m^2/g)	Graft step - Monomer	Order of addition/ reaction solvent	Ce(IV) (mmol/g M-PVA)	Monomer presented (mmol/g M-PVA)	Target DP (units)	React^n (%)	DP (units)	Spacing (Å)	Monomer installed (mmol/g M-PVA)	Polymer (g/g M-PVA)	Polymer (g/g support)	Monomer installed (mmol/g support)	
Mixed-4.1	4	55	1 - NIPAAm	Std/H_2O	0.22	55	250	10.7	26.8	6.45	4.53	0.512	0.249	2.04	[$pNIPAAm_{26.8}$ + $pVI_{26.4}$] – 4.6 Å
			2 - VI	Std/H_2O	0.22	22	100	26.4	26.4	4.56	5.81	0.546	0.265	2.61	
											10.3	1.058	0.514	4.65	
Mixed-4.2	4	55	1 - VI	Std/H_2O	0.22	22	100	17.7	17.7	6.45	3.89	0.366	0.203	2.16	[$pVI_{17.7}$ + $pNIPAAm_{26.3}$] – 4.6 Å
			2 - NIPAAm	Std/H_2O	0.22	55	250	10.5	26.3	4.56	5.78	0.440	0.244	3.20	
											9.67	0.806	0.446	5.35	
Mixed-4.3	4	55	1 - NIPAAm	Std/H_2O	0.22	55	250	8.5	21.3	6.45	4.68	0.529	0.214	1.89	[$pNIPAAm_{21.3}$ + $pVBIDA_{17}$] – 4.6 Å
			2 - VBIDA	Std/H_2O	0.22	22	100	17.0	17.0	4.56	3.74	0.940	0.381	1.52	
											8.42	1.469	0.595	3.41	
Mixed-4.4	4	55	1 - VBIDA	Std/H_2O	0.22	22	100	17.9	17.9	6.45	3.94	0.991	0.400	1.59	[$pVBIDA_{17.9}$ + $pNIPAAm_{19.5}$] – 4.6 Å
			2 - NIPAAm	Std/H_2O	0.22	55	250	7.8	19.5	4.56	4.29	0.485	0.196	1.73	
											8.23	1.476	0.596	3.32	

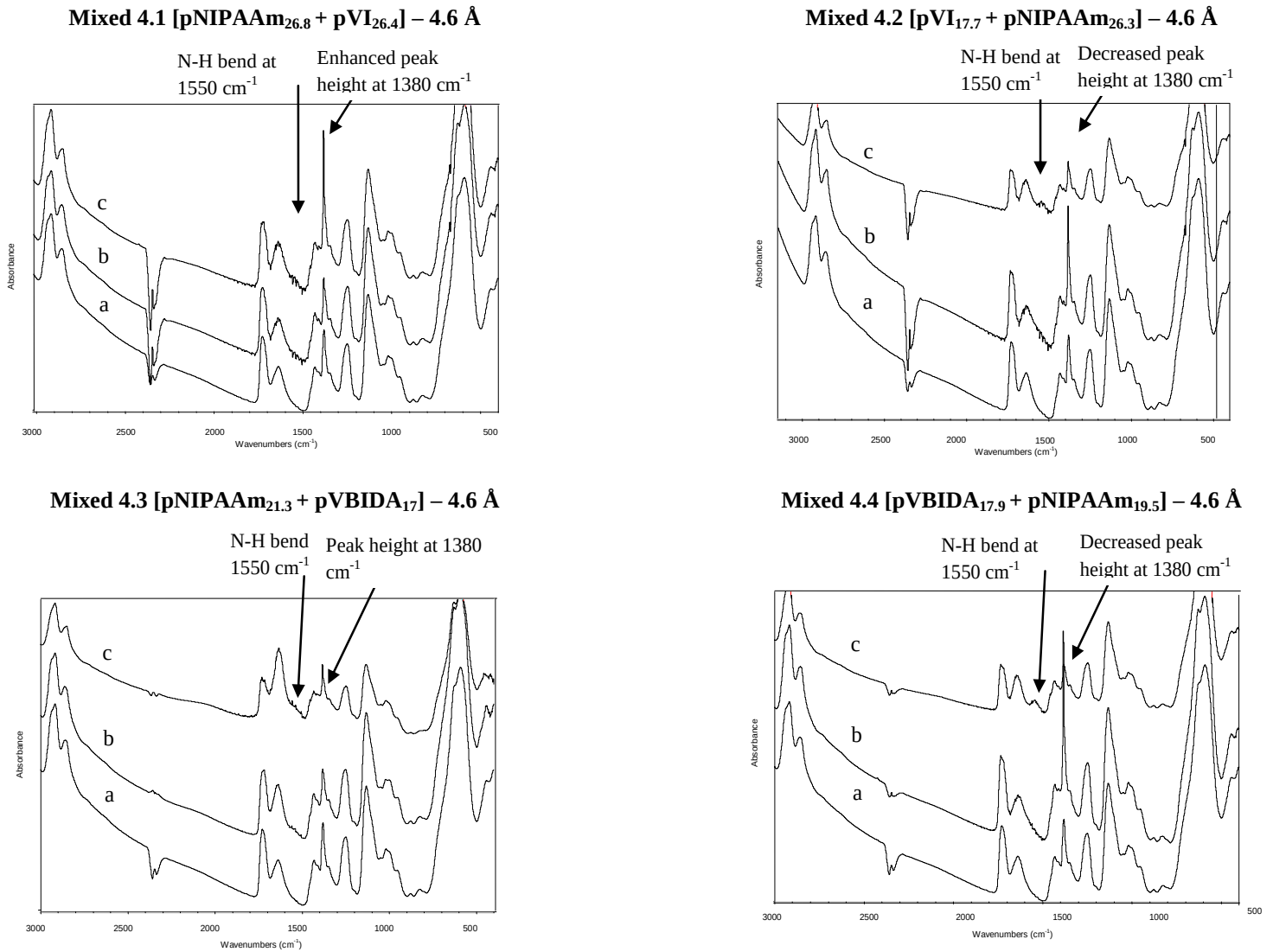

Figure 4.6 FT-IR spectra of mixed polymer brushes by cerium (IV) sequential grafting: **a**- Unmodified M-PVA, batch 4; **b**- First graft; **c**- Second graft.

4.4.1.2 Investigation of possible polymerisation onto polymers backbones during the second grafting step

During the construction of mixed brushes, three different monomers were used in various combinations (i.e. NIPAAm, VI and VBIDA). Depending the structure of each monomer (and its corresponding polymer), when grafted onto a surface could be a candidate for cerium (IV) initiation polymerisation reaction. In Fig. 4.7, the two possible brush architectures using sequential cerium (IV) grafting is shown. At (a), the real regime of the mixed brush is illustrated, while at (b) a likely deviating arrangement has been drawn.

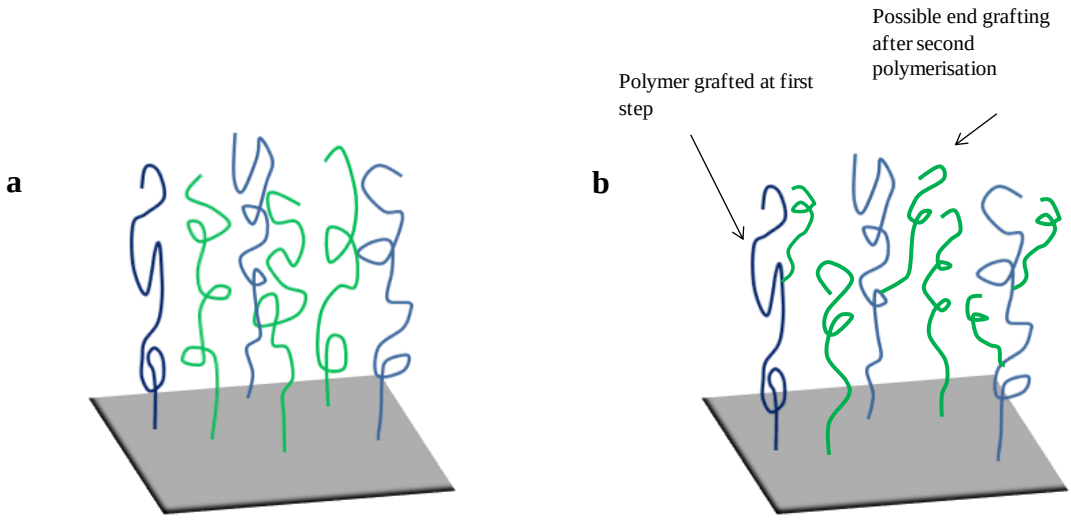

Figure 4.7 Possible brush architectures after the second cerium (IV) initiated polymerisation reaction: **a**- Real regime of mixed polymer brush; **b**- Polymer brush with the second polymer installed onto the backbone of the first one.

In order to investigate the possibility of end grafting, cerium (IV) initiation reactions were performed in solution and their resulting products were analysed with FT-IR. The first reaction that took place in solution was that of pNIPAAm in the presence of cerium (IV) and the VI monomer under complete exclusion of oxygen. After the reaction, the resulting product was isolated from any remaining VI, then dried and finally mixed with KBr. In Fig. 4.8, the

obtained FT-IR scan is compared with that of pure pNIPAAm. Observation of these spectra indicates that VI could not graft onto pNIPAAm via cerium reaction as: (i) the product's spectra (b) corresponds with that of pure pNIPAAm (a) and (ii) there is no significant reduction of the C=O stretch peak at 1680 cm^{-1} with respect of the other peaks (this bond is the only available site for cerium (IV) reaction.

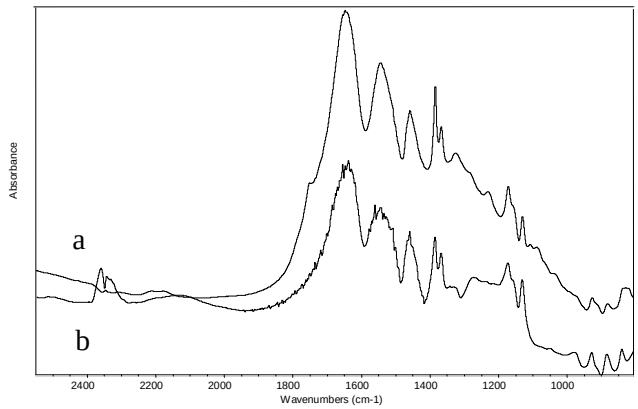

Figure 4.8 Cerium (IV) reaction of poly-N-isopropylacrylamide and N-vinylimidazole in solution: (a) Pure pNIPAAm, (b) Product of the reaction.

These findings, confirm that the mixed brushes constructed by adding pNIPAAm at the first step of the sequential reactions, are near the desired regime of a mixed brush (Fig. 4.7, a), i.e. the chains of the two polymers (pNIPAAm and pVI) are distributed adjacent to each other.

In order to test the same hypothesis where pVI is grafted at the first step, a reaction of pVI in the presence of NIPAAm and cerium (IV) took place under complete exclusion of oxygen. In Fig. 4.9, the FT-IR spectra of pure pVI (a), pure NIPAAm (b) and that of their product (c) after the reaction and NIPAAm evaporation, are shown.

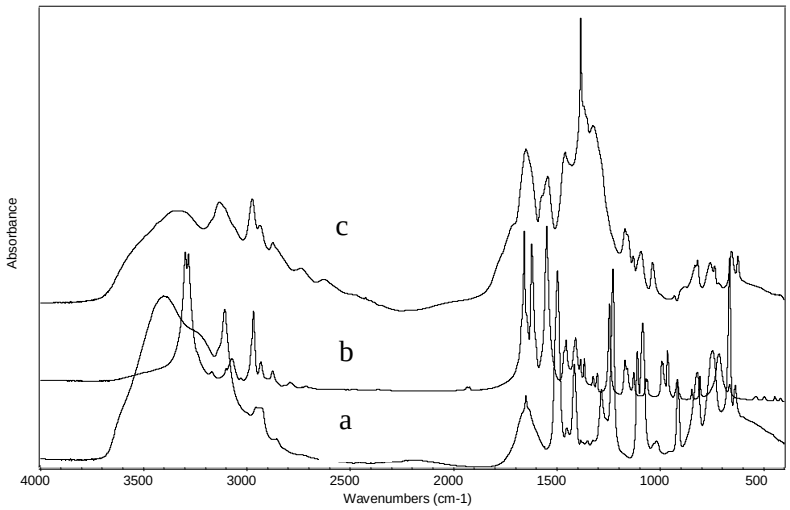

Figure 4.9 Cerium (IV) reaction of poly-*N*- vinylimidazole and *N*- isopropylacrylamide in solution: **a**- pVI; **b**- NIPAAm; and **c**- Product of pVI and NIPAAm after cerium (IV) reaction in solution.

The spectrum (c) of the reaction product indicates the appearance of peaks corresponding to pVI and/or pNIPAAm polymers. In such case, there are two possibilities. Either the NIPAAm is polymerised in the solution or is grafted onto the pVI backbone. Based on observations of the supernatants after cerium (IV) grafting (ATR FT-IR spectra and viscosity), no polymer was formed in solution. In addition, as mentioned before, due to the high concentration of –OH groups onto the PVA polymer coating, the affinity of cerium (IV) for initiation from the surface is high to allow for any further initiation from other groups. In Fig. 4.10, the structures of the polymers (pNIPAAm, pVI and pVBIDA) employed are presented.

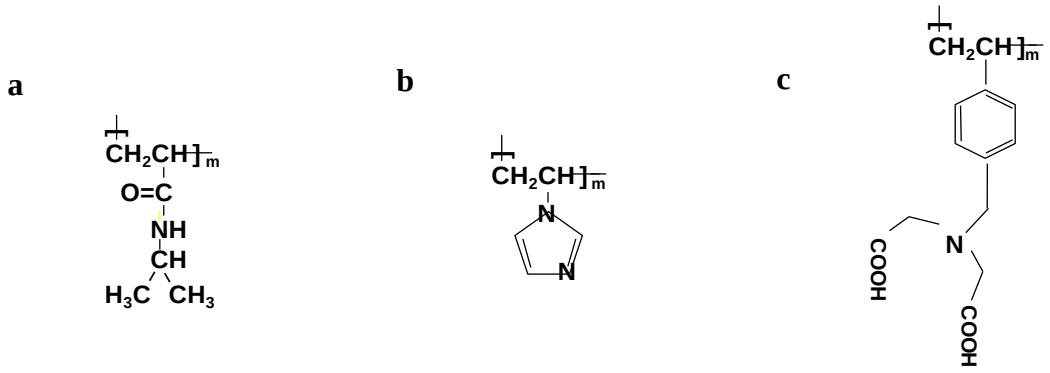

Figure 4.10 Structure of polymers used for the construction of mixed brushes: **a**- the thermoresponsive polymer pNIPAAm; **b** - the metal chelating polymer pVI; **c**- the metal chelating polymer pVBIDA.

By observing the structures of all the polymers (Fig. 4.10), not such reactive sites can be identified where cerium (IV) reaction can initiate polymerisation. Although polymerisation may take place in solution, when the same reaction takes place onto the backbone of the PVA (graft polymerisation), the same scenario would be more unlikely, given the much higher affinity of Ce(IV) for hydroxylated materials such as PVA. In addition, the optimum concentration of ACN for the prevention of polymerisation in solution was utilised in this work, which was based on previous studies on cerium (IV) grafting of poly acrylic acid.

On the other hand, if some 'alive' radicals remained after the first polymerization reaction able to engage further polymerization reactions with other monomers, the free radical quenching agent prior to conducting the second cerium (IV) grafting was utilised, making sure that these radicals were 'killed'.

4.4.1.3 Flory radii and regime of mixed polymer chains

The average Flory Radius (R_F) of the mixed polymer chains was estimated following three different methods, by taken account the proportion of each monomer in the brush layer and relating the R_F with respect to the average of monomer size:

a. In this method, the average $R_F^{'}$ is related to the number of monomer units at each polymer chain, and can be estimated by the following equation:

$$R_F^{'} = \frac{R_{F1} \cdot n_1 + R_{F2} \cdot n_2}{n_1 + n_2} \qquad \text{Eq. (4.1)}$$

At Eq. 4.1, R_{F1} and R_{F2} are the Flory radii of the two monomers grafted respectively, and n_1 and n_2 are the number of monomer units of each polymer present.

b. In the second method, the average $R_F^{''}$ is related to average R_F of each polymer which is based to the number of chains of each polymer present (equal weighting), and can be estimated by Eq. 4.2:

$$R_F^{''} = \frac{R_{F1} \cdot N_1 + R_{F2} \cdot N_2}{N_1 + N_2} \qquad \text{Eq. (4.2)}$$

At Eq. 4.2, R_{F1} and R_{F2} are the Flory radii of the two monomers grafted respectively, and N_1 and N_2 are the number of chains of each polymer present, based on number of initiator groups.

c. In this method, the average R_F''' is related to the weighted average of the R_F of each polymer and their number of chains present, while the average is weighted towards the chains of higher R_F values, and can be estimated using Eq. 4.3:

$$R_F''' = \frac{R_{F1}^2 \cdot N_1 + R_{F2}^2 \cdot N_2}{R_{F1}N_1 + R_{F2}N_2} \qquad \text{Eq. (4.3)}$$

At Eq. 4.3, R_{F1} and R_{F2} are the Flory radii of the two monomers grafted respectively, and N_1 and N_2 are the number of chains of each polymer present, based on number of initiator groups.

In Table 4.2, the average R_F', R_F'' and R_F''' and their corresponding s/($2R_F$) ratios for all the mixed brushes are presented. The estimations were based on (a) 100 % cerium (IV) consumption based on cerium color disappearance observations in this work; (b) 70 % of cerium (IV) consumption based on findings of Gupta and Sahoo (2001); and (c) 2 % of cerium (IV) consumption based on findings of Hritcu *et al*. (1999).

Following method c, higher R_F values are obtained as the estimation is weighted towards the species of more monomer units. However, all three averaging techniques gave consistent results, indicating that the mixed polymer chains are in the 'true' brush regime.

Table 4.2 R_F and $s/(2R_F)$ values obtained under different % cerium (IV) assumed consumption, following method (a) averaging based on number of monomer units; (b) averaging based on the number of polymer chains with equal weighting; and (c) averaging according to number of chains, weighted with respect to those of higher R_F.

100 % cerium (IV) consumption												
Support #	Graft step - Monomer	Ce(IV) (mmol/g M-PVA)	s (Å)	DP (units)	Segment length *l* (Å)	R_F (Å)	R_F' (Å)	$s/(2R_F')$	R_F'' (Å)	$s/(2R_F'')$	R_F''' (Å)	$s/(2R_F''')$
Mixed-4.1	1 - NIPAAm	0.22	4.56	26.8	3.0	21.9	38.3	0.06	38.4	0.06	45.7	0.05
	2 - VI	0.22		26.4	7.74	55.2						
Mixed-4.2	1 - VI	0.22	4.56	17.7	7.74	43.4	30.2	0.08	32.4	0.07	36.1	0.06
	2 - NIPAAm	0.22		26.3	3.0	21.3						
Mixed-4.3	1 - NIPAAm	0.22	4.56	21.3	3.0	18.8	26.7	0.09	27.7	0.08	30.6	0.07
	2 - VBIDA	0.22		17	6.70	36.7						
Mixed-4.4	1 - VBIDA	0.22	4.56	17.9	6.70	37.8	27.4	0.08	27.8	0.08	31.4	0.07
	2 - NIPAAm	0.22		19.5	3.0	17.8						
70 % cerium (IV) consumption												
Support #	Graft step - Monomer	Ce(IV) (mmol/g M-PVA)	s (Å)	DP (units)	Segment length *l* (Å)	R_F (Å)	R_F' (Å)	$s/(2R_F')$	R_F'' (Å)	$s/(2R_F'')$	R_F''' (Å)	$s/(2R_F''')$
Mixed-4.1	1 - NIPAAm	0.154	5.46	29.4	3.0	22.8	48.4	0.06	45.9	0.06	57.0	0.05
	2 - VI	0.154		37.7	7.74	68.4						
Mixed-4.2	1 - VI	0.154	5.46	25.3	7.74	53.7	37.4	0.07	40.1	0.07	44.7	0.06
	2 - NIPAAm	0.154		37.5	3.0	26.4						
Mixed-4.3	1 - NIPAAm	0.154	5.46	30.4	3.0	23.3	33.1	0.08	34.4	0.08	37.9	0.07
	2 - VBIDA	0.154		24.3	6.70	45.4						
Mixed-4.4	1 - VBIDA	0.154	5.46	25.6	6.70	46.8	34.0	0.08	34.5	0.08	38.9	0.07
	2 - NIPAAm	0.154		27.9	3.0	22.1						
2 % cerium (IV) consumption [a]												
Support #	Graft step - Monomer	Ce(IV) (mmol/g M-PVA)	s (Å)	DP (units)	Segment length *l* (Å)	R_F (Å)	R_F' (Å)	$s/(2R_F')$	R_F'' (Å)	$s/(2R_F'')$	R_F''' (Å)	$s/(2R_F''')$
Mixed-4.1	1 - NIPAAm	0.0044	32.27	1029.5	3.0	192.62	408.6	0.04	384.8	0.04	480.8	0.03
	2 - VI	0.0044		1320.5	7.74	577.00						
Mixed-4.2	1 - VI	0.0044	32.27	884.1	7.74	453.56	315.7	0.05	338.3	0.05	377.6	0.04
	2 - NIPAAm	0.0044		1313.6	3.0	222.95						
Mixed-4.3	1 - NIPAAm	0.0044	32.27	1063.6	3.0	196.43	279.5	0.06	290.0	0.06	320.1	0.05
	2 - VBIDA	0.0044		850.0	6.70	383.47						
Mixed-4.4	1 - VBIDA	0.0044	32.27	895.5	6.70	395.64	286.6	0.06	291.0	0.06	328.6	0.05
	2 - NIPAAm	0.0044		975.0	3.0	186.43						

[a] Note: As mentioned in Chapter 3 (section 3.4.6) the range of values obtained for 2 % consumption is rather unlikely as homopolymerisation was not detected at supernatants as observed at Hritcu *et al*. (1999) work.

4.4.2 Protein (haemoglobin) binding studies onto manufactured mixed brushes

Subsequently to the characterization of the mixed brushes, all the supports were tested for protein adsorption at 20 ºC. Haemoglobin (Hb) was used for binding studies on mixed polymer supports, which affinity for metal-charged adsorbents is well documented and can be attributed to the number, geometry and accessibility of its exposed histidines (Hemdan *et al.*, 1989; Todd *et al*., 1994, O'Brien *et al.*, 1996). Hb binding onto homopolymer brushes of pVI, pVBIDA or pNIPAAm was studied in the previous chapter. The metal affinity interactions were exploited by performing the above studies in the presence and absence of Cu^{2+} ions. During binding, the pH of the solution was kept at 6.9 so that the histidines in the protein structure could coordinate to the Cu^{2+} ions. At lower pH value, the degree of protonation increases and the coordination ability decreases (Garipcan, 2004). The experiments took place in 100 mM Sodium Phosphate, 1 M NaCl buffer in order to investigate the effect of high salt concentration in protein binding on mixed brushes containing pNIPAAm. High salt concentrations reduce unspecific binding, eliminate the ionic interactions and do not affect the metal chelating interactions with protein (Marshak, 1996; Amersham, 2007; Kumar *et al.*, 1998a and references therein). However the addition of NaCl lowers the LCST of pNIPAAm compounds due to salting-out effect (i.e. accelerated de-hydration) (Inomata *et al*., 1992; Park and Hoffman, 1993; Kanazawa *et al.*, 1996 and 1998; Suwa *et al*., 1998; Freitag and Garret-Flaudy, 2002). It has been reported that at concentration of 1.0 M NaCl, the LCST of pNIPAAm decrease from 32 °C to 20 °C (Kanazawa *et al.*, 1996 and 1998; Freitag and Garret-Flaudy, 2002). In the case of NIPAAm-VI copolymers synthesised by Kumar *et al.* (1998a), the incorporation of hydrophilic imidazole moieties of vinyl imidazole increased the LCST. This effect was more pronounced when the copolymer was charged with copper ions. Considering these findings, we assume that the pNIPAAm chains on supports are still in their

extended form (or at least partial collapsed) when the supports are charged, however completely collapsed while being uncharged.

In Fig. 4.11, the equilibrium adsorption isotherms of all the supports including that of the base matrix (unmodified M-PVA) are represented. The predicted Langmuir parameters for all the supports are summarised in Table 4.3.

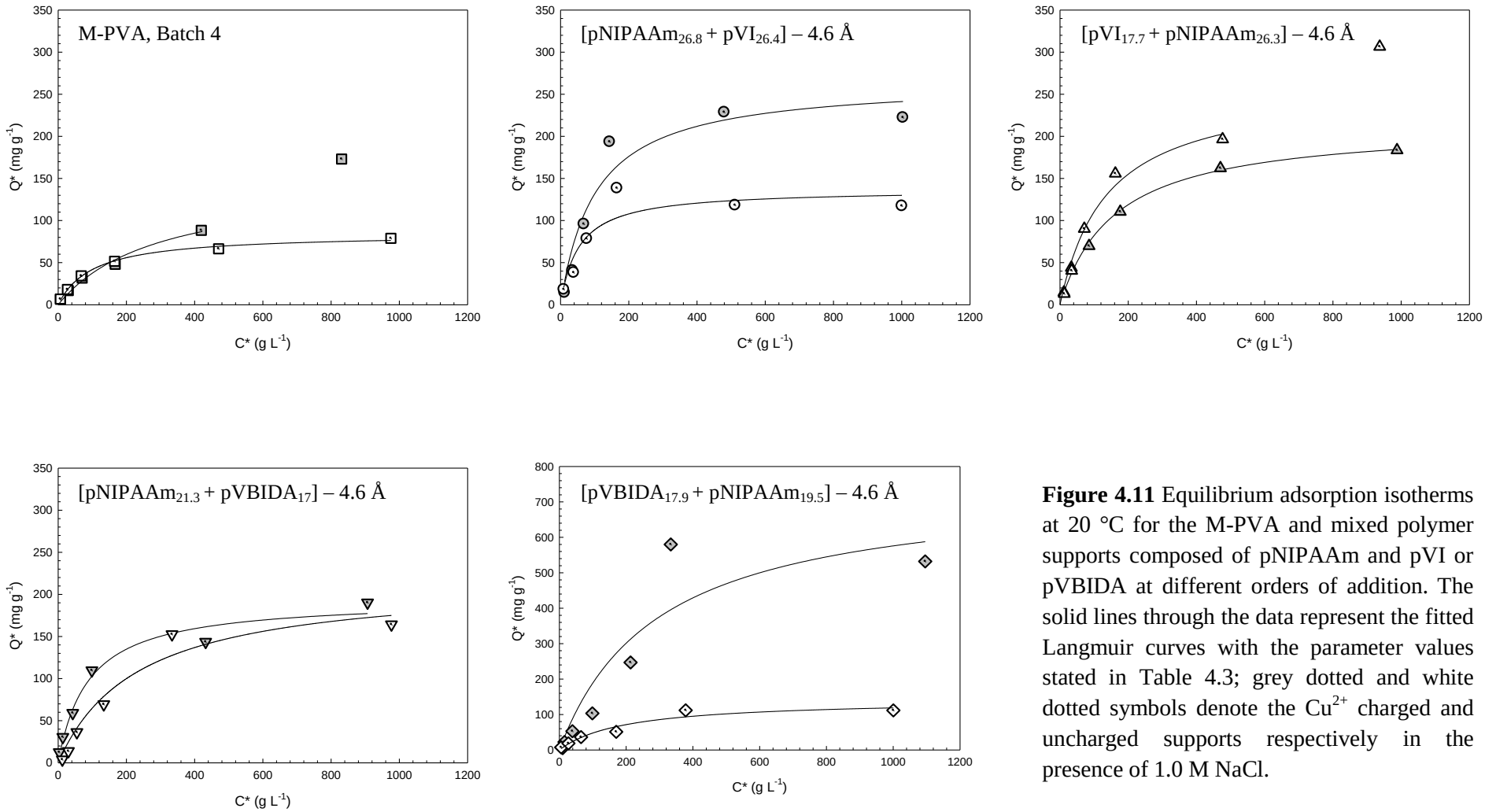

Figure 4.11 Equilibrium adsorption isotherms at 20 °C for the M-PVA and mixed polymer supports composed of pNIPAAm and pVI or pVBIDA at different orders of addition. The solid lines through the data represent the fitted Langmuir curves with the parameter values stated in Table 4.3; grey dotted and white dotted symbols denote the Cu^{2+} charged and uncharged supports respectively in the presence of 1.0 M NaCl.

Table 4.3 Langmuir predicted parameters for the curves fitted in Fig. 4.11.

Support #	Batch # and description	NaCl conc^{n} in binding buffer (M)	Q_{max} (mg/g)	K_d (μM)	Initial slope (L/g)	Affinity ligand (mmol/g support)	NIPAAm (mmol/g support)
	M-PVA, batch 4	1	88	1.58	0.87	0	0
Mixed-4.1	[$pNIPAAm_{26.8}$ + $pVI_{26.4}$] – 4.6 Å	1	136	0.82	2.57	2.61	2.04
Mixed-4.2	[$pVI_{17.7}$ + $pNIPAAm_{26.3}$] – 4.6 Å	1	260	2.11	1.91	2.16	3.20
Mixed-4.3	[$pNIPAAm_{21.3}$ + $pVBIDA_{17}$] – 4.6 Å	1	217	3.63	0.93	1.52	1.89
Mixed-4.4	[$pVBIDA_{17.9}$ + $pNIPAAm_{19.5}$] – 4.6 Å	1	142	3.07	0.72	1.59	1.73
	M-PVA, batch 4	1	148	4.56	0.5	0	0
Mixed-4.1	Cu^{2+}-[$pNIPAAm_{26.8}$ + $pVI_{26.4}$] – 4.6 Å	1	266	1.58	2.61	2.61	2.04
Mixed-4.2	Cu^{2+}-[$pVI_{17.7}$ + $pNIPAAm_{26.3}$] – 4.6 Å	1	214	2.48	1.34	2.16	3.20
Mixed-4.3	Cu^{2+}-[$pNIPAAm_{21.3}$ + $pVBIDA_{17}$] – 4.6 Å	1	194	1.36	2.2	1.52	1.89
Mixed-4.4	Cu^{2+}-[$pVBIDA_{17.9}$ + $pNIPAAm_{19.5}$] – 4.6 Å	1	740	4.23	2.71	1.59	1.73

According to Table 4.3 and considering the assumptions made above (pNIPAAm chains fully or partially extended when charged) it is estimated that haemoglobin's access to and interaction with metal chelating residues of the metal chelating chains (copper charged supports) depends on the amount of the available grafted affinity ligand. However, for the mixed-4.4 support the binding capacity is surprisingly high and further investigation on that may be required. For the rest supports, i.e. charged mixed-4.1, mixed-4.2 and mixed-4.3 supports, the binding capacity increases linearly with the affinity ligand content (Table 4.3). Taking account the previous findings that Cu^{2+} may coordinate with pNIPAAm backbone, it is expected that the haemoglobin will also bind to these sites however at less capacity and specificity (i.e. for homo-1.3 / Cu^{2+}-$pNIPAAm_{14}$ – 4.6 Å support: Q_{max} = 86 mg g^{-1}, K_d = 11.3 μM). In addition, it is expected that the size of the pVI and pVBIDA chains will be higher than that of pNIPAAm as estimated before (Table 4.2).

All of the supports delivered high binding capacities of increased specificity with respect of that of the unmodified M-PVA support. Binding of haemoglobin onto the base matrix delivered 88 mg g^{-1} maximum capacity, whereas above the 500 g L^{-1} added protein the binding was unspecific (Fig. 4.11) with respect to all the other modified supports. Incorporation of Cu^{2+} ions increased the binding capacity of the matrix (as explained in Chapter 3). However in all cases after functionalisation the binding characteristics of the supports were considerably changed.

By comparing the binding characteristics of the above supports with that of homopolymer brushes of pVI and pVBIDA onto the same particles (batch 4), the protein binding capacity has been considerably increased in the case of mixed polymer brushes. The main difference constructing these supports is that although the final grafting density between the two different polymers (pNIPAAm and pVI) is the same i.e. 4.6 Å, the density of the chains of the same polymers (pNIPAAm or pVI) is actually at 6.5 Å. The configuration of the chains is different (wider spacing) and so the metal chelating interactions. In addition, the incorporated pNIPAAm chains of increased length (employing 1:250 ratio between Ce(IV) and NIPAAm) at 1.0 M NaCl may influence the way protein interacts with the matrix.

The increased protein binding capacity of the uncharged supports can be attributed to the effect of high salt concentration (1.0 M NaCl) on the LCST, where the pNIPAAm chains at 20 °C are most probably collapsed. As a consequence, Hb interacts and adsorbed more easily on the support due to the introduced hydrophobic interactions (Prime and Whitesides, 1991 Ding *et al*., 1999).

4.4.3 Protein desorption studies from mixed brushes by temperature transitions

In these experiments the protein desorption efficiency during transitions between the hydrophilic and hydrophobic state (i.e. 'collapse-expansion' and the reverse) of pNIPAAm chains within the mixed brushes has been examined. Batch binding studies of haemoglobin (Hb) and the hexahistidine tagged Green Fluorescent Protein (GFP) onto Cu^{2+} charged supports was performed and then followed by eight sequential cycles of temperature shifts across pNIPAAm's LCST (either from 20 °C to 45 °C -hot transition or from 45 °C to 20 °C - cold transition). The binding of both proteins was conducted at 20 °C, in order to initialise desorption below the LCST where elution is more efficient as mentioned in Chapter 3 (see section *3.4.6.5*). Before any temperature change, the supports were washed with the binding buffer at the same temperature (20 °C) to wash away any protein loosely bound. For most of the experiments the composition of the buffers did not change. The desorption experiments of haemoglobin utilising 'hot-cold' transitions were repeated also in the presence of elution buffer (imidazole) in four cycles. For the mixed brush supports the cumulative sum of eluted protein was set to 100 % corresponding to that of protein totally firmly bound after washing. This was based on the results obtained from the amount of protein eluted after stripping. After washing with NaOH the remaining protein bound was completely removed at high enough amounts. This allowed a much more accurate quantification at this step in comparison with that of protein measured after each temperature shift cycle (very dilute samples).

The first attempt employing temperature desorption cycles was conducted to Cu^{2+} charged pNIPAAm and pVI homo-polymer brushes which were used as controls to the experiments carried out onto mixed brushes.

4.4.3.1 Protein (haemoglobin and GFP) binding and desorption studies with pNIPAAm and pVI homopolymer brushes

Two homopolymer grafted supports, designated such as $pVI_{30.9}$- 4.6 Å and $pNIPAAm_{10.3}$- 4.6 Å (characterisation is given in Table 3.1), were introduced into sequential hot and cold transitions. Both of the supports were charged with Cu^{2+} ions and protein (haemoglobin and GFP) binding and desorption was performed as described above. Hb experiments took place in 100 mM Sodium phosphate, 1.0 M NaCl buffer, while GFP in 20 mM Sodium Phosphate, 200 mM NaCl buffer. The pH of both buffers was adjusted to 6.8-6.9. In Fig. 4.12, the percentage of Hb or GFP released from total bound after each temperature cycle and the corresponding cumulative percentages for each support are presented. At the end the supports were eluted with 0.2 M imidazole at pH 7.0.

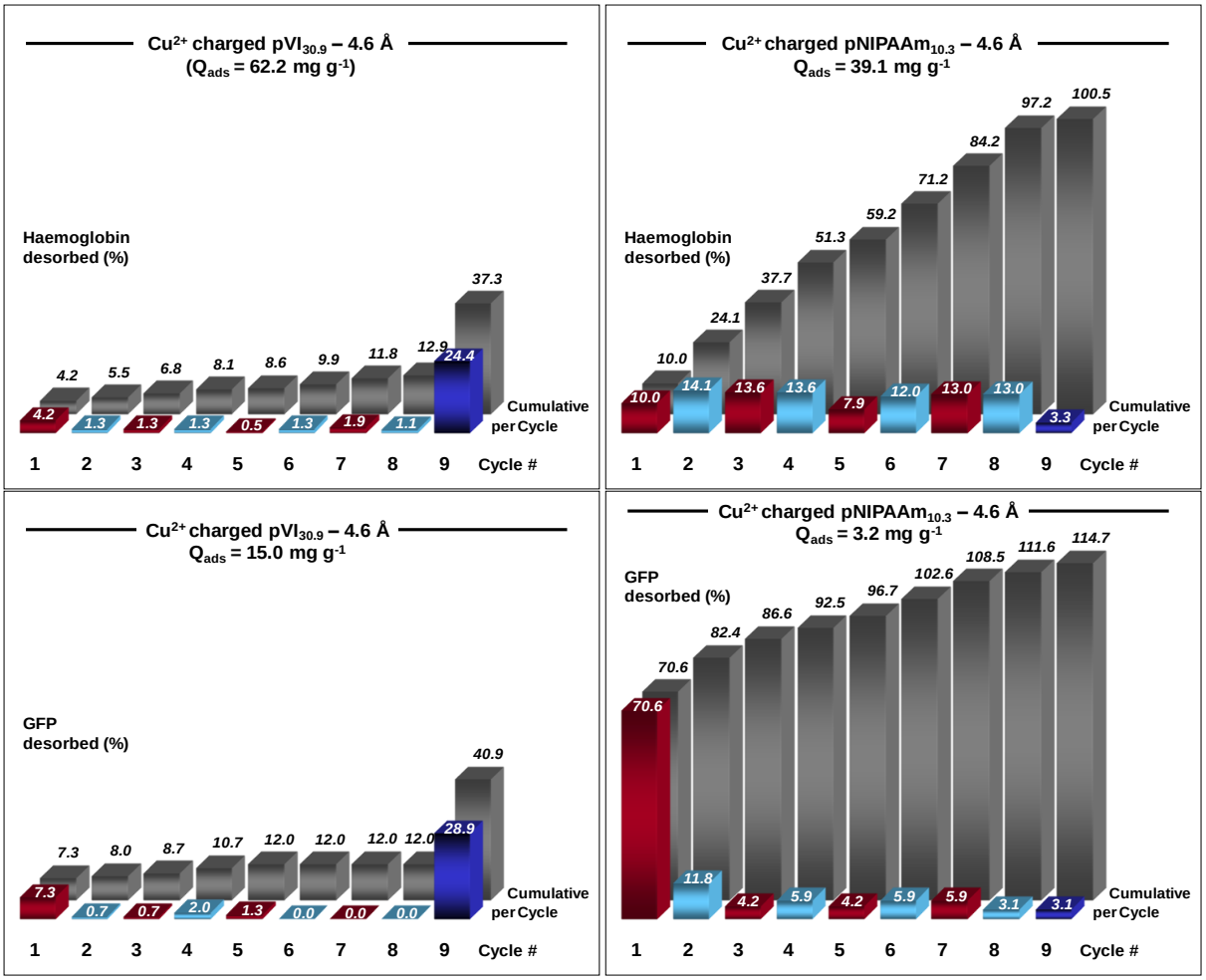

Figure 4.12 Protein (Hb and GFP) desorption experiments with Cu^{2+} charged $pVI_{30.9}$ – 4.6 Å and $pNIPAAm_{10.3}$ –4.6 Å modified M-PVA supports: Protein desorbed from 20 °C to 45 ° C (red bars); protein desorbed from 45 °C to 20 °C (light blue bars); protein desorbed with 0.2 M imidazole (pH 7.0) (deep blue bars); cumulative protein desorption from each support (grey bars).

The higher binding capacity of the supports for Hb than GFP (i.e. 62.2 mg g^{-1} versus 15.0 mg g^{-1}) can be attributed to the difference of available histidines for binding (i.e. 16 versus 6 for Hb and GFP respectively). In addition, Hb is a soft and bigger molecule which tends to stick even on 'neutral' hydrophilic surfaces (Matsui, 2008). However the very low GFP adsorption onto the support indicates that the vinyl imidazole is a relative weak affinity ligand. In addition as the pVI chains are grafted very close to each other, there is no room for the protein

to penetrate the film layer and so interacts only with the surface exposed Cu^{2+} charged VI moieties.

After the eight temperature transitions only 12.9 % and 12.0 % of Hb and GFP were desorbed from the total bound respectively. Washing of the supports with elution buffer (imidazole), more protein was desorbed (i.e. 24.4 % and 26.9 % of Hb and GFP elution). As expected, in this set of experiments, the elution buffer was more efficient than the hot-cold transition. However, for the charged $pNIPAAm_{10.3}$ –4.6 Å support, almost complete desorption was achieved with temperature changes for both proteins. The much lower amount of protein released from the pVI support in comparison with that of pNIPAAm, can be explained as (i) the amount and the way Cu^{2+} is bound onto the pVI support where the histidines of the protein can interact is higher and stronger and (ii) during the temperature transitions, the pNIPAAm chains change conformation (either expansion or collapse) promoting Hb release from the magnetic support.

4.4.3.2 Protein (haemoglobin and GFP) binding and desorption studies with [$pNIPAAm_{26.8}$ + $pVI_{26.4}$] – 4.6 Å support

The binding/desorption of Hb and GFP onto the [$pNIPAAm_{26.8}$ + $pVI_{26.4}$] – 4.6 Å mixed brush support is presented in Fig. 4.13. As in these experiments uncharged supports were tested, the concentration of salt in the buffer was lowered from 1.0 to 0.2 M for Hb binding experiments, in order to make sure that the pNIPAAm chains are not collapsed (hydrophobic). The buffer of GFP binding remained the same (i.e. 20 mM Sodium Phosphate, 200 mM NaCl buffer). The pH of both buffers was kept to 6.8-6.9. These conditions remained the same for all the

experiments with the rest of mixed supports. After the eight standard 'hot-cold cycles', the supports were washed three times with elution buffer and finally stripped with NaOH.

After protein batch binding, 59.7 mg g^{-1} of Hb was bound on the charged support while 39.7 mg g^{-1} on the uncharged. Although Hb could interact with the surface of the uncharged support, when the same material was charged with Cu^{2+} ions, the metal chelating interactions delivered higher and more specific protein binding. For both charged and uncharged support, over 40 % of Hb was desorbed after the eight successive hot-cold transitions. Subsequent washing of the charged support with elution buffer (three times) desorbed 8.4 % of Hb. Washing of the uncharged support with the same buffer could not remove much Hb (i.e. just 0.8 %) due to lack of metal chelating interactions.

A total amount of 18.1 mg g^{-1} GFP was firmly bound on the same support while being charged. From that, 60.8 % was desorbed after the first 'cold-hot' transition and 89.2 % was totally desorbed after the eight transitions. The much higher desorption of GFP in comparison with that of Hb can be attributed mainly to lower binding of GFP as well as to the differences in nature/structure of the two proteins, such as: a. GFP has 6 exposed histidines *cf.* 16 histidines of Hb available for metal chelating interactions; Hb is bigger molecule than GFP (i.e 64.5 kDa *cf.* 30 kDa), soft and can easily adhere on surfaces; GFP is more resistant to denaturation by heat providing better overall stability than that of Hb, i.e. is extremely compact and heat stable molecule which complete denaturation occurs upon rapid heating to 80 °C (Ward *et al.* 1982 and references therein; Nagy *et al*., 2004).

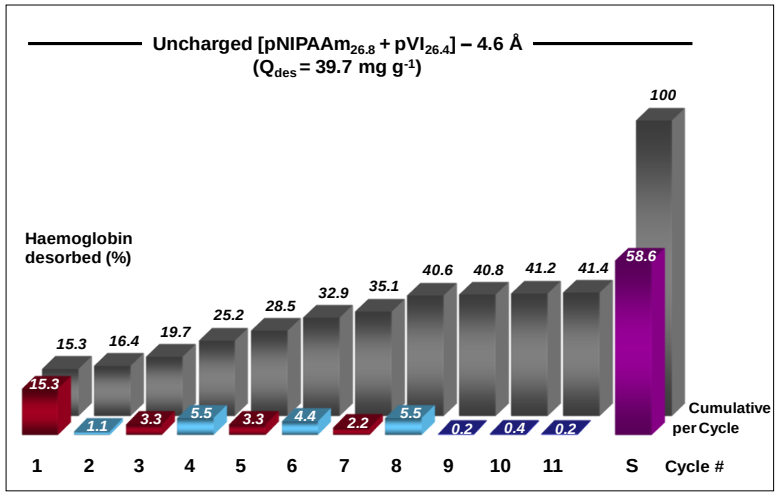

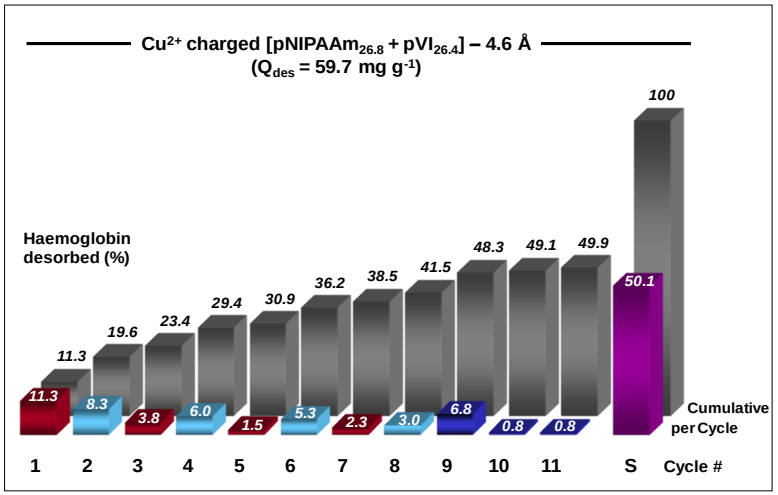

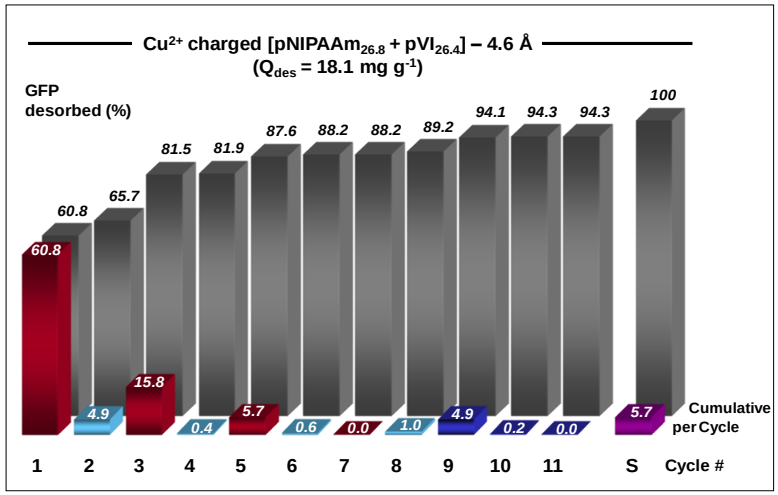

Figure 4.13 Protein (haemoglobin and GFP) desorption experiments with [pNIPAAm$_{26.8}$ + pVI$_{26.4}$] – 4.6 Å modified M-PVA support: Protein desorbed from 20 °C to 45 °C (red bars); protein desorbed from 45 °C to 20 °C (light blue bars); protein desorbed with 0.2 M imidazole (pH 7.0) (deep blue bars); protein desorbed with stripping agent (NaOH) (purple bar); cumulative protein desorption from each support (grey bars).

4.4.3.3 Protein (haemoglobin and GFP) binding and desorption studies with [$pVI_{17.7}$ + $pNIPAAm_{26.3}$] – 4.6 Å support

The Hb and GFP binding / temperature desorption onto charged / uncharged supports in binding buffer (and subsequent washes with imidazole and NaOH) was also performed for the mixed brush designated as [$pVI_{17.7}$ + $pNIPAAm_{26.3}$] – 4.6 Å, under the same conditions. In Fig. 4.14, the result of all the above desorption experiments are presented.

From the Hb bound onto the charged mixed brush (36.2 mg g^{-1}) a total amount of 21.6 % was released after the eight temperature transitions. This brush delivered lower Hb binding in comparison with the previous mixed brush [$pNIPAAm_{26.8}$ + $pVI_{26.4}$] – 4.6 Å as according to supports characterisation, much less pVI was grafted onto support i.e. 216 mmol/g *cf*. 261 mmol/g support (Table 4.1). The lower protein release can be also explained as less pNIPAAm was grafted onto the support, i.e. 2.04 mmol/g *cf.* 3.20 mmol/g support.

The same support uncharged demonstrated increased protein release at 31.5 % from the total bound (25.4 mg g^{-1} Hb). The higher desorption efficiency of the uncharged support can be attributed to the lack of Cu^{2+} ions or otherwise metal chelating interactions which promote stronger protein binding. In addition, due to the presence of metal chelating interactions, 12.8 % of protein was removed from the charged support while quite less from the uncharged one (1.6 %) when applying elution buffer.

As before, much less GFP was bound on the charged support than Hb (i.e. 12.5 mg g^{-1}) and higher desorption efficiency was achieved (i.e. 42.2 % at the first step and total 66.9 % after the eighth transition).

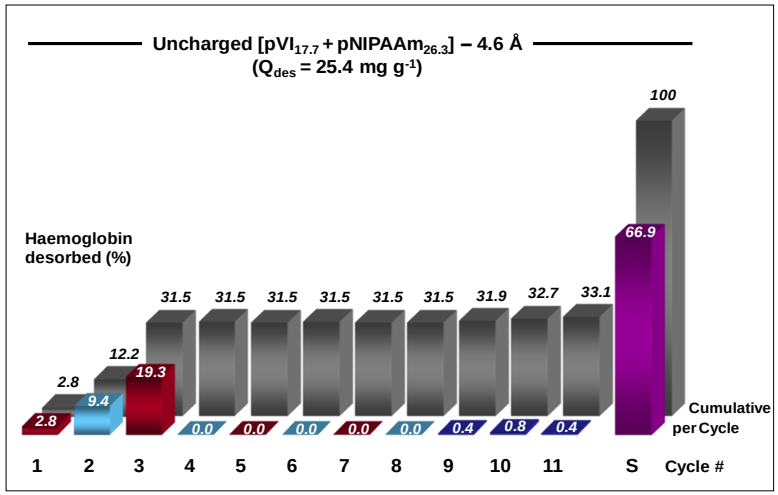

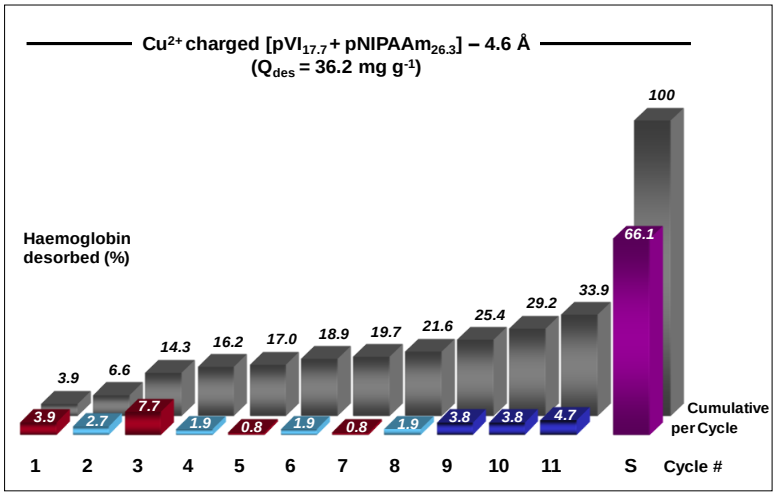

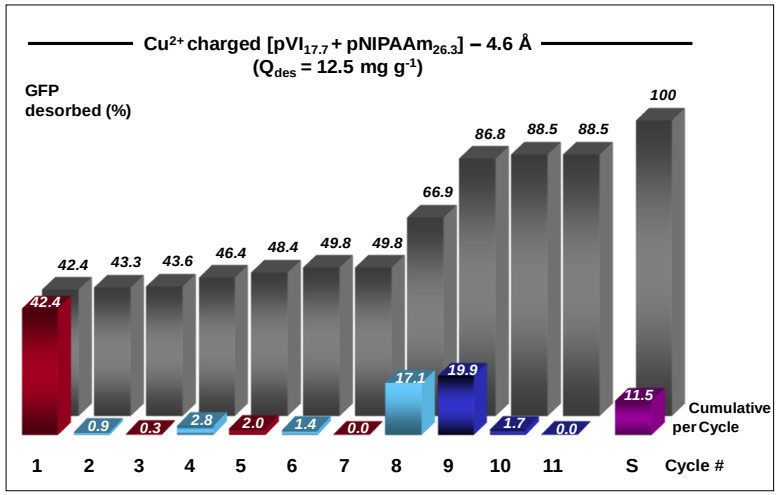

Figure 4.14 Protein (haemoglobin and GFP) desorption experiments with [$pVI_{17.7}$ + $pNIPAAm_{26.3}$] – 4.6 Å modified M-PVA support: Protein desorbed from 20 °C to 45 °C (red bars); protein desorbed from 45 °C to 20 °C (light blue bars); protein desorbed with 0.2 M imidazole (pH 7.0) (deep blue bars); protein desorbed with stripping agent (NaOH) (purple bar); cumulative protein desorption from each support (grey bars).

4.4.3.4 Protein (haemoglobin) binding and desorption studies with [pNIPAAm$_{21.3}$ + pVBIDA$_{17}$] – 4.6 Å support

The Hb binding / temperature desorption onto charged / uncharged supports in binding or imidazole buffer (and subsequent washes with imidazole and NaOH) of that containing VBIDA instead of VI, i.e. the mixed brush designated as [pNIPAAm$_{21.3}$ + pVBIDA$_{17}$] – 4.6 Å, is shown in Fig. 4.15.

After batch binding of Hb onto the support, a total amount of 30.9 mg g^{-1}, was bound. After the standard eight cycles of temperature transitions, there was no significant protein release (only 5.2 %). The inefficiency of this mixed brush for protein desorption can be explained from the type of the affinity ligand used. VBIDA forms very strong complexes with metal ions and can coordinate with more Cu^{2+} ions than VI, i.e. each VBIDA forms a complex with two Cu^{2+} ions whereas 2-3 VI groups associates with one Cu^{2+} ion (Kumar *et al*., 1998a; Kumar *et al*., 1999; Ivanov *et al*., 2001, Porath, 1992). The protein (diameter of 55 Å) bounds onto the polymer brushes (spacing 4.6 Å) by interacting only with the surface exposed Cu^{2+} ions, so the length of the affinity polymer chains is not so important. As a consequence, the higher concentration of Cu^{2+} ions onto the VBIDA grafted support surface delivers much stronger Hb binding than that of VI, although the pVBIDA grafted supports are of lower chain lengths (i.e. 17 monomers length of VBIDA *c.f.* 26 and 18 monomer lengths of VI onto the other brushes).

From the uncharged support, 36.7 % of protein was released due to the absence of metal chelating interactions and the very low amount of protein bound on the support (i.e. 7.9 mg g^{-1}).

Unfortunately, due to the full consumption of the support, no further experiments could be employed with GFP. However, for the next support where pVBIDA has been grafted aside with pNIPAAm direct comparison of both proteins has been performed.

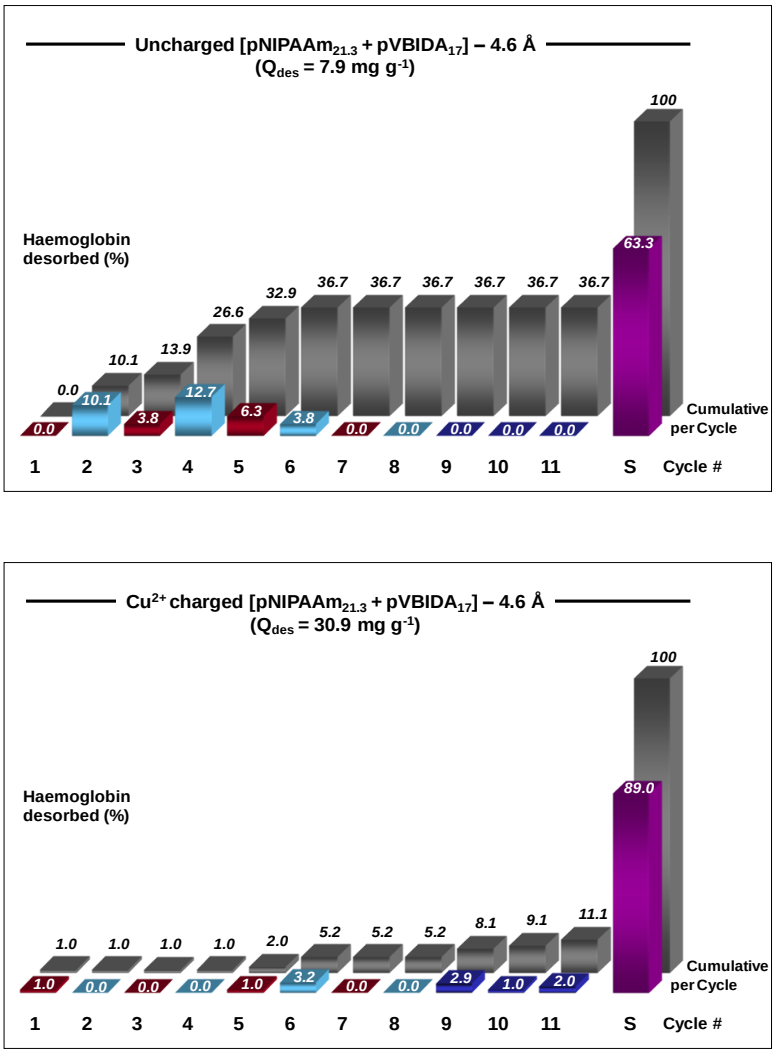

Figure 4.15 Protein (haemoglobin and GFP) desorption experiments with [pNIPAAm$_{21.3}$ + pVBIDA$_{17}$] – 4.6 Å mixed brush support: Protein desorbed from 20 °C to 45 °C (red bars); protein desorbed from 45 °C to 20 °C (light blue bars); protein desorbed with 0.2 M imidazole (pH 7.0) (deep blue bars); protein desorbed with stripping agent (NaOH) (purple bar); cumulative protein desorption from each support (grey bars).

4.4.3.5 Protein (haemoglobin and GFP) binding and desorption studies with [pVBIDA$_{17.9}$ + pNIPAAm$_{19.5}$] – 4.6 Å support

This mixed brush where VBIDA was grafted first onto the M-PVA was fully tested for Hb and GFP desorption while being charged or uncharged in binding and/or imidazole buffer (Fig. 4.16).

The charged support with Cu^{2+} ions, bound 24.9 mg g^{-1} Hb and from that only 4 % was totally desorbed after the eight temperature transition cycles in binding buffer (protein release was demonstrated only within the first two cycles). Further washing of the support with imidazole buffer (three cycles) didn't deliver any significant protein elution. A very low amount of Hb was bound on the uncharged support (3.5 mg g^{-1}) and most of it (83 %) was removed with NaOH stripping. The GFP bound onto the charged support at a concentration of 9.5 mg g^{-1}, and from that 52 % was desorbed after the first cycle. The rest temperature transitions contributed to another 9.2 % protein release (i.e. 61.2 % total desorption after eight cycles). Further serial washing of supports with imidazole buffer (three cycles) delivered 26 % desorption indicating that the elution buffer was more efficient than the temperature transitions. However the low binding capacity of pVBIDA mixed brush for GFP needs further investigation by performing experiments on pVBIDA homobrushes as in the case of Hb.

Based on these results, the very tight binding of Hb onto the mixed brush containing VBIDA has been demonstrated where elution of protein hardly feasible with means of thermoresponsiveness.

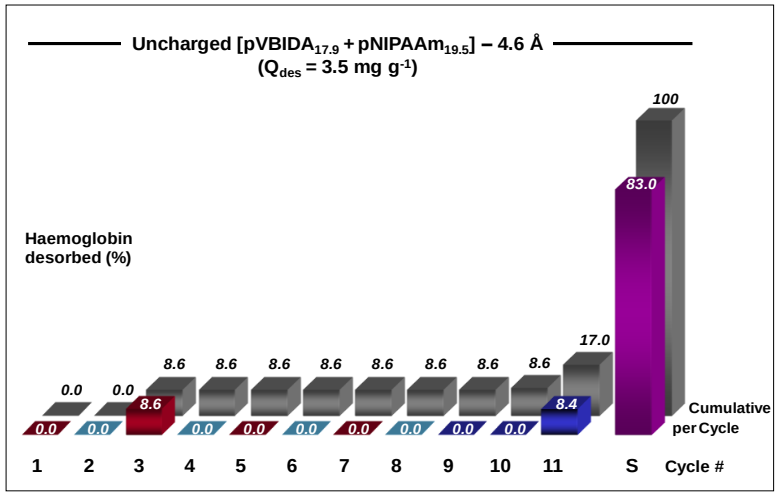

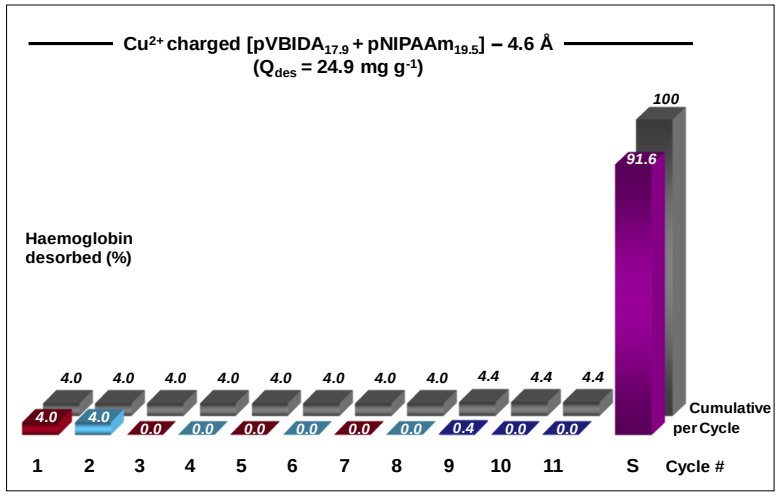

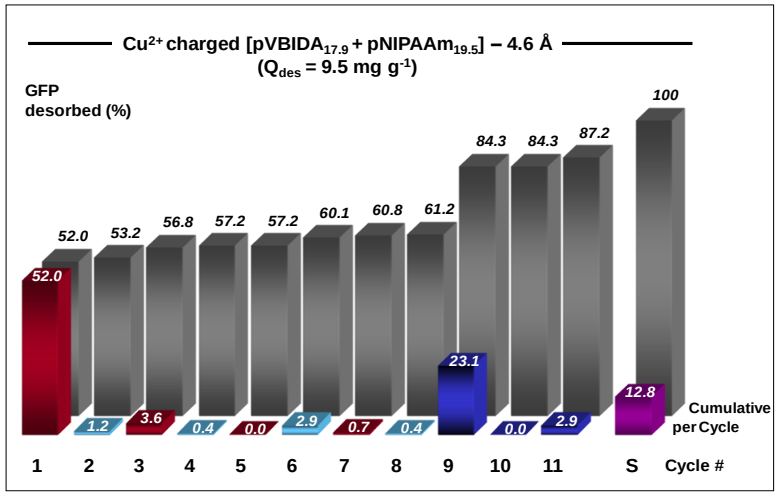

Figure 4.16 Protein (haemoglobin and GFP) desorption experiments with [pVBIDA$_{17.9}$ + pNIPAAm$_{19.5}$] – 4.6 Å mixed brush support: Protein desorbed from 20 °C to 45 °C (red bars); protein desorbed from 45 °C to 20 °C (light blue bars); protein desorbed with 0.2 M imidazole (pH 7.0) (deep blue bars); protein desorbed with stripping agent (NaOH) (purple bar); cumulative protein desorption from each support (grey bars).

4.4.3.6 Comparison of protein desorption by 'hot-cold' transitions in binding buffer and 'hot-cold' transitions in elution buffer

Four temperature transition cycles were applied on charged supports in elution buffer and compared with those that took place in binding buffer. The results for three different supports are shown in Fig. 4.17.

For the [$pNIPAAm_{26.8}$ + $pVI_{26.4}$] – 4.6 Å support the hot-cold elution in binding buffer delivered 29.4 % Hb desorption while the transitions in elution buffer 23.2 %. In this case incorporation of imidazole was not advantageous and it seems that temperature transitions were more beneficial in protein desorption. Incorporation of elution buffer was not advantageous neither for the [$pVI_{17.7}$ + $pNIPAAm_{26.3}$] – 4.6 support (i.e. 16.2 % and 16 % desorption in binding and elution buffer respectively). Heating and cooling in the presence of salt (binding buffer: 100mM Sodium Phosphate, 200mM NaCl at pH 6.9) it is expected to shift the LCST and decrease the ionic interactions while promoting precipitation of polymer and protein desorption. On the other hand, the protein upon heating partial deforms on the polymer film and associates with that firmly hindering the elution in both cases. For these supports clearly the hot-cold transitions are more beneficial than the elution buffer. However is not the same case for the [$pVBIDA_{17.9}$ + $pNIPAAm_{19.5}$] – 4.6 Å support, where desorption was achievable only in elution buffer. The type of affinity ligand seems to play a crucial role in temperature assisted desorption. If the ligand employed develops very strong metal chelating interactions (eg. VBIDA), then it is very difficult to release the adsorbed protein and probably higher amounts of pNIPAAm are required. On the other hand if the affinity ligand is weaker (e.g. VI), then is much easier to facilitate desorption with temperature and no other means.

Observations of the supernatants after each imidazole-temperature cycle appeared as colored solutions of darker to lighter blue shades, indicating the removal of copper ions at high concentrations from the pVI or pVBIDA grafted supports. However ligand utilization in dense brushes can be related only to the exterior surface available affinity sites of the polymer film. In addition, at high temperatures the protein molecules are deformed either by interacting with the polymer chains or by electrostatic interactions (Shamim, 2006). In this case where the electrostatic interactions have been minimized by adding salt, the lower protein desorption from that expected can be attributed to the strong attachment of Hb onto the polymer film while is partially deformed at elevated temperatures.

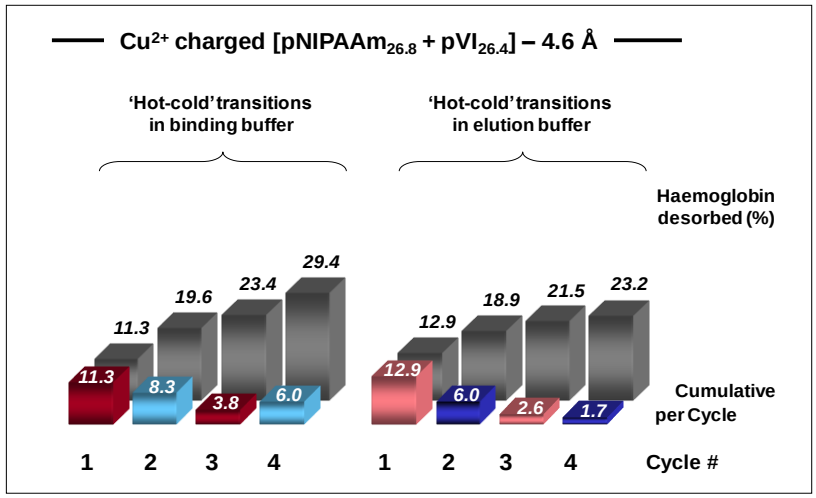

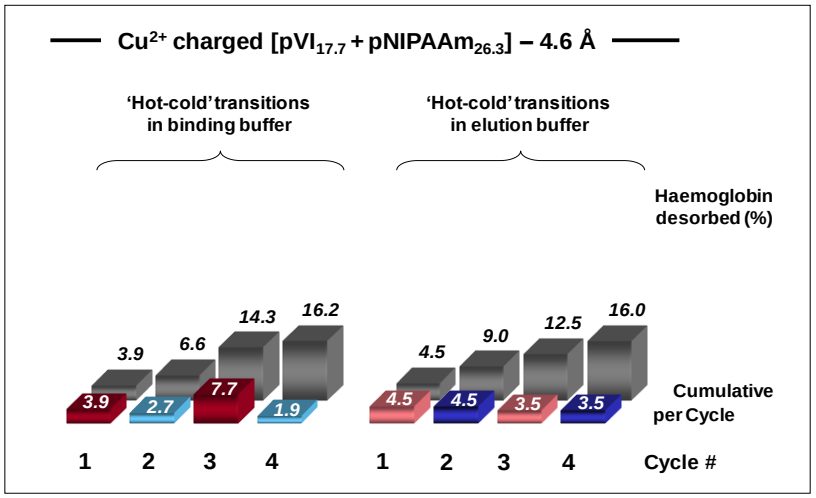

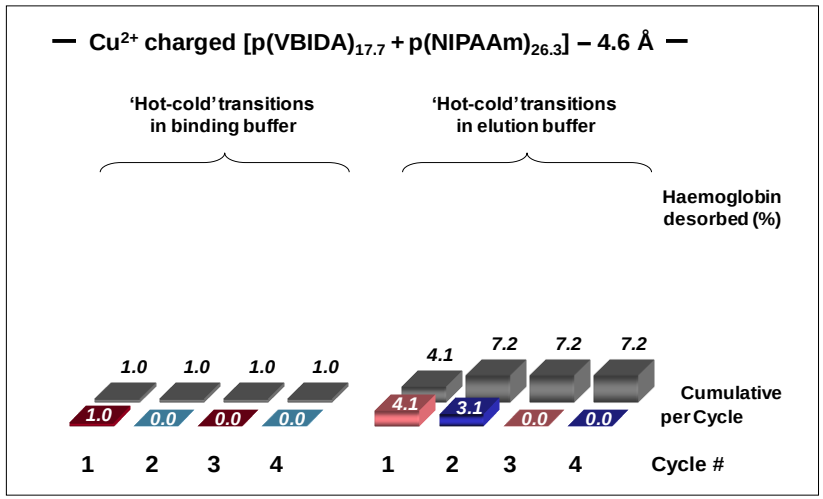

Figure 4.17 'Protein desorbed by 'hot-cold' transitions in binding and elution buffer with mixed brush supports: Protein desorbed from 20 °C to 45 °C in binding buffer (red bars); protein desorbed from 45 °C to 20 °C in binding buffer (light blue bars); protein desorbed from 20 °C to 45 °C in 0.2 M imidazole (pH 7.0) elution buffer (pink bars); protein desorbed from 45 °C to 20 °C in imidazole elution buffer (deep blue bars).

4.5 Conclusions

Sequential cerium (IV) initiated 'graft from' polymerisation was employed to manufacture mixed functionality brushes, i.e. polymer brushes onto magnetic M-PVA support composed of thermoresponsive and affinity ligand polymer chains adjacent to each other at fixed density. FT-IR analysis of solid products and ATR FTIR of liquid supernatants from each step reaction, were used to confirm the polymerisations and characterise the supports in terms of polymer chain lengths and composition. The effect of order of polymer addition at the two-step reaction was explored by investigating the possibility of polymerisation onto the backbones of polymers added. From observations of the structures of the polymers employed, no reactive sites were identified able to initiate polymerisation in the presence of cerium (IV). Although polymerisation can be observed in solution, when the same reaction takes place onto the backbone of the PVA (graft polymerisation) and at certain cerium (IV) concentration, the polymerisation is initiated from the PVA given the much higher affinity of Ce(IV) for hydroxylated materials.

The configuration of the mixed brushes was further investigated by estimating their average Flory Radious (R_F) with three different methods. Based on the resulting $s/(2R_F)$ ratios and assuming different levels of % cerium consumption, all the mixed polymer supports were in the 'true' brush regime.

Haemoglobin binding studies onto mixed polymer supports in high concentration of salt, delivered high binding capacities (> 194 mg g^{-1}) of protein. The incorporated pNIPAAm chains of increased length (employing 1:250 ratio between Ce(IV) and NIPAAm) influenced the way protein interacted with the matrix. The haemoglobin's access to and interaction with metal chelating residues of the metal chelating chains (copper charged supports) was

dependent on the amount of affinity ligand introduced. On the other hand, the increased protein binding capacity of the uncharged supports can be attributed to the effect of high salt concentration on the LCST, where the pNIPAAm chains at 20 °C are most probably collapsed. As a consequence, Hb interacted and adsorbed more easily on the support of increased hydrophobicity.

The efficiency of polymer brush supports, in terms of protein binding and subsequent desorption employing serial temperature transitions cycles, was evaluated. Complete desorption of both proteins (Hb and GFP) via temperature changes across the LCST was achievable from the charged $pNIPAAm_{10.3}$ –4.6 Å support. Such desorption was not observed for the charged $pVI_{30.9}$ – 4.6 Å support (control), as proteins interacted stronger with the base matrix and the VI polymer chains remained hydrophilic with temperature change. From the charged and uncharged [$pNIPAAm_{26.8}$ + $pVI_{26.4}$] – 4.6 Å mixed brush, over 40 % of Hb was desorbed after the eight successive hot-cold transitions. The charged [$pVI_{17.7}$ + $pNIPAAm_{26.3}$] – 4.6 Å support demonstrated lower protein binding and release than the [$pNIPAAm_{26.8}$ + $pVI_{26.4}$] – 4.6 Å support, due to lower pVI and pNIPAAm grafting, and the extend of the pNIPAAm chains length in relation with that of pVI.

As a general trend, the uncharged supports performed better than the charged ones (higher % desorption) as the protein bound on them without strong interactions (lack of metal chelating interactions) and at less amounts. The mixed brushes composed of pVI showed better desorption characteristic than those of pVBIDA. This accounts mainly to the stronger protein binding (i.e. each VBIDA unit coordinate with more Cu^{2+} ions than VI). The efficiency of the supports was also dependent on the type of protein used during batch binding and desorption. Shift of temperature (or otherwise change of pNIPAAm chains conformation), resulted in

much more GFP desorption than Hb. This is aspect to different characteristic of the two proteins. Hb interacts differently than GFP does with the polymer brush film, as it is a 'soft' and relative big molecule with the tendency to stick onto the surfaces. In addition, is less stable than GFP in temperature and so conformational changes will be more pronounced. Generally, the way each protein interacts with a functionalised support depends on the brush architecture, the temperature and the type of metal affinity ligand. Desorption via temperature changes, depends on protein concentration, strength of binding and polymers employed content.

As shown in Chapter 3, the cerium (IV) grafted homopolymer and copolymer brush supports demonstrated thermoresponsive behaviour. Based on these findings, it is expected that the mixed brush supports should also demonstrate thermoresponsive behaviour, given the spacing and length of pNIPAAm chains employed. However, the same assay should be also applied to the mixed brush supports in order to detect their exact LCST and further examine the effect of salt and Cu^{2+} addition on pNIPAAm chains collapse.

5. Synthesis of mixed functionality polymer brushes using Atom Transfer Polymerisation Reaction (ATRP) on M-PVA supports and their application for protein binding and subsequent desorption via temperature transitions

5.1 Abstract

A method to produce controlled activation of M-PVA surface for the attachment of polymers at different configurations via ATRP has been developed. The effects of several parameters on the reaction have been investigated, such as that of Cu(I)Br concentration, the different levels of bromination to create graft sites as well as the monomer to initiator ratio (final polymer chain lengths). In addition, the living character of the reaction was studied for the preparation of di-block polymers. All the reactions were confirmed qualitative with FT-IR in solids and further quantified by employing ATR FT-IR to liquid supernatants. The ATRP reactions of both monomers employed (NIPAAm and VI) did not reach completion evidence of premature chain termination reactions taking place. Sequential partial bromination in combination with ATRP at two steps was performed successfully for the preparation of mixed polymer supports. The polymer chains were grafted in high density but at relative short lengths. Estimation of the $s/(2R_F)$ ratios indicated that the polymer chains were in brush regime. Finally, the efficiency of most of the supports for protein binding and subsequent desorption via temperature transition cycles or elution buffer or their combination was evaluated. The efficiency of the above supports was less than those manufactured with cerium (IV) grafting due to architecture differences (more packed and shorter chains).

5.2 Introduction

Although the conventional free radical polymerisation reaction is applicant for a vast of vinyl monomers and has been very useful by operating in mild conditions, it suffers from poor control to prepare well defined polymeric networks (polydispersity of chains, composition fluctuations, and lack of site-specific functionality). In the past decade, the development of Controlled/Living Polymerisation (CPR) methods was such that to overcome these problems and since then it is used widespread. Nowadays, the most interesting CPR methods are: (a) the stable free radical polymerization (SFRP), (b) the reversible addition fragmentation chain transfer (RAFT) polymerization and (c) the transition-metal-catalyzed atom transfer radical polymerization (ATRP) (Matyjaszewski and Spanswick, 2005).

Atom transfer radical polymerization (ATRP) is a recently developed 'controlled' radical polymerization method, which allows the preparation of well-defined (co)polymer brushes with "living" chain ends on various types of substrates via surface-initiated techniques (Wang and Matyjaszewski, 1995; Pyun *et al*., 2001; Coessens *et al.*, 2001; Matayjaszewski and Xia, 2001). Among other controlled/living polymerization techniques, ATRP is considered as the most versatile in terms of reaction conditions and monomers, easy experimental set up, cheap catalysts and availability of commercially easily prepared initiators (Kizhakkedathu *et al*., 2004; Matyjaszewski, 2005). Several polymer brushes have been synthesised using ATRP to a plethora of substrates, as it has many advantages over other conventional polymerisation techniques, such as narrow polydispersity, accurate control over polymer weight or brush thickness, suppression of termination reactions and ability to create block polymers regenerating the end groups (living character) (Matyjaszewski, 2005).

The basic mechanism of ATRP (reaction scheme is illustrated in Fig. 2.2, section 2.3.1) involves the abstraction of a halogen from an alkyl halide using a lower-oxidation-state metal complex. By this way, a radical centre is generated and polymerisation starts in the presence of a monomer. The reaction proceeds until the higher-oxidation-state metal complex deactivates the active centre and creates the dormant species (Kamigaito *et al*., 2001; Pintauer *et al*., 2004; Tsarevsky *et al*., 2007). The formation of radicals during the ATRP process is reversible (Pintauer and Matyjaszewski, 2005). Many catalytic systems have been identified. Among them, the copper based is the most promising in terms of efficiency (Queffelec *et al*., 2000). Chloride and bromide are the most used counterions, whereas higher rates are achieved with bromide.

The control over the polymerisation depends on the position of equilibrium and on the reaction dynamics. The chains during this reaction are initiated instantaneous promoting the simultaneous growth of all chains (Matyjaszewski, 2005). The equilibrium is pushed to the left-hand side (deactivation) where the dormant species are in excess due to the persistent radical effect (PRE) (Fischer, 2001), i.e. the radicals are stable (or persistent) suppressing the bimolecular termination between the living monomers. The persistent radical effect in conjunction with the reversible reaction of propagating radicals is the basis of living radical polymerisation (Odian, 2004). Research on theoretical aspects of living radical polymerisations has been achieved by numerical methods related to molecular weight distribution and conversion rates. Although, these methods help to understand the mechanism of the reactions taking place, they arise from specific systems of their own kinetic parameters. This makes their generalisation and reproducibility difficult. For this reason, analytical equations are more useful for polymerisation data analysis, but again are valid for ideal systems (Fischer, 2001). Generally, the main problems that may occur during ATRP and

affect its performance are: the complexity of equilibrium, the side effects, the solubility, the presence of metal ions in the higher oxidation state, and the low reactivity of the initiation system (Matyjaszewski *et al.*, 1997; Parker *et al.*, 2000; Hou *et al.*, 2006). As in all CPR systems, chain breaking reactions (termination, transfer) are also unavoidable at ATRP. However, the contribution of transfer reactions is relative small in comparison with that of termination reactions. The contribution of transfer increases with chain length, so the molecular weights should be limited by the appropriate monomer to initiator ratio. On the other hand, the rate of termination in CPR systems can be limited by the low concentration of active species. The termination is of second order, whereas propagation is of first order with respect to radical concentration. Most CPRs are consequently slower than conventional systems. On the other hand, by targeting low molecular weights and/or incorporating highly reactive monomers we can obtain fast ATRPs. The rate of propagation of ATRP is controlled by adjusting the concentration of activator or deactivator, since this reaction is based on the catalysis (Patten and Matyjaszewski, 1999). On the other hand, the efficiency of the catalyst can be controlled by the appropriate selection of a ligand or addition of a solvent (Xia and Matyjaszewski, 1997; Xia *et al*., 1998; Matyjaszewski *et al*., 1998).

Recently, dense polymer brushes grafted onto surfaces have attracted lots of interest due to their potential in many applications (Zhao *et al.*, 2000). Adapting the development of ATRP methods, several efforts have been described to synthesise polymer films of controllable thickness, functionality and properties onto surfaces by several groups (Matyjaszewski *et al*., 1999; Husseman *et al*., 1999; Yamamoto *et al*., 2000; Jeyaprakash *et al*., 2002). In addition, ATRP offers the possibility to synthesise diblock copolymers by extending the first grafted polymer chain (Zhang and Matyjaszewski, 1999; Zhao and Brittain, 1999; Zhao *et al*., 2000).

Patterning of initiators on surfaces, offers the option to graft patterned polymer brushes suitable for many applications (Becer *et al.,* 2007). One such method is the introduction of allyl groups on a given surface and subsequent bromination of these groups. Burton and Harding (1997) reported the attachment of ligands at high densities to brominatd allyl chromatographic supports. By adding controlled amounts of Br_2 to the available allyl groups (electrophilic addition), partial brominated sites are generated where ATRP 'graft from' route can be also applied. Grafting polymer brushes on the brominated sites may provide better control on polymer chains density as the bromination level can be easily regulated. In summary, the procedure is based on a two-stage reaction involving: (a) the introduction of double bonds onto the matrix (M-PVA) for example by reacting it with allyl glycidyl ether (AGE); and (b) the partially addition of bromine onto these bonds to obtain ATRP initiation sites at specific spacing. The efficiency of this initiation procedure can be explored for its ability to serve as a template for introducing polymer chains onto the magnetic particles at fixed spacing via ATRP.

Depending on the type of polymer brush we want to create (i.e. mixed or block copolymer brush), two different routes can be followed. For mixed brushes, after performing the first polymerisation, termination takes place and a second partial bromination is performed followed by ATRP of the second monomer of interest. For di-block polymer brushes, no further bromination is required and ATRP is employed directly onto the ends of the chains already grafted before (no termination took place so they should be still 'alive'). The aqueous ATRP employed here involves a catalytic system of CuBr and 2,2-dipyridyl in water at room temperature. The Cu^I complex abstracts the bromine atom from the initiator and an initiating radical is produced. Then, it is possible for monomer units to be added to this radical until the propagating radical is recapped and become halogen-terminated 'dormant' chain. This cycle

is repeated allowing the growth of polymer chains from the initiated surface. The methods described above are summarised in Fig. 4.1.

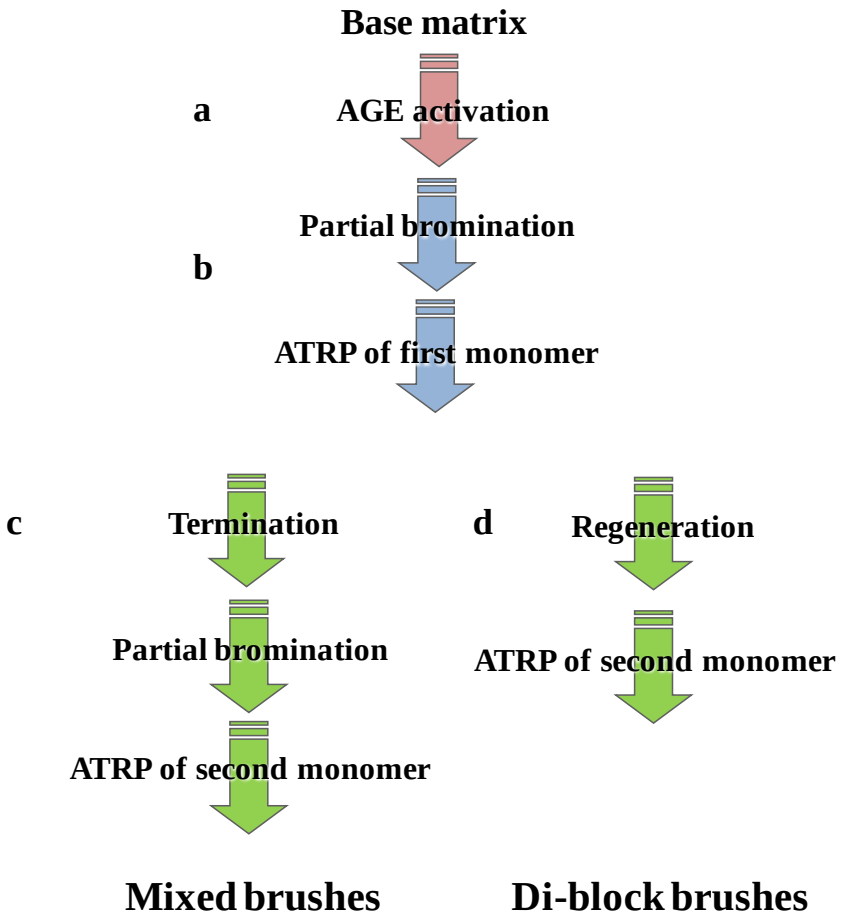

Figure 5.1 Summary of steps that can be employed for the construction of mixed or di-block brushes: **a**- AGE activation of base matrix (introduction of double bonds); **b**- Subsequent partial bromination and ATRP performance of the first monomer to be grafted (at fixed spacing); **c**- Route followed for mixed brush construction: termination, second partial bromination and ATRP performance of the second monomer to be grafted (at fixed spacing); **c**- Route followed for di-block brush construction: regeneration of the reaction is possibly as no termination takes place and ATRP is performed by applying fresh catalyst and the second monomer of interest.

The aims of the work in this Chapter are outlined such as: (a) to introduce and quantify brominated sites on the M-PVA surface; (b) to create homopolymer brush supports, characterise them with FT-IR and in parallel investigate the effect of CuBr concentration on

the reaction; (c) to examine the livingness of the grafted polymer end groups following route d, for copolymer preparation; (d) prepare mixed polymer supports of NIPAAm and VI and characterise them; (e) to perform preliminary protein binding and desorption studies with temperature.

5.3 Materials and Methods

5.3.1 Materials

M-PVA 012 particles (M_r 130,000; acetyl content: 10.0-11.6 %; degree of hydrolysis 86.8 - 88.7 %; 2 µm mean diameter) used (batch 4, R2-0109027), were received as a gift from Chemagen Biopolymer-Technologie AG (Baesweiler, Germany). *N*-isopropylacrylamide (NIPAAm), *1*-vinylimidazole (VI), Dimethyl Sulfoxide (DMSO), Allyl Glycidyl Ether (AGE), 2,2′-Dipyridyl, Imidazole, haemoglobin from bovine blood (lyophilized powder), Bromine (Br_2) and Bromine (bromide-bromate) volumetric standard solution (0.05 M Br_2, 0.1 N) were purchased from Sigma-Aldrich Company Ltd. (Gillingham, UK). Green fluorescence protein (GFP) was received as a gift from Joerg Becker at Karlsruhe Institute of Technology and purified as described in Chapter 4 (section *4.3.1.1*). All other chemicals used were of analytical grade and most of the consumables were supplied by Sarstedt Ltd. (Leicester, UK).

A Vortex mixer (VM20, Chiltern Scientific, Bucks, UK), a shaking plate (CAMLAB, Serring Science, Cambridge, UK), a magnetic stirrer (SM1, Stuart Scientific Co Ltd, UK), a water bath (OLS 200, Grant Instruments, Cambridgeshire, UK) and a weighing machine (Mettler AT261, Delta range, Leicester, UK) were used. For analytical purposes, a Spectrophotometer UVIKON 922 (Kontron Instruments, Northstar Scientific, Bedfordshire, UK) and FT-IR

(Nicolet 380, Thermo Scientific, Waltham, MA, USA) were used. During all the washing stages and functionalisations, the magnetic beads were separated from solvents using magnetic blocks (Chemagic Stand 50k Type A and Chemagic Stand 2x12; Chemagen Biopolymer-Technologie AG, Baesweiler, Germany).

5.3.2 Washing procedure before and after AGE activation

Eight batches of 250 mg of beads were transferred to 50 mL screw cap tubes. The solvent (water) was removed using a magnetic block and the beads were washed sequentially with 20 mL portions of the following solutions: twice with deionised distilled water; once with 50 % methanol in deionised distilled water; once with 100% methanol; once with 50 % methanol in acetone; once with 100% methanol; twice with deionised distilled water; once with 1 M NaCL; three times with deionised distilled water. During each step, the particles were mixed for 30 s into the solvent using a vortex mixer (VM20, Chiltern Scientific, Bucks, UK).

After AGE activation the supports were allowed to cool at room temperature and washed with water, 50% ethanol in water and then several times with water. The beads were then suspended in 20 ml water and stored at 4^{o}C.

5.3.3 Activation of magnetic supports with Allyl Glycidyl Ether (AGE)

After washing each batch of M-PVA support as described in section 5.3.2, a total of 2 g of beads were transferred to a 50 mL screw cap tube. Then, 30 mL of water containing 16 g of NAOH, 333 mg of $NABH_4$ and 8.93 g of NA_2SO_4 were added to the beads, the tube was

sealed and placed to the water batch (OLS 200, Grant Instruments, Cambridgeshire, UK) at 50 °C The mixture was shaken for 1 h at 150 rpm (Fig. 5.2, a). Then, the temperature was lowered to 40 ^{o}C, and 10 mL of AGE were added and the reaction continued for 15 h at 170 rpm (Fig. 5.2, b). The introduced double bonds were quantified using the acidified bromine assay as described in section *5.3.7.1*.

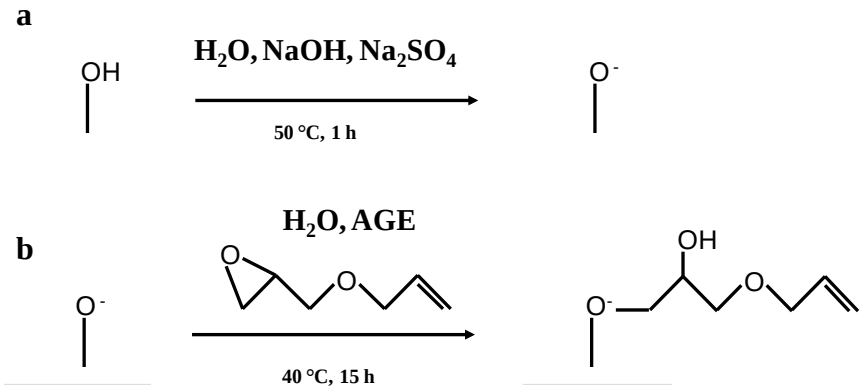

Figure 5.2 Scheme of AGE activation of M-PVA support: **a-** Deprotonation of M-PVA hydroxyls; and **b-** AGE reaction at deprotonated hydroxyl sites.

5.3.4 Partial bromination of AGE activated supports

Controlled bromination was performed on 5 mg samples of AGE modified M-PVA supports. The supports were washed with water and reacted with 100, 80 , 75, 60, 50, 45, 30, 25, 15 and 10 % of the amount of Br_2 required to completely react with the available total AGE double bonds on the supports (i.e. corresponding to 0.0027 moles g^{-1} support as found following the acidified bromine assay, section *5.3.7.1*). Before partial bromination, the supports were washed with 1.5 mL DMSO for at least five times. A stock solution of bromine solution in DMSO was prepared and the supports were reacted for 120 s with the corresponding diluted

solution. The supernatant was removed and the samples were washed five times with 1 mL DMSO. The introduced C=C bonds of AGE were assayed using again the acidified bromine assay described in section *5.3.7.1*.

5.3.5 ATRP on partially brominated supports

Initially, ATRP was performed at molar ratios of initiator:CuBr:dipyridyl of increasing CuBr concentration, to study the effect of this component in the reaction. For the construction of the polymer brushes, the initiator:CuBr:dipyridyl:monomer ratio was kept constant either at 1:10:20:100 or 1:10:20:250 (aiming for 100 or 250 monomer length chains respectively).

The general procedure followed for all the reactions was: 50 mg AGE modified M-PVA was mixed with a dilute solution of bromine in DMSO (corresponding to 50 % or 20 % bromination). The brominated support was washed with 5 mL DMSO for 120 s five times and two times with 5 mL water, suspended in 5 mL water (containing the monomer at the required concentration) and purged with nitrogen for 0.5 h. Meanwhile, Cu(I)Br and dipyridyl were added separately to a 15 mL screw cap tube and the tube was purged with nitrogen for 0.25 h. The M-PVA with monomer mixture was then added to the degassed tube under a nitrogen blanket. The tube was sealed and mixed overnight (15 h). The supernatant was removed from the support and analysed later with ATR FT-IR. A small amount of support (1-2 mg) was also kept and mixed with 300 mg KBr and tested with FTIR. After this reaction, two different routes were followed depending on the required position of the second polymer (i.e. copolymer or mixed brush support), such as:

(a) For the mixed polymer brushes: After the first polymerisation, the reaction mixture was removed under a Nitrogen stream and the grafted support was quenched by removing any radicals which could interfere with subsequent reactions, by adding 4-ethoxyphenol inhibitor (10 mg in 5 mL water) to the reaction mixture. The supports were washed twice with 5 mL DMSO and mixed with 5 mL of 1.0 M NaOH for 1 h. Finally, the supports were washed three times with 5 mL of water and again mixed with a dilute solution of bromine in DMSO (50% or 20%) and ATRP was followed to graft the second polymer.

(b) For the di-block polymer brush: The second ATRP onto the support was performed directly, without terminating the first reaction or adding initiator. The procedure described above was repeated, by adding the second monomer with fresh catalyst into the reaction.

5.3.6 Protein (haemoglobin and green fluorescence protein) batch binding and release studies with temperature

The selected functionalised supports (2 mg) were charged with Cu^{2+} ions by suspending them in 1.0 mL of 50 mM $CuCl_2$. The solutions were mixed using an orbital shaker (IKA®-Werke GmbH, Staufen, Germany) at 1800 rpm for 0.3 h (twice). The supports were then equilibrated and washed from any unbound Cu^{2+} ions with 1.0 mL binding buffer for 0.3 h twice. The supports were then incubated for 1 h with haemoglobin or GFP solution at 300 mg g^{-1} in an OLS 200 water bath (Grant Instruments, Shepreth, UK) at 20 ºC. After protein binding, the samples were washed twice with 1.0 mL of binding buffer at 20 ºC to remove any loosely bound protein from the matrix. These materials were washed with the same binding buffer at temperatures above and below the estimated LCST, i.e. at 42 ºC and 20 ºC, to investigate any protein elution via phase transition of polymers (due to the expansion or collapse of the

polymer chains). Each sample was introduced in eight temperature shifting cycles for at least 360 s. The same procedure was also repeated for the uncharged supports. Both charged and uncharged supports were afterwards eluted with 1.0 mL of 0.2 M imidazole at pH 7.0. Finally, the remaining protein was stripped off the support with 1.0 mL of 0.5 M NaOH by incubation for 1 h using the orbital shaker.

5.3.7 Analytical methods

5.3.7.1 Determination of C=C bonds introduced onto PVA of magnetic supports (Acidified bromine assay)

The amount of C=C bonds introduced onto M-PVA supports after the AGE activation was assayed by the acidified bromine assay. An acidified bromine solution ($KBr/KBrO_3$) was prepared by mixing 2.5 mL of 0.1 M $KBr/KBrO_3$ with 5 mL of 0.5 M H_2SO_4 for 2 min (Eq. 5.1).

$$BrO_3^- + 5\ Br^- + 6\ H^+ \rightarrow 3\ Br_2 + 3\ H_2O \qquad \text{Eq. (5.1)}$$

A volume of 0.150 mL of this solution was added to 1.35 mL of 0.2 M H_2SO_4 and the absorbance of this was measured at 410 nm. An amount of 5 mg M-PVA support was reacted for 10 s with 1.5 mL of undiluted acidified mixture. Then 0.150 mL of the supernatant was added to 1.35 mL of 0.2 M H_2SO_4 and its absorbance reading was taken at 410 nm.

The assay was repeated and each time a fresh stock acidified solution was prepared. The absorbance of the stock solution was taken also at the end of the assay in order to confirm the stability of the acidified solution. Different concentrations of bromine were also tested with the same method and a calibration curve was obtained (see Appendix section, Fig. 7.12). Using this calibration curve, the amount of Br_2 reacted with the AGE activated support was estimated. The AGE activated M-PVA support was found to consume 0.0027 moles Br_2 per g support (corresponding to 1.84 Å spacing), whereas there was no Br_2 consumption for the unmodified M-PVA support (control).

5.3.7.2 Solid based detection of polymers grafted onto M-PVA supports using Fourier Transform Infrared Spectroscopy (FT-IR) technique in solids

After each reaction step, the functionalized supports were subsequently washed, dried and 1-2 mg of each was mixed and crushed with 300 mg potassium bromide (KBr) to form a very thin powder. Then, these mixtures were pressed between pellets at 10 tons, and the resulting discs were tested with the Nicolet 380 FTIR spectrometer (Thermo Fisher Scientific, Waltham, MA, USA). The FTIR spectra of unmodified beads and modified beads were compared in order to detect the appearance of new bands corresponding to the polymers grafted on the supports.

5.3.7.3 Liquid based analysis of monomer consumption using Attenuated Total Reflection Fourier Transform Infrared Spectroscopy (ATR FT-IR) technique

The concentration of the monomers remained in the supernatants after each step of the reaction was measured using the same method described at paragraph *3.3.6.5* in Chapter 3. However, in this work new calibration curves were constructed by diluting the monomers (NIPAAm or VI) into solutions containing CuBr and dipyridyl at the equivalent amounts used for ATRP. The slopes of these calibration curves (peak area units per g L^{-1}) were used to estimate the amount of unreacted monomer concentration at supernatant solutions (see correlation factors > 0.99 in Appendix, section 7.5, Fig 7.13 and Fig. 7.14).

5.3.7 4 Assays for protein content

The concentration of protein bound and released onto/from the supports was defined by estimating the protein remained in supernatants. For this purpose a calibration curve of Hb in binding buffer measuring the absorbance of different concentrations of protein at 405 nm was used. The same calibration curve was used to estimate the Hb washed and released from the supports. The Hb stripped with the addition of NaOH was estimated by constructing a calibration graph of protein in NaOH and measuring the absorbance at 210 nm. The GFP bound onto or washed from the support and stripped in NaOH was determined by using the standard Better Bradford Assay in the corresponding solvents. The GFP eluted from the support (low quantities) was determined using the Better Bradford assay of microtest protocol. For the measurements a UVICON 922 Spectrophotometer (Kontron Instruments, Bletchley, UK) was employed. All the above curves are given in the Appendix, section 7.3, Fig. 7.8 - 7.11.

5.4 Results and discussion

5.4.1 Activation of M-PVA surface with Allyl Glycidyl Ether (AGE) and partial bromination of PVA surface

M-PVA support (batch 4) was activated with AGE by introducing C=C bonds onto the surface as shown at the reaction scheme of Fig. 5.2. After washing, the allyl density of the AGE activated material was assayed by reacting with the acidified bromine solution (Eq 5.1), and was found 2.7 mmol g^{-1}.

$$–C=C + Br_2 \rightarrow –CBr–CBr \qquad \text{Eq. (5.2)}$$

Partial bromination of the AGE activated surface of M-PVA was utilised to create initiation sites at various concentrations enabling to employ ATRP at any desired spacing. This involved the addition of controlled amount of Br_2 to the activated support. So partial bromination reactions were carried out (Fig. 5.3) by reacting the AGE-activated M-PVA with different amounts of bromine in DMSO (0 – 5 mmol Br_2 per g support), washing with DMSO and then assaying the remaining C=C bonds.

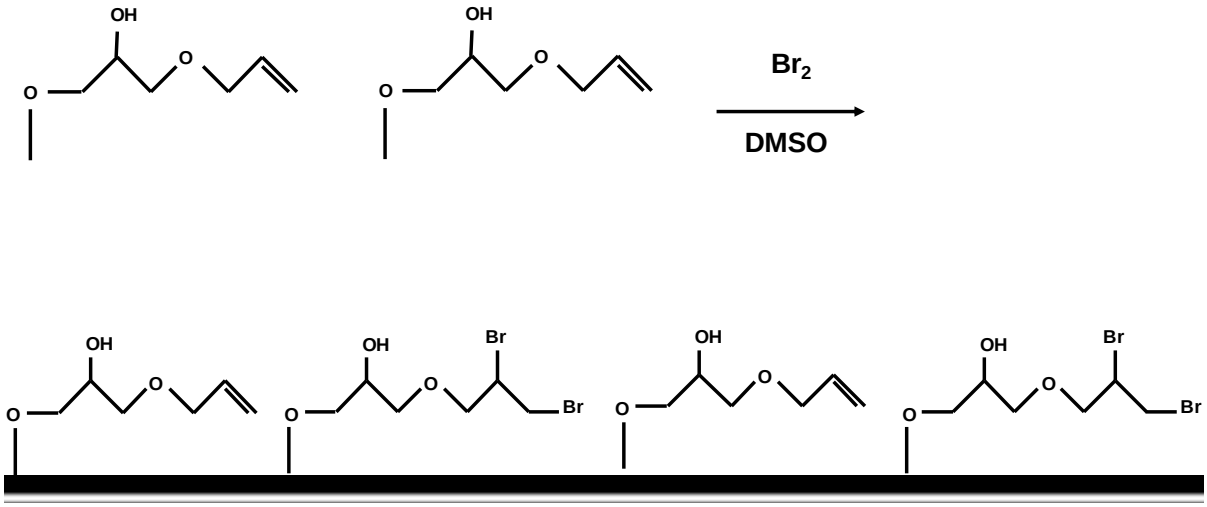

Figure 5.3 Partial bromination reaction on allyl activated M-PVA support.

In Fig. 5.4, the different levels of Br_2 consumed onto the support after partial brominations, and the corresponding estimated spacing between the initiation sites (-CBr-CBr) are presented.

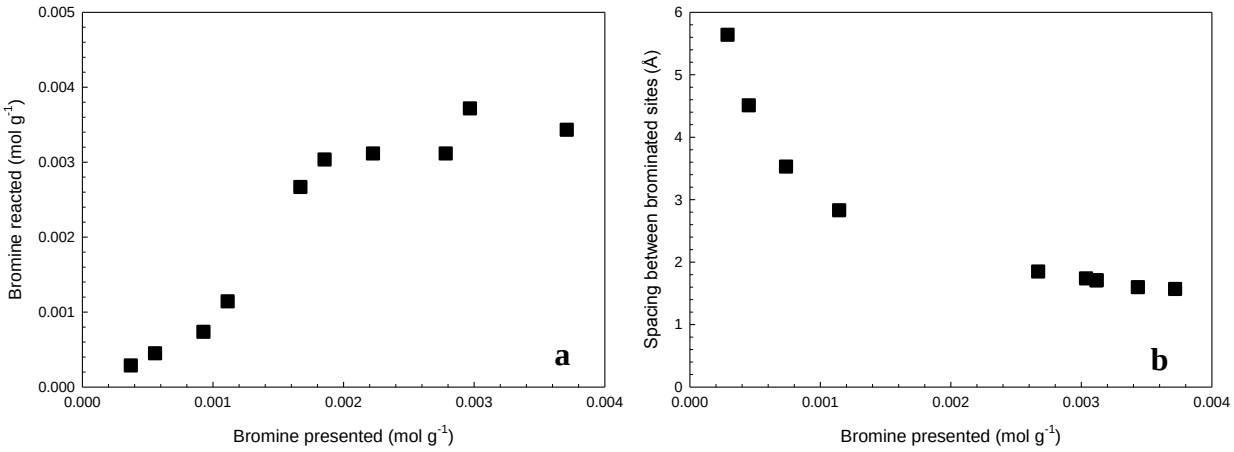

Figure 5.4 a- Br_2 presented versus Br_2 reacted on AGE activated M-PVA (batch 4). Prior assay of the allyl density of the two supports gave values of 2.7 mmol g^{-1} for this batch material; **b**- Effect of level of bromine addition on estimated spacing of –CBr–CBr initiator sites introduced onto AGE–activated M-PVAs.

A linear relationship between the amount of bromine added and that consumed was revealed up to a certain concentration (Fig. 5.4, **a**). Under the same conditions unmodified M-PVA

consumed negligible levels of Br_2. The specific surface area per g of M-PVA batch 4 has been determined as ca. 55 m^2 g^{-1}. Using this value and the data presented in Fig. 5.4 **a**, the minimum spacing between the adjacent initiator sites was estimated (Fig. 5.4, **b**). The same activation procedure has been repeated for M-PVA batch 5 delivering similar results, indicating that the AGE/bromination route is probable able to take different batches of M-PVA and create very similar activation chemistries on their surfaces.

5.4.2 Atom Transfer Polymerisation reaction (ATRP) onto partial brominated M-PVA supports

The radical reaction can be initiated by Copper(I) Bromide from a group containing a C-Br bond. The radical is generated through a reversible redox process catalysed by Cu(I)Br complex which undergoes a one-electron oxidation to Cu(II)Br with concomitant abstraction of Br atom from the C-Br group on the M-PVA surface. The formed radicals can initiate the polymerization by adding across the double bond of a vinyl monomer. Reactivation of the dormant species allows for the polymer chains to grow again, only to be deactivated later. Under optimum conditions, such a process results in a polymer chain that slowly, but steadily, grows and has a well-defined end group (Fig. 5.5).

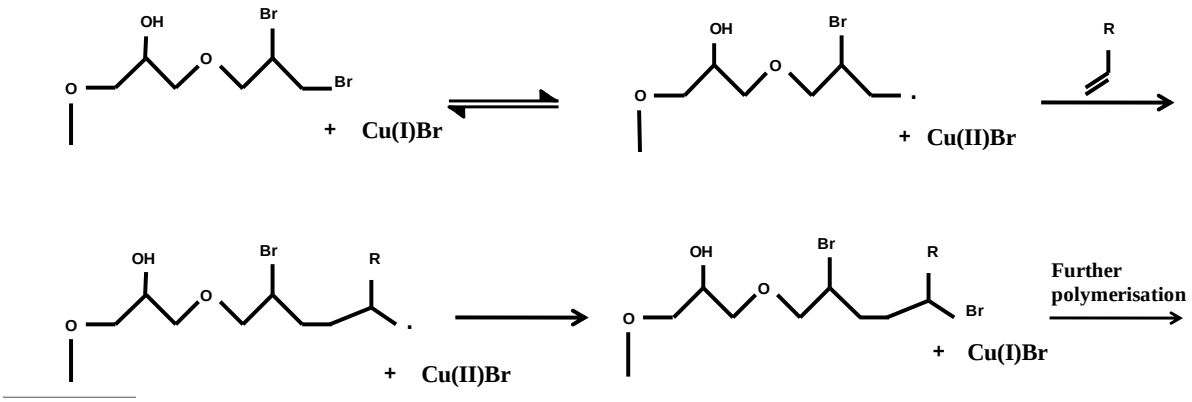

Figure 5.5 ATRP scheme onto brominated M-PVA support.

In this reaction 2,2'-bipyridine (bpy), an efficient bromine atom transfer promoter was used as complexing ligand to Cu(I)Br, represented by the formula $[Cu^{I}(bpy)2]^{+}[Br]^{-}$. The stochiometric ratio between the components Initiator:Cu(I)Br:bpy:monomer of the reaction, for a 100 monomer units length polymer, would be 1:1:2:100. In this work, an excess of Cu(I)Br/bpy was used, to study the effect of the catalytic system and simplify the kinetic analysis. The ratio of Cu(I)Br:bpy was kept constant at 1:2 during all the reactions, as the highest values of activation for Cu(I)Br have been obtained at this range for polar solvents (Nanda and Matyjaszewski, 2003).

5.4.2.1 Preparation of homopolymer supports and FT-IR characterization

ATRP was performed onto M-PVA brominated supports (20% activation, 4.1 Å target spacing), by altering the ratio of Initiator:Cu(I)Br and keeping the other parameters constant. The colour change of the reaction mixture was also observed at several time intervals, to further identify the conversion of metal complex. The following initiator:Cu(I)Br ratios were used: 1:0, 1:1, 1:2, 1:5 and 1:10. All the reactions took place for the same time period, and the

monomer (NIPAAm) installed onto the support was determined by ATR FT-IR quantitative analysis of supernatants. The reactions were also confirmed qualitative by FT-IR analysis on solids in KBr discs. In Table 5.1, the reaction conditions and the results of the quantification are summarised, while in Fig. 5.6, the scans of all the supports before and after the bromination and ATRP are presented.

According to Table 5.1, the monomer consumed after all the reactions is between 8.2 – 12.8 %, and no increasing trend is observed by increasing the amount of Cu(I)Br, indicating that this component has no effect in the reaction. This is in accordance to literature, where the molecular weights are defined mostly by the monomer to initiator ratio and are not affected by the concentration of the transition metal (Braunecker and Matyjaszewski, 2007).

Table 5.1 Homo polymer brush supports prepared by 'AGE / partial bromination / ATRP' route.

Support #	M-PVA starting material		Partial bromination & ATRP parameters					Support characterization							Polymer brush description on finished support
	Batch	SA (m^2/g)	Monomer employed	mmol Br_2 added per g M-PVA *(% bromination)*	Cu(I)Br (mmol/g M-PVA)	Bpy (mmol/g M-PVA	Monomer presented (mmol/g M-PVA)	React^n (%)	DP (units)	Spacing (Å)	Monomer installed (mmol/g M-PVA)	Polymer (g/g M-PVA)	Polymer (g/g support)	Monomer installed (mmol/g support)	
Homo-4.10	4	55	NIPAAm	0.54 *(20)*	0	0	54	0	-	-	-	-	-	-	-
Homo-4.11	4	55	NIPAAm	0.54 *(20)*	0.54	1.08	54	12.85	12.9	4.12	6.94	0.784	0.374	3.31	$pNIPAAm_{12.9}$ – 4.1 Å
Homo-4.12	4	55	NIPAAm	0.54 *(20)*	1.08	2.16	54	12.29	12.3	4.12	6.64	0.750	0.288	2.55	$pNIPAAm_{12.3}$ – 4.1 Å
Homo-4.13	4	55	NIPAAm	0.54 *(20)*	2.70	5.40	54	8.21	8.2	4.12	4.43	0.501	0.277	2.45	$pNIPAAm_{8.2}$ – 4.1 Å
Homo-4.14	4	55	NIPAAm	0.54 *(20)*	5.40	10.80	54	11.51	11.5	4.12	6.22	0.703	0.349	3.09	$pNIPAAm_{11.5}$ – 4.1 Å

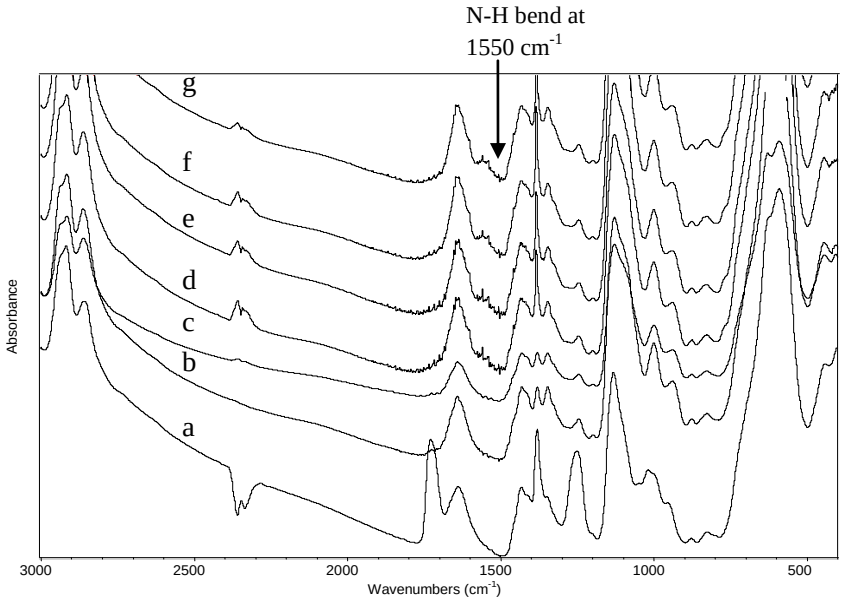

Figure 5.6 FTIR spectra of the M-PVA supports before and after partial bromination and ATRP for pNIPAAm homopolymers: **a**- unmodified M-PVA support; **b**- AGE activated M-PVA support; **c**, **d**, **e**, **f** and **g**: AGE activated M-PVA supports after performing ATRP with ratios of Initiator:Cu(I)Br:bpy:monomer at 1:0:0:100, 1:1:2:100, 1:2:4:100, 1:5:10:100 and 1:10:20:100 respectively.

In Fig. 5.6, spectrum b corresponds to AGE activated M-PVA. Modification of the support is observed by the disappearance of the carbonyl moiety peak at 1720 cm^{-1} after the reaction. These carbonyl groups found on the surface of the M-PVA may originated from: either (a) the oxidation of the -OH groups during the synthesis of the supports or; (b) residual hydrolysed acetate groups during the synthesis of PVA from poly vinyl acetate. In both cases these groups would appear on the surface of the supports as: M-PVA is non-porous; and acetate groups are unlikely to be within the matrix as hydrogen bonds are favoured between the PVA hydroxyls. At d, e, f, g spectra the appearance of N-H bend at 1550 cm^{-1} indicates the pNIPAAm grafting onto the supports with no significant differences of peak areas/heights obtained.

Observation of the reaction mixture color, indicated that the reaction was initiated within the first 15 min, (i.e. change from greenish to blue color of the reaction mixture referred to conversion of Cu(I)Br to Cu(II)Br).

The low conversions obtained with ATRP can be attributed to several factors. Firstly, when chains are grown from a surface at high density, the kinetics of the reaction are affected or the polydispersity of the chains increases, due to geometric constrains, when compared with that observed in solution at the same conditions (Matyjaszewski *et al*., 1999). In addition, chain breaking reactions (termination and transfer) are possible during an ATRP.

Grafting of pNIPAAm onto surfaces of particles via ATRP is not very common as the thickness of the resulting brushes is not well-controlled (Wu *et al*., 2008). In literature just few examples have been reported, where nanoparticles have been either cross-linked with pNIPAAm or contain pNIPAAm shells using ATRP (Kim *et al.*, 2005; Zhang *et al.*, 2007). The reasons for the not well controlled reaction have been attributed to the type of the monomer and solvent, the high concentration of radicals promoting chain transfer and termination reactions as well as the type of the catalytic system (CuX/bpy) (Wu *et al*., 2008). Teodorescu and Matyjaszewski (1999) and Rademacher *et al.*, (2000) attribute the lack of control in ATRP of (meth)acrylamides utilising the copper catalyst system to: (a) the inactivation of catalyst due to polymer complexation; (b) the strong bond between bromine and the terminal monomer unit in the polymer; and (c) the nucleophilic displacement of terminal bromine by the penultimate amide group.

Although the immobilisation and concentration of the initiator can be controlled with the partial bromination method, when ATRP is employed, the efficiency of the catalytic system for the ‘true’ initiator utilisation is not known. For this reason, we initially assume that 100 %

utilisation has taken place, in order to estimate the theoretical chain lengths obtained to be make easier the comparison of the different types of brushes constructed in this work.

5.4.2.1.1 Flory radii and regime of homopolymer chains

The Flory radii (R_F) of the homopolymer chains grafted on the supports were estimated under two different considerations: (a) assuming 100 % utilisation of brominated sites; (b) assuming 16 % utilisation of brominated sites based on findings of Wu *et al*., (2008). The estimated $s/(2R_F)$ values for both assumptions (Table 5.2) were found much less than 1, indicating that the chains are configured at the brush regime.

Table 5.2 Grafting parameters such as density, degree of polymerisation, R_F and $s/(2R_F)$ ratio under different assumptions of % Br_2 consumption.

100 % Br_2 consumption								
Support #	Monomer employed	mmol Br_2 added per g M-PVA	Monomer installed (mmol/g M-PVA)	DP (units)	s (Å)	Segment length *l* (Å)	R_F (Å)	$s/(2R_F)$
Homo-4.11	NIPAAm	0.54	6.94	12.9	4.12	3.0	13.91	0.15
Homo-4.12	NIPAAm	0.54	6.64	12.3	4.12	3.0	13.52	0.15
Homo-4.13	NIPAAm	0.54	4.43	8.2	4.12	3.0	10.60	0.19
Homo-4.14	NIPAAm	0.54	6.22	11.5	4.12	3.0	12.99	0.16
16 % Br_2 consumption								
Support #	Monomer employed	mmol Br_2 added per g M-PVA	Monomer installed (mmol/g M-PVA)	DP (units)	s (Å)	Segment length *l* (Å)	R_F (Å)	$s/(2R_F)$
Homo-4.11	NIPAAm	0.09	6.94	80.3	10.3	3.0	41.69	0.12
Homo-4.12	NIPAAm	0.09	6.64	76.9	10.3	3.0	40.60	0.13
Homo-4.13	NIPAAm	0.09	4.43	51.3	10.3	3.0	31.85	0.16
Homo-4.14	NIPAAm	0.09	6.22	72.0	10.3	3.0	39.04	0.13

5.4.2.2 Preparation of mixed polymer supports, copolymer supports and FT-IR characterization

ATRP onto partial brominated M-PVA supports was performed at two steps to graft mixed polymer brushes of NIPAAm and VI. The mixed brushes were manufactured by incorporating a termination step before the second monomer reaction making sure that polymerisation initiated from the surface and no other site. In the first set of experiments the AGE-PVA surface was brominated at 50 % at each ATRP step, which corresponds to 1.84 Å final spacing assuming complete utilisation of the initiator. Three supports were prepared by setting the initiator to monomer ratio either 1:100 or 1:250, and inverting the order of monomer addition. According to FT-IR characterisation (Table 5.3), the increase of monomer concentration (i.e. 250 versus 100 monomers target length) delivered longer polymer chains for both pNIPAAm and pVI. The order of monomer addition had no significant effect onto the final % conversion. In the second set of experiments the AGE-PVA surface was brominated at 20 % before each ATRP step, which corresponds to 2.91 Å final spacing assuming complete utilisation of the initiator. Three supports were again prepared by setting the initiator to monomer ratio either at 1: 100 or 1:250, and inverting the order of monomer addition. By decreasing the % bromination, the final length of the polymer chains obtained was higher during both steps of ATRP. In addition, as before (50 % bromination), by increasing the presented monomer concentration onto the reaction, polymer chains of increasing length are obtained.

FT-IR of solid samples in KBr discs was performed during both ATRP steps for all the above functionalised supports. In Fig. 5.7, the spectra of unmodified M-PVA (a), AGE activated M-PVA (b) and that of the products obtained after each reaction (c and d) with 50 % bromination

are shown. In all cases, the grafting of pNIPAAm is confirmed with the appearance of N-H bend peak at 1550 cm^{-1}. As before, modification of the support with pVI is followed with the enhanced height of peak at 1380 cm^{-1} as well as the increase of peak area and height at 1633 cm^{-1} (C=C stretch vibration appearance of imidazole ring) (Hummel and Scholl, 1990). In Fig. 5.8, the spectra obtained from the products delivered after each reaction (c and d) with 20 % bromination are shown. Again, the grafting of pNIPAAm is confirmed with the appearance of N-H bend peak at 1550 cm^{-1}, and that of VI with the change of peak height at 1633 cm^{-1} and 1380 cm^{-1}. For the [pVI_7 + $pNIPAAm_{11}$] – 2.9 Å (Mixed 4.10) support, the increased height of peak at 1380 cm^{-1} obtained after VI polymerisation was considerably decreased after pNIPAAm addition onto the same support (similar trend was observed at cerium (IV) mixed brush grafting).

Table 5.3 Mixed brush and copolymer brush supports prepared by the 'AGE / partial bromination / ATRP' route.

Support #	M-PVA starting material		Partial bromination & ATRP parameters					Support characterization							Polymer brush description on finished support
	Batch	SA (m^2/g)	Graft step - Monomer	mmol Br_2 added per g M-PVA *(% bromination)*	Cu(I)Br (mmol/g M-PVA)	Bpy (mmol/g M-PVA	Monomer presented (mmol/g M-PVA)	React^n (%)	DP (units)	Spacing (Å)	Monomer installed (mmol/g M-PVA)	Polymer (g/g M-PVA)	Polymer (g/g support)	Monomer installed (mmol/g support)	
Mixed-4.5	4	55	1 - NIPAAm 2 - VI	1.35 *(50)* 1.35 *(50)*	13.5 13.5	27.0 27.0	135 135	4.87 4.74	4.9 4.7	2.61 1.84	6.58 6.40 12.98	0.743 0.601 1.344	0.280 0.227 0.507	2.48 2.42 4.90	[$pNIPAAm_{4.9}$ + $pVI_{4.7}$] – 1.8 Å
Mixed-4.6	4	55	1 - NIPAAm 2 - VI	1.35 *(50)* 1.35 *(50)*	13.5 13.5	27.0 27.0	337.5 337.5	4.69 2.69	11.7 6.7	2.61 1.84	15.83 9.08	1.789 0.853 2.642	0.453 0.216 0.669	4.01 2.30 6.31	[$pNIPAAm_{11.7}$ + $pVI_{6.7}$] – 1.8 Å
Mixed-4.7	4	55	1 - VI 2 - NIPAAm	1.35 *(50)* 1.35 *(50)*	13.5 13.5	27.0 27.0	135 135	4.25 3.32	4.3 3.3	2.61 1.84	5.74 4.48	0.539 0.506 1.046	0.229 0.215 0.444	2.43 1.90 3.33	[$pVI_{4.3}$ + $pNIPAAm_{3.3}$] – 1.8 Å
Mixed-4.8	4	55	1 - NIPAAm 2 - VI	0.54 *(20)* 0.54 *(20)*	5.4 5.4	10.8 10.8	135 135	9.69 7.90	24.2 19.8	4.12 2.91	13.08 10.71	1.478 1.006 2.485	0.390 0.265 0.655	3.45 2.82 6.27	[$pNIPAAm_{24.2}$ + $pVI_{19.8}$] – 2.9 Å
Mixed-4.9	4	55	1- VI 2 - NIPAAm	0.54 *(20)* 0.54 *(20)*	5.4 5.4	10.8 10.8	54 54	4.94 17.70	4.9 17.7	4.12 2.91	2.68 9.56	0.251 1.080 1.331	0.095 0.409 0.504	1.01 3.62 4.63	[$pVI_{4.9}$ + $pNIPAAm_{17.7}$] – 2.9 Å
Mixed-4.10	4	55	1- VI 2 - NIPAAm	0.54 *(20)* 0.54 *(20)*	5.4 5.4	10.8 10.8	54 54	7.0 11.0	7.0 11.0	4.12 2.91	3.80 5.94	0.357 0.671 1.028	0.153 0.287 0.440	1.62 2.54 4.16	[pVI_7 + $pNIPAAm_{11}$] – 2.9 Å
Co-4.9	4	55	1 - NIPAAm 2 - VI	0.54 *(20)* - *(0)*	5.4 5.4	10.8 10.8	54 54	11.51 7.41	11.5 7.4	4.12 4.12	6.22 4.00	0.702 0.376 1.078	0.294 0.157 0.451	2.60 1.67 4.27	$pNIPAAm_{11.5}$ –*co*– $pVI_{7.4}$ – 4.1 Å

Mixed 4.5 [pNIPAAm$_{4.9}$ + pVI$_{4.7}$] – 1.8 Å

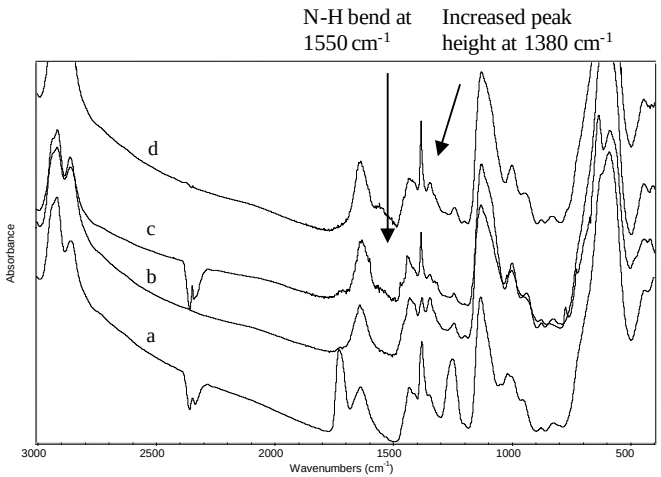

Mixed 4.6 [pNIPAAm$_{11.7}$ + pVI$_{6.7}$] – 1.8 Å

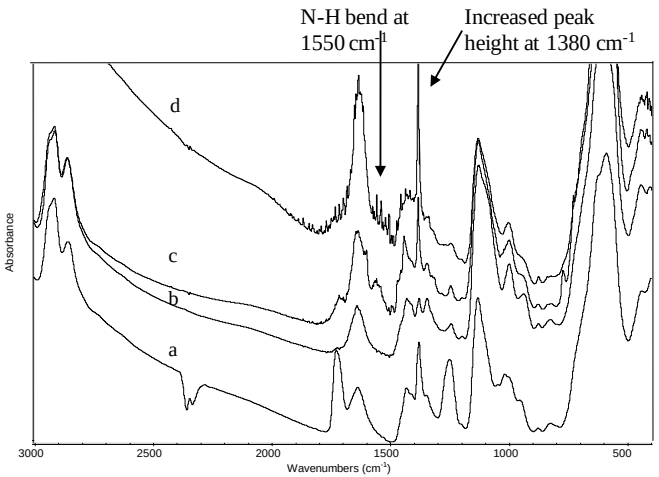

Mixed 4.7 [pVI$_{4.3}$ + pNIPAAm$_{3.3}$] – 1.8 Å

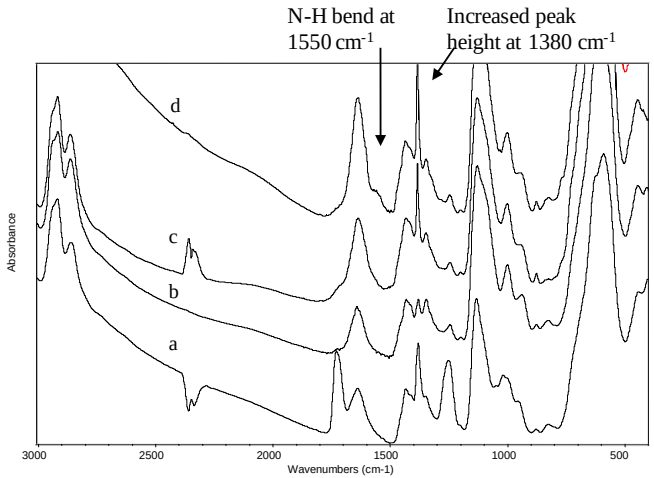

Figure 5.7 FT-IR spectra of mixed polymer supports prepared by the 'AGE / partial bromination / ATRP' route, where 50 % bromination was utilised twice for 1.8 Å target spacing. **a**- Unmodified M-PVA; **b**- AGE activated M-PVA; **c**- First polymer installed via ATRP; **d**- Second polymer installed via ATRP.

Mixed 4.8 [pNIPAAm$_{24.2}$ + pVI$_{19.8}$] – 2.9 Å

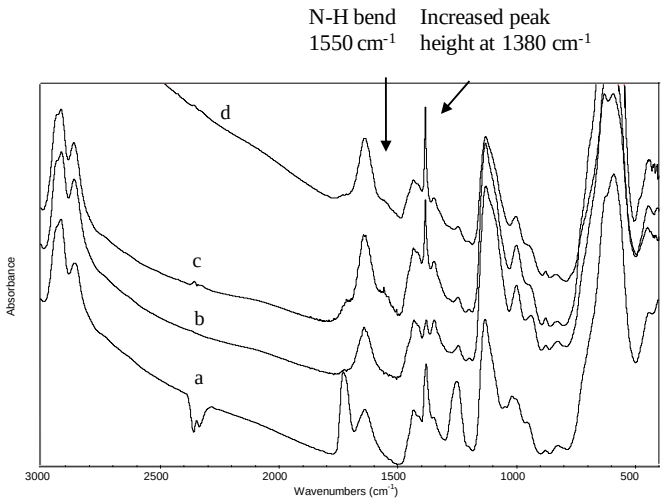

Mixed 4.9 [pVI$_{4.9}$ + pNIPAAm$_{17.7}$] – 2.9 Å

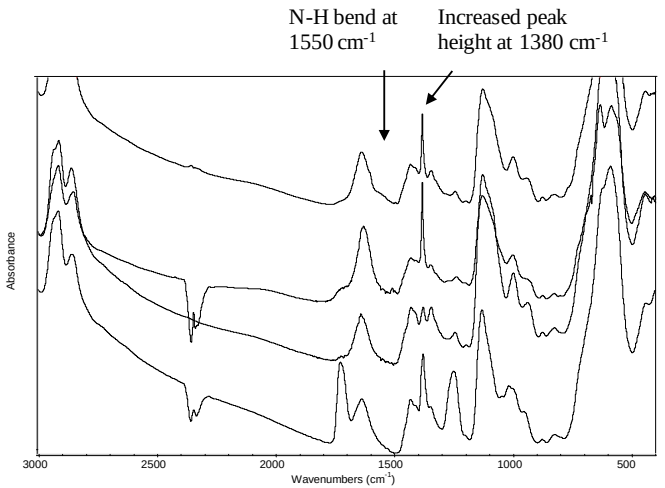

Mixed 4.10 [pVI$_7$ + pNIPAAm$_{11}$] – 2.9 Å

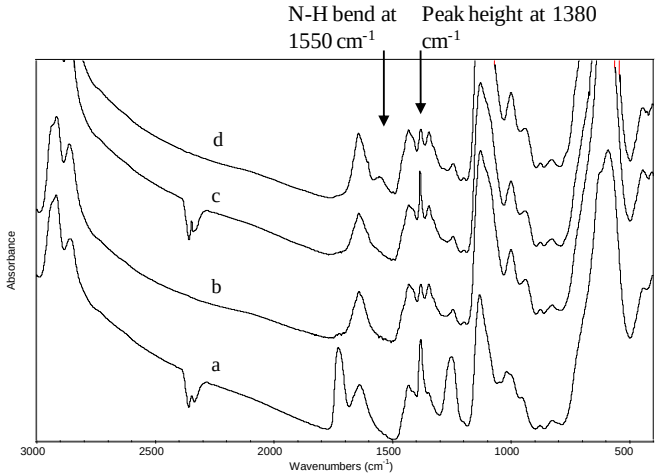

Figure 5.8 FT-IR spectra of mixed polymer supports prepared by the 'AGE / partial bromination / ATRP' route, where 20 % bromination was utilised twice for 2.9 Å target spacing. **a**- Unmodified M-PVA; **b**- AGE activated M-PVA; **c**- First polymer installed via ATRP; **d**- Second polymer installed via ATRP.

Well-controlled molecular architectures are essential to study the materials structure-property relationships, especially in biomedical applications. Atom transfer radical polymerization (ATRP) is a versatile technique for the preparation of well-defined polymers with different compositions, macromolecular architecture, and end-functional groups (Wang and Matyjaszewski, 1995; Zhang and Matyjaszewski, 1999; Matyjaszewski *et al*., 1999; Kamigaito *et al*., 2001). To evaluate the living character of the system, VI was used as the second monomer (sequential addition) for further polymerisation (block copolymer). For this reason, ATRP of VI onto pNIPAAm grafted M-PVA support ($pNIPAAm_{11.5}$ – 4.1 Å in Table 5.1 and spectrum **g** in Fig 5.6) was utilised without any further initiator addition. This reaction was characterised measuring the monomer consumption after the reaction (Table 5.2) and investigating the FT-IR spectra of the modified support (Fig. 5.7). The reduction of VI concentration at the supernatant after the reaction (monomer consumption of 7.41 %) indicates polymerisation of VI onto the support. As no further initiator was added onto the reaction it may assumed that the polymerisation took place at the end of the pNIPAAm backbone resulting in block copolymerisation.

In Fig. 5.9, between spectrum c and d, two main differences are observed at peaks of 1550 and 1380 cm^{-1}. The first one (NH bend) becomes smoother while the second one (C-H bend) is reduced. The same support modifications were observed for the [pVI_7 + $pNIPAAm_{11}$] – 2.9 Å mixed support (Fig. 5.8). Based on previous argumentation (incomplete utilisation of the initiator) it could be also possible that polymerisation was initiated from residual dibrominated sites from the first polymerisation. As a consequence, for confirmation of the polymer chains end functionality, further examination is required.

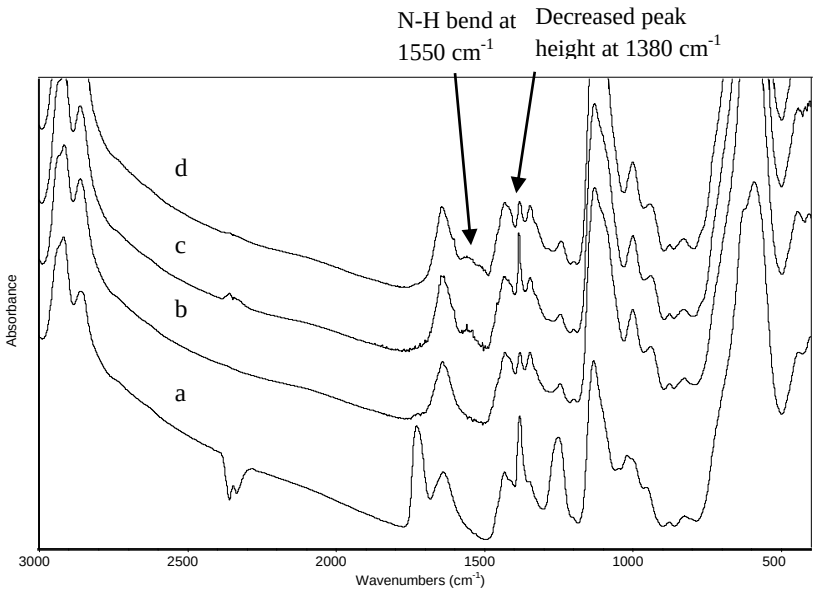

Figure 5.9 FTIR spectra obtained during VI grafting onto non-terminated pNIPAAm grafted supports (block copolymerisation): **a**- unmodified M-PVA support; **b**- AGE activated M-PVA support; **c**- first grafting (pNIPAAm) **d**- second grafting (VI).

5.4.2.2.1 Flory radii and regime of mixed polymer chains

The average Flory Radius (R_F) of the mixed polymer chains was estimated following the three methods described in section *4.4.1.3* (Eq. 4.1, 4.2 and 4.3). The estimations were based on 100 %, and 16 % utilisation of brominated sites (Wu *et al.*, 2008). In Table 5.4, the $s/(2R_F)$ ratios (much less than 1) indicate that the mixed polymer chains are in 'true' brush regime.

Table 5.4 R_F and $s/(2R_F)$ values obtained under different % Br_2 assumptions, following method (a) averaging based on number of monomer units; (b) averaging based on the number of polymer chains with equal weighting; and (c) averaging according to number of chains, weighted with respect to those of higher R_F.

100 % Br_2 consumption												
Support #	Graft step - Monomer	mmol Br_2 added per g M-PVA	s (Å)	DP (units)	Segment length *l* (Å)	R_F (Å)	R_F' (Å)	s/(2RF')	R_F'' (Å)	s/($2R_F''$)	R_F''' (Å)	s/($2R_F'''$)
Mixed-4.5	1 - NIPAAm	1.35	1.84	4.9	3	7.8	13.6	0.07	13.7	0.07	16.3	0.06
	2 - VI	1.35		4.7	7.74	19.7						
Mixed-4.6	1 - NIPAAm	1.35	1.84	11.7	3	13.1	17.2	0.05	18.7	0.05	20.3	0.05
	2 - VI	1.35		6.7	7.74	24.2						
Mixed-4.5	1 - VI	1.35	1.84	4.3	7.74	18.6	13.2	0.07	12.4	0.07	15.5	0.06
	2 - NIPAAm	1.35		3.3	3	6.1						
Mixed-4.8	1 - NIPAAm	0.54	2.91	24.2	3	20.3	32.1	0.05	33.4	0.04	38.5	0.04
	2 - VI	0.54		19.8	7.74	46.4						
Mixed-4.9	1- VI	0.54	2.91	4.9	7.74	20.1	17.5	0.08	18.5	0.08	18.6	0.08
	2 - NIPAAm	0.54		17.7	3	16.8						
Mixed-4.10	1- VI	0.54	2.91	7.0	7.74	24.9	17.4	0.08	18.8	0.08	20.8	0.07
	2 - NIPAAm	0.54		11.0	3	12.6						
16 % Br_2 consumption												
Support #	Graft step - Monomer	mmol Br_2 added per g M-PVA	s (Å)	DP (units)	Segment length *l* (Å)	R_F (Å)	R_F' (Å)	s/(2RF')	R_F'' (Å)	s/($2R_F''$)	R_F''' (Å)	s/($2R_F'''$)
Mixed-4.5	1 - NIPAAm	0.22	4.56	30.5	3	23.3	41.0	0.06	41.2	0.06	49.0	0.05
	2 - VI	0.22		29.6	7.74	59.1						
Mixed-4.6	1 - NIPAAm	0.22	4.56	73.3	3	39.5	51.7	0.04	56.2	0.04	61.2	0.04
	2 - VI	0.22		42.0	7.74	72.9						
Mixed-4.5	1 - VI	0.22	4.56	26.6	7.74	55.4	39.2	0.06	36.9	0.06	46.2	0.05
	2 - NIPAAm	0.22		20.7	3	18.5						
Mixed-4.8	1 - NIPAAm	0.0864	7.28	151.4	3	61.0	96.3	0.04	100.3	0.04	115.7	0.03
	2 - VI	0.09		124.0	7.74	139.5						
Mixed-4.9	1- VI	0.09	7.28	31.0	7.74	60.8	52.8	0.07	55.6	0.07	56.1	0.06
	2 - NIPAAm	0.09		110.6	3	50.5						
Mixed-4.10	1- VI	0.09	7.28	44.0	7.74	74.9	52.4	0.07	56.5	0.06	62.5	0.06
	2 - NIPAAm	0.09		68.8	3	38.0						

5.4.3 Preliminary protein desorption studies from mixed polymer brushes by temperature transitions

In this section, the protein desorption efficiency during transitions across the LCST of the brushes manufactured via ATRP has been investigated. The procedure followed is the same with that used before for testing the mixed brushes prepared by cerium (IV) initiated 'graft from' route. In these studies, three supports were selected (of varying spacing and polymer lengths), i.e. the mixed-4.6, mixed-4.8 and mixed-4.10 materials due to the higher amounts of pNIPAAm and pVI grafted in comparison with other supports (Table 5.2). For the mixed-4.6 and mixed-4.8 supports, Hb was used during batch binding and desorption with temperature. For the mixed- 4.10 support both Hb and GFP desorption was tested. The buffers were kept at the same composition of those utilised in Chapter 4, i.e. 100 mM Sodium Phosphate, 200 mM NaCl buffer and 20 mM Sodium Phosphate, 200 mM NaCl buffer for the Hb and GFP respectively.

5.4.3.1 Protein (haemoglobin) binding and desorption studies with [pNIPAAm$_{11.7}$ + pVI$_{6.7}$] – 1.8 Å support

The Hb binding / temperature desorption with charged / uncharged supports in binding buffer (and subsequent washes with imidazole and NaOH), of [pNIPAAm$_{11.7}$ + pVI$_{6.7}$] – 1.8 Å support, is shown in Fig. 5.10.

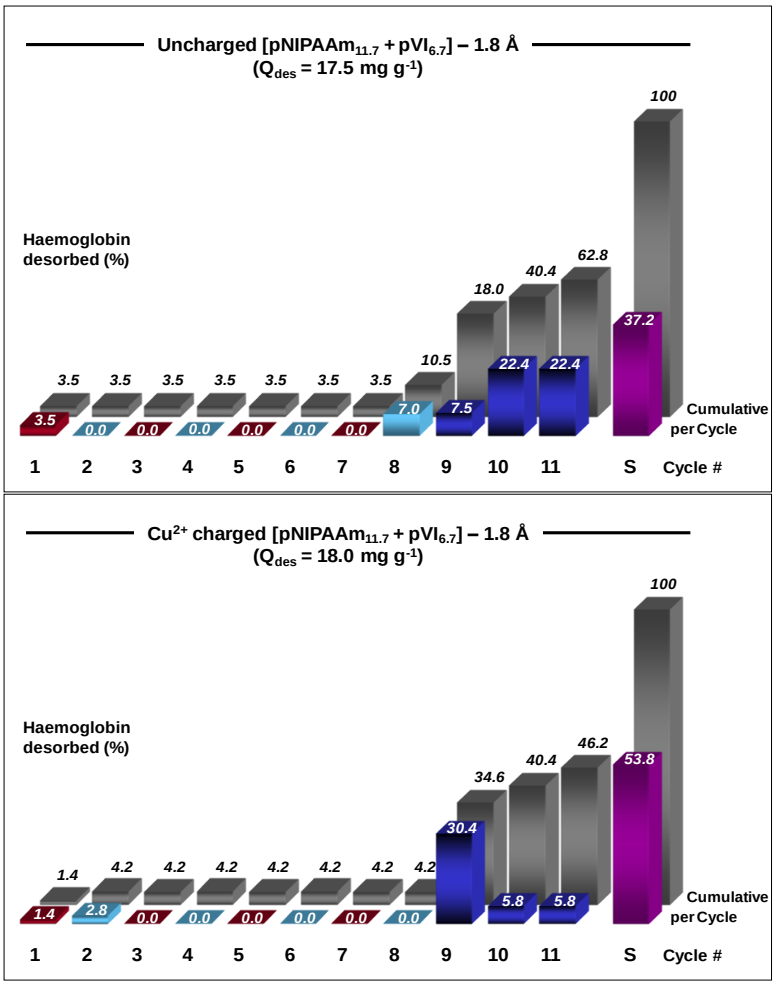

Figure 5.10 Protein (haemoglobin) desorption experiments with [pNIPAAm$_{11.7}$ + pVI$_{6.7}$] – 1.8 Å mixed brush support: Protein desorbed from 20 °C to 45 °C (red bars); protein desorbed from 45 °C to 20 °C (light blue bars); protein desorbed with 0.2 M imidazole (pH 7.0) (deep blue bars); protein desorbed with stripping agent (NaOH) (purple bar); cumulative protein desorption from each support (grey bars).

After batch binding of Hb for 1 h, a total amount of 17.7 and 18.0 mg g^{-1} of protein firmly bound on the uncharged and charged support respectively. Due to the very short length of the pVI chains (i.e. 6.7 monomer units), the binding capacity for Hb was also very low with a small increase after charging. Employing the standard eight cycles of temperature transitions, no significant protein release was detected (i.e. only 3.5 and 4.5 % respectively). The low efficiency of this mixed for protein release can be attributed to many reasons. Based on the assumption that all the initiator has been utilized, the density of the chains incorporated to this

material are estimated to be very close (1.84 Å for 100 % consumption) and crowding of polymer chains at a polymer brush, may result to less contraction as steric crowding may inhibit collapse (Kilbey *et al.*, 2001; Toomey and Tirrell, 2008). Washing this support with elution buffer, 52.3 and 42.0 % of the total protein bound was eluted from the uncharged and charged support respectively. By further washing the supports with imidazole (three cycles) and NaOH the rest of the protein was completely removed.

5.4.3.2 Protein (haemoglobin) binding and desorption studies with [pNIPAAm$_{24.2}$ + pVI$_{19.8}$] – 2.9 Å support

In Fig. 5.11, the results of protein (Hb) protein binding and desorption at [pNIPAAm$_{24.2}$ + pVI$_{19.8}$] – 2.9 Å while being charged or uncharged are shown. A total amount of 23.9 mg g^{-1} of Hb was bound to the charged support and 14.0 mg g^{-1} onto the uncharged. The much higher pVI chain lengths (i.e. 19.8 monomer units) in comparison with the previous support (i.e. 6.7 monomer units), resulted in increasing binding capacity for Hb. After the eight temperature transitions, 15.3 and 17.3 % of Hb was released from each support respectively. The desorption efficiency of this support in comparison with the previous one was also higher (especially for the charged material), due to the differences in morphology (spacing, chain length) between the two brushes. The increased pNIPAAm chain length at wider spacing allowed the free expansion and collapse of the polymer for protein release enhancement. The increased amount of Hb removed with imidazole from the charged support in comparison with the uncharged one can be attributed to the higher amount of protein bound and at more specific way.

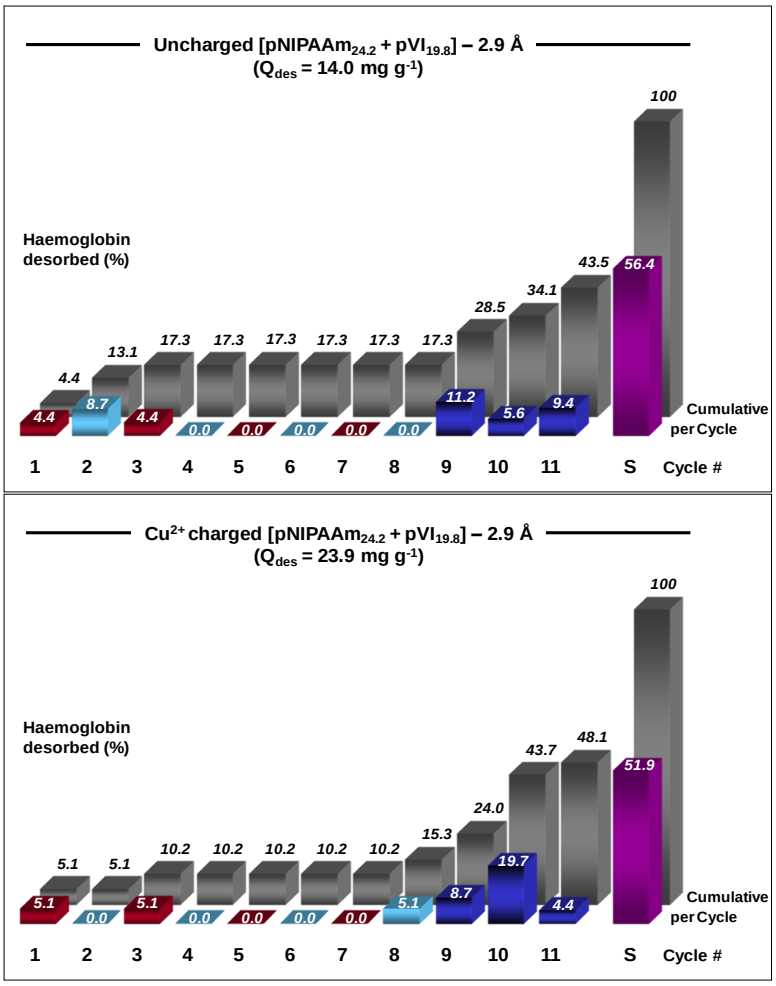

Figure 5.11 Protein (haemoglobin) desorption experiments with [pNIPAAm$_{24.2}$ + pVI$_{19.8}$] – 2.9 Å mixed brush support: Protein desorbed from 20 °C to 45 °C (red bars); protein desorbed from 45 °C to 20 °C (light blue bars); protein desorbed with 0.2 M imidazole (pH 7.0) (deep blue bars); protein desorbed with stripping agent (NaOH) (purple bar); cumulative protein desorption from each support (grey bars).

5.4.3.3 Protein (haemoglobin and GFP) binding and desorption studies with [pVI$_7$ + pNIPAAm$_{11}$] – 2.9 Å polymer support

In this section, the protein desorption and elution efficiency of the [pVI$_7$ + pNIPAAm$_{11}$] – 2.9 Å support is presented. Hb was bound to the charged support at 23.7 mg g^{-1} and from that 30.9 % was released. Imidazole washing (three cycles) eluted 23 % while NaOH removed the

rest of the protein (Fig. 5.12). This support demonstrated better Hb release efficiency with temperature transitions than the other supports; even though the resulting lengths of pVI and pNIPAAm have been estimated to 7 and 11 monomer units respectively. However, the grafting at 2.9 Å between the graft sites indicates that the spacing is a very important parameter both in protein binding and in pNIPAAm transition with temperature change. For example, this support delivered higher Hb binding capacity than the [$pNIPAAm_{11.7}$ + $pVI_{6.7}$] – 1.8 Å of similar chain lengths but of wider density. In addition the pVI chains of this support are much shorter than the [$pNIPAAm_{24.2}$ + $pVI_{19.8}$] – 2.9 Å support and as a consequence their conformation may influenced more by the pNIPAAm expansion/collapse.

A total amount of 17.9 mg g^{-1} GFP was bound on the charged support and from that 62.9 % was eluted. The less amount of GFP bound on these supports and the higher percentage of protein release in comparison with Hb can be attributed to the differences between the structures of the proteins as already outlined in Chapter 4 (i.e. differences in size, thermal stability etc.).

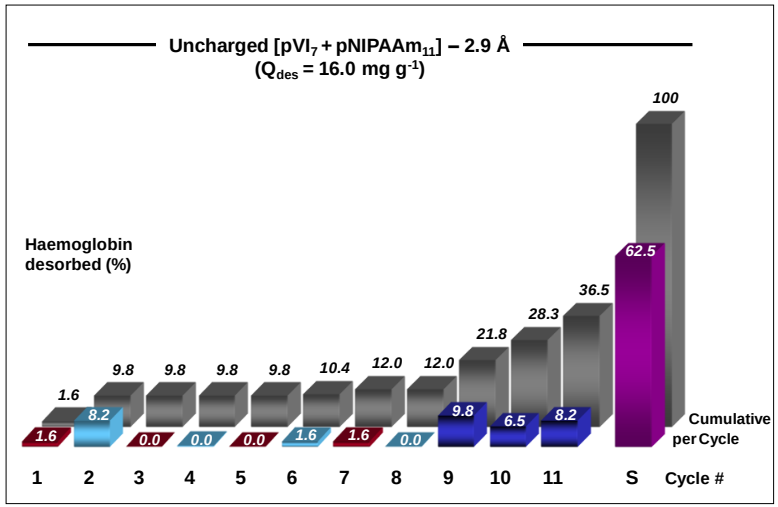

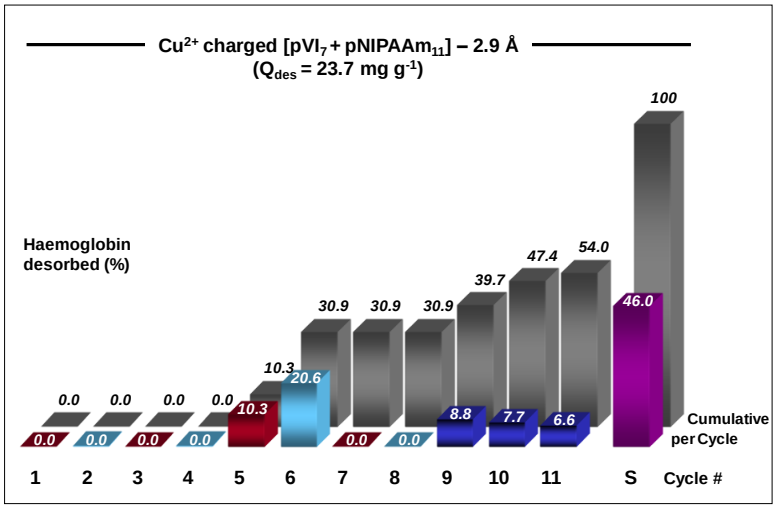

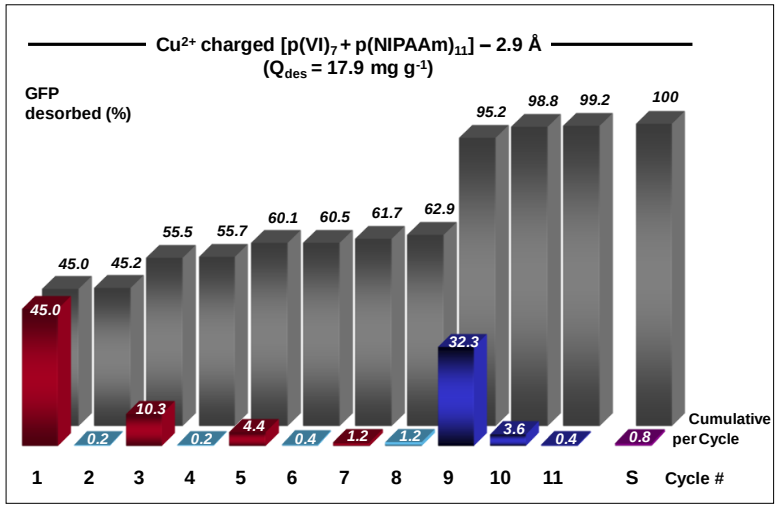

Figure 5.12 Protein (haemoglobin) desorption experiments with [pVI_7 + $pNIPAAm_{11}$] – 2.9 mixed brush support: Protein desorbed from 20 °C to 45 °C (red bars); protein desorbed from 45 °C to 20 °C (light blue bars); protein desorbed with 0.2 M imidazole (pH 7.0) (deep blue bars); protein desorbed with stripping agent (NaOH) (purple bar); cumulative protein desorption from each support (grey bars).

5.4.3.4 Comparison of protein desorption by 'hot-cold' transitions in binding buffer and 'hot-cold' transitions in elution buffer

Four temperature transition cycles were applied on charged supports in elution buffer and compared with those that took place in binding buffer. The results for two supports are shown in Fig. 5.13.

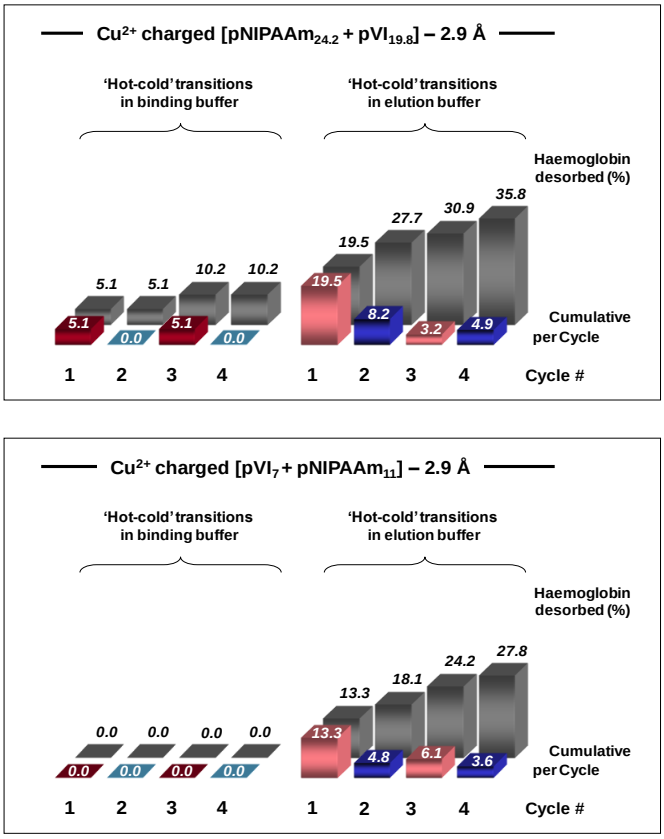

Figure 5.13 Protein desorbed by 'hot-cold' transitions in binding and elution buffer with mixed brush supports: Protein desorbed from 20 °C to 45 °C in binding buffer (red bars); protein desorbed from 45 °C to 20 °C in binding buffer (light blue bars); protein desorbed from 20 °C to 45 °C in 0.2 M imidazole (pH 7.0) elution buffer (pink bars); protein desorbed from 45 °C to 20 °C in imidazole elution buffer (deep blue bars).

For both supports, the desorption achieved from 'hot-cold' transitions in elution buffer was higher than that in binding buffer. These results indicate that the supports prepared with ATRP are less efficient in comparison with most of those prepared with cerium (IV) initiated

polymerization in terms of pNIPAAm ability to improve desorption. Generally, the mixed brush supports prepared with cerium (IV) grafting of higher lengths and at wider spacing, were superior in both protein higher binding and release with temperature transitions, than those prepared by the 'AGE / partial bromination / ATRP' route.

5.5 Conclusions

Controlled partial bromination of the AGE activated M-PVA support enabled the immobilisation of the initiator at sites of varying spacing to graft different polymers (pNIPAAm and VI) in the form of mixed brushes using sequential ATRP. The polymer conversions did not reach completion after ATRPs, resulting in short polymer chain lengths than it was expected. The deficiency of the catalytic system, the steric hindrances between the chains growing close to each other, the types of monomers employed and other side reactions resulted in the premature termination of the reactions. Increasing the amount of Cu(I)Br/bpy in the reaction mixtures, revealed no significant effect in the polymerisation degree. There is evidence of possible regeneration of the reaction (ATRP living character), however further investigation is required in case that reaction was also initiated from remaining surface brominated sites after the first ATRP.

Manufacturing of mixed brushes was achieved by employing sequential ATRP reaction onto partial brominated supports incorporating a termination (quenching) reaction between the two steps. From these preliminary studies, it was shown that by increasing the monomer to initiator ratio, polymer chains of higher length were obtained for both pNIPAAm and pVI regardless the bromination level. Both the homopolymer and mixed polymer chains were in brush regime based on the estimation of the $s/(2R_F)$ values. However, the brushes prepared

with ATRP were of lower polymer chain lengths and tighter spacing than those prepared by the cerium (IV) initiated grafting. This resulted in different brush behaviour in terms of protein binding and release with temperature. The higher efficiency of the supports for GFP desorption in comparison with that of Hb is again attributed to the difference in nature between the two proteins.

Some authors indicate that employing ATRP on surfaces, not only termination reactions are possible, but also reduced utilisation of the initiator may be observed. For example, Wu *et al.* (2008), estimated a 16 % utilisation of the initial initiator added to the reaction. As a consequence, estimations of the actual initiator utilised in this work is also required. The followings have been proposed to overcome such limitations: (a) the use of a 'sacrificial' free initiator in the polymerisation mixture at the beginning of the reaction provides a better control over the process (Ejaz *et al*., 2001; Zampano *et al*., 2009); (b) adding a sufficient amount of deactivator at the beginning of the reaction course (Matyjaszewski *et al*., 1999); and (c) appropriate selection of optimum reaction conditions in accordance with the system employed (Kowalewski *et al*., 2003).

A general conclusion from this chapter is that although ATRP system is considered well-controlled when takes place in aqueous media, when it is applied onto surfaces (of particles) limitations may arise. Further information for the behavior of these materials in terms of pNIPAAm chains collapse aside to the pVI chains, can be obtained by performing thermoresponsive studies of uncharged and Cu^{2+} charged supports under different levels of salinity.

6. General conclusions and future work

The current status of downstream processing in the production of bio-therapeutics requires not only the need for improvement of the current bioseparation methods, but also further research towards alternative techniques and materials. Magnetic separations techniques become increasingly widespread due to their possible application in bioscience. The magnetic particles that are employed in these methods can be easily separated, deal with large volumes and can be functionalised with various ligands (e.g. affinity). However, it is possible to improve the efficiency of these materials in terms of protein binding and elution behaviour. The potential of 'stimuli responsive' or 'smart' polymers seems very promising in numerous applications, including bioseparations. Lately, the thermoresponsive polymers have been extensively used as means to facilitate separations in cost effective ways. Considering the recent advances in the development of adaptive surfaces and chemistry routes, the aim of this work was to fabricate polymer brushes composed of thermoresponsive and affinity polymers in different designs on magnetic particles for protein binding and release purposes. To achieve this, the 'grafting from' approach, onto magnetic supports, employing both cerium (IV) initiated system and Atom Transfer Polymerisation Reaction (ATRP), was utilised for studies of forced thermoresponsive desorption in assisting the cleaning adsorbed difficult to remove materials from supports (e.g. haemoglobin).

In Chapter 3, the cerium (IV) initiated polymerisation was extensively investigated in terms of different monomers grafting onto M-PVA supports. The optimum conditions were identified, while both the initiator and feed composition in the reaction were regulated to deliver polymer chains at brush regime. This was mainly achieved by characterising the polymer grafted supports in terms of resulting spacing and polymer chain lengths. Premature termination of

cerium (IV) initiated reactions onto M-PVA supports were unavoidable, due to the high polymerisation rates and termination reactions between the growing polymer chains. Investigation on one-pot cerium (IV) polymerisation to mixtures of two monomers (thermoresponsive and affinity) showed that di-block instead of alternating copolymers were constructed, due to the reactivity (solubility) differences between the monomers. Grafted pNIPAAm chains onto M-PVA supports either as homopolymer or di-block copolymer brushes with pVI, demonstrated thermoresponsiveness at the reported temperature range as a function of polymer chain length, spacing and pVI interruption. Brush behaviour demonstrated sharp transition upon heating, i.e. hydrophobic interactions favoured the discontinuous collapse of the polymer film. Haemoglobin binding studies onto homo-brushes or di-block brushes at different conditions showed that the protein binds to the modified matrices via many interactions (metal chelate, hydrophobic, ionic). The pNIPAAm single chains could form weak complexes with Cu^{2+} ions making possible the protein binding. It was demonstrated that protein interacted more strongly with the pNIPAAm modified surfaces above their LCST, while below the LCST the non-specific interactions were minimised. At elevated temperatures the development of strong interactions, the increased retention of metal ions and the partial haemoglobin unfolding, made the elution of protein difficult at these temperature ranges.

In Chapter 4, a method to construct mixed functionality brushes onto magnetic particles via sequential cerium (IV) initiated reactions was developed. Characterisation of the resulting brushes after modification of supports revealed that cerium (IV) chemistry can be used to graft polymers aside to each other at defined spacing onto the PVA surface. Haemoglobin binding studies in the presence of high salt concentration (1.0 M NaCl), delivered high capacities for all the mixed type charged supports (> 195 mg g^{-1}), whereas the protein binding

capacities increased with the amount of affinity ligand grafted onto the support. Protein could also interact with the uncharged supports as the pNIPAAm chains were collapsed (hydrophobic) in the presence of salt in high concentration. The performance of the above materials for protein release (without change of buffer) was evaluated by employing temperature transitions across their LCST. Complete desorption of both proteins employed (Hb and GFP) via temperature changes across the LCST in eight cycles was demonstrated from the charged $pNIPAAm_{10.3}$ –4.6 Å homopolymer support. On the other hand not such effect was observed for the homopolymer $pVI_{30.9}$ – 4.6 Å support (control). The mixed brush support grafted with the higher pNIPAAm length (and pVI aside), demonstrated better performance in comparison with the other mixed brushes (41.5 and 89.2 % of Hb and GFP was totally desorbed respectively after eight successive temperature transition cycles). The protein desorption of supports was correlated to the type of affinity ligand grafted onto them. Generally, pVI is a relative weak ligand, whereas pVBIDA much stronger. The strong protein binding onto the pVBIDA containing brushes made difficult its release even after eight temperature transition cycles. In all cases, the efficiency of supports for GFP desorption was much superior to haemoglobin. This is mainly attributed to the different structure characteristics of the two proteins and the way they interact with the polymer film at different temperatures. Addition of salt and Cu^{2+} charging of the materials is expected to influence the LCST of the homopolymer and mixed polymer brushes. For this reason, further studies to identify the exact transition temperature are required. In addition, further work to identify the optimum conditions for protein release, such as buffer composition (salt concentration), pNIPAAm chain length, exact range of transition temperature, kinetics studies regarding the protein interaction with the polymer brushes, and time required for complete pNIPAAm chains expansion/collapse, is required.

Atom transfer radical polymerization (ATRP) is a recently developed ‘controlled’ radical polymerization method, which allows the preparation of well-defined (co)polymer brushes with “living” chain ends on various types of substrates via surface-initiated techniques. In addition, ATRP offers the possibility to synthesise di-block copolymers by extending the first grafted polymer chain. In Chapter 5, sequential ATRP reaction onto partial brominated supports was employed to manufacture polymer brushes. The controlled partial bromination was achieved by firstly AGE activating the PVA surface. Then ATRP reaction was initiated from these groups by employing the Copper(I) Bromide catalytic system. The reactions onto the magnetic particles were difficult to control, while the polymer conversions were found rather low. The reasons of that can be attributed to several factors as the standard reaction conditions need optimisation when performed onto surfaces of small particles such as M-PVA. The regeneration of the reaction (ATRP living character) could not be excluded. However further investigation is required on that. This could be very advantageous in terms of di-block, tri-block etc. copolymers grafting. Further work should concentrate onto finding optimum reaction procedures and in parallel investigating other catalytic systems or controlled polymerisation reactions such as that of reversible addition fragmentation chain transfer (RAFT) reaction. Preliminary studies of protein adsorption/release via temperature change from supports prepared with ATRP made possible to compare the efficiency of these brushes with those prepared with cerium (IV) grafting. Both protein binding and release was much higher in the case of cerium (IV) initiated polymerised mixed brushes. ATRP prepared mixed brushes where of tighter spacing and/or lower polymer lengths delivering lower protein binding capacities and less desorption with temperature changes across the LCST. As a consequence, for ATRP made materials desorption was more efficient with elution buffer, whereas for the cerium (IV) initiated prepared materials desorption was more efficient with

temperature shifts. Thermoresponsive studies to identify the exact range of transition temperature and time required for pNIPAAm chains expansion/collapse (continuous or discontinuous phase separation) of these materials may help to identify the optimum conditions for protein binding and subsequent release.

Further investigation on pVI binding and desorption behaviour via pH changes is also possible. However, due to this ligand weak protein binding it is recommended to select other types of ligands (e.g. ionic exchangers or triazine dyes such as Cibacron Blue). Finally, as both cerium (IV) and ATRP 'grafting from' routes can be utilised for mixed functionality polymer supports construction, it is recommended to be applied to other types of chromatographic supports for similar applications and advantages.

7. Appendix

7.1 Proton NMR analysis of *N-(4-vinyl)-benzyl Iminodiacetic acid* (VBIDA)

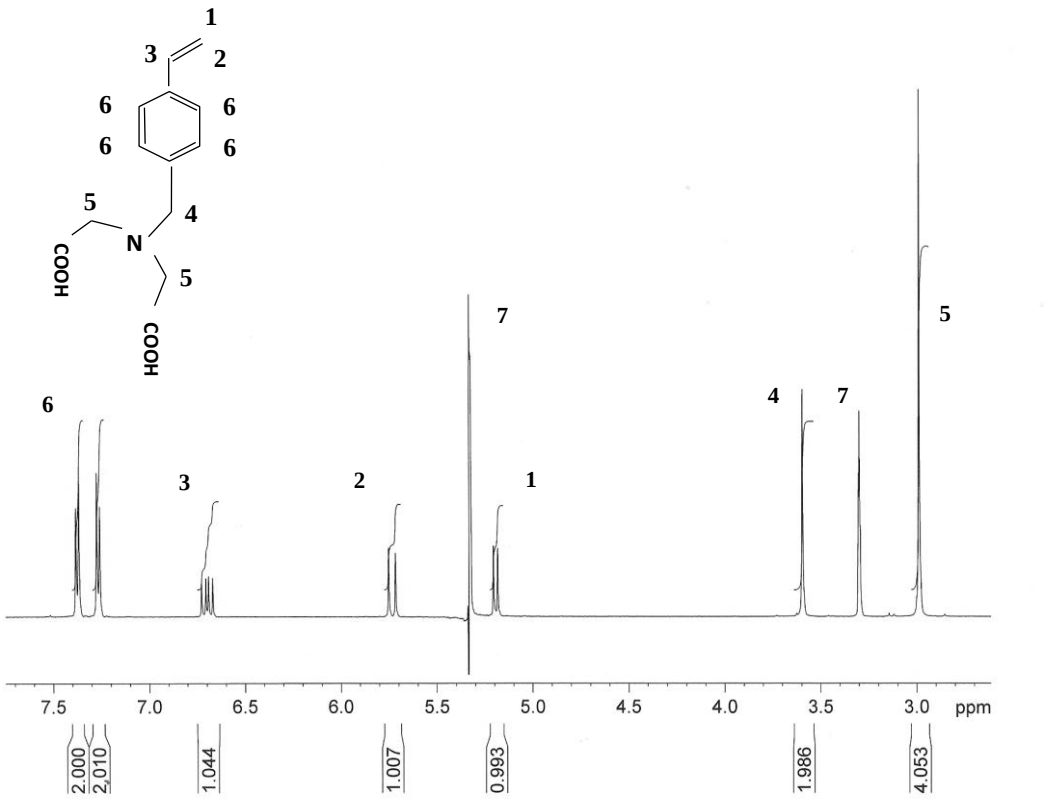

Figure 7.1 Proton NMR spectrum of VBIDA, (6 MHz): The distinctive peaks obtained from NMR spectrum have been assigned (numbered) according to available protons of the VBIDA molecule (top left corner). The peaks at 5.3 and 3.3 ppm (**7**) refer to protons from residual solvent (MeOH).

7.2 ATR FT-IR analysis

7.2.1 FT-IR Theory

The infrared spectroscopy method is based upon the vibration of the atoms of a molecule (chemical bonds stretch, contract and bend when light interacts with matter). When IR radiation is passed through a sample, some of the radiation is absorbed from the sample and some is transmitted through it. The amount of the radiation absorbed or transmitted is used to obtain an infrared spectrum which peaks correspond to the frequency of a vibration of a molecule (Thermo Nicolet Corporation, 2001; Stuart, 2004). As a consequence infrared spectroscopy is widely used to detect the characteristic vibrations of chemical functional bonds in samples.

According to Beer-Lambert Law, the amount of light transmitted by a sample is proportional to the thickness and the concentration of the sample:

$$A=\varepsilon c l \qquad \text{Eq. (7.1)}$$

In Eq. 7.1, A is the absorbance of the solution, c the concentration, *l* the path-length of the sample, while the Greek letter ε is the constant of proportionality (molar absorptivity) (Stuart, 2004). From this relationship it is noticeable that the absorbance is directly proportional with the concentration in a linear manner and a gradient of εl. The IR absorbance values of a sample are related to its concentration, analogous to the way concentration is related to absorbance in transmission spectroscopy through the Beer-Lambert law. As a consequence, by choosing a suitable band from the spectra of known concentrations of a substance, a calibration graph can be constructed and used for the analysis of samples of unknown concentrations. Therefore, the infrared spectroscopy can be very useful for both qualitative

(identification of unknown materials) and quantitative (amount of a component in a sample) purposes.

IR spectra can be obtained from samples in different forms (liquid, solid, gas). Typically, pellets are used for solid samples, where the sample is finely ground and mixed with dry potassium bromide powder (KBr). One of the most versatile tools of FT-IR is the Attenuated Total Reflectance (ATR), which is very useful for the fast analysis of many materials such as highly absorbing solids and liquids. The main advantages of this mode, is the thin sampling path length and the depth of penetration of the IR beam into the sample as well as the bypass of sample preparation (Hsu, 1997).

7.2.2 ATR FT-IR calibrations of monomers in liquid samples for analysis in Chapter 3 and 4

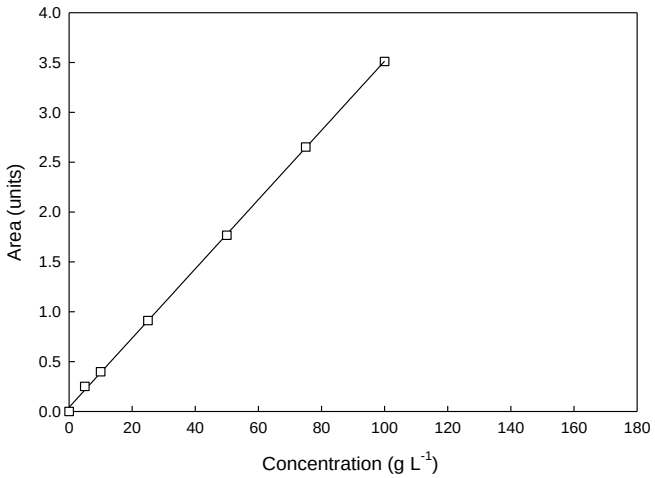

Figure 7.2 ATR FT-IR calibration curve of NIPAAm in the reaction mixture with main solvent the H_2O. The area under the peak of N-H bend (1550 cm^{-1}) of each standard's spectrum was calculated, keeping the same region and baseline at 1625-1500 cm^{-1} during all the readings. The slope of this curve was found 0.0353 peak area units per g L^{-1} with a correlation factor of 0.9992.

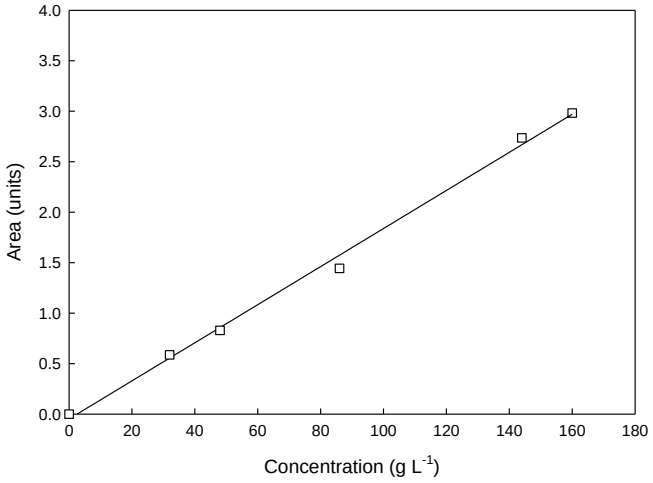

Figure 7.3 ATR FT-IR calibration curves of NIPAAm in the reaction mixture with main solvent the DMSO. The area under the peak of N-H bend (1550 cm^{-1}) of each standard's spectrum was calculated, keeping the same region and baseline at 1585-1504 cm^{-1} during all the readings. The slope of this calibration was found 0.0185 peak area units per g L^{-1} with a correlation factor of 0.9957.

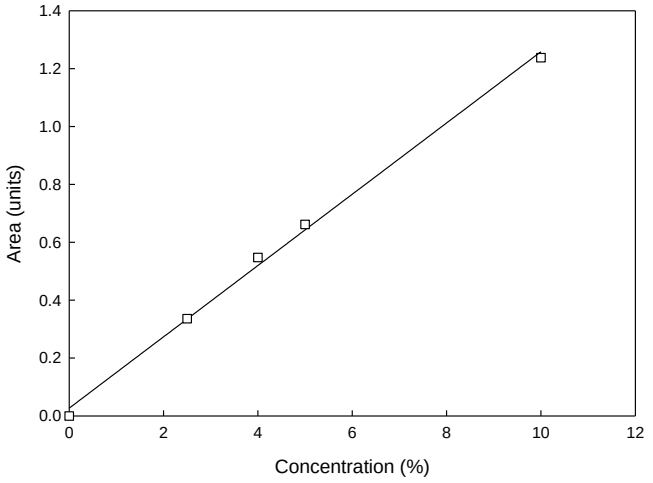

Figure 7.4 ATR FT-IR calibration curve of VI in the reaction mixture with main solvent the H_2O. The area under the peak of C-C stretch in ring (1500 cm^{-1}) of each standard's spectrum was calculated, keeping the same region and baseline at 1535-1450 cm^{-1} during all the readings. The slope of this calibration was found 0.1271 peak area units per (%) with a correlation factor of 0.9956.

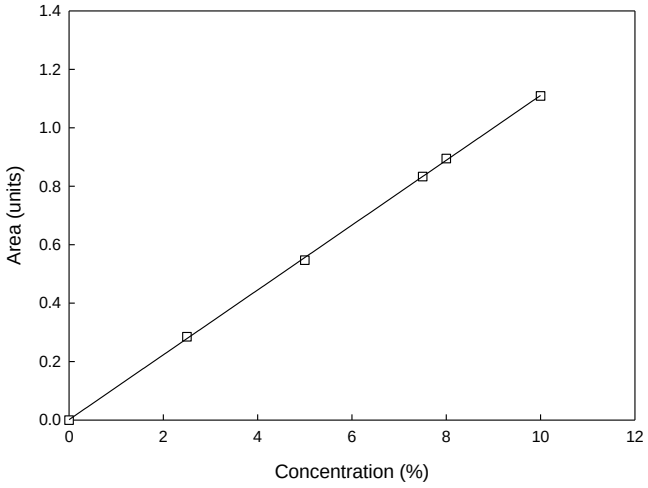

Figure 7.5 ATR FT-IR calibration curve of VI in the reaction mixture with main solvent the DMSO. The area under the peak of C-C stretch in ring (1500 cm^{-1}) of each standard's spectrum was calculated, keeping the same region and baseline at 1519-1450 cm^{-1} during all the readings. The slope of this calibration was found 0.1111 peak area units per (%) with a correlation factor of 0.9998.

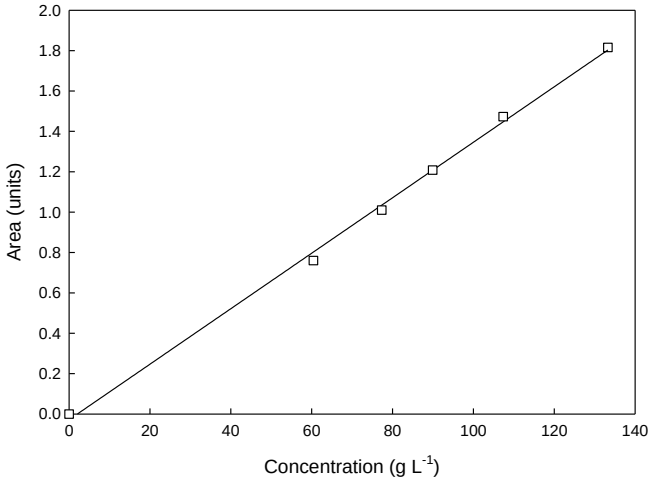

Figure 7.6 ATR FT-IR calibration curve of VBIDA in the reaction mixture with main solvent the H_2O. The area under the peak of C-C stretch in ring (1613 cm^{-1}) of each standard's spectrum was calculated, keeping the same region and baseline at 1540-1600 cm^{-1} during all the readings. The slope of this calibration was found 0.0135 peak area units per g L^{-1} with a correlation factor of 0.9975.

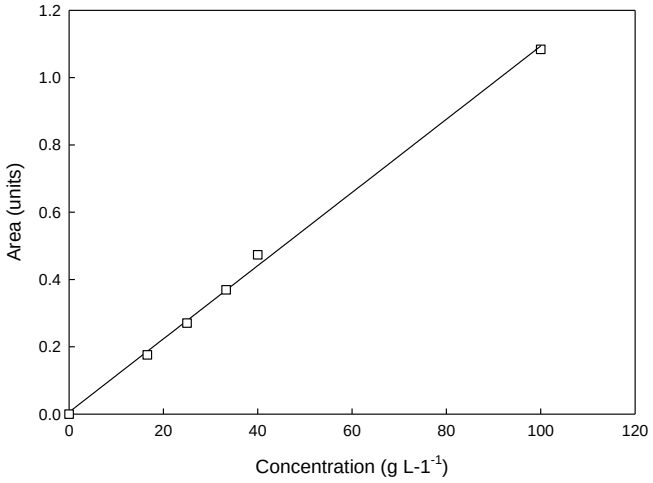

Figure 7.7 ATR FT-IR calibration curve of VBIDA in the reaction mixture with main solvent the DMSO. The area under the peak of 1720cm^{-1} of each standard's spectrum was calculated, keeping the same region and baseline at 1760-1695 cm^{-1} during all the readings. The slope of this calibration was found 0.011 peak area units per g L^{-1} with a correlation factor of 0.998.

7.3 Calibration curves for protein analysis in Chapter 3, 4 and 5

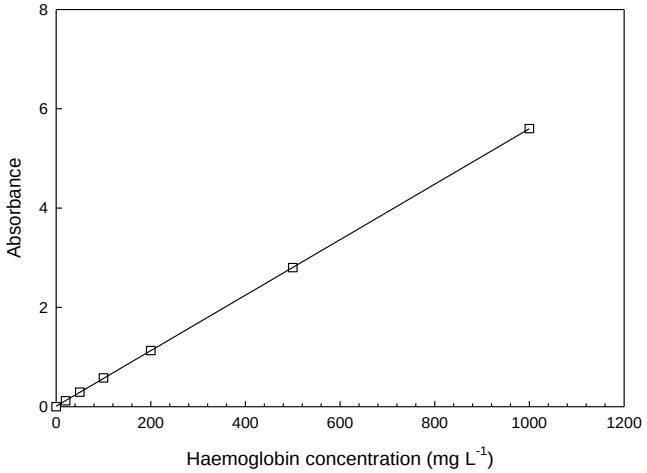

Figure 7.8 Calibration curve used for calculation of haemoglobin concentration in binding buffer after measurement of solution absorbance at 405 nm. The slope of this calibration was found 0.0056 absorbance units per mg L^{-1} with a correlation factor of 1.

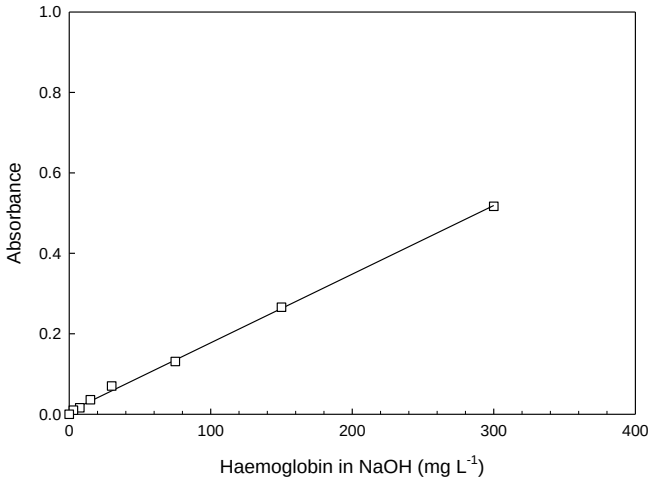

Figure 7.9 Calibration curve used for calculation of haemoglobin concentration in NaOH after measurement of solution absorbance at 210 nm. The slope of this calibration was found 0.0017 absorbance units per mg L^{-1} with a correlation factor of 0.9981.

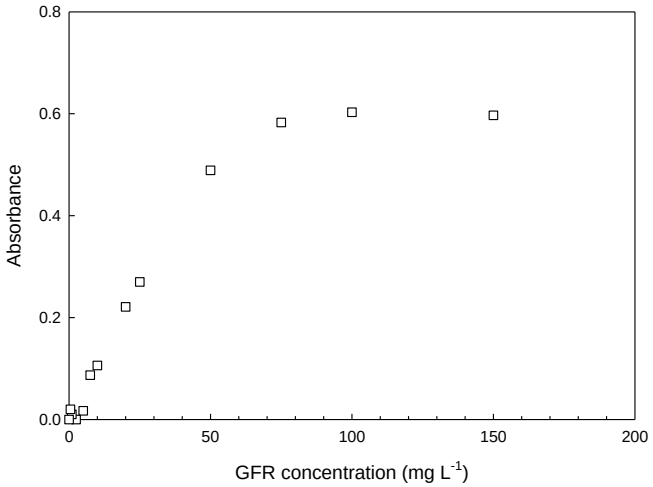

Figure 7.10 Calibration curve of green fluorescent protein (GFP) concentration in binding buffer using the Standard Better Bradford Assay (measurement of solution absorbance at 595 nm).

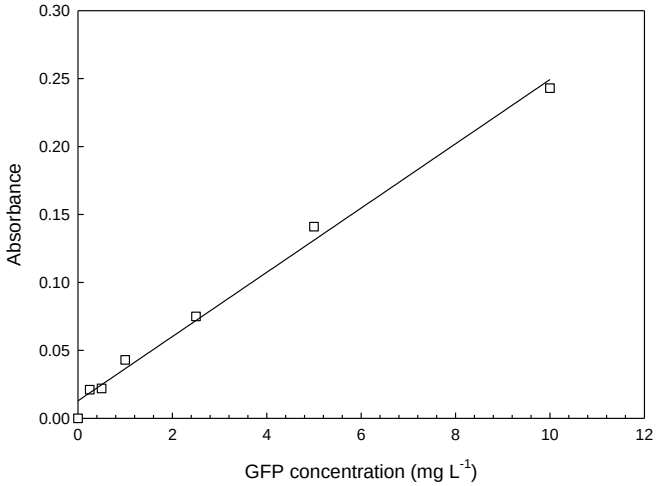

Figure 7.11 Calibration curve of green fluorescent protein (GFP) concentration in binding buffer using the Better Bradford Assay Microtest (measurement of solution absorbance at 595 nm). The slope of this calibration was found 0.0128 absorbance units per mg L^{-1} with a correlation factor of 0.9959.

7.4 Bromine assay used in Chapter 5

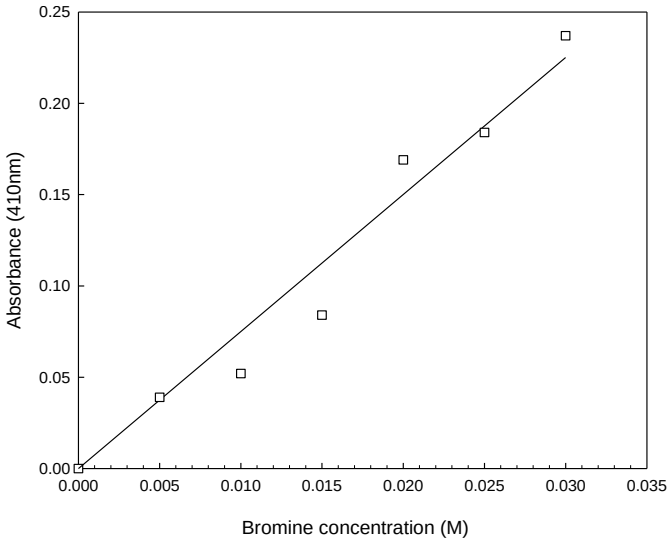

Figure 7.12 Bromine assay calibration curve by measuring the absorbance of bromine solutions at 410 nm. The slope of this calibration was found 7.501 absorbance units per mol L^{-1} with a correlation factor of 0.9598.

7.5 ATR FT-IR calibrations of monomers in liquid samples for analysis in Chapter 5

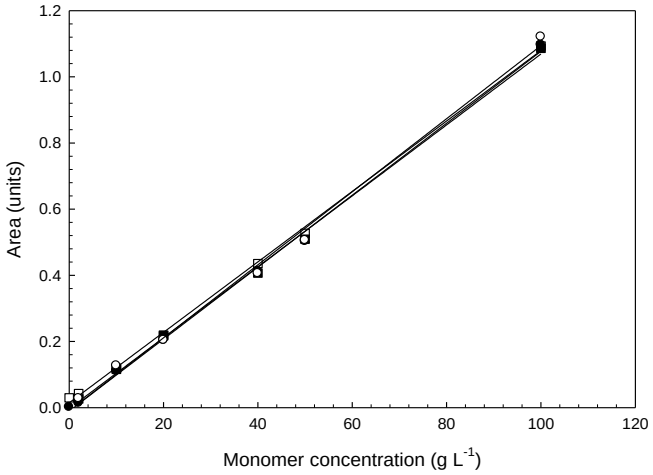

Figure 7.13 Calibration curves of NIPAAm in different amounts of Cu(I)Br and bpy. The monomer concentration has been plotted against the area obtained at 1500 cm^{-1} peak (both region and baseline kept between 1581-1508 cm^{-1}) from ATR-FT-IR analysis. The equations for lines of best fit and the corresponding R^2 for initiator:Cu(I)Br:bpy ratios have been estimated: for 1:1:2 of initiator:Cu(I)Br: bpy ratio, y=0.0106x+0.00147 and R^2=0.998 (white square); for 1:2:4 of initiator:Cu(I)Br: bpy ratio, y=0.0107x-0.0032, R^2=0.998 (black square); for 1:5:10 of initiator:Cu(I)Br: bpy ratio, y=0.0108x-0.0103, R^2=0.998 (white circle); for 1:10:20 of initiator:Cu(I)Br: bpy ratio , y=0.011x-0.0099, R^2=0.995 (black circle).

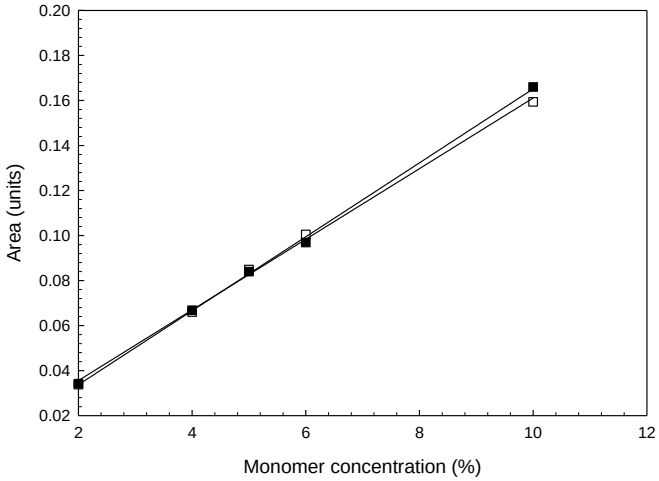

Figure 7.14 Calibration curves used for VI concentration calculations after 20 % and 50 % activation for 1:10:20 ratio of initiator:Cu(I)Br:bpy. The monomer concentration has been plotted against the area obtained at region and baseline between 1095-1078 cm^{-1} from ATR-FT-IR analysis. The equations for lines of best fit and the corresponding R^2 for initiator:Cu(I)Br:bpy ratios have been estimated: for 50 % activation, y=0.0157x+0.0042 and R^2=0.998 (white square); for 50 % activation, y=0.0164x+0.0009 and R^2=0.998 (black square).

7.6 EDX analysis of M-PVA supports under different conditions and modifications

7.6.1 Elemental analysis of sample stub and different batches of M-PVA supports (washed and unwashed)

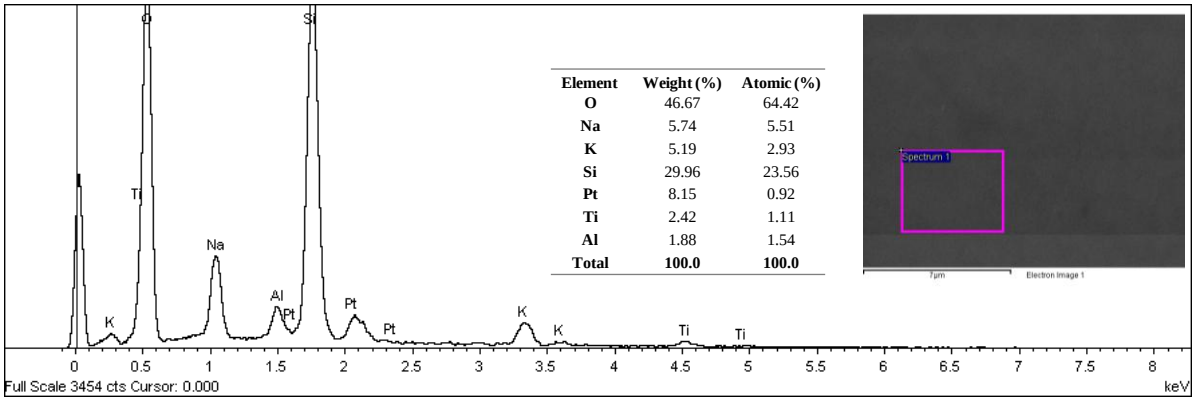

Element	Weight (%)	Atomic (%)
O	46.67	64.42
Na	5.74	5.51
K	5.19	2.93
Si	29.96	23.56
Pt	8.15	0.92
Ti	2.42	1.11
Al	1.88	1.54
Total	**100.0**	**100.0**

Figure 7.15 EDX spectrum, SEM image and elemental analysis of slide (sample stub) used as base surface where all the samples were introduced.

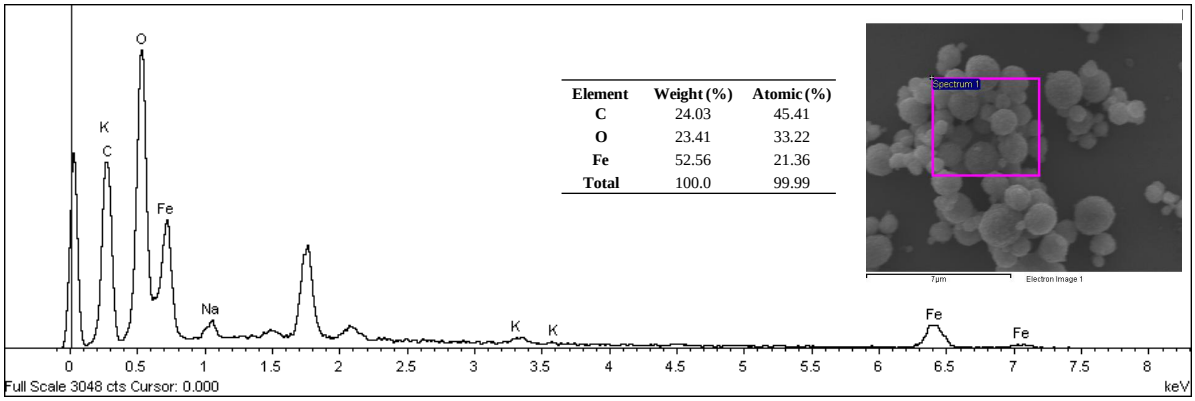

Element	Weight (%)	Atomic (%)
C	24.03	45.41
O	23.41	33.22
Fe	52.56	21.36
Total	100.0	99.99

Figure 7.16 EDX spectrum, SEM image and elemental analysis of M-PVA (batch 4) after washing using the standard protocol.

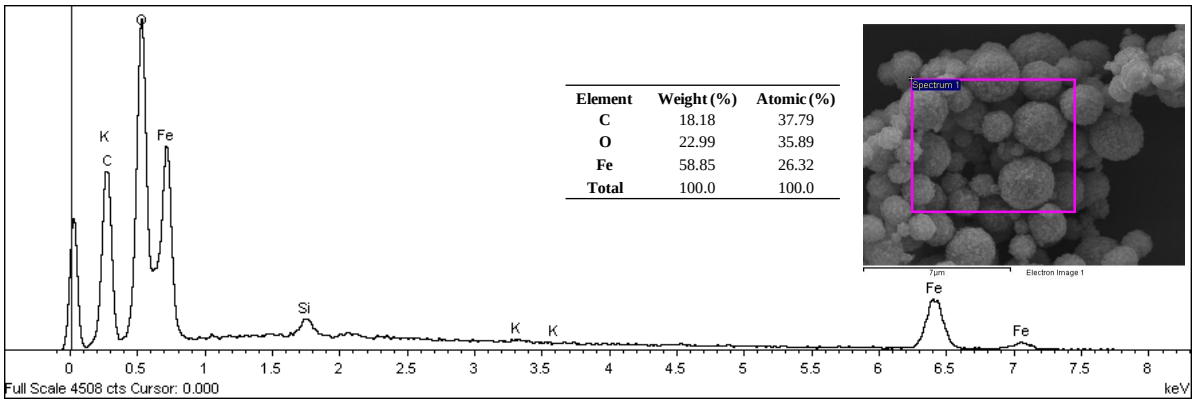

Element	Weight (%)	Atomic (%)
C	18.18	37.79
O	22.99	35.89
Fe	58.85	26.32
Total	100.0	100.0

Figure 7.17 EDX spectrum, SEM image and elemental analysis of M-PVA (batch 5) as supplied (unwashed).

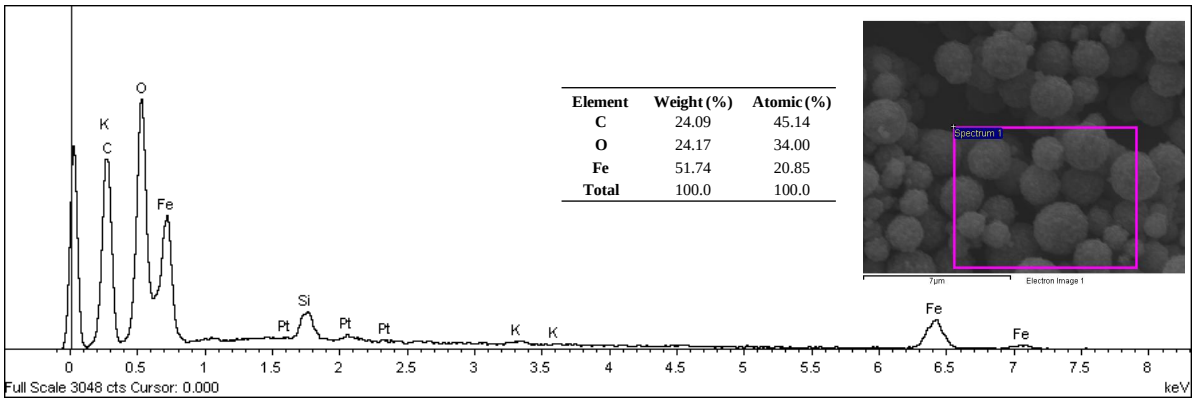

Element	Weight (%)	Atomic (%)
C	24.09	45.14
O	24.17	34.00
Fe	51.74	20.85
Total	100.0	100.0

Figure 7.18 EDX spectrum, SEM image and elemental analysis of M-PVA (batch 5) after washing using the standard protocol.

7.6.2 Elemental analysis of unmodified M-PVA supports at buffers of different ionic strength, while being uncharged or charged with Cu^{2+} ions

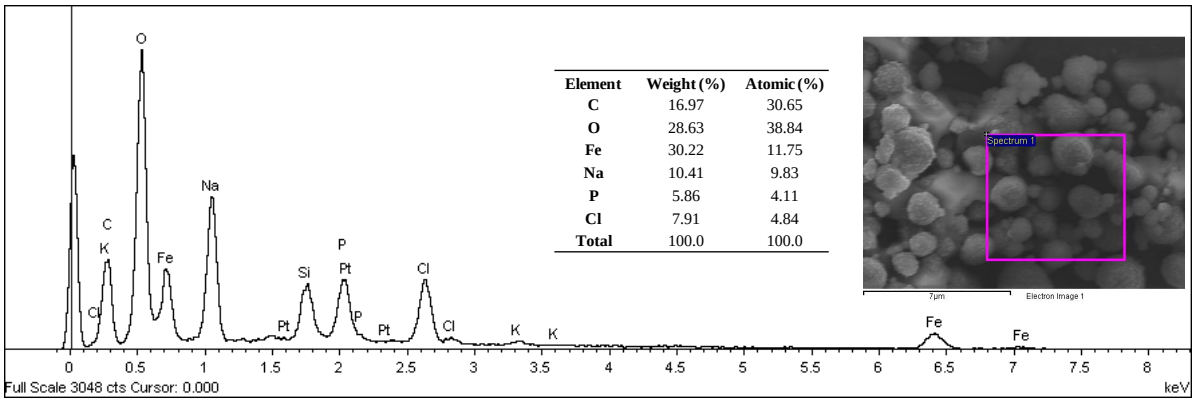

Element	Weight (%)	Atomic (%)
C	16.97	30.65
O	28.63	38.84
Fe	30.22	11.75
Na	10.41	9.83
P	5.86	4.11
Cl	7.91	4.84
Total	100.0	100.0

Figure 7.19 EDX spectrum, SEM image and elemental analysis of M-PVA (batch 4), washed and introduced into 100 mM Sodium Phosphate and 1 M NaCl buffer.

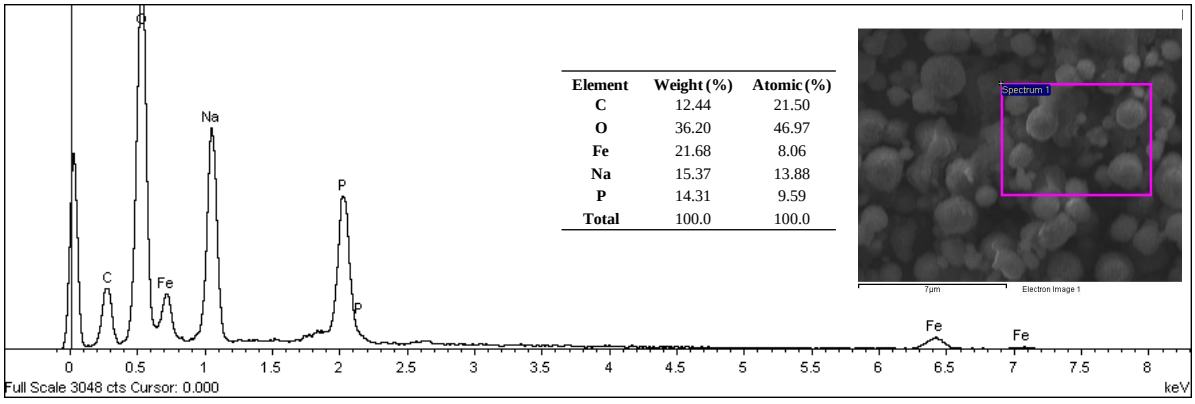

Element	Weight (%)	Atomic (%)
C	12.44	21.50
O	36.20	46.97
Fe	21.68	8.06
Na	15.37	13.88
P	14.31	9.59
Total	100.0	100.0

Figure 7.20 EDX spectrum, SEM image and elemental analysis of M-PVA (batch 4), washed and introduced into 100 mM Sodium Phosphate buffer.

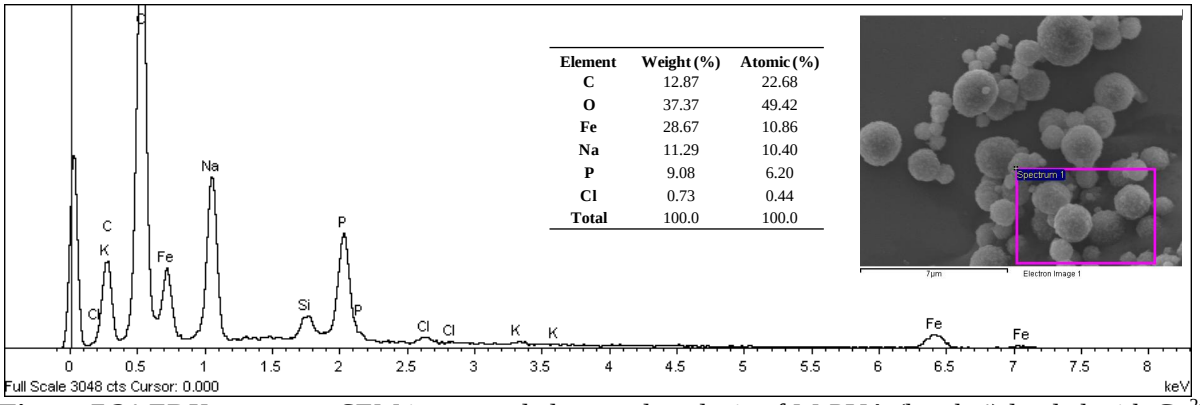

Element	Weight (%)	Atomic (%)
C	12.87	22.68
O	37.37	49.42
Fe	28.67	10.86
Na	11.29	10.40
P	9.08	6.20
Cl	0.73	0.44
Total	100.0	100.0

Figure 7.21 EDX spectrum, SEM image and elemental analysis of M-PVA (batch 4) loaded with Cu^{2+} ions, washed and introduced into 100mM Sodium Phosphate buffer.

7.6.3 Elemental analysis of modified M-PVA supports installed with affinity ligands while being uncharged or charged with Cu^{2+} ions at buffers of different ionic strength

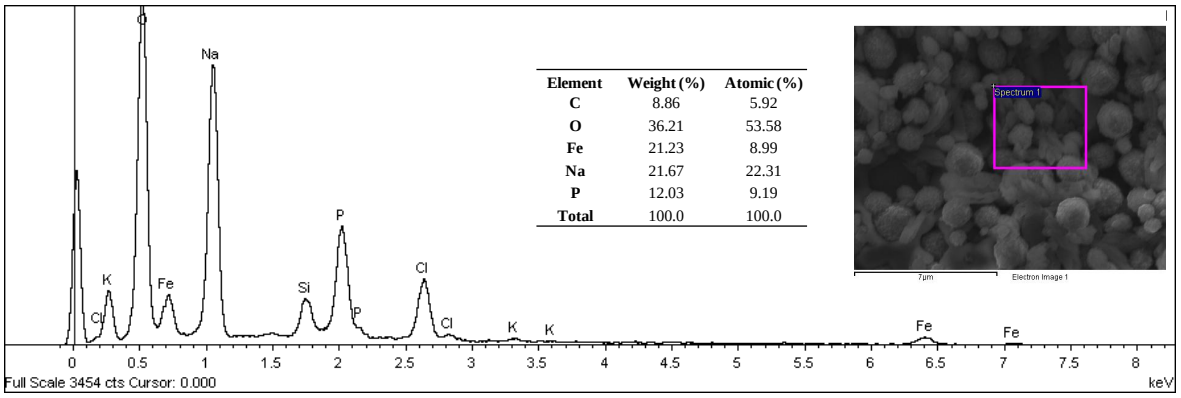

Element	Weight (%)	Atomic (%)
C	8.86	5.92
O	36.21	53.58
Fe	21.23	8.99
Na	21.67	22.31
P	12.03	9.19
Total	100.0	100.0

Figure 7.22 EDX spectrum, SEM image and elemental analysis of M-PVA (batch 4) installed with pVBIDA (uncharged - $pVBIDA_{16}$ - 4.6 Å), washed and introduced into 100 mM Sodium Phosphate and 1 M NaCl buffer.

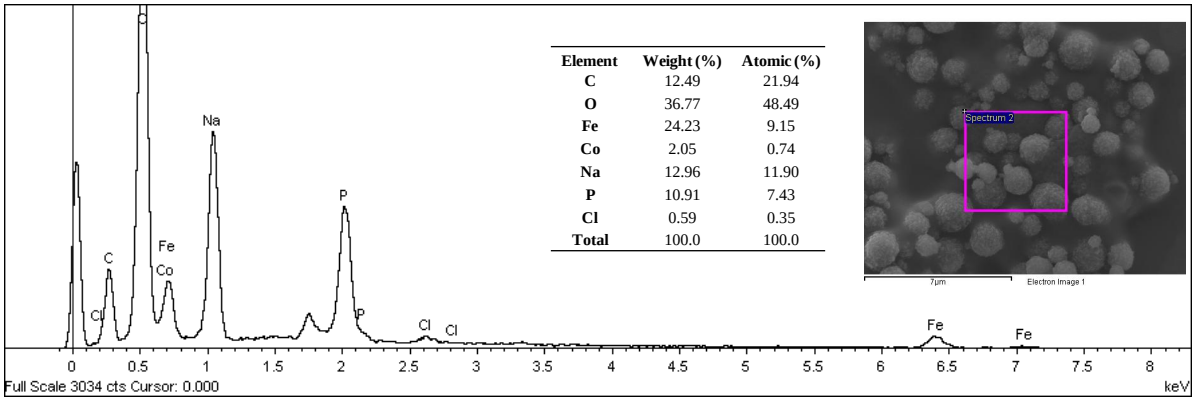

Element	Weight (%)	Atomic (%)
C	12.49	21.94
O	36.77	48.49
Fe	24.23	9.15
Co	2.05	0.74
Na	12.96	11.90
P	10.91	7.43
Cl	0.59	0.35
Total	100.0	100.0

Figure 7.23 EDX spectrum, SEM image and elemental analysis of M-PVA (batch 4) installed with pVBIDA (uncharged - $pVBIDA_{16}$ - 4.6 Å), washed and introduced into 100 mM Sodium Phosphate buffer.

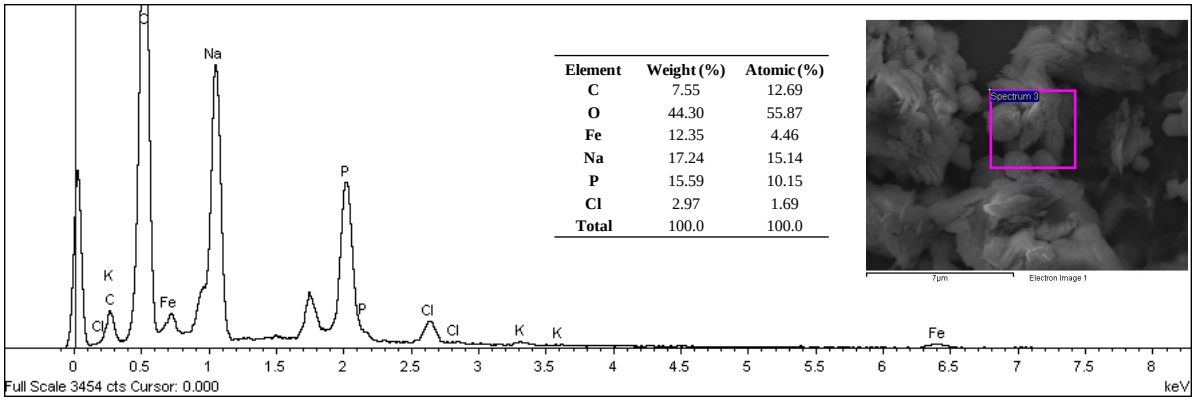

Element	Weight (%)	Atomic (%)
C	7.55	12.69
O	44.30	55.87
Fe	12.35	4.46
Na	17.24	15.14
P	15.59	10.15
Cl	2.97	1.69
Total	100.0	100.0

Figure 7.24 EDX spectrum, SEM image and elemental analysis of M-PVA (batch 4) installed with pVBIDA and loaded with Cu^{2+} ions (Cu^{2+} - $p(VBIDA)_{16}$ - 4.6 Å), washed and introduced into 100mM Sodium Phosphate.

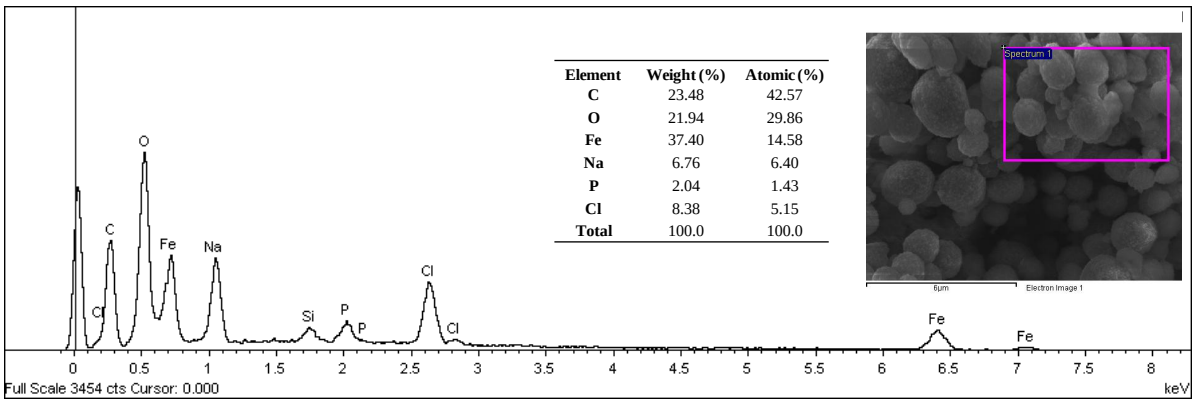

Element	Weight (%)	Atomic (%)
C	23.48	42.57
O	21.94	29.86
Fe	37.40	14.58
Na	6.76	6.40
P	2.04	1.43
Cl	8.38	5.15
Total	100.0	100.0

Figure 7.25 EDX spectrum, SEM image and elemental analysis of M-PVA (batch 4) installed with pVI (uncharged - $pVI_{36.7}$ - 4.6 Å), washed and introduced into 100 mM Sodium Phosphate buffer 1 M NaCl.

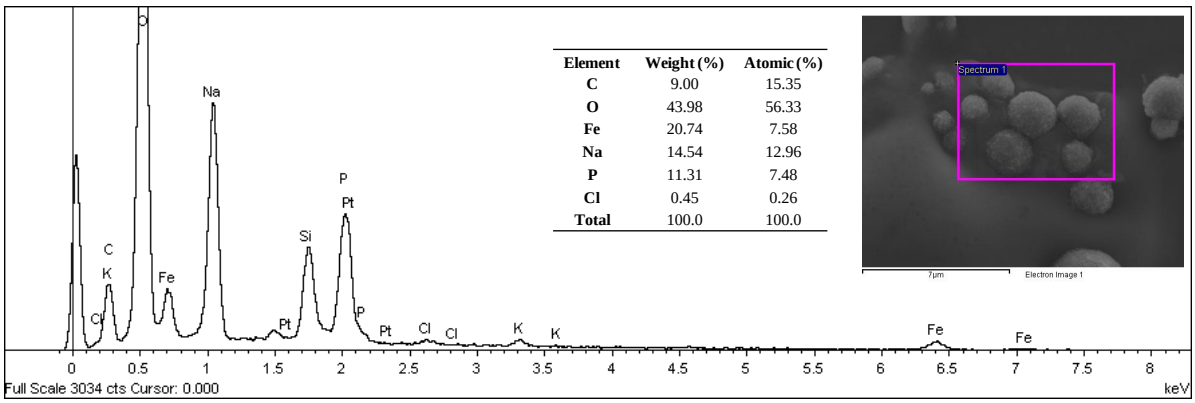

Element	Weight (%)	Atomic (%)
C	9.00	15.35
O	43.98	56.33
Fe	20.74	7.58
Na	14.54	12.96
P	11.31	7.48
Cl	0.45	0.26
Total	100.0	100.0

Figure 7.26 EDX spectrum, SEM image and elemental analysis of M-PVA (batch 4) installed with pVI (uncharged - $pVI_{36.7}$ - 4.6 Å), washed and introduced into 100 mM Sodium Phosphate buffer.

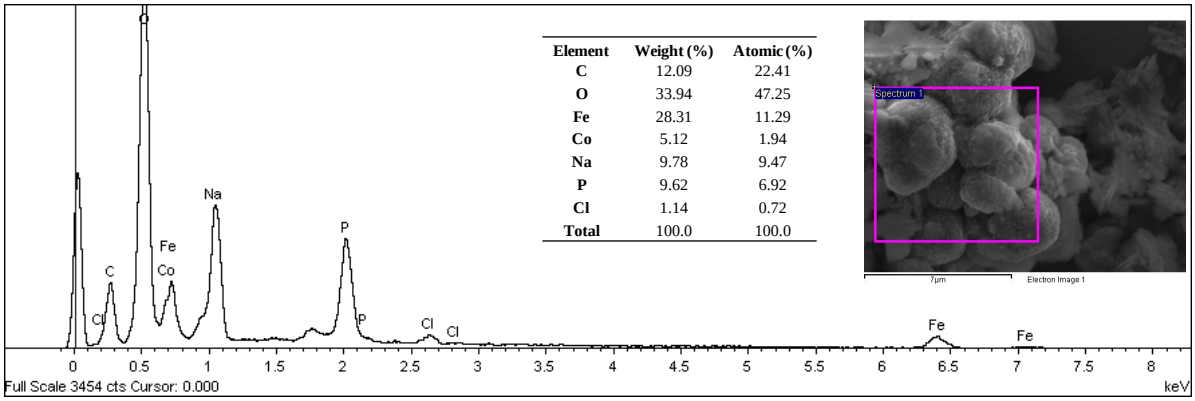

Figure 7.27 EDX spectrum, SEM image and elemental analysis of M-PVA (batch 4) installed with pVI and loaded with Cu^{2+} ions (Cu^{2+} - $pVI_{36.7}$ - 4.6 Å), washed and introduced into 100 mM Sodium Phosphate buffer. Note: Co element appears only due to its similar X-Ray properties with Fe and not because it is present in the sample.

7.6.4 Elemental analysis of M-PVA supports activated with Cerium (IV)

Two samples of M-PVA support (batch 4) were activated by introducing ACN (0.44 mmol g^{-1}) under nitrogen for 3 h. The first sample was analysed without any prior washing (Fig. 7.28) while the other sample was washed extensively with milliQ water and then analysed (Fig. 7.29).

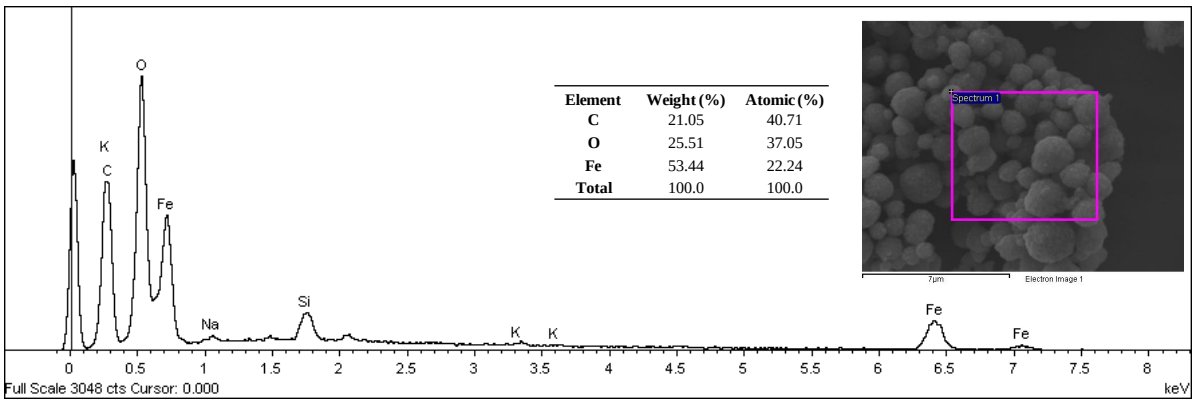

Figure 7.28 EDX spectrum, SEM image and elemental analysis of M-PVA (batch 4) after activation with 0.44 mmol g^{-1} Cerium (IV) and no washing afterwards.

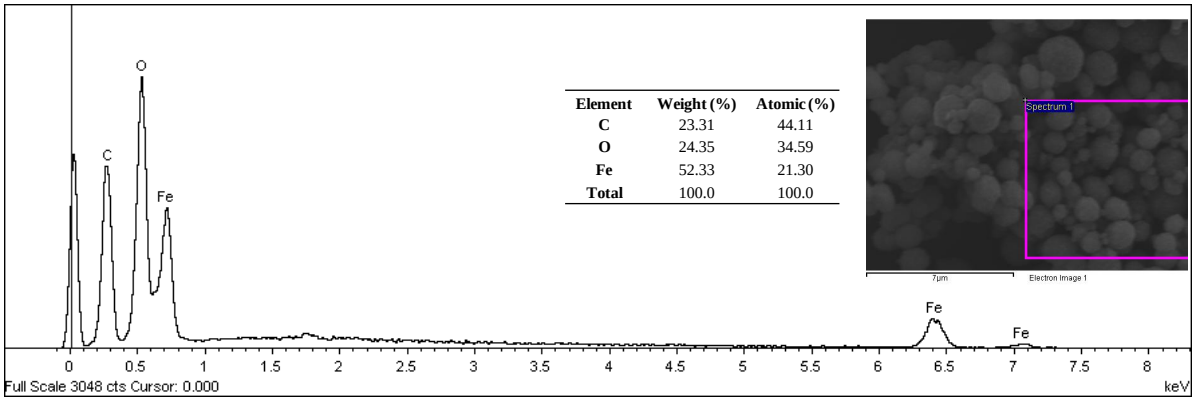

Element	Weight (%)	Atomic (%)
C	23.31	44.11
O	24.35	34.59
Fe	52.33	21.30
Total	100.0	100.0

Figure 7.29 EDX spectrum, SEM image and elemental analysis of M-PVA (batch 4) after activation with 0.44 mmol g^{-1} Cerium (IV) and washing with milliQ water afterwards.

The relative X-Ray intensities for Kα and Lα lines of Cerium (Ce) are at 4.8403 and 0.8831 keV respectively for the different oxidation states (i.e. 3 and 4). The peak at Lα line is very near with that of Fe, so it would not be possible to distinct from each other. There is no a distinctive peak at Kα line, however the amount of cerium added to the support (0.44 mmol g^{-1}) is very low and so it is the contribution to the overall sample.

7.6.5 Elemental analysis and SEM imaging of modified M-PVA supports with pNIPAAm

A pNIPAAm modified support ($pNIPAAm_{13.2}$ – 4.6 Å) was also examined with EDX analysis as shown in Fig. 7.30. No difference was observed between the elemental analysis of this support and that of M-PVA batch 4 supports (Fig. 7.16).

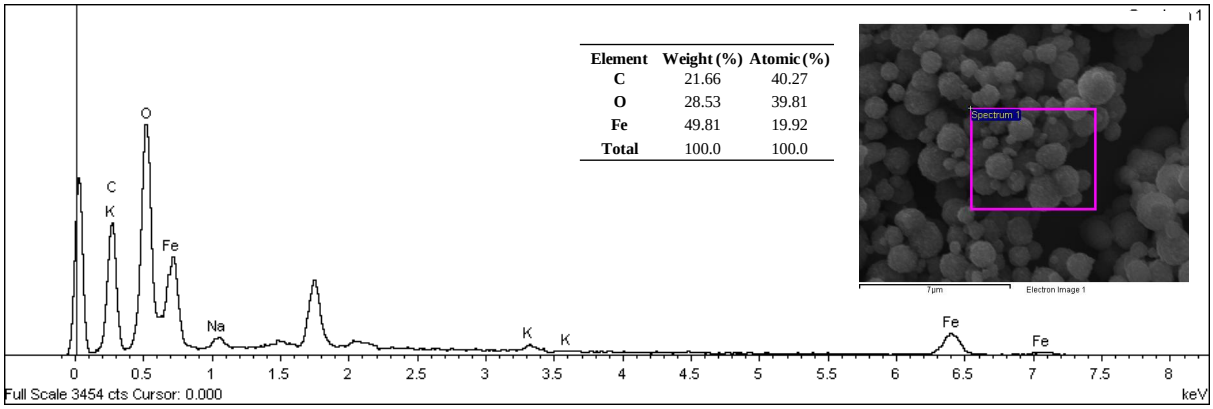

Element	Weight (%)	Atomic (%)
C	21.66	40.27
O	28.53	39.81
Fe	49.81	19.92
Total	100.0	100.0

Figure 7.30 EDX spectrum, SEM image and elemental analysis of M-PVA (batch 4) modified with pNIPAAm ($pNIPAAm_{13.2}$ – 4.6 Å) in water.

8. References

Afroze F., Nies E., Berghmans H. (2000), Phase transitions in the system poly(*N*-isopropylacrylamide) / water and swelling behaviour of the corresponding networks, *J. Mol. Struct.*, 554: 55–68.

Albertsson P. Å. (1972), Partition of Cell Particles and Macromolecules, 2nd edition, Almquist and Wiksell, Stockholm: p. 323.

Albertsson P. Å. (1986), Partition of Cell Particles and Macromolecules (3rd ed.), J. Wiley, N.Y.

Albertsson P. Å., Johansson G., Tjerneld F. (1996), Ucon-benzoyl dextran aqueous two-phase systems: protein purification with phase component recycling, *J. Chromatogr. B.*, 680: 65-70.

Aldridge, S. (2006), Downstream processing needs a boost *Gen. Eng. Biotech. News*, 26(1).

Amersham Biosciences (2007), Affinity chromatography handbook: Principles and methods, 18-1022-29, Edition AD., available online at the following link: (http://www1.gelifesciences.com/aptrix/upp00919.nsf/Content/91D3DF5DE303E8B6C1256EB400417F34/$file/18102229AE.pdf).

Annenkov V. V., Danilovtseva E. N., Tenhu H., Aseyev V., Hirvonen S. -P., Mikhaleva A. I. (2004), Copolymers of 1-vinylimidazole and (meth)acrylic acid: Synthesis and polyelectrolyte properties, *Eur. Polym. J.*, 40: 1027–1032.

Ansbach F. B., Curbelo D., Harttman R., Garke G., Deckwer W. D. (1999), Expanded bed chromatography in primary protein purification, *J. Chromatogr. A*, 865(1-2): 129-144.

Arnold F. H. (1991), Metal affinity separations: a new dimension in protein processing, *Bio/Technology*, 9: 151-156.

Arnold F. H., Blanch H. W., Wilke C. R. (1985), Analysis of affinity separations. I. Predicting the performance of affinity adsorbers, *Chem. Eng. J.*, 30**:** B9–B23.

Arvidsson P., Ivanov A. E., Galaev I. Y., Mattiasson B. (2001), Polymer versus monomer as displacer in immobilized metal affinity chromatography, *J. Chromatogr. B*, 753: 279–285.

Ayano E., Nambu K., Sakamoto C., Kanazawa H., Kikuchi A., Okano T. (2006), Aqueous chromatography system using pH- and temperature-responsive stationary phase with ion-exchange groups, *J. Chromatogr. A*, 1119: 58–65.

Balamurugan S., Mendez S., Balamurugan S. S., O'Brien II M. J., Lopez G. P. (2003), Thermal response of poly(*N*-isopropylacrylamide) brushes probed by surface plasmon resonance, *Langmuir*, 19: 2545-2549.

Bashir W., Paull B., (2002), Ionic strength, pH and temperature effects upon selectivity for transition and heavy metal ions when using chelation ion chromatography with an iminodiacetic acid bonded silica gel column and simple inorganic eluents, *J. Chromatogr. A*, 942: 73–82.

Bashir W., Tyrrll E., Feeney O., Paull B. (2002),Retention of alkali, alkaline earth and transition metals on an itaconic acid cation-exchange column. Eluent pH, ionic strength and temperature effects upon selectivity, *J. Chromatogr. A*, 964: 113–122.

Baulin V. A., Halperin A. (2003), Signatures of a concentration-dependent Flory χ parameter: Swelling and collapse of coils and brushes, *Macromol. Theory Simul*, 12: 549-559.

Baulin V. A., Zhulina E. B., Halperin A. (2003), Self-consistent field theory of brushes of neutral water-soluble polymers. *J. Chem. Phys.* 119:10977–88.

Becer C. R., Haensch C., Hoeppener S., Schubert U. S. (2007), Patterned polymer brushes grafted from bromine-functionalized, chemically active surface templates, *Small*, 3(2):220-225.

Behari, K., Agarwal, U., Das R. (1993), Cerium (IV) - sorbose - initiated polymerization of acrylamide and methacrylamide, *Polymer*, 34(21): 4557-4561.

Birkenmeier G., Vijayalakshmi M. A., Stigbrand T., Kopperschläger G., (1991), Immobilized metal ion affinity partitioning IMAP: a method combining metal protein interaction and partition of proteins in aqueous two phase systems, *J. Chromatog.*, 539: 267-277.

Boutris C., Chatzi E., and Kiparissides C. (1997), Characterization of the LCST behaviour of aqueous poly(N-isopropylacrylamide) solutions by thermal and cloud point techniques**,** *Polymer*, 38: 2567-2570.

Boyes S. G., Granville A. M., Baum M., Akgun B., Mirous B. K., Brittain W. J. (2004), Polymer brushes-surface immobilized polymers, *Surface Science*, 570: 1–12.

Brandrup, J., Immergut E. H. (1989), Polymer Handbook, 3rd ed., Wiley-lnterscience, New York.

Braunecker W. A., Matyjaszewski K. (2007), Controlled/living radical polymerization: Features, developments, and perspectives, *Prog. Polym. Sci*., 32: 93–146.

Brittain W. J., Minko S. (2007), A Structural definition of polymer brushes, *J. Polym. Sci. Part A: Polym. Chem.*, 45: 3505-3512.

Brown N. G. (2008), Advances in magnetic particle based bioprocessing, Ph.D. thesis, University of Birmingham, School of Chemical Engineering, UK

Burton S. C, Harding D. R. K. (1997), High-density ligand attachment to brominated allyl matrices and application to mixed mode chromatography of chymosin, *J. Chromatogr. A.*, 775: 39-50.

Caner H., Yilmaz E., Yilmaz O. (2007), Synthesis, characterization and antibacterial activity of poly(*N*-vinylimidazole) grafted chitosan, *Carbohydr. Polym.*, 69: 318–325.

Carey, F. A. (1992), *Organic Chemistry*, 2nd ed.; McGraw-Hill: New York.

Carlsson J., Jansson J.-C., Sparrman M. (1998), Chapter 10: Affinity chromatography, In: Protein purification (2nd edition), Janson J.-C. & Rydén L. (eds), Wiley & Sons, Inc., New York, USA; Shukla and Yigzaw, 2007.

Coessens V., Pintaeur T., Matyjaszewski K. (2001), Functional polymers by atom transfer radical polymerisation, *Prog. Polym., Sci.*, 26: 337-377.

Curling J., Gottschalk U. (2007), Process Chromatography: Five decades of innovation, *BioPharm International*, 20: 10–19.

Dagani R. (1995), Polymeric 'smart' materials respond to changes in their environment, *Chem. Eng. News (Sept*), 73: 30–33.

Dhara, D., Chatterji P. R. (2000), Phase transition in linear and cross-linked poly(*N*-isopropylacrylamide) in water: effect of various types of additives., *J. Macromol. Sci., Rev. Macromol. Chem. Phys*., *C40*, 51-68.

Digel I., Maggakis-Kelemen C., Zerlin K. F., Linder P., Kasischke N., Kayser P., Porst D., Temiz Artmann A., Artmann G. M. (2006), Body temperature-related structural transitions of monotremal and human haemoglobin, *Biophys. J.*, 91: 3014–3021.

Dimitrov I., Trzebicka B., Axel H.E., Muller A. H. E., Dworak A., Tsvetanov C. B. (2007), Thermosensitive water-soluble copolymers with doubly responsive reversibly interacting entities, *Prog. Polym. Sci*., 32: 1275–1343.

Ding X. B., Sun Z. H., Wan G. X., Jiang Y. Y. (1998), Preparation of thermosensitive magnetic particles by dispersion Polymerization, *React. Funct. Polym.*, 38: 11–15.

Ding X. B., Sun Z. H., Zhang W. C..Peng Y. X., Wan G. X., Jiang Y. Y (1999), Adsorption/desorption of protein on magnetic particles covered by thermosensitive polymers, *J. Appl. Polym. Sci*., 77: 2915–2920.

Ding X. B., Sun Z., Zhang W., Peng Y., Chan A. S. C., Li P. (2000), Characterization of Fe3O4/poly(styrene-co-*N*-isopropylacrylamide) magnetic particles with temperature sensitivity, *Colloid Polym. Sc*i., 278: 459-463.

Draper J., Luzinov I., Tokarev I., Minko S. and Stamm M. (2002), Morphology and wettability of hybrid polymer brushes, *Polym. Mater. Sci. Eng*., 87: 187- 188.

Dunlop, E. H., Feiler, W. A., and Mattione, M. J., 1984, Magnetic separation in biotechnology, *Biotech. Advs.*, 2: 63-74.

Dunnill P., Lilly M. D. (1974), Purification of enzymes using magnetic bio-affinity materials, *Biotechnol Bioeng*, 16(7): 987-990.

Ehrehneim P. (2006), GE Healthcare presentation at biologic Asia, Mumbai, India, Nov 28-29.

Ejaz M., Tsuji Y., Fukuda T. (2001), Controlled grafting of a well-defined polymer on a porous glass filter by surface-initiated atom transfer radical polymerization, *Polymer*, 42:6811–6815.

Elaissari M., Bourrel V. (2001), Thermosensitive magnetic latex particles for controlling protein adsorption and desorption, *J. Magn. Magn. Mater.*, 225: 151-155.

Elaïssari A., Rodrigue M., Meunier F., Herve C. (2001), Hydrophilic magnetic latex for nucleic acid extraction, purification and concentration, *J. Magn. Magn. Mater.*, 225(1-2): 127-133.

Elefterov A. I., Kolpachnikov M. G., Nesterenko P. N., Shpgun O. A.(1997), Ion-exchange properties of glutamic acid-bonded silica, *J. Chromatogr. A*, 769, 179-188.

Eriksson K.-O. (1998), Chapter 7: Hydrophobic Interaction chromatography, In: Protein purification (2nd edition), Janson J.-C. & Rydén L. (eds), Wiley & Sons, Inc., New York, USA.

Farkas T., Strålbrand H., Tjerneld F. (1996), Partitioning of a β-mannanase and α-galactosidase from *Aspergillus niger* in Ucon/Reppal aqueous two-phase systems and using temperature induced phase separation, *Bioseparation*, 6: 147–157.

Figueroa, A., Corradini C., Feibush B., Karger B. L. (1986), High-performance immobilized-metal affinity chromatography of proteins on iminodiacetic acid silica-based bonded phases, *J. Chromatogr.*, 371: 335−352.

Fischer H. (2001), The persistent radical effect: A principle for selective radical reactions and living radical polymerizations, *Chem. Rev.*, 101: 3581-3610.

Franco T. T., Galaev I. Y., Hatti-Kaul R., Holmberg N., Bülow L., Mattiasson B (1997), Aqueous two-phase system formed by thermoreactive vinyl imidazole/vinyl caprolactam copolymer and dextran for partitioning of a protein with a polyhistidine tail, *Biotechnol. Techn.* 11**:** 231–235.

Franzreb M., Siemann-Herzberg M., Hobley T., Thomas O.R.T. (2006), Protein purification using magnetic adsorbent particles, *Appl. Microbiol. Biotechnol.*, 70(5): 505-516.

Freitag R., Garret-Flaudy F. (2002), Salt effects on the thermoprecipitation of Poly-(*N*-isopropylacrylamide) oligomers from aqueous solution, *Langmuir*, 18*:* 3434-3440.

Galaev I. Y., Gupta M. N., Mattiasson B. (1996), Use Smart polymers for bioseparations, *ChemTech*, 26: 19-25.

Galaev I. Y., Kumar A., Agarwal R., Gupta M. N., Mattiasson, B. (1997), Imidazole - a new ligand for metal affinity precipitation. Precipitation of kunitz soybean trypsin inhibitor using Cu(II)-loaded copolymers of *1*-Vinylimidazole with *N*-Vinylcaprolactam or *N*-Isopropylacrylamide, *Appl. Biochem. Biotechnol*, 68: 121-133.

Galaev I. Y., Mattiasson B. (1999), 'Smart' polymers and what they can do in biotechnology and medicine, *Trends Biotechnol*, 17(8): 335-340.

Galaev, I. Y., Kumar, A., Agarwal, R., Gupta, M. N. and Mattiasson, B. (1997), Imidazole - a new ligand for metal affinity precipitation. Precipitation of kunitz soybean trypsin inhibitor using Cu(II)-loaded copolymers of *1*-vinylimidazole with *N*-vinylcaprolactam or *N*-isopropylacrylamide, *Appl. Biochem. Biotechnol*, 68: 121-133.

Garipcan B., Andac M., Uzun L., Denizli A. (2004), Methacryloylamidocysteine functionalized poly(2-hydroxyethyl methacrylate) beads and its design as a metal-chelate affinity support for human serum albumin adsorption, *React. Funct. Polym.,* 59: 119-128.

Gerber R., Birss R. R. (1983), High gradient magnetic separation, Wiley and Sons Ltd, Chichester, UK.

Gonen S. and Kohn D. H. (1981), Graft copolymerisation I. Grafting of hydroxyalkyl methacrylates on poly(vinyl alcohol), *J. Polym. Sci., Part A: Polym. Chem,* 19: 2215-2228.

Gupta K. C., and Khandekar K. (2003), Temperature-responsive cellulose by Ceric(IV) ion-initiated graft copolymerisation of *N*-isopropylacrylamide, *Biomacromolecules*, 4: 758-765.

Gupta K. C., Sahoo S. (2001), Grafting of acrylonitrile and methyl methacrylate from their binary mixtures on cellulose using ceric ions, *J. Appl. Polym. Sci.* , 79: 767–778.

Gupta M. N., Kaul R., Guoqiang D., Dissing U., Mattiasson B. (1996), Affinity precipitation of proteins, *J. Mol. Recognit.,* 9: 356-359.

Gupta, M. N., Mattiasson, B. (1994), Affinity precipitation in Highly selective separations in biotechnology, G. Street (ed.), Blackie Academic & Professional, London., pp. 7-33.

Gurau M., C., Lim S. M., Castellana E. T., Albertorio F., Kataoka, S., Cremer P. S. (2004), On the Mechanism of the Hofmeister Effect , *J. Am. Chem. Soc.*, *126*: 10522-10523.

Hage D. S. (1999), Affinity chromatography: A review of clinical applications, *Clin. Chem.,* 45(5), 593-615.

Hagel L. (1998), Chapter 3: Gel Filtration, In: Protein purification (2^{nd} edition), Janson J.-C. & Rydén L. (eds), Wiley & Sons, Inc., New York, USA.

Halling P. J., Dunnill P. (1980), Magnetic supports for immobilised enzymes and bioaffinity adsorbents, *Enzyme Microb. Technol.,* 2: 2–10.

Halperin A. (1998), Compression induced phase transitions in PEO brushes: the n-cluster model, *Eur. Phys. J. B.*, 3: 359-364.

Halperin A. (1999), Polymer brushes that resist adsorption of model proteins: Design parameters, *Langmuir*, 15: 2525-2533.

Halperin A., Leckband D. E. (2000), From ship hulls to contact lenses: repression of protein adsorption and the puzzle of PEO, *C R Acad Sci [IV] Physc*, 1: 1171-1178.

Halperin A., Tirrell M., Lodge T. P. (1992), Tethered chains in polymer microstructures, *Adv Polym Sci*, 100, 31-71.

Heebøll-Nielsen A. (2002), High gradient magnetic fishing, support functionalisation and application for protein recovery from unclarified bioprocess liquors, Ph.D. thesis, Technical University of Denmark, Published by BioCentrum-DTU, Lungby, Denmark.

Heebøll-Nielsen A., Dalkiaer M., Hubbuch J. J., Thomas O. R. T. (2004), Superparamagnetic adsorbents for high-gradient magnetic fishing of lectins out of legume extracts, *Biotechnol Bioeng*, 87: 311–323.

Hellferich F. (1961), 'Ligand exchange': a novel separation technique, *Nature*, 189: 1001-1002.

Hemdan E.S., Zhao Y. –J., Sulkowski E., Porath, J. (1989), Surface topography of histidine residues: a facile probe by immobilised metal ion affinity chromatography, *Proc. Natl. Acad. Sci. USA*, 86: 1811-1815.

Hermanson G. T., Mallia A. K., Smith P.K. (1992), Immobilized affinity ligand techniques, London: Academic Press.

Heskins M., Guillet J.E. (1968), Solution properties of poly(N-isopropylacrylamide). *J. Macromol. Sci. Chem., Part A*, 2(8): 1441–1455.

Hiemenz and Rajagopalan (1997), Chapter 2: Sedimentation and Diffusion and their equilibrium in Principles of Colloid and Surface Chemistry, By Paul C. Hiemenz, Raj Rajagopalan, 3rd Edition, Published by CRC Press, p. 97.

Hoffmeister F. (1888), *Arch. Exp. Pathol. Pharmacol*., *24*, 247.

Hou C., Qu R., Ji C., Wang C., Sun C. (2006), ATRP of acrylonitrile catalyzed by $FeCl_2$/Succinic acid under microwave irradiation, *J. Appl. Polym. Sci*., 101: 1598–1601.

Hritcu D., Muller W, Brooks D. E. (1999), Poly(styrene) latex carrying Cerium(IV)-initiated terminally attached cleavable chains: Analysis of grafted chains and model of the surface layer, *Macromolecules*, 32: 565-573.

http://www.biology-online.org/dictionary

http://www.bionity.com/news/e/63927

http://www.britannica.com/EBchecked/topic/165892/disproportionation).

http://www.chemagen.de

http://www.contractpharma.com/articles/2008/05/biocapacity-in-2012

Hu T., You Y., Pan Cm, Wu C. (2002), The Coil-to-Globule-to-Brush Transition of Linear Thermally Sensitive Poly(*N*-isopropylacrylamide) Chains Grafted on a Spherical Microgel, *J. Phys. Chem. B* , 106*:* 6659-6662.

Hubbuch J. J., (2000), Development of adsorptive separation systems for recovery of proteins from crude bioprocess liquors, Ph.D. thesis, Technical University of Denmark, Published by BioCentrum-DTU, Lungby, Denmark.

Hubbuch J. J., Mattheiesen D. B., Hobley T. J., Thomas O. R. T. (2001), High gradient magnetic separation versus expanded bed adsorption: a first principle comparison, *Bioseparation*, 10(1-3): 99-112.

Hubbuch J. J., Thomas O. R. T. (2002), High gradient magnetic affinity separation of trypsin from porcine pancreatin, *Biotcehnol. Bioeng.*, 79(3): 301-313.

Hummel, D. O., Scholl F. (1990), Atlas of polymer and plastic analysis (2nd ed.), Munich: Hanser.

Husseman M., Malmström E. E., McNamara M., Mate M., Mecerreyes D., Benoit D. G., Hedrick J. L., Mansky P., Huang E., Russell T. P., Hawker C. J. (1999), Controlled synthesis of polymer brushes by "living" free radical polymerization techniques, *Macromolecules*, 32: 1424-1431.

Inomata H., Goto S., Otake K., Saito S. (1992), Effect of additives on phase transition of N-isopropylacrylamide gels, *Langnuir*, 8: 687-690.

Israelachvili J. (1991), *Intermolecular and Surface Forces*, 2nd ed.; Academic Press: San Diego, CA.

Ista L. K., Pérez-Luna V. H., López G. P. (1999), Surface-grafted, environmentally sensitive polymers for biofilm release, *App.l Environ. Microbiol.*, 65(4): 1603-1609.

Ivanov A. E., Kazakov S. V., Galaev I. Y., Mattiasson B. (2001), Thermosensitive copolymer of N-vinylcaprolactam and 1-vinylimidazole: molecular characterization and separation by immobilized metal affnity chromatography, *Polymer*, 42: 3373-3381.

Janson J.-C., Jönsson J.-Å. (1998), Chapter 2: Introduction to chromatography, In: Protein purification (2nd edition), Janson J.-C. & Rydén L. (eds), Wiley & Sons, Inc., New York.

Jeyaprakash J. D., Samuel S., Dhamodharan R., Rühe J. (2002), Polymer brushes via ATRP: Role of activator and deactivator in the surface-initiated ATRP of styrene on planar substrates, *Macromol. Rapid Commun.*, 23(4): 277-281.

Jones P. Nesterenko P. N. (1997), High-performance chelation ion chromatography A new dimension in the separation and determination of trace, *J. Chromatogr. A*, 789: 413–435.

Kågedal L. (1998), Chapter 8: Immobilized metal ion affinity chromatography, In: Protein purification (2nd edition), Janson J.-C. & Rydén L. (eds), Wiley & Sons, Inc., New York, USA; Ueda E.K.M., Gout P.W., Morganti L. (2003), Corrent and prospective applications of metal ion-protein binding, *J. Chromatogr. A*, 988: 1-23.

Kamigaito M, Ando T, Sawamoto M. (2001), Metal-catalyzed living radical polymerization, *Chem Rev.*, 101(12): 3689-746.

Kanazawa H., Kashiwase Y., Yamamoto K., Matsushima Y., Kikuchi A., Sakurai Y., Okano T. (1997), Temperature-responsive liquid chromatography. 2. Effects of hydrophobic groups in N-isopropylacrylamide copolymer-modified silica, *Anal. Chem.*, 69: 823-830.

Kanazawa H., Matsushima Y., Okano T. (1998), Temperature-responsive chromatography, *Trends Anal. Chem (TrAC),* 17(7): 435-440.

Kanazawa H., Yamamoto K., Matsushima Y. (1996), Temperature-responsive chromatography using poly(N-isopropylacrylamide)-modified silica, *Anal. Chem.***,** 68(1): 100-105.

Karlsson E., Rydén L., Brewer J. (1998), Chapter 4: Ion-exchange chromatography, In: Protein purification (2nd edition), Janson J.-C. & Rydén L. (eds), Wiley & Sons, Inc., New York, USA.

Kato K., Uchida E., Kang E. -T., Uyama Y., Ikada Y. (2003), Polymer surface with graft chains, *Prog. Polym. Sc.i.* 28**:** 209–259.

Kawai T., Saito K., Lee W. (2003), Protein binding to polymer brush, based on ion-exchange, hydrophobic, and affinity interactions, *J. Chromatogr. B*, 790: 131–142.

Kidoaki S., Ohya S., Nakayama Y., Matsuda T. (2001), Thermoresponsive structural change of a poly(*N*-isopropylacrylamide) graft layer measured with an atomic force microscope, *Langmuir*,17: 2402-2407.

Kikuchi A., Okano T. (2002), Intelligent thermoresponsive polymeric stationary phases for aqueous chromatography of biological compounds, *Prog. Polym. Sci.*, 27: 1165-1193.

Kikuchi A., Okuhara M., Karikusa F., Sakurai Y., Okano T. (1998), Two-dimensional manipulation of confluently cultured vascular endothelial cells using temperature-responsive poly(*N*-isopropylacrylamide)-grafted surfaces, *J Biomater Sci, Polym Ed*, 9(18):1331-1348.

Kilbey S. M., Watanabe H, Tirrell M. (2001), Structure and scaling of polymer brushes near the theta condition, *Macromolecules*, 34: 5249–5259.

Kim D. J., Kang S. M., Kong B., Kim W. J., Paik H. J., Choi H, Choi I. S. (2005), Formation of thermoresponsive gold nanoparticle/PNIPAAm hybrids by surface-initiated, atom transfer radical polymerization in aqueous media, *Macromol. Chem. Phys*, 206(19): 1941–1946.

Kim D. J., Kong B., Jung Y. H., Kim K. S., Kim W. J., Lee K., Kang S. M., Jeon S., Choi I. S. (2004), Formation of thermoresponsive surfaces by surface-initiated, aqueous atom-transfer radical polymerization of *N*-isopropylacrylamide: Application to cell culture, *Bull. Korean Chem. Soc.*, 25(11): 1629-1630.

Kizhakkedathu J. N., Jones N. R. and Donald E. Brooks E. D. (2004), Synthesis of well-defined environmentally responsive polymer brushes by aqueous ATRP, *Macromolecules*, 37: 734-743.

Kobayashi J., Kikuchi A., Sakai K., Okano T. (2003), Cross-linked thermoresponsive anionic polymer-grafted surfaces to separate bioactive basic peptides, *Anal. Chem.*, 75(13): 3244−3249.

Kolpachnikova M. G., Penner N. A., Nesterenko P. N. (1998), Effect of temperature on retention of alkali and alkaline-earth metal ions on some aminocarboxylic acid functionalised silica based ion exchangers, *J. Chromatogr. A*, 826: 15-23.

Kowalewski T., McCullough R. D., Matyjaszewski K. (2003), Complex nanostructured materials from segmented copolymers prepared by ATRP, *Eur. Phys. J. E*, 10: 5–16.

Kubota K., Fujishige S., Ando I. (1990), Single-Chain Transition of Poly (N-isopropylacrylamide) in Water, *J. Phys. Chem.*, Vol. 94(12): 5154-5158.

Kumar A., Kamihira M., Galaev I. Y., Mattiasson B., Iijima S. (2001), Type-specific separation of animal cells in aqueous two-phase systems using antibody conjugates with temperature-sensitive polymers, *Biotcehnol. Bioeng.*, 75: 570-580.

Kumar A., Galaev I. Y., Mattiasson B. (1999), Metal chelate affinity precipitation: a new approach to protein purification, *Bioseparation*, 7: 185–194.

Kumar A., Galev I. Y., Mattiasson B. (1998a), Affinity precipitation of α-amylase inhibitors from wheat meal by metal chelate affinity binding using Cu(II)-loaded copolymers of 1-vinylimidazole with *N*-isopropylacrylamide, *Biotechnol Bioeng* 59(6): 695–704.

Kumar A., Galev I. Y., Mattiasson B. (1998b), Isolation and separation of α-amylase inhibitors I-1 and I-2 from seeds of ragi (Indian finger millet, *Eleusine coracana*) by metal chelate affinity precipitation, *Bioseparation*, 7: 129–136.

Kumar A., Kamihara M., Mattiasson B. (2002), Two-phase affinity partitioning of animal cells: Implications of multipoint interactions, In Methods for affinity-based separations of proteins/enzymes, Gupta M. N., ed. (Basel, Switzerland: Birk imhauser Verlag): 163–180.

Kumar A., Kamihira M., Galaev I. Y., Iijima S., Mattiasson B. (2003), Binding of Cu(II)-Poly(*N*-isopropylacrylamide/ vinylimidazole) copolymer to histidine-tagged protein: a surface plasmon resonance study, *Langmuir*, 19(3): 865-871.

Kumar A., Srivastava A., Galaev I. Y., Mattiasson B. (2007), Smart polymers: Physical forms and bioengineering applications, *Prog. Polym. Sci*., 32(10): 1205–1237.

Lakhiari H., Okano T., Nurdin N., Luthi C., Descouts P., Muller D., Jozefonvicz J. (1998), Temperature-responsive size-exclusion chromatography using poly (*N*-isopropylacrylamide) grafted silica, *Biochemica et Biophysica Acta*, 1379: 303–313.

Langer E.S. (2007a), Downstream production challenges in 2007, *BioProcess International*, June: 22-28).

Langer E.S. (2007b), Downstream production impacts overall capacity, *BioWorld EUROPE*, March: 38-40.

Lightfoot E. N., Moscariello J. S (2004), Bioseparations, *Biotechnol. Bioeng.*, 87(3): 259-273.

Lukin J. A., Kontaxis G., Simplaceanu V., Yuan Y., Bax A., Ho C. (2003), Quaternary structure of hemoglobin in solution, *PNAS,* 100(2): 517-520.

Luzinov I., Minko S., Tsukruk V. V. (2004), Adaptive and responsive surfaces through controlled reorganization of interfacial polymer layers, *Prog. Polym. Sci.*, 29(7): 635-698.

Ma Z. Y., Guan Y. P., Liu X. Q., Liu H. Z. (2005), Synthesis of magnetic chelator for high-capacity immobilized metal affinity adsorption of protein by cerium initiated graft polymerization, *Langmuir,* 21: 6987-6994.

Mahadevaiah D. T. (2007), Polymerisation kinetics of methylmethacrylate by oxidation: reduction system using Cerium(IV)/Lactic acid in aqueous medium, *J. Appl. Polym. Sci*., 103: 3498-3505.

Maharjan P., Woonton B. W., Bennett L. E., Smithers G. W., DeSilva D., Milton T.W., Hearn M. T. W (2008), Novel chromatographic separation - The potential of smart polymers, *Innovative Food Science and Emerging Technologies*, 9: 232–242.

Maisano F., Testori S. A., Grandi G. (1989), Immobilised metal-ion affinity chromatography of human growth hormone, *J. Chromatogr.*, 472: 422-427.

Marshak D. R. (1996), Strategies for protein purification and characterization: a laboratory course manual, Cold Spring Harbor Laboratory Press (U.S), p. 8.

Matsui M., Nakahara A., Takatsu A., Kato K., Matsuda N. (2008), In situ observation of the state and stability of hemoglobin adsorbed onto glass surface by Slab Optical Waveguide (SOWG) Spectroscopy, *International Journal of Chemical and Biomolecular Engineering*, 1(2): 73-76.

Matyjaszewski K. (2005), Macromolecular engineering: From rational design through precise macromolecular synthesis and processing to targeted macroscopic material properties, *Prog. Polym. Sci*., 30: 858–875.

Matyjaszewski K., Woodworth B. E., Zhang X., Gaynor S. G., Zack Metzner (1998), Simple and efficient synthesis of various alkoxyamines for stable free radical polymerization, *Macromolecule,* 31: 5955-5957.

Matyjaszewski K., and Xia J. (2001), Atom Transfer Radical Polymerization, *Chem. Rev*., 101(9): 2921-2990.

Matyjaszewski K., Davis K., Patten T.E., Wei M. (1997), Observation and analysis of a slow termination process in the atom transfer radical polymerization of styrene, *Tetrahedron*, 53(45): 15321-15329.

Matyjaszewski K., Miller P. J., Shukla N., Immaraporn B., Gelman A., Luokala B. B., Siclovan T. M., Kickelbick G., Vallant T., Hoffmann H., Pakula T. (1999), Polymers at interfaces: Using atom transfer radical polymerization in the controlled growth of homopolymers and block copolymers from silicon surfaces in the absence of untethered sacrificial initiator, *Macromolecule,* 32, 8716-8724.

Matyjaszewski K., Müller A. H. E. (2006), Editorial: 50 years of living polymerization, *Prog. Polym. Sci.*, 31: 1039–1040.

Matyjaszewski K., Spanswick J. (2005), Controlled/living radical polymerisation, *Mater. Today*, 8: 26–33.

Matyjaszewski K., Xia J. (2001), Atom transfer radical polymerization, *Chem. Rev.*, 101: 2921-2990.

Michnik A., Drzazga Z., Kluczewska A., Michalik K. (2005), Differential scanning microcalorimetry study of the thermal denaturation of haemoglobin, *Biophys. Chem.*, 118: 93-101.

Milner T. S. (1991), Polymer brushes, *Science*, 251, 905-915.

Minko S. Usov D., Goreshnik E., Stamm M. (2001), Environment-adopting surfaces with reversibly switchable morphology, *Macromol. Rapid Commun*. 22 (3): 206-211.

Minko S., Sidorenko A., Stamm M., Gafijchuk G., Senkovsky V., Voronov S. (1999), Radical polymerization initiated from a solid substrate. 2. Study of the grafting layer growth on the silica surface by in situ ellipsometry, *Macromolecules,* 32: 4532-4538.

Minko S., Usov D., Motornov M., Ionov L. and Stamm M. (2003), Smart responsive interface, *Polym. Mater. Sci. Eng*., 89: 156

Minko, S., Müller, M., Usov, D., Scholl, A., Froeck, C., Stamm, M. (2002), Lateral versus perpendicular segregation in mixed polymer brushes, *Physical Review Letters*, 88(3): 035502/1-035502/4.

Mino G. and Kaizerman S. (1958), A new method for the preparation of graft copolymers. Polymerization initiated by ceric ion redox systems, *J. Polymer Science*, 31: 242-243.

Mino G., Kaizerman S., Rasmussen E. (1959), The oxidation of pinacols by ceric sulphate, *J. Am. Chem. Soc.*, 81: 1494–1502.

Misra G. S., Bajpai U. D. N. (1982), Redox polymerisation, *Prog. Polym. Sci.*, 8: 61-131.

Mu Q., Fang Y. E (2006), Preparation of thermal-responsive chitosan-graft-*N*-isopropylacrylamide membranes *via* γ-ray irradiation, *Chin. Chem. Lett.*, 17(9): 1236-1238.

Müller W. (1990), New ion exchangers for the chromatography of biopolymers, *J. Chromatogr.*, 510: 133-140.

Nagy A., Malnasi-Csizmadia A., Somogyi B., Lorinczy D. (2004), Thermal chemically stability of denatured green fluorescent protein (GFP) - A preliminary study, *Thermochim. Acta*, 410: 161–163.

Nanda A. K., Matyjaszewski, K. (2003), Effect of [bpy]/[Cu(I)] ratio, solvent, counterion, and alkyl bromides on the activation rate constants in atom transfer radical polymerization, *Macromolecules*, 36(3), 599-604.

Netopilík M., Bohdanecký M., Chytrý V., Ulbrich K. (1997), Cloud point of poly(N-isopropylmethacrylamide) solutions in water: is it really a point?, *Macromol. Rapid Commun.*, 18: 107-111.

O'Brien S. M., Thomas O. R. T., Dunnill P. (1996), Non-porous magnetic chelator supports for protein recovery by immobilised metal affinity adsorption, *J. Biotechnol.*, 50(1): 13-25.

Odian G. (2004), Principles of polymerisation (4rth Ed.), Wiley N.Y., p. 315.

Okano T., Yamada N., Okuhara M., Sakai H., Sakurai Y, (1995), Mechanism of cell detachment from temperature-modulated, hydrophilic-hydrophobic polymer surfaces, *Biomaterials*, 16(4): 297-303.

Okano T., Yamada N., Sakai H., Sakurai Y. (1993), A novel recovery system for cultured cells using plasma-treated polystyrene dishes grafted with poly (*N*-isopropylacrylamide), *J Biomed Mater Res*, 27: 1243-1251.

Okieimen F. E., Ogbeifun D. E. (1996), Graft copolymerizations of modified cellulose, grafting of acrylonitrile, and methyl methacrylate on carboxy methyl cellulose, *J. Appl. Polym. Sci*, 59: 981-986.

Ozturk T., Cakmak . (2007), Synthesis of block copolymers via redox polymerization process: a critical review, *Iran. Polym. J.*, 16 (8): 561-581.

Park T. G., Hoffman A.S. (1993), Sodium chloride-induced phase transition in nonionic poly(*N*-isopropylacrylamide)gel, *Macromolecules*, 26: 5045-5048.

Parker J., Jones R. G., Holder S. J. (2000), Direct evidence for the interaction of the mechanisms of thermally initiated and atom transfer radical polymerization, *Macromolecules*, 33**:** 9166-9168**.**

Patten T. E., Matyjaszewski K. (1999), Copper(I)-Catalyzed Atom Transfer Radical Polymerizations , *Acc. Chem. Res.*, 32: 895- 903.

Paull B., Bashir W. (2003), Non-trivial temperature effects on the cation exchange chromatography and chelation ion chromatography of metal ions *The Analyst*, 128(4): 335-44.

Pieters, B.R., Williams, R.A. and Webb, C. (1991) Magnetic carrier technology, Williams R. A. (Ed.), *Colloid and Surface Engineering: Applications in the Process Industries*. Butterworth-Heinemann, Oxford, UK, pp. 248-286.

Pietruszka N, Galaev I. Yu., Kumar A., Brzozowski Z.K., Mattiasson B. (2000), New polymers forming aqueous two-phase polymer systems, *Biotechnol Prog*, 16: 408-415.

Pintauer T., Braunecker W., Collange E., Poli, R., Matyjaszewski K. (2004), Determination of rate constants for the activation step in atom transfer radical polymerization using the stopped-flow technique; *Macromolecules*, 37: 2679-2682.

Pintauer T., Matyjaszewski K. (2005), Structural aspects of copper catalyzed atom transfer radical polymerization, *Coord. Chem. Rev.*, 249: 1155–1184.

Pitfield I. D. (1992), Perflurocarbon chromatographic supports, Ph.D. thesis, University of Cambridge, United Kingdom.

Plomer J. J. Ryland J. R., Matthews M.-A. H.,Traylor D. W., Milne E. E., Durfee S. L. Mathews A. J., Neway J. O. (1996), Purification of haemoglobin, WO 1996015151 (patent).

Plunkett K. N., Xi Z, Moore J. S., Leckband D. E. (2006), PNIPAM chain collapse depends on the molecular weight and grafting density, *Langmuir*, 22: 4259-4266.

Porath J. (1988), IMAC - Immobilized metal ion affinity based chromatography, *Trends Anal. Chem.,* 7(7): 254-259.

Porath J., Carlsson J., Olsson I., Belfrage G. (1975), Metal chelate affinity chromatography, a new approach to protein fractionation, *Nature*, 258: 598-599.

Porath J., Olin B. (1983), Immobilized metal ion affinity adsorption and immobilized metal ion affinity chromatography of biomaterials. Serum protein affinities for gel-immobilized iron and nickel ions, J. *Biochem.*, 22: 1621–1630.

Prigogine I., Defay R. (1954), Chapter XX in Chemical thermo-dynamics translated by Everett D., Longmans Green and Co, London · New York · Toronto.

Prime K. L., Whitesides G. M. (1991), Self-assembled organic monolayers: model systems for studying adsorption of proteins at surfaces, *Science*, 252: 1164-1167.

Przybycien T. M., Pujar N. S., Steele L. M. (2004), Alternative bioseparation operations: life beyond packed-bed chromatography, *Curr. Opin. Biotechnol.*, 15: 4 69–478.

Purcell, E. M., 1984, Electricity and magnetism, in *Berkely Physics Course, Volume 2*, 2nd Edition, McGraw-Hill Science Engineering, Blacklick, Ohio, USA.

Pyun J., Matyjaszewski K., Kowalewski T., Savin D., Patterson G., Kickelbick G., Huesing N. (2001), Synthesis of well-defined block copolymers tethered to polysilsesquioxane nanoparticles and their nanoscale morphology on surfaces, *J. Am. Chem. Soc.*,123*:* 9445-9446.

Qiu J., Charleux B., Matyjaszewski K. (2001), Controlled/living radical polymerization in aqueous media: homogeneous and heterogeneous systems, *Progr. Polym. Sci*., 26:2083–134.

Queffelec J., Gaynor S.G., Matyjaszewski K. (2000), Optimization of atom transfer radical polymerization using Cu(I)/tris(2-(dimethylamino)ethyl)amine as a catalyst, *Macromolecules*, 33 (23): 8629-8639.

Rademacher J. T., Baum M., Pallack M. E., Brittain W. J., Simonsick W. J (2000), Atom transfer radical polymerization of *N,N*-Dimethylacrylamide, *Macromolecules*, 33: 284-288.

Rai S. K.., Shivakumar K., Sherigara B. S. (2000), Polymerization of acrylonitrile initiated by the manganese (III)-glycine redox system: a kinetic study, *Eur. Polym. J.*, 36: 1339-1346.

Reyes Z., Rist C. E., Russell C. R. (1966), Grafting vinyl monomers to starch by ceric ion. I. Acrylonitrile and acrylamide, *J. Polym. Sci., Part A: Polym. Chem*, 4(5): 1031-1043.

Robinson P. J., Dunnill P., Lilly M. D. (1973), Properties of magnetic supports in relation to immobilized enzyme reactors, *Biotechnol Bioeng*, 15(3): 603-606.

Roohi F. (2008), Synthesis and evaluation of thermo-responsive monolithic stationary phases for chromatography, Presentation at Monolith Summer School and Symposium (MSS), Portorož, Slovenia.

Roy I. and Gupta M. N. (2003), Smart Polymeric Materials: Emerging Biochemical Applications, *Chem. Biol.*, 10: 1161–1171.

Russel, T. P. (2002), Surface-responsive materials, *Science*, 297(5583): 964-967.

Safaric I., Much P., Pecho J., Stoklasa J., Safarikova M. (2001), Separation of magnetic affinity biopolymer adsorbents in a Davis tube magnetic separator, *Biotechnol. Lett*, 23: 851–855.

Safaric I., Safaricova M., (2004), Magnetic techniques for the isolation and purification of proteins and peptides, *BioMagn Res Technol.*, 2: 7-14.

Safaric I., Safaricova M., Forsythe S. J. (1995), The application of magnetic separations in applied microbiology. *J. Appl. Bacteriol.* 78: 575–585.

Safaricova M., Safaric I., (1999), Magnetic solid-phase extraction. *J. Magn. Magn. Mater.,* 194: 108–112.

Sarac A. S. (1996), Redox polymerization in Polymeric encyclopedia of materials by Salamone J. C. (Vol. 10), CRC Press Inc., Boca Raton, FL, p. 7446.

Sarac A. S. (1999), Redox polymerisation, *Prog. Polym. Sci.,* 24(8): 1149-1204.

Scarpa J S., Mueller, D. D, Klotz I. M. (1967), Slow hydrogen-deuterium exchange in a non-a-helical polyamide, *J. Am. Chem. Soc*, 89(24): 6024-6030.

Schild H. G. (1992), Poly(*N*-isopropylacrilamide): experiment, theory and application, *Prog. Polym. Sci.*, 17:163-249.

Schild H. G., Tirrell D. A. (1991), Interaction of poly(*N*-isopropylacrylamide) with sodium n-alkyl sulfates in aqueous solution, *Langmuir***,** 7: 665-671.

Schulz R., Renner G., Henglein A., Kern W. (1954), Untersuchungen über die radikalpolymerisation von acrylamid, *Makromol. Chem.***,** 12 (1): 20-34.

Selezneva I. I., Gorelov A. V., Rochev Y. A. (2006), Use of thermosensitive polymer material on the basis of *N*-isopropylacrylamide and *N*-tert-butylacrylamide copolymer in cell technologies, *Bull. Exp. Biol. Med.,* 2(4):538-541.

Shamim N., Hong L., Hidajat K., Uddin M. S. (2006), Thermosensitive-polymer-coated magnetic nanoparticles: Adsorption and desorption of Bovine Serum Albumin, *J. Colloid Interface Sci.,* 304: 1–8.

Shan J., Chen J., Nuopponen M., Tenhu H. (2004), Two phase transitions of poly(*N*-isopropylacrylamide) brushes bound to gold nanoparticles, *Langmuir , 20:* 4671-4676.

Sharma B. R., Kumar V., Soni P. L. (2002), Ceric ammonium nitrate-initiated graft copolymerization of acrylamide onto *Cassia tora* gum, *J. Appl. Polym. Sci.,* 86: 3250–3255.

Sheth S. R. And Leckband D. (1997), Measurements of attractive forces between proteins and end-grafted poly(ethylene glycol) chains, *Proc. Natl. Acad. Sci. USA,* 94: 8399–8404.

Shukla A.A. and Yigzaw Y. (2007), Chapter 6: Modes of preparative chromatography, In: Process scale bioseparations for the biopharmaceutical industry, Shukla A.A., Etzel M.R. & Gadam S. (eds), CRC Press, Boca Raton, USA.

Sidorenko A., Minko S., Schenk-Meuser K., Duschner H., Stamm M. (1999), Switching of polymer brushes, *Langmuir, 15:* 8349-8355.

Simon J., Bajpai A. (2003), Application of thermal analysis to study the macroredox polymerization of styrene with hydroxy-terminated polybutadiene, *Eur. Polym. J.*, 39: 2077–2089.

Singh B. C., Misra B. K., Rout A., Mallick N., Rout M. K. (1979), Kinetics of inhibited or retarted polymerization- investigation on the cerium(IV)-toluene-acrylonitrile system, *Makromol. Chem.*, 180: 953-1968.

Sivars U., Abramson J., Iwata S., Tjerneld F. (2000), Affinity partitioning of poly(histidine)-tagged integral membrane protein, cytochrome bo3 ubiquinol oxidase, in a detergent-polymer aqueous two-phase system containing metal-chelating polymer, *J Chromtagr B*, 743: 307-316.

Soga K. G., Zuckermann J. M. and Guo H. (1996), Binary polymer brush in a solvent, *Macromolecules*, 29: 1998-2005.

Sommerfeld S., Strube J. (2005), Challenges in biotechnology production – generic processes and process optimisation for monoclonal antibodies, *Chem. Eng. Process* 44**:** 1123–1137.

Stuart B. H. (2004), Chapter 1: Introduction and Chapter 3: Spectral analysis, In Infrared Spectroscopy: Fundamentals and applications, *AnTs*, John Wiley and Sons, p. 2, 57.

Sugawara T., Matsuda T. (1994), Novel surface graft copolymerization method with micron-order regional precision, *Macromolecules*, 27(26): 7809-7814.

Sulkowski E. (1996), Immobilized metal-ion affinity chromatography: imidazole proton pump and chromatographic Sequelae. II. Chromatographic Sequelae, *J. Mol. Recognit*., 9: 494-498.

Suwa K.,Yamamoto K., Akashi M., Takano K., Tanaka N., Kunugi S.(1998), Effects of salt on the temperature and pressure responsive properties of poly(N-vinylisobutyramide) aqueous solutions, Colloid Polym Sci, 276 :529-533.

Suwa M., Wada Y., Kikunada Y., Morishita K., Kishida A., Akashi M. (1996), Synthesis and functionalities of Poly(*N*-vinylalkylamide). IV. Synthesis and free radical polymerization of *N*-vinylisobutyramide and thermosensitive properties of the polymer, 35(9): 1763 – 1768.

Svoboda J, Fujita T. 2003, Recent developments in magnetic methods of material separation, *Miner. Eng.*, 16: 785–792.

Szwarc M. (1956), 'Living' polymers, *Nature*, 176**:** 1168–1169.

Tager A. A., Safronov A. P., Sharina S. V., Galaev I. Y. (1993), Thermodynamic study of poly(*N*-vinyl caprolactam) hydration at temperatures close to lower critical solution temperature, *Colloid. Polym. Sci.*, 271: 868–872.

Takezawa T., Yuichi M., Yoshizato K.(1990), Cell Culture on a Thermo-Responsive Polymer Surface, *Bio/Technology*, 8: 854 – 856.

Taylor L. D., Cerankowski L. D. (1975), Preparation of films exhibiting a balanced temperature dependence to permeation by aqueous solutions - a study of lower consolute behavior, *J. Polym. Sci.*, Part A: Polym. Chem**.**, 13(11): 2551-2570.

Teal H. M., Hu Z., Root D. D. (2000), Native purification of biomolecules with temperature-mediated hydrophobic modulation liquid chromatography, *Anal. Biochem.*, 283: 159–165.

Teodorescu M., Matyjaszewski K. (1999), Atom transfer radical polymerization of (meth)acrylamides, *Macromolecules*, 32: 4826-4831.

Thermo Nicolet Corporation booklet (2001), Introduction to Fourier Transform Infrared Spectrometry, WI, USA

Thomas O.R. T., Franzreb M. (2007), "Magnetic Separations", In: *Bioseparation Processes*, Chapter 8, Jungbauer A., Kieran P. (Co-Editors), John Wiley & Sons Inc., New York.

Todd R. J., Johnson R. D., Arnold F. H. (1994), Multiple site binding interactions in metal-affinity chromatography. I. Equilibrium binding of engineered histidine-containing cytochromes *c*., *J. Chromatogr.* A, 662: 13–26.

Toomey R., Tirrell M. (2008), Functional polymer brushes in aqueous media from self-assembled and surface-initiated polymers, *Annu. Rev. Phys. Chem.*, 59:493–517.

Tsarevsky N. V., Bencherif S. A., Matyjaszewski K. (2007), Graft copolymers by a combination of ATRP and two different consecutive click reactions, *Macromolecules*, 40: 4439.

Tsukruk V. V. (1997), Assembly of supramolecular polymers in ultrathin films, *Prog. Polym. Sci.*, 22: 247-311.

Ueda E.K.M., Gout P.W., Morganti L. (2003), Current and prospective applications of metal ion-protein binding, *J. Chromatogr. A*, 988: 1-23.

Uenouama S., Hoffman A. S. (1988), Synthesis and characterisation of acrylamide-*N*-isopropylacrylamide copolymer grafts on silicone rubber substrates, *Int. J. Radiat. Appl. lnstrum., Part C, Radiat. Phys. Chem.*, 32(4): 605-608.

Ulbricht M, Riedel M. (1998), Ultrafiltration membrane surface with grafted polymer tentacles: preparation, characterization and application for covalent protein binding, *Biomaterials*, 19: 1229–37.

Van Dam M. E., Wuenschell G. S., Arnold, F. H. (1989), Metal affinity precipitation of proteins, *Biotechnol. Appl. Biochem.,* 11: 492- 502.

Vunnum S., Gallant S., Cramer S. (1996), Immobilized metal affinity chromatography: Displacer characteristics of traditional mobile phase modifiers, *Biotechnol. Prog*., 12: 84-91.

Wang J., Matyjaszewski K. (1995), Control1ed "living" radical polymerization. Atom transfer radical polymerization in the presence of transition-metal complexes, *J. Am. Chem. Soc.*, 117: 5614-5615.

Ward W. W., Bokman S. H. (1982), Reversible denaturation of *Aequorea* Green-Fluorescent Protein: Physical separation and characterization of the renatured protein?, *Biochemistry,*21: 4535-4540.

Wenning L., Müller M., K. Binder K. (2005), How does the pattern of grafting points influence the structure of one-component and mixed polymer brushes?, *Europhys. Lett.*, 71(4): 639–645.

Willett T. (2009), Ph.D. thesis, University of Birmingham, School of Chemical Engineering, UK

Winnik M. F. (1990), Phase transition of aqueous poly(*N*-isopropylacrylamide) solutions: a study by non-radiative energy transfer, *Polymer,* 1990, 31: 2125-2134.

Wu T., Zhang Y., Wang X., Liu S. (2008), Fabrication of hybrid silica nanoparticles densely grafted with thermoresponsive poly(*N*-isopropylacrylamide) brushes of controlled thickness via surface-initiated atom transfer radical polymerization, *Chem. Mater., 20:* 101–109.

Wu T., Efimenko K., Genzer J. (2002), Combinatorial study of the mushroom-to-brush crossover in surface anchored polyacrylamide, *J. A,. Chem. Soc.*, 124: 9394-9395.

Xia J., Gaynor S. G.. Matyjaszewski K. (1998), Controlled/“living” radical polymerization. Atom transfer radical polymerization of acrylates at ambient temperature, *Macromolecules*, 31: 5958-5959.

Xia J., Matyjaszewski K. (1997), Controlled/“living” radical polymerization. Atom transfer radical polymerization using multidentate amine ligands, *Macromolecules*, 30(25): 7697-7700.

Xu J., Zeng F., Wu S., Liu X., Hou C., Tong Z. (2007), Gold nanoparticles bound on microgel particles and their application as an enzyme support, *Nanotechnology*, 18: 1-8.

Yamamoto S., Ejaz M., Tsujii Y., Fukuda T. (2000), Surface interaction forces of well-defined, high-density polymer brushes studied by atomic force microscopy. 2. Effect of graft density. *Macromolecules*, 33: 5608–5612.

Yan Y.-B., Wang Q., He H.-W., Zhou H.-M. (2004), Protein thermal aggregation involves distinct regions: sequential events in the heat-induced unfolding and aggregation of haemoglobin, *Biophys. J.*, 86: 1682–1690.

Yim H., Kent M. S., Mendez S., Balamurugan S., Balamurugan S. S., Lopez G. P., Satija S. (2004), Temperature-dependent conformational change of PNIPAM grafted chains at high surface density in water, *Macromolecules:* 37: 1994-1997.

Yim H., Kent M. S., Satija S., Mendez S., Balamurugan S. S., Balamurugan S., Lopez G. P. (2005), Evidence for vertical phase separation in densely grafted, high-molecular-weight poly(*N*-isopropylacrylamide) brushes in water. *Phys. Rev. E,* 72: 051801.1-051801.7.

Yoshida R., Ichijo H., Hakuta T., Yamaguchi T. (1995), Self-oscillating swelling and deswelling of polymer gels, Macromol. Rapid Commun., 16, 305-310.

Zampano G., Bertoldo M., Bronco S. (2009), Poly(ethyl acrylate) surface-initiated ATRP grafting from wood pulp cellulose fibers, *Carbohydr. Polym.*, 75: 22–31.

Zhang K., Ma J., Zhang B., Zhao S., Li Y., Xu Y., Yu W., Wang W. (2007), Synthesis of thermoresponsive silica nanoparticle/PNIPAM hybrids by aqueous surface-initiated atom transfer radical polymerization, *Mater. Lett.*, 61: 949–952.

Zhang X., Matyjaszewski K. (1999), Synthesis of well-defined amphiphilic block copolymers with 2-(dimethylamino)ethyl methacrylate by controlled radical polymerization, *Macromolecules,* 32: 1763-1766.

Zhang Y., Cremer P. S. (2006), Interaction between macromolecules and ions: the Hofmeister series, 10(6): 658-663.

Zhao B. (2003), Synthesis of binary mixed homopolymer brushes by combining atom transfer radical polymerization and nitroxide-mediated radical polymerization, *Polymer*, 44: 4079-4083.

Zhao B., Brittain J. W. (1999), Synthesis of tethered polystyrene-*block*-poly(methyl methacrylate) monolayer on a silicate substrate by sequential carbocationic polymerization and atom transfer radical polymerization, *J. Am. Chem. Soc., 121:* 3557-3558.

Zhao B., Brittain J. W., Zhou W. and Cheng Z. D. S. (2000), Nanopattern forrmation from tethered PS-*b*-PMMA brushes upon treatment with selective solvents, *J. Am. Chem. Soc.,* 122: 2407-2408

Zhao B., Brittain W. J. (2000), Polymer brushes: surface-immobilized macromolecules, *Prog. Polym. Sci.,* 25: 677-710.

Zhou F., Huck W. T. S. (2006), Surface grafted polymer brushes as ideal building blocks for ‘‘smart’’ surfaces, *Phys. Chem. Chem. Phys.,* 8: 3815–3823.

Zhou F., Jiang L., Liu W., Xue Q. (2004), Fabrication of chemically tethered binary polymer-brush pattern through two-step surface-initiated atomic transfer radical polymerization, *Macromol. Rapid Commun.,* 25: 1979-1983.

Zhu P. W., Napper D. H. (1994), Experimental observation of coil-to-globule type transitions at interfaces, *J. Colloid Interface Sci.,* 164: 489-494.

Zhu P. W., Napper D. H. (1997), Conformational transitions of poly(*N*-isopropylacrylamide) chains loopily absorbed at the surfaces of poly(*N-tert*-butylacrylamide) latex particles in water, *J. Phys. Chem. B,* 101, 3155-3160.

Zhu X., Yan C., Winnik F. M., Leckband D. (2007), End-grafted low-molecular-weight PNIPAM does not collapse above the LCST, *Langmuir*, 23: 162-169.

Zhulina E. B., Borisov O. V., Pryamitsyn V. A., Birshtein T. M. (1991), Coil-globule type transitions in polymers. 1. Collapse of layers of grafted polymer chains, *Macromolecules*, 24: 140-149.